

Soils and Rocks

An International Journal of Geotechnical
and Geoenvironmental Engineering



Volume 42, N. 1
January-April 2019

SOILS and ROCKS

An International Journal of Geotechnical and Geoenvironmental Engineering

Editor Paulo Scarano Hemsí - Aeronautics Institute of Technology, Brazil

Co-editor José Couto Marques - University of Porto, Portugal

Executive Board

Waldemar Coelho Hachich
University of São Paulo, Brazil
Antônio Topa Gomes
University of Porto, Portugal

Renato Pinto Cunha
University of Brasília, Brazil
Rafaela Cardoso
University of Lisbon, Portugal

José Antônio Schiavon (*Secretary*)
Aeronautics Institute of Technology, Brazil

Associate Editors

H. Einstein
MIT, USA
John A. Hudson
Imperial College, UK
Kenji Ishihara
University of Tokyo, Japan
Michele Jamiolkowski
Studio Geotecnico Italiano, Italy
Willy A. Lacerda
COPPE/UFRJ, Brazil

E. Maranha das Neves
Lisbon Technical University, Portugal
Nielen van der Merve
University of Pretoria, South Africa
Paul Marinos
NTUA, Greece
James K. Mitchell
Virginia Tech., USA
Lars Persson
SGU, Sweden

Harry G. Poulos
University of Sidney, Australia
Niek Rengers
ITC, The Netherlands
Fumio Tatsuoka
Tokyo University of Science, Japan
Luiz González de Vallejo
UCM, Spain
Roger Frank
ENPC-Cermes, France

Editorial Board Members

Roberto F. Azevedo
Federal University of Viçosa, Brazil
Milton Kanji
University of São Paulo, Brazil
Kátia Vanessa Bicalho
Federal University of Espírito Santo, Brazil
Omar Y. Bitar
IPT, Brazil
Lázaro V. Zuquette
University of São Paulo at São Carlos, Brazil
Fabio Taioli
University of São Paulo, Brazil
Tarcisio Celestino
University of São Paulo at São Carlos, Brazil
Edmundo Rogério Esquivel
University of São Paulo at São Carlos, Brazil
Nilo C. Consoli
Federal Univ. Rio Grande do Sul, Brazil
Sandro S. Sandroni
Consultant, Brazil
Sérgio A.B. Fontoura
Pontifical Catholic University, Brazil
Ennio M. Palmeira
University of Brasília, Brazil
Luciano Décourt
Consultant, Brazil
Faïçal Massad
University of São Paulo, Brazil
Marcus Pacheco
University of the State of Rio de Janeiro, Brazil
Paulo Maia
University of Northern Rio de Janeiro, Brazil
Renato Cunha
University of Brasília, Brazil

Orencio Monje Vilar
University of São Paulo at São Carlos, Brazil
Maria Eugenia Boscov
University of São Paulo, Brazil
Eda Freitas de Quadros
BGTECH, Brazil
Tácio de Campos
Pontifical Catholic University of Rio de Janeiro, Brazil
Richard J. Bathurst
Royal Military College of Canada
Robert Mair
University of Cambridge, UK
Serge Leroueil
University of Laval, Canada
Mario Manassero
Politécnico di Torino, Italy
Luis Valenzuela
Consultant, Chile
Jorge G. Zornberg
University of Texas/Austin, USA
Andrew Whittle
MIT, USA
Pierre Bérest
LCPC, France
Peter Kaiser
Laurentian University, Canada
He Manchao
CUMT, China
Teruo Nakai
Nagoya Inst. Technology, Japan
Claudio Olalla
CEDEX, Spain
Frederick Baynes
Baynes Geologic Ltd., Australia

R. Kerry Rowe
Queen's University, Canada
R. Jonathan Fannin
University of British Columbia, Canada
Laura Caldeira
LNEC, Portugal
Antônio S. Cardoso
University of Porto, Portugal
José D. Rodrigues
Consultant, Portugal
Antônio G. Coelho
Consultant, Portugal
Luís R. Sousa
University of Porto, Portugal
Rui M. Correia
LNEC, Portugal
João Marcelino
LNEC, Portugal
Antônio C. Mineiro
University of Lisbon, Portugal
Antônio P. Cunha
LNEC, Portugal New
Antônio G. Correia
University of Minho, Portugal
Carlos D. Gama
Lisbon Technical University, Portugal
José V. Lemos
LNEC, Portugal
Nuno Grossmann
LNEC, Portugal
Luís L. Lemos
University of Coimbra, Portugal
Ricardo Oliveira
COBA, Portugal

“Ad hoc” Reviewers (2019)

Soils and Rocks is indebted to all “ad hoc” reviewers.

A complete list of reviewers that contributed to the current volume of Soils and Rocks will be published here in the December issue.

Soils and Rocks publishes papers in English in the broad fields of Geotechnical Engineering, Engineering Geology and Geoenvironmental Engineering. The Journal is published in April, August and December. Subscription price is US\$ 90.00 per year. The journal, with the name “Solos e Rochas”, was first published in 1978 by the Graduate School of Engineering, Federal University of Rio de Janeiro (COPPE-UFRJ). In 1980 it became the official magazine of the Brazilian Association for Soil Mechanics and Geotechnical Engineering (ABMS), acquiring the national character that had been the intention of its founders. In 1986 it also became the official Journal of the Brazilian Association for Engineering Geology and the Environment (ABGE) and in 1999 became the Latin American Geotechnical Journal, following the support of Latin-American representatives gathered for the Pan-American Conference of Guadalajara (1996). In 2007 the journal acquired the status of an international journal under the name of Soils and Rocks, published by the Brazilian Association for Soil Mechanics and Geotechnical Engineering (ABMS), Brazilian Association for Engineering Geology and the Environment (ABGE) and Portuguese Geotechnical Society (SPG). In 2010, ABGE decided to publish its own journal and left the partnership.

Soils and Rocks

1978,	1 (1, 2)
1979,	1 (3), 2 (1,2)
1980-1983,	3-6 (1, 2, 3)
1984,	7 (single number)
1985-1987,	8-10 (1, 2, 3)
1988-1990,	11-13 (single number)
1991-1992,	14-15 (1, 2)
1993,	16 (1, 2, 3, 4)
1994-2010,	17-33 (1, 2, 3)
2011,	34 (1, 2, 3, 4)
2012-2018,	35-41 (1, 2, 3)
2019,	42 (1,

ISSN 1980-9743

CDU 624.131.1

SOILS and ROCKS

An International Journal of Geotechnical and Geoenvironmental Engineering

Publication of**ABMS - Brazilian Association for Soil Mechanics and Geotechnical Engineering****SPG - Portuguese Geotechnical Society****Volume 42, N. 1, January-April 2019****Table of Contents****ARTICLES**

Geomembrane as an Upstream Impermeable Blanket of Embankment Dams - Laboratory and Numerical Study

R.C. Pierozan, S.H.C. Teixeira, G.L.S. Araújo, C.A. Teixeira 3

Predicting the Shear Strength of Unfilled Rock Joints with the First-Order Takagi-Sugeno Fuzzy Approach

Y.M.P. Matos, S.A. Dantas Neto, G.A. Barreto 21

Analysis of the Physical-Mechanical Behavior of Clayey Sand Soil Improved with Coir Fiber

L.C.P. Menezes, D.B. Sousa, S.F. Sukar, S.R.M. Ferreira 31

Numerical Simulation of Vertical Pullout of Plate Anchors Embedded in Reinforced Sand

A.T. Siacara, L. Festugato 43

Obtaining the Mechanical Parameters for the Hardening Soil Model of Tropical Soils in the City of Brasilia

J.F.R. Rebolledo, R.F.P. León, J. Camapum de Carvalho 61

TECHNICAL NOTES

Rockburst From Floors

S.S. Andreyko, T.A. Lyalina 77

Maximum Tensile Strength of Sand - Coal Fly Ash - Lime Blends for Varying Curing Period and Temperature

C. Silvani, M. Benetti, N.C. Consoli 83

DISCUSSION

Behavior of Geosynthetic-Encased Stone Columns in Soft Clay: Numerical and Analytical Evaluations

N.R. Alkhorshid, G.L.S. Araújo, E.M. Palmeira 93

Articles

Soils and Rocks
v. 42, n. 1

Geomembrane as an Upstream Impermeable Blanket of Embankment Dams - Laboratory and Numerical Study

R.C. Pierozan, S.H.C. Teixeira, G.L.S. Araújo, C.A. Teixeira

Abstract. The use of geosynthetics has been a common practice in geotechnical engineering when the improvement of local soil characteristics is necessary. This paper presents an experimental and numerical study of the performance of HDPE geomembrane as impermeable blanket installed upstream of embankment dams, a treatment technique for very permeable foundation. Data based on project, field and laboratory tests of the Brazilian Salto Hydroelectric Power Plant were presented to gather information about the constructive method and to support further studies. A small-scale seepage model was constructed to represent the transverse section geometry of a hypothetical embankment dam, whose geometry was adopted based on Salto Hydroelectric Power Plant. Likewise, a numerical model was elaborated referring to the small-scale seepage model to perform several parametric analyses. The obtained results indicated that the geomembrane sealing system acts increasing the flow path through the dam foundation, resulting in lower pore-pressures into the dam. Additionally, the hydraulic parameters in the soil mass may vary considerably in case of damage to the geomembrane. In general, the study has shown that the use of synthetic membranes can be a good solution for treatment of pervious foundations and possible defects can lead to the reduction of their performance.

Keywords: earth dam, geomembrane, impermeable blanket, numerical model, scaled model.

1. Introduction

Embankment dams are normally large, complex, and costly works. Studies of alternatives to improve technical characteristics and to reduce construction cost of dams are important. One current alternative for improving soils, which has been common in geotechnical engineering works, is the use of geosynthetics. These materials have additional advantages compared to traditional materials as, for example, lower costs, shorter execution time and better ease of installation (Shukla, 2002; Koerner, 2012; Nicholson, 2015). The increasing use of geosynthetics in recent years has attracted the attention of engineers and researchers around the world, since those materials have peculiar characteristics when compared to traditional geotechnical materials. For this reason, new researches and design models became necessary, especially when geosynthetics are applied in embankment dams.

Geomembranes are among the most common types of geosynthetics. They are defined as a very low permeability synthetic membrane used with any geotechnical engineering related material, with the purpose of controlling liquid or gas migration in a human-made work, structure or system (ASTM, 2015). High density polyethylene (HDPE) geomembranes are commonly used for the construction of reservoirs as liners for water, chemical products, mining

tailings, among others (Giroud & Bonaparte, 1989; Tao *et al.*, 1996; FHWA, 1998; Whitfield, 1996; Poulain *et al.*, 2011, for instance). However, the efficiency of these barriers depends on the integrity of the synthetic membrane (Giroud & Touze-Foltz, 2003), in addition to other aspects, like the service life (Needham *et al.*, 2006).

Some researchers have studied aspects related to dam failure (*e.g.* Mahinroosta *et al.*, 2015; Petaccia *et al.*, 2016). Failures in dams and reservoirs protected by geomembranes have also been reported in the literature (*e.g.* Wu *et al.*, 2008; Messerklinger, 2014; Dong *et al.*, 2016; Bhowmik *et al.*, 2018) indicating the need for further studies.

Additionally, geomembranes can also be applied for the construction of impermeable upstream blankets for embankment dams over permeable foundations. Scuero & Vaschetti (2004) pointed out that PVC geomembranes may be installed in the upstream portion of dams in order to minimize uncontrolled water presence inside the dam, improving safety. Among the existing literature about this kind of application, Cardoso *et al.* (2010) studied the project constraints and performed a numerical analysis that supported the application of the foundation treatment in the São Salvador Hydropower Plant.

This paper presents a research (Pierozan, 2014) whose main objective is to evaluate the efficiency of foundation treatment of embankment dams by upstream imper-

Rodrigo César Pierozan, D.Sc., Postdoctoral Fellow, The University of Texas at Austin, Center for Transportation Research, Austin, TX, U.S.A., e-mail: rodrigopierozan@hotmail.com.

Sidnei Helder Cardoso Teixeira, D.Sc., Professor, Universidade Federal do Paraná, Departamento de Construção Civil, Curitiba, PR, Brazil. e-mail: s.teixeira@ufpr.br.

Gregório Luís Silva Araújo, D.Sc., Professor, Universidade de Brasília, Departamento de Engenharia Civil e Ambiental, Brasília, DF, Brazil. e-mail: gregorio@unb.br.

Celimar Azambuja Teixeira, D.Sc., Professor, Universidade Tecnológica Federal do Paraná, Departamento Acadêmico de Construção Civil, Curitiba, PR, Brazil. e-mail: celimar@utfpr.edu.br.

Submitted on January 24, 2018; Final Acceptance on December 13, 2018; Discussion open until August 30, 2019.

DOI: 10.28927/SR.421003

meable geomembrane blankets. Firstly, data from field and laboratory tests of the Brazilian Salto Hydroelectric Power Plant are briefly presented to bring together information concerning the constructive method. A cross-section of the dam was selected to represent the overall behavior of the dam and to support further studies. Based on this cross-section, a small-scale seepage model was constructed to represent the behavior of a dam with geomembrane as upstream impermeable blanket, allowing the researchers to calibrate significant parameters. This small-scale model was built taking into consideration the characteristics of Salto Hydroelectric Power Plant, however it is a simplification of the prototype. Finally, a numerical model was elaborated based on the small-scale seepage model and considering the calibrated parameters, which permitted several parametric analyses.

2. Case History Used as a Reference for the Model

The Salto Hydroelectric Power Plant, located in Rio Verde, belongs to the Paraná River Basin in the state of Goiás - Brazil. The plant started its operation in 2010 with two generation units and an installed capacity of 116 MW. Figure 1A shows a photograph of the dam. This type of solution has been used in just a few dams around the world (*e.g.* Salto Hydroelectric Power Plant and São Salvador

Hydroelectric Power Plant) and limited information regarding this kind of foundation treatment may be found in the literature (*e.g.* Cruz, 2004; Cardoso *et al.*, 2010). For this reason, studies that consider the use of geomembranes as upstream impermeable blankets of dams are very important for the advancement of the knowledge on the topic.

The left side of the earth dam has a crest with approximately 580 m length and a maximum height of approximately 25 m. Due to the geotechnical properties of the dam foundation soil, an impermeable blanket was executed upstream on the left side of the dam. A HDPE geomembrane has been used as a liner to reduce the water flow throughout the dam foundation. The applied geomembrane is a 1.5 mm thick flexible synthetic HDPE membrane, textured on both sides. According to the dam designers, a textured geomembrane was chosen in order to avoid slippage between geomembrane and compacted soil.

The setting of the geomembrane on the foundation soil was made by means of a previously excavated anchor trench 0.80 m deep and 0.50 m wide, as presented in Fig. 1B. In both cases, backfill compaction was done by hand-operated equipment near the geomembrane. Several procedures were observed to prevent damaging the membrane. The geomembrane anchor trench at the upstream face of the dam is 2 m wide and was executed after the embankment construction. These geometric attributes were

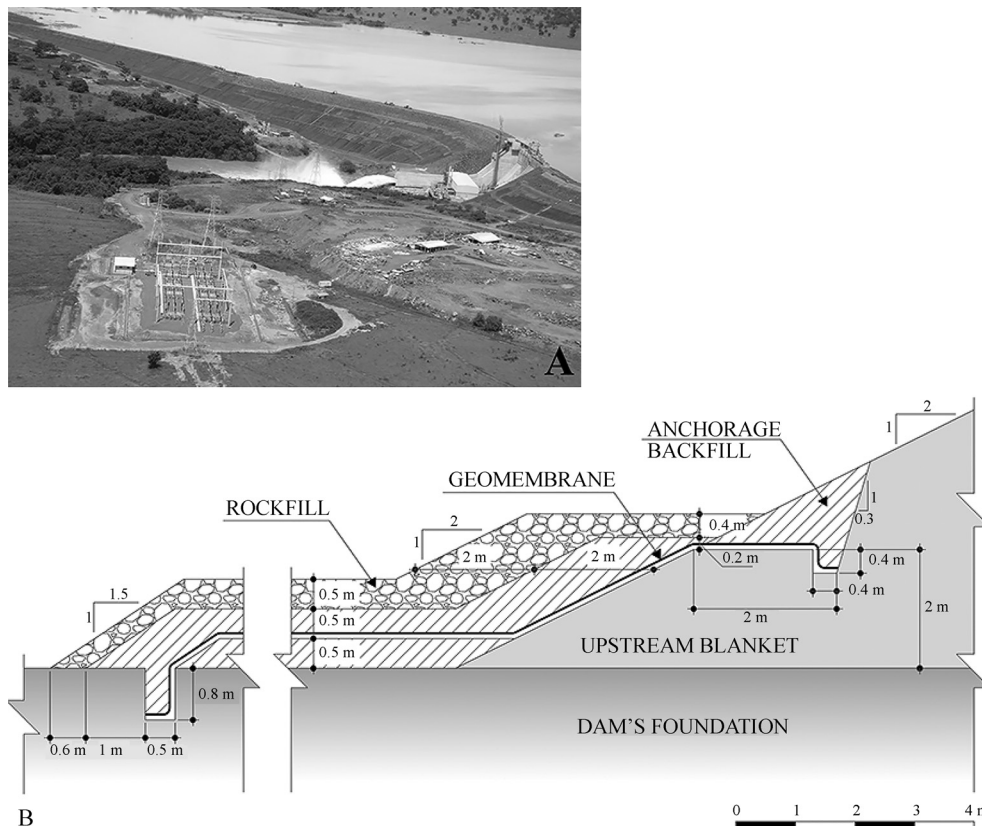


Figure 1 - Salto Hydroelectric Power Plant: (A) Aerial view and (B) Geomembrane anchor trench at upstream dam face and foundation.

based on the experience of the engineers involved in the design and further explanation regarding the anchor trench at the upstream face of the dam is discussed in this paper.

The seams between geomembrane panels were executed by using a dual welding process through the application of heat melted polymer, forming an air-tight channel between the weld lines. From the channel, it was possible to identify eventual defects, check the quality of the sealing procedure and fix the eventually identified defects.

Aiming to protect the geomembrane and to mitigate the effects of an eventual local failure, due to some mechanical effect, a 50 cm layer of compacted soil was executed over the geosynthetic. Over the compacted soil layer, an additional protective 50 cm thick layer of compacted rockfill was constructed.

2.1. Data source and analyses

The data used in this research were obtained from contractors documentation such as project drawings, topographic survey and results of field and laboratory tests. In Table 1, the main geometric characteristics of the left abutment of Salto Hydroelectric Dam are presented.

The instrumentation of Salto Hydroelectric Dam consists on standpipe piezometers, V-notch flow meters, water level indicators and surface marks. The V-notch flow meters are responsible for measuring the water flow from the internal drainage system. Five sections on the left side of the dam were instrumented.

The thickness of the permeable foundation soil layer was determined based on field permeability tests in boreholes located in several points on the left side of the dam foundation. The adopted hydraulic conductivities for foundation layers were the average values of several tests for each layer. The anisotropy relative to permeability, due to the constructive process of the embankment, was determined by the ratio between the horizontal hydraulic conductivity (k_h) and the vertical hydraulic conductivity (k_v), as suggested by Cruz (2004).

The vertical and horizontal average hydraulic conductivities of the embankment dam used in the analyses were determined from results of laboratory permeability

tests. Based on tests performed in samples from undisturbed blocks of dam embankment, an average horizontal coefficient of permeability equal to 1×10^{-5} cm/s and a vertical coefficient of permeability equal to 2×10^{-6} cm/s were obtained. Thus, the horizontal permeability is approximately five times greater than the vertical permeability. The foundation bedrock consists mainly of basalt, covered by its weathered products. The average hydraulic conductivity of foundation bedrock is equal to 1×10^{-6} cm/s.

3. Small-Scale Seepage Modelling

Laboratory tests for soil geotechnical characterization and small-scale modelling were performed at the CESEC/UFPR (Center for Studies on Civil Engineering/ Federal University of Paraná) facilities. The small-scale model consisted of a percolation tank filled with sand and other materials in the interest of representing the cross-section geometry of a hypothetical embankment dam, in the scale 1:100, taking into consideration some properties of Salto Hydroelectric Dam.

3.1. Geometric and boundary conditions of modelling

The geometry of the cross-section model was defined based on geometric characteristics of Salto Hydroelectric Dam, such as upstream and downstream slope inclination, crest width, dam height and thickness of foundation layers. It is important to highlight that the small-scale model was a simplification of Salto Hydroelectric dam instrumented cross-sections and, consequently, average parameters were adopted. The model itself is not equivalent to any of the instrumented sections and reproduces the overall observed behavior. The small-scale model did not have the objective to be the same as the prototype, since the prototype was anisotropic with properties ranging in the three dimensions (3D), and the small-scale model was isotropic and properties ranged just in two dimensions (2D). Considering that the small-scale model represents a hypothetical dam and not exactly Salto Hydroelectric Power Plant, the small-scale model has not the same hydraulic characteristics as the prototype.

Table 1 - Main characteristics of the left abutment of Salto Hydroelectric Dam.

Crest	Width = 6 m; Elevation = 449.50 m;
Downstream and upstream slope inclination	For El. < 447.50 m: 1V:2H; For El. > 447.50 m: 1V:1.5H; Upstream slope protected by riprap and crushed stone;
Berms	At El. 429.00 and 439.50 m; Width = 3 m;
Internal drainage system	80 cm wide chimney drain and horizontal blanket drain.

The length of the treated area with geomembrane on the foundation was defined from geometric data of several instrumented sections of the Salto Hydroelectric dam. Thus, the ratio between the length of upstream dam foundation treatment (L) and dam height (H) was reproduced in the small-scale model ($L = 4H$). The internal drainage system used in the model consisted of a vertical filter and blanket drain and had similarity with the dam prototype.

The boundary conditions imposed to the small-scale model were: a) reservoir water level, b) downstream water level and c) restriction to flow through the upstream impermeable blanket. The upstream water level was set to represent the maximum normal water elevation in Salto Hydroelectric reservoir (Elevation 446.50).

3.2. Model instrumentation

Internally, the tank was 250 cm long, 60 cm high and 45 cm wide, resulting in a volume of 0.75 m³. Flow visualization could be done by a lateral plexiglass wall. Water percolates through the embankment and foundation of the model as in the prototype. The flow was collected by a water outlet located at the end of the tank, allowing determination of the flow rate.

The seepage tank was instrumented with piezometers to determine the pressure head at different points. The interpretations of total heads were made by means of a reading panel. Figure 2 shows the piezometers location in the model. In this paper, piezometers in the embankment are named as PE and piezometers in the foundation are named as PF.

3.3. Geotechnical materials

The materials used for simulating the embankment and foundation soil on small-scale models were submitted to some tests, such as particle size distribution, specific gravity, permeability and maximum and minimum void ratio. The material used as drain layer was submitted to particle size distribution and permeability tests. Based on the results of particle size distribution tests, the suitability of materials to be applied as filter and drain was evaluated by the Terzaghi filter criterion.

It is important to highlight that the small-scale model was intended to simulate the cross-section geometry of a hypothetical embankment dam, based on the geometry and some characteristics found on Salto Hydroelectric Power Plant. The purpose of the scale-model was to understand how the use of geomembrane as an upstream impermeable blanket would impact the flow through the dam and its foundation. The small-scale model (2D) is a simplification of the behavior observed on the prototype (3D). It was not possible to build the small-scale model with the same geotechnical characteristics of the prototype, since the geotechnical properties were not isotropic in the field. Considering the construction of the small-scale model, laboratory available materials were used, and they were not the same found in the prototype.

3.4. Small-scale model construction

For construction of the small-scale model, granular material was deposited in the tank by means of a technique known as “sand pluviation”. This technique gives to the soil mass a standardized condition of compaction and permeability. It consists on promoting sand precipitation in pre-

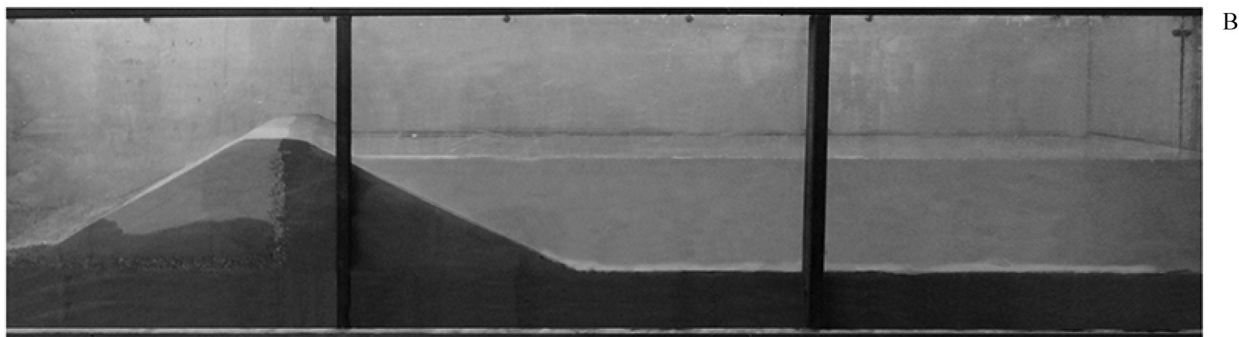
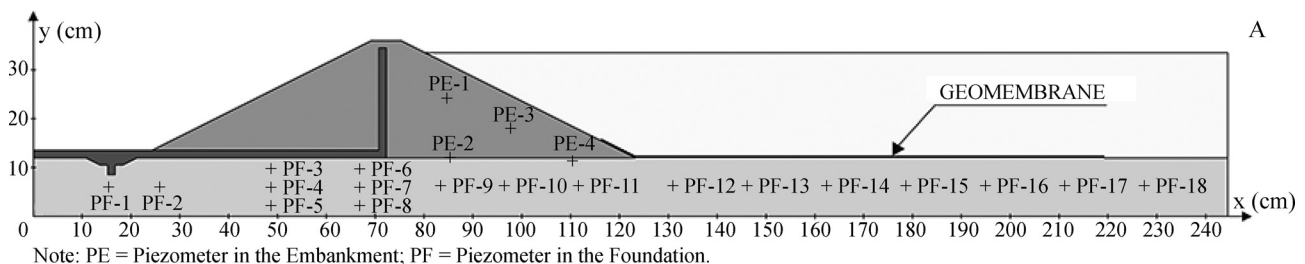


Figure 2 - Piezometers location in the small-scale model: (A) Model cross section setup and (B) Photo from laboratory tests.

established conditions, in order to obtain a material as homogeneous as possible (Rad & Tumay, 1987; Brandon *et al.*, 1991; Lo Presti *et al.*, 1992).

The sand deposition flow rate was kept constant by using 5 mm opening funnels. Because soil compaction also depends on the material falling height in this method, a calibration curve relating falling height and material relative density was obtained. Based on the curves relating the sand fall height with the obtained soil density, it was selected a fall height equal to 12 cm, for both embankment and foundation materials in small-scale models. This fall height was adopted once small variation of the density has been verified for greater heights.

The dam slopes were drawn in internal faces of the tank walls to geometrically orientate the construction of the small-scale dam model, drainage system and foundation. Successive layers of gauze and paraffin were applied over the dam upstream soil to represent the impermeable membrane. Figure 3 presents some photographs of the model assembly. Wooden sticks were placed temporarily within the vertical filter (Fig. 3 - B) as leveling references.

3.5. Small-scale model simulations

Three distinct scenarios were simulated, allowing to evaluate the effect of an upstream impermeable membrane over the dam: a) no foundation treatment, b) use of geomembrane upstream of the dam and c) use of damaged

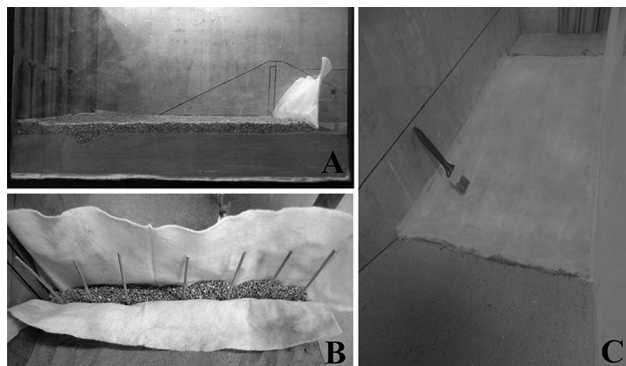


Figure 3 - Construction of the small-scale model: (A) Drainage blanket and foundation soil, (B) Vertical filter, and (C) Impermeable layer (Pierozan, 2014).

geomembrane upstream of the dam. For each simulation, readings of total heads and percolation flow rates were made. Figure 4 shows a small-scale model sketch.

In the model simulating the existence of defects on the geomembrane, longitudinal openings were made in the sealing material upstream of the dam model to simulate defects that can occur during geomembrane installation and at the end of the construction of the dam. The objective of this simulation was to verify if the geomembrane sealing system would be able to maintain a minimum performance even with generalized failure. According to Nosko *et al.* (1996), this consideration is acceptable since most of the leaks occur during the procedure of covering the liner with soil or stone, while other types of defects that could influence the system proper behavior (*e.g.* seam failure between geomembrane rolls) may be identified and fixed at the same time as the geomembrane installation quality control. Other studies (*e.g.* Rollin *et al.*, 1999; Rollin *et al.*, 2002; Rollin *et al.*, 2004) also presented similar conclusions.

3.6. Results of small-scale seepage modelling

The geometric characteristics of the model are summarized in Table 2 and illustrated in Fig. 5. It is important to observe that the dimensions adopted on the small-scale model were not exactly the same from Salto Hydroelectric

Table 2 - Small-scale model characteristics.

Characteristic	Description
Scale of model	1:100
Crest width	6 cm
Slopes	Inclination: 1V:2H (upstream and downstream);
Height (H)	24 cm;
Foundation thickness (t)	12 cm (t = H/2);
Boundary conditions	Free board: 3 cm;
	Water level: 33 cm above tank bottom;
	Downstream water outlet: 10 cm above the tank bottom;
Geomembrane length (L)	96 cm (L = 4H).

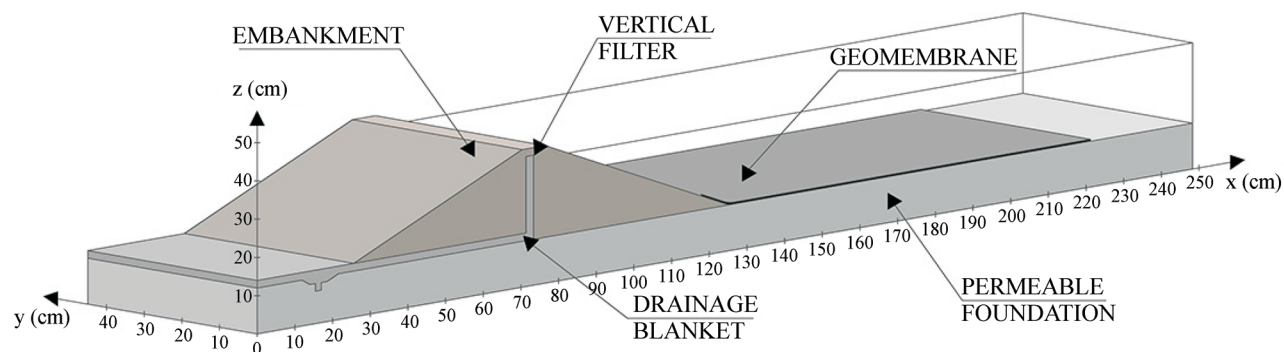


Figure 4 - Small-scale model.

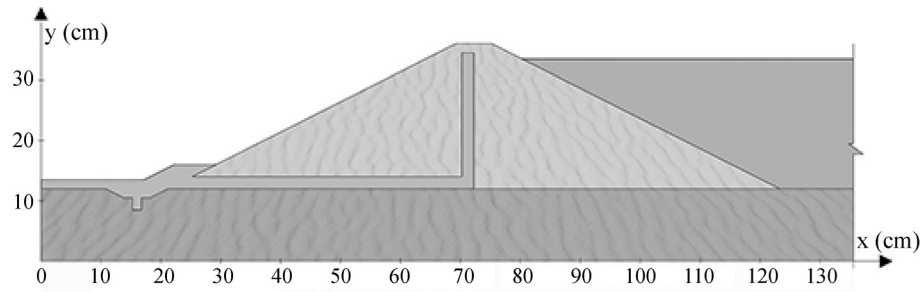


Figure 5 - Dimensions of the small-scale model.

Dam, once five sections were analyzed from the prototype and just one section was analyzed in the small-scale model.

The results of the characterization tests, maximum and minimum void ratio and permeability of materials are presented in Table 3. Based on grain size distribution curves of the materials, their suitability for using in filtration and drainage was verified.

Figure 6 shows the total head values obtained on the section of the small-scale models. The piezometers were divided into 3 arrangements to simplify the analysis of the results, considering that the arrangements are referring to the same cross-section of the dam and analyzing a distinct set of piezometers.

According to Fig. 6, the presence of nondamaged geomembrane upstream of the dam model reduced the total flow through the embankment and foundation by approxi-

Table 3 - Results of laboratory tests on material used on small-scale models.

Test	Material		
	Foundation	Dam	Drain
Water content during construction (%)	0.25	0.56	0.11
Specific gravity of solids	2.656	2.643	Not determined
Maximum void ratio	0.672	0.762	Not determined
Minimum void ratio	0.484	0.535	Not determined
Permeability (cm/s)	1×10^{-2}	2×10^{-4}	5×10^0

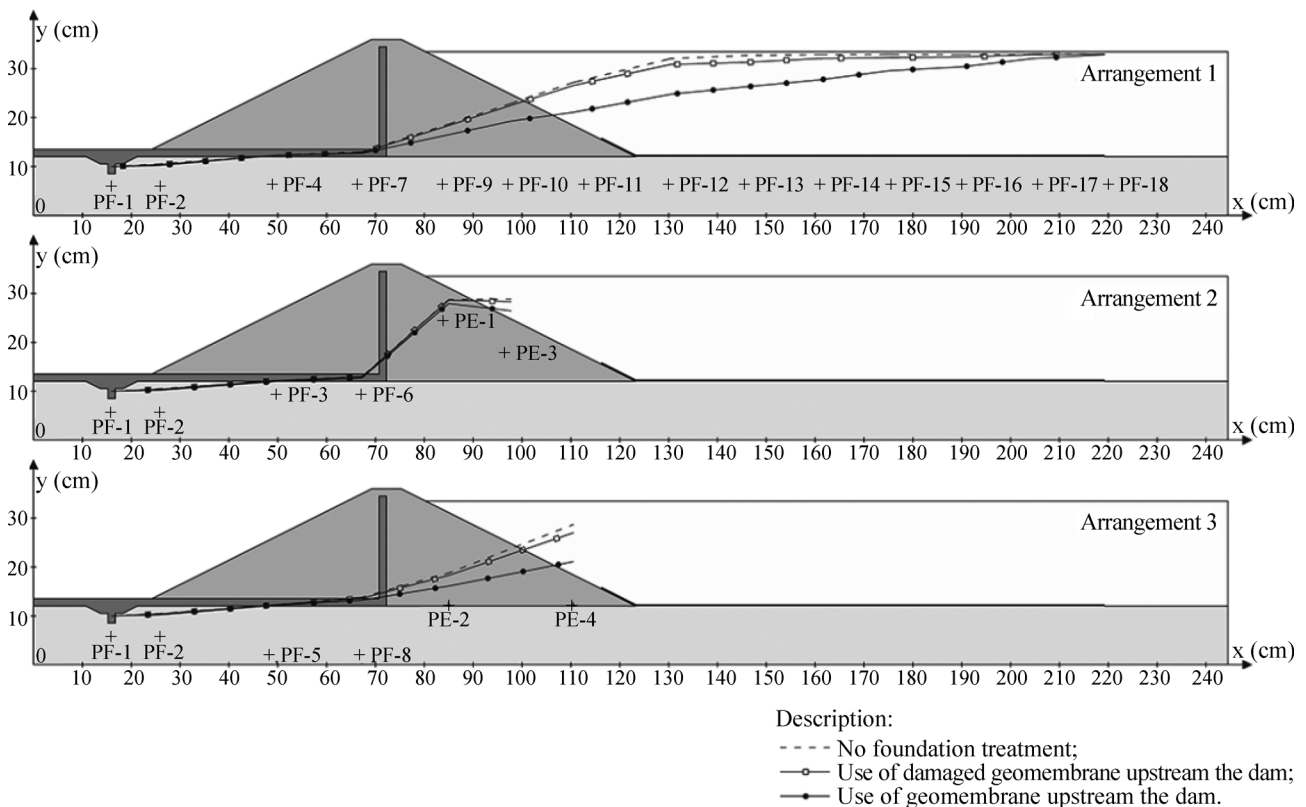


Figure 6 - Total hydraulic head obtained in tests with small-scale models.

mately 46%. On the other hand, the presence of a geomembrane with defects reduced the water flow by only 8% when comparing to the scenario without treatment.

Based on the results obtained in Arrangement 1 (Fig. 6), the presence of geomembrane upstream of the dam model leads to lower total heads. It can also be observed that the reduction of the hydraulic heads occurs primarily upstream from the chimney drain. The presence of defects leads to a lower efficiency of the foundation treatment.

The foundation treatment with upstream impermeable blanket had little influence on hydraulic heads over the dam embankment material, as shown in Arrangement 2. On the other hand, some influence can be noticed in the hydraulic heads at the interface between the dam embankment and foundation materials, as shown in Arrangement 3 (PE-2 and PE-4).

4. Numerical Analysis

Based on the results of the small-scale models, a hypothetical case with the same characteristics as the laboratory model has been simulated, in prototype dimensions. SEEP/W® software (GEO-SLOPE, 2012) was used to perform numerical analyses. This software provides two-dimensional analysis of groundwater flow within porous materials.

The following assumptions were admitted for the numerical analysis:

a) Geometric characteristics: The geometry of the dam and its foundation corresponded to that assumed in the small-scale models, except for scale and unit width (Width = 1 m). Table 4 presents the main geometric characteristics considered in the numerical analysis.

b) Saturated steady-state flow, governed by Darcy’s Law. This assumption corresponds to a constant flow rate and volumetric water content at any position below the water table. The unsaturated flow at the downstream side was disregarded in the simulations. The seepage flow rate col-

Table 4 - Numerical model geometric characteristics.

Characteristic	Description
Crest width	6 m;
Slopes	Inclination: 1V:2H (upstream and downstream);
Height (H)	24 m;
Foundation thickness (t)	12 m (t = H/2);
Geomembrane length (L)	96 m (L = 4H).

lected by the drainage system was measured in two sections: one between the vertical drain and the upstream blanket of the embankment, corresponding to the flow through the embankment (Section A-A’, Fig. 7-A), and another between the horizontal drain and the foundation, corresponding to the flow through the foundation (Section B-B’, Fig. 7-A). The sum of the two contributions resulted in the total flow;

c) Boundary conditions: The adopted boundary conditions were (Fig. 7-B) a) total head equal to 33 m in the reservoir (12 m of foundation thickness plus 24 m of dam height, minus 3 m for the free board) and b) pressure head equal to atmospheric pressure in the vertical filter and in the blanket drain. These boundary conditions are reasonable since the unsaturated flow did not represent a considerable amount of the total flow, according to previous simulations (Pierozan, 2014). For this reason, the unsaturated flow was not considered when dealing with the numerical model. In the geomembrane region, no boundary condition was applied, in other words, the geomembrane was considered impermeable.

d) Material properties: The hydraulic conductivity of the foundation was equal to 1×10^{-2} cm/s and the hydraulic conductivity of the embankment was equal to 2×10^{-4} cm/s vertically and 1×10^{-3} cm/s horizontally. These values have been adopted the same as for the small-scale tests Also, it

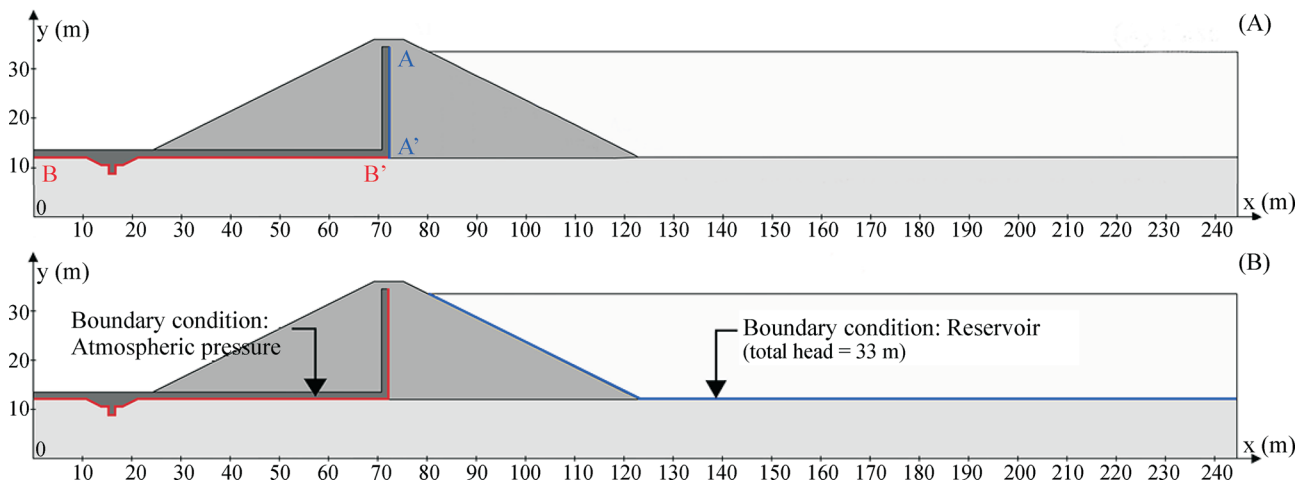


Figure 7 - Numerical model: (A) Seepage flow rate collected by the drainage system and (B) Boundary conditions of the numerical model.

was considered that the embankment material had hydraulic conductivity in horizontal direction 5 times greater than in vertical direction, which is the ratio found from laboratory tests on undisturbed samples of the Salto Dam embankment.

Once calibrated with appropriate parameters from physical and experimental data, the numerical analysis could simulate several not physically evaluated conditions to study some hypothetical cases with different boundary conditions. The behavior of the flow throughout the embankment dam and its foundation was evaluated in terms of flow rates, pressure heads and hydraulic gradients.

4.1. Validation and calibration

For the case with no geomembrane foundation treatment, the obtained flow rates were slightly higher than those obtained by the physical model. For anisotropy of the dam equal to 1, the predicted percolation flow rate has been 3% higher than the value obtained for the small-scale model. For anisotropy of the dam equal to 5, this difference was 16% and for anisotropy equal to 10, the difference was 33%.

The numerical analyses with geomembrane treatment also obtained flow rates higher than those obtained in the physical model. In this case, for anisotropy of the dam equal to 1, the predicted percolation flow rate was 10% higher than the value obtained for the small-scale model. For anisotropy equal to 5, this difference was 33% and, for anisotropy equal to 10, 62%.

The predicted values of hydraulic head were similar to those measured in the small-scale models (Fig. 6), with slight variations relative to the anisotropy coefficients.

According to the numerical analyses with no geomembrane foundation treatment, the differences between the predicted pressure heads in relation to the small-scale tests (Fig. 6), within the dam foundation for the piezometers PF-12, PF-13, PF-14, PF-15, PF-16, PF-17 and PF-18 varied between zero and 1% for the studied anisotropy coefficients. For the dam foundation in the location of piezometers PF-1, PF-2, PF-3, PF-4 and PF-5, the predictions have shown a difference between -30% and -8%, once the chimney drain highly influences this area. However, this variation is considered small for engineering practice. On the other hand, for the piezometers PF-6, PF-7, PF-8, PF-9, PF-10 and PF-11, this difference has ranged between -11% and 1%. Finally, for the embankment dam in the location of piezometers PE-1, PE-2, PE-3 and PE-4, this difference has ranged between -11% and -1%.

It was observed that the use of geomembrane as impermeable blanket has resulted in a pressure head reduction measured under it at locations corresponding to piezometers PF-12, PF-13, PF-14, PF-15, PF-16, PF-17 and PF-18 of the small-scale model (Fig. 6). Predictions for these piezometers and considering anisotropy of the dam equal to 1 have presented differences of 12%, 11%, 9%,

9%, 5%, 5% and 2%, respectively, when comparing to the small-scale tests. On the other hand, applying an anisotropy of the dam equal to 5, the differences were 2%, 10%, 8%, 9%, 5%, 5% and 2%, respectively. Lastly, for anisotropy of the dam equal to 10, the differences between predictions and measurements have been 12%, 10%, 9%, 9%, 13%, 5% and 2%, respectively.

The use of geomembrane can also reduce the pressure head in the dam foundation, according to the numerical analysis. For piezometers PF-9, PF-10 and PF-11, this reduction has ranged between 17% and 29%, which is similar to that observed in the small-scale model (Fig. 6). Additionally, the numerical analyses also predicted a reduction of the hydraulic head between 4% and 8% for the piezometers PF-6, PF-7 and PF-8, located in the dam foundation below the vertical filter. For piezometers PF-6, PF-7, PF-8, PF-9, PF-10 and PF-11 and considering anisotropy of the dam equal to 1, the predicted pressure heads have reduced 12%, 4%, 5%, 8%, 10% and 7%, respectively, when comparing to the small-scale model. When considering the anisotropy of the dam equal to 5, the differences have been 12%, 3%, 5%, 8%, 9% and 65%, respectively. Finally, the differences have been 12%, 3%, 5%, 7%, 8% and 6%, respectively, for anisotropy equal to 10.

The region within the embankment, corresponding to piezometers PE-1, PE-2, PE-3 and PE-4, presented a pressure head reduction between 20% and 45% due to the presence of the geomembrane. For these piezometers, the simulations have diverged -10%, -10%, -8% and -9% when comparing to the small-scale tests, respectively. However, when the anisotropy of the dam was considered equal to 5, the differences have been 13%, -8%, 2% and -8%, respectively. Following the results, the differences have been 20%, -8%, 7% and -7%, respectively, for anisotropy of the dam equal to 10.

Based on these results, it can be inferred that the anisotropy coefficient from the embankment influences the percolation flow rates and the pressure heads, for the case studied. The anisotropy coefficient that leads to results closest to the values obtained in small-scale modelling is equal to 1. However, it must be considered that compacted soils in actual dams present anisotropy relative to permeability. For this reason and in accordance with Salto Dam results, the anisotropy coefficient adopted for the embankment in the numerical model was $k_h/k_v = 5$. This is acceptable, once in the field some factors cannot be simulated, such as heterogeneity.

4.2. Parametric analysis and results

After validation and calibration, parametric analyses were performed to identify the influence of some factors on the internal flow through dam. In these analyses, some parameters were varied and others remained the same. In all analyses the following independent variables were kept constant: a) the dam geometry, b) the thickness of the foun-

dation permeable soil and c) the hydraulic conductivity of embankment and foundation. The following evaluations have been made:

1) Use of a single geomembrane barrier as impermeable blanket, evaluating the geomembrane application in dams by the following simulations (Fig. 8 - A):

(1a) No treatment for dam embankment and foundation;

(1b) Treatment with geomembrane only for foundation, with anchor height equivalent to 15% of the dam height (geomembrane over surface A2-A3-A4);

(1c) Treatment with geomembrane only for the dam upstream slope along all length (geomembrane over surface A1-A3);

(1d) Treatment with geomembrane over the dam upstream slope and foundation (geomembrane over surface A1-A3-A4).

The height equivalent to 15% of the dam height is equivalent to that observed in Salto Hydroelectric dam. The geomembrane length on the foundation is also the same found in Salto Hydroelectric dam ($L = 4H$).

2) Use of a single barrier of compacted soil as impermeable blanket, with the same material and permeability coefficient of the dam (2×10^{-4} cm/s), evaluating the foundation treatment through a single barrier of compacted soil with the following thicknesses (t) (Fig. 8 - B):

(2a) $t = 80$ cm;

(2b) $t = 300$ cm;

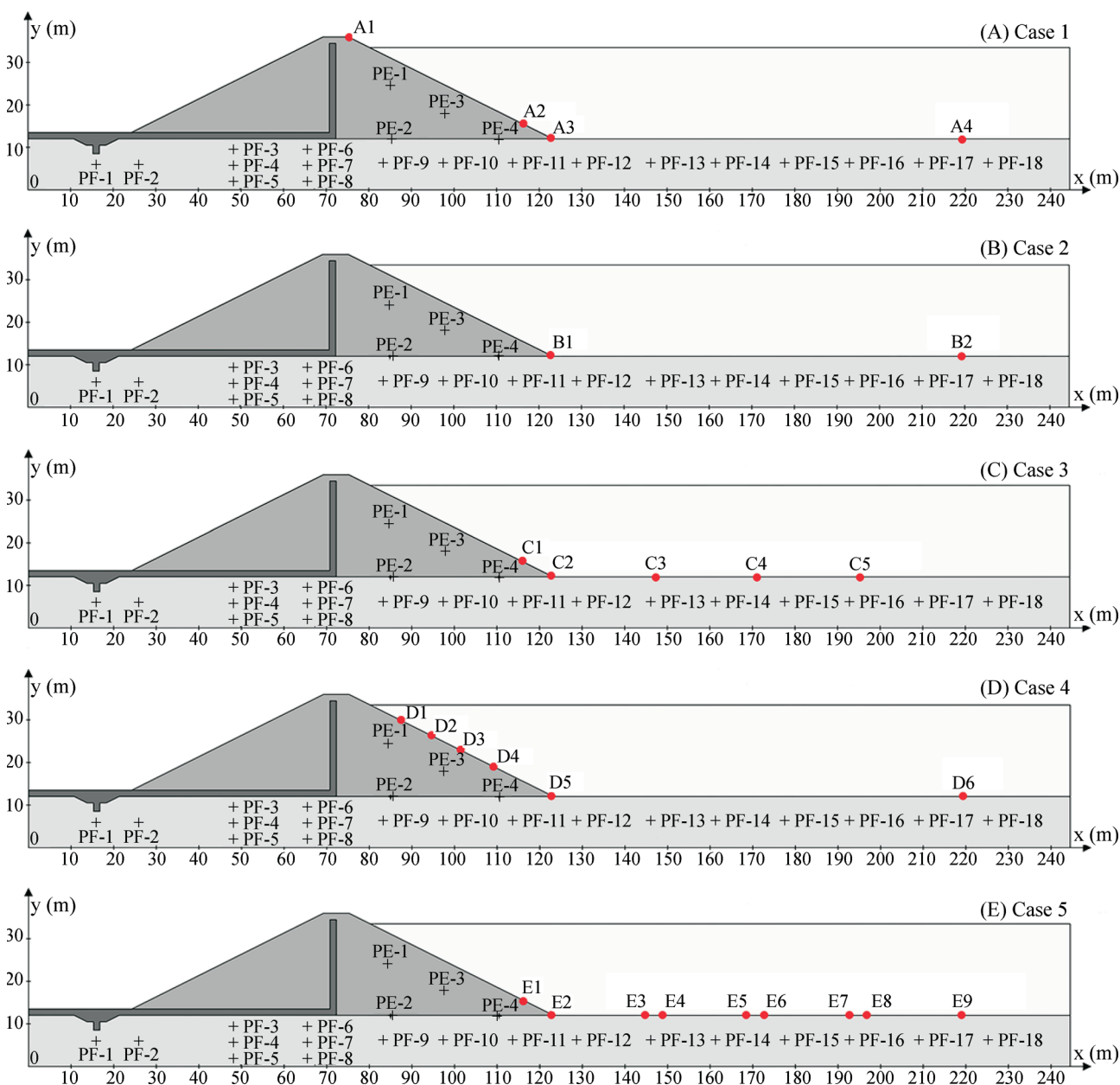


Figure 8 - Parametric analysis: (A) Case 1, (B) Case 2, (C) Case 3, (D) Case 4, and (E) Case 5.

(2c) $t = 600$ cm.

The foundation treatment length was the same considered for the geomembrane ($L = 4H$), over surface B1-B2.

3) Length of the upstream dam foundation treatment (without soil blanket), evaluating the geomembrane length on the foundation (L) in relation to the total height of the dam (H) (Fig. 8 - C):

(3a) $L=H$ (geomembrane over surface C1-C2-C3);

(3b) $L = 2.H$ (geomembrane over surface C1-C2-C4);

(3c) $L = 3.H$ (geomembrane over surface C1-C2-C5).

All the simulations considered the anchor height equivalent to 15% of the dam height (surface C1-C2).

4) Length of the geomembrane over the upstream slope of the dam, evaluating the geomembrane anchorage height (H_a) as a function of the total height of the dam (H) (Fig. 8 - D):

(4a) $H_a = 30\%.H$ (geomembrane over surface D4-D5-D6);

(4b) $H_a = 45\%.H$ (geomembrane over surface D3-D5-D6);

(4c) $H_a = 60\%.H$ (geomembrane over surface D2-D5-D6);

(4d) $H_a = 75\%.H$ (geomembrane over surface D1-D5-D6).

The foundation treatment length was considered constant and equal to $L = 4H$, over surface D5-D6.

5) Longitudinal defects in the geomembrane, simulating a set of defects and evaluating the effect of an 80 cm thick compacted soil as a secondary barrier. Considering that the software used in the analysis supports only two-dimensional simulations, these defects were simulated as a single longitudinal tear on the geomembrane, with unit width (1 m). The idea is to simulate a very adverse condition related to problems that can occur in the field such as during the placement of the cover soil over the geomembrane, since this constructive stage may result in geomembrane defects if not properly implemented. More reasonable parameters could be obtained with the use of three-dimensional modeling.

The following simulations were made (Fig. 8- E):

(5a) Presence of one 4 m long defect at half the length of the geomembrane, no secondary soil barrier (geomembrane over surface E1-E2-E9, defect over surface E5-E6);

(5b) Presence of one 4 m long defect at half the length of the geomembrane, and secondary soil barrier (geomembrane over surface E1-E2-E9, defect over surface E5-E6);

(5c) Presence of three 4 m long defects equally spaced along the geomembrane, no secondary soil barrier (geomembrane over surface E1-E2-E9, defect over surfaces E3-E4, E5-E6 and E7-E8);

(5d) Presence of three 4 m long defects equally spaced along the geomembrane, and secondary soil barrier geomembrane over surface E1-E2-E9, defect over surfaces E3-E4, E5-E6 and E7-E8).

The results of parametric analyses are presented and discussed according to hydraulic head, flow rate and hydraulic gradient, as follows.

4.2.1. Pressure head

The pressure heads obtained by the analyses considering or not the presence of the geomembrane (Case 1) are shown in Fig. 9. When geomembrane was used, the heads were significantly reduced, indicating that the geomembrane caused the reduction of pressure head in the soil. Foundation treatment with geomembrane increased the dam safety, since a pressure head and water flow decrease were observed.

The pressure heads measured in further simulations are presented in relation to the piezometer locations (Fig. 9). This procedure was adopted to synthesize the evaluated data. Slight variations were detected for piezometers PF-1 to PF-8, once they are installed in the dam foundation below the downstream embankment and are not suitable for evaluating the geomembrane performance.

Figure 10 presents the pressure heads of the embankment piezometers and analyzes are presented as follows.

With the presence of the geomembrane (Case 1), based on the results (Fig. 9), it is possible to understand that pressure heads are heavily influenced by the upstream embankment and foundation treatment with geomembrane. If the design purpose is to reduce the pressure heads in the embankment to ensure dam stability, Case 1c has the best cost-benefit. However, the installation of geomembrane over the upstream embankment may not be viable when the embankment has low hydraulic conductivity and the design purpose of the geomembrane installation is to minimize the flow rates along the foundation soil. In this case, Case 1b has the best cost-benefit. Case 1d may be the best solution for cases when both embankment and foundation have high hydraulic conductivity.

The use of a compacted soil barrier (Case 2) resulted in small pressure changes in the embankment, with exception of piezometer PE-4, which is located near the anchor trench.

In relation to the study concerning the geomembrane length relative to the total height of the dam (Case 3), small changes in pressure head were detected for the embankment piezometers (Fig. 10), except for piezometer PE-4. For this reason, for the studied case, it is possible to conclude that the length of the treatment does not heavily influence the upstream embankment stability, as long as the pressure heads remain below projected levels.

According to the results of Case 4 (Fig. 10), the pressure heads within the embankment have reduced when the geomembrane height along the slope increased. In relation to Case 1b, pressure heads of piezometer PE-1 have reduced 3%, 15%, 38% and 100%, for Cases 4a, 4b, 4c and 4d, respectively. Again, when comparing to Case 1b, pressure heads of piezometer PE-2 have reduced 13%, 25%,

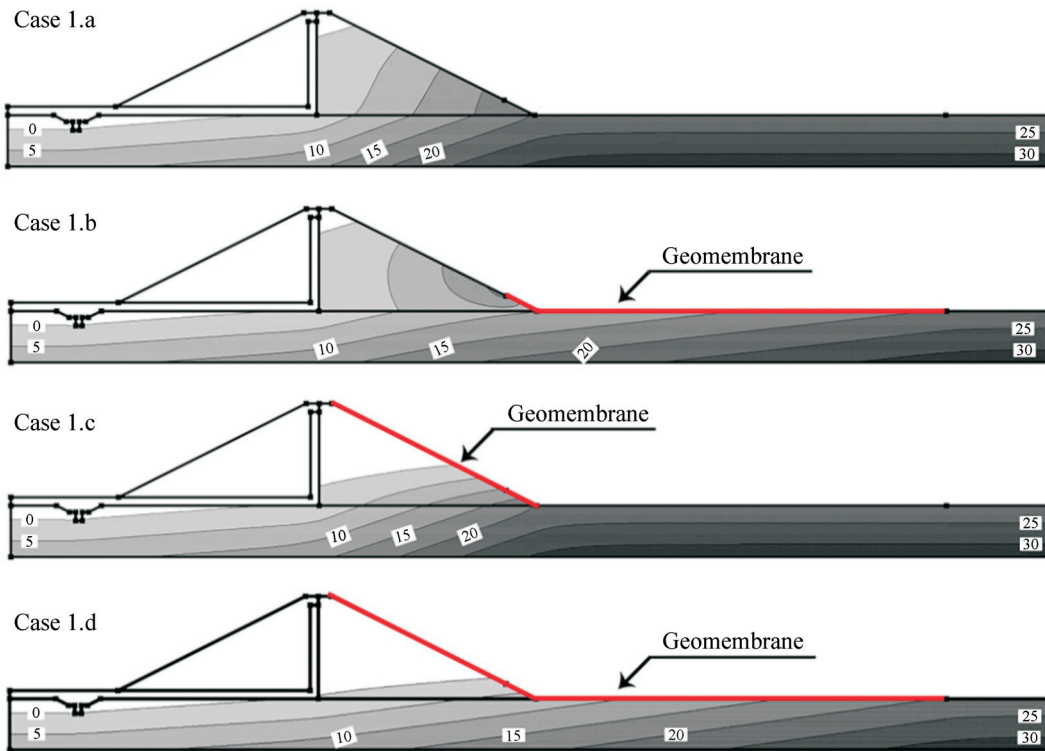


Figure 9 - Pressure head for Case 1 (in meters of water column).

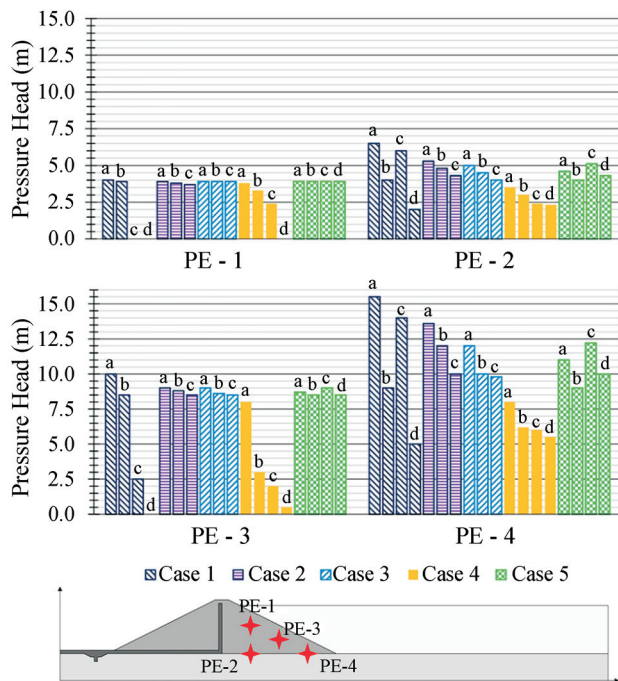


Figure 10 - Pressure heads for embankment piezometers.

40% and 43%, for Cases 4a, 4b, 4c and 4d, respectively. Pressure heads of piezometer PE-3 have reduced 6%, 65%, 76% and 94%, for Cases 4a, 4b, 4c and 4d, respectively, compared to the case with geomembrane with 15% embankment height. The same kind of analyses was made for

the pressure heads of piezometer PE-4 and showed a reduction of 11%, 31%, 33% and 39%, for Cases 4a, 4b, 4c and 4d, respectively. However, considering the embankment soil has satisfactory permeability, the use of geomembrane along the embankment should just be long enough to construct the anchor trench, such as in Case 1b. Greater lengths may be adopted when the embankment stability may get reduced by the higher pressure heads.

According to Case 5 (Fig. 10), small oscillations of pressure head were detected for embankment piezometers PE-1, PE-2 and PE-3, with the presence of longitudinal defects in the geomembrane. Contrasting with Case 1b, PE-4 presented an increase of pressure head equal to 22% and 36% for Cases 5a and 5c. However, these values were just 0% and 11% for Cases 5b and 5d, respectively, which considered the existence of an 80 cm thick compacted soil as a secondary barrier. In this case, the compacted soil had an important role as a secondary barrier.

Figure 11 presents the pressure heads for foundation piezometers located below the embankment dam and analyses are presented as follows.

For Case 1, piezometers located below the upstream embankment of the dam are highly influenced by the geomembrane treatment (Fig. 11). Considering piezometer PF-9, the pressure heads have reduced in relation to Case 1a (without geomembrane) 26%, 4% and 41%, for Cases 1b, 1c and 1d, respectively. For piezometer PF-10, on the other hand, the pressure heads have reduced compared to Case 1a 29%, 4% and 44%, for Cases 1b, 1c and 1d, respectively.

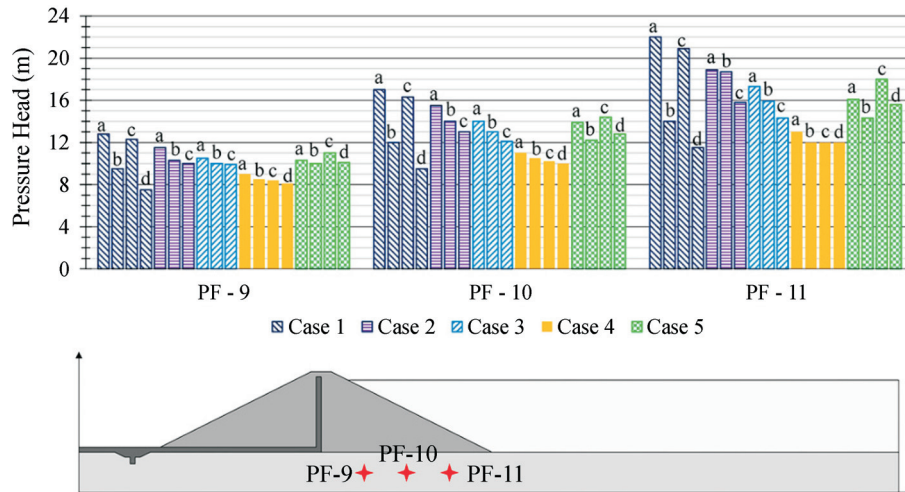


Figure 11 - Pressure heads for foundation piezometers located below the upstream embankment of the dam.

Piezometer PF-11 presented reduction of pressure heads, in relation to Case 1a, equal to 36%, 5% and 48%, for Cases 1b, 1c and 1d, respectively. For this reason, Cases 1b and 1d have better cost-benefit when the geomembrane purpose is to reduce pressure head in the foundation.

Considering the use of a compacted soil layer (Case 2), variations in pressure heads were detected for piezometers located below the upstream embankment of the dam (Fig. 11), however the effect of the geomembrane in pressure head reduction is lower than with the use of geomembrane (Case 1b).

The pressure head for foundation piezometers located below the upstream embankment of the dam (Fig. 11) presented small changes for piezometer PF-9 and more considerable changes for PF-10 and PF-11, which are located nearest to the treated area. In relation to Case 3a, which corresponds to a geomembrane length equal to the total height of the dam, the maximum reduction of pressure head (Case 3c) was 6%, 14% and 17% for piezometers PF-9, PF-10 and PF-11, respectively.

According to the results of Case 4, the pressure head within the foundation soil upstream of the dam had small variations in relation to the geomembrane length installed over the upstream slope of the dam.

For Case 5, an increase of pressure head was observed for foundation piezometers located below the upstream embankment of the dam (Fig. 11), when comparing to Case 1b. The increase of pressure head is a consequence of the flow rate increment on foundation soil below the dam. However, Cases 5b and 5d presented lower increase of pressure head, once an 80 cm thick compacted soil was considered as secondary barrier, with the same hydraulic conductivity of the dam.

Figure 12 presents the pressure head for foundation piezometers located upstream of the dam, and analyses are presented as follows.

Considering Case 1, pressure heads from piezometers PF-12 to PF-18 (Fig. 12) have reduced with the installation

of geomembrane along the foundation (Cases 1b and 1d). The reduction of pressure head was equal to 39%, 33%, 27%, 20%, 15%, 9% and 4% for piezometers PF-12, PF-13, PF-14, PF-15, PF-16, PF-17 and PF-18, respectively, for Case 1b in relation to Case 1a. On the other hand, the reduction of pressure head was equal to 49%, 39%, 33%, 26%, 19%, 10% and 4% for piezometers PF-12, PF-13, PF-14, PF-15, PF-16, PF-17 and PF-18, respectively, when analyzing the difference between Case 1d and Case 1a. For this reason, it may be concluded that the geomembrane effect is greater for the foundation area near the dam and lower for the area located more distantly. Small variations were detected in the foundation soil for Case 1c.

Regarding the use of compacted soil barrier (Case 2), the reduction of pressure in the foundation is lower in magnitude than that observed for geomembrane application, indicating that the use of a single compacted soil barrier is less effective than the use of geomembrane for the evaluated case, even with high values of thickness (6 m). It must be considered that the studied soil liner has the same permeability of the embankment dam (2×10^{-4} cm/s) and better results might be achieved with the use of soils with lower permeability. However, even when geomembranes are applied, a protective layer is normally recommended for geomembrane protection. In the specific case of this research, a compacted soil barrier was used with the purpose of acting as a watertight defense if the geomembrane is subjected to damage, also cooperating in the geomembrane protection. It is important to highlight that thick layers of polypropylene geotextile might be used with the purpose of protecting the geomembrane rather than compacted soil layers, since the installation of the synthetic layers may lead to lower risks of damaging the geomembrane. Besides, some researchers (e.g. Touze-Foltz, 2009) have shown that when the compacted soil over the geomembrane becomes saturated and is subjected to an applied load, the flow rate through the geomembrane defects may increase.

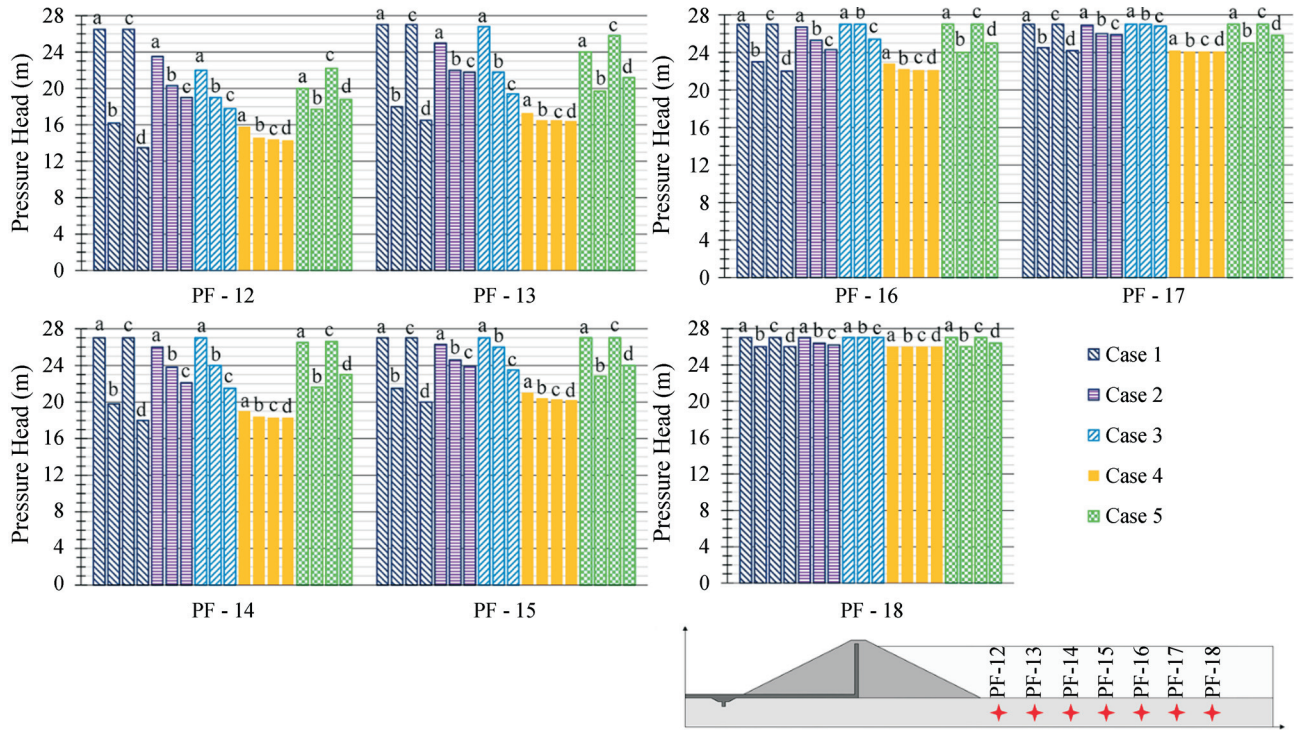


Figure 12 - Pressure heads for foundation piezometers located upstream of the dam.

Additionally, for Case 2, piezometers PF-12 and PF-13 exhibited considerable reduction of total head with the use of a compacted soil barrier. Contrasting with Case 1a, piezometer PF-12 had decrease of total head equal to 11%, 23% and 28% for Cases 2a, 2b and 2c, respectively. Also, when contrasting with Case 1a, piezometer PF-13 had decrease of total head equal to 7%, 19% and 19% for Cases 2a, 2b and 2c, respectively. However, the increase in thickness from 0.8 m to 3 m or 6 m may not be economically viable when considering the amount of material necessary and the other possibilities of foundation treatment, such as geomembrane.

For Case 3, pressure head reduction was detected in the foundation soil treated with geomembrane, upstream of the dam (Fig. 12). The magnitude of the reduction is directly proportional to the treated foundation extension. For this reason, more significant pressure head reduction was recorded for Case 3c, which corresponds to a geomembrane length of 3 times the total height of the dam.

In practical terms, the increase of the treated extension (Case 3) results in higher costs and the engineers should select a suitable treatment depending on the budget of the project. As an example, Salto Hydroelectric Dam has treated foundation extension variable according to the evaluated cross-section.

According to the results of Case 4, the pressure head below the upstream embankment of the dam had small variations in relation to the geomembrane length installed over the upstream slope of the dam. This was expected once this

analysis considered the length of geomembrane over the upstream slope of the dam.

The occurrence of defects in the geomembrane (Case 5) increased the pressure head in the foundation soil upstream of the dam (Fig. 12), especially for piezometers located near the damage. For example, for piezometer PF-12 located near the dam, the pressure head from this piezometer (Case 1b), contrasted with Cases 5a and 5c, resulted in an increase of 23% and 37%, respectively. For piezometer PF-18, on the other hand, these values were just 4% for both situations.

Only a small increase of this pressure was recorded when an 80 cm thick compacted soil layer was placed above the geomembrane with defects (Fig. 12). As an example, the pressure head from PF-12 (Case 1b), contrasted with Cases 5b and 5d, resulted in an increase of 9% and 16%, respectively. Therefore, based on the results, the use of geomembrane associated to a compacted clay layer above it is an interesting solution to reduce the risk of the loss of efficiency of the system.

4.2.2. Seepage flow rate

For the hypothetical case when geomembrane was not used (Case 1a), the obtained flow rates were 255.1 L/(h.m) and 1371.1 L/(h.m) through the embankment and the foundation, respectively. Figure 13 presents the flow values from all the simulations and the reductions in total flow compared to Case 1a.

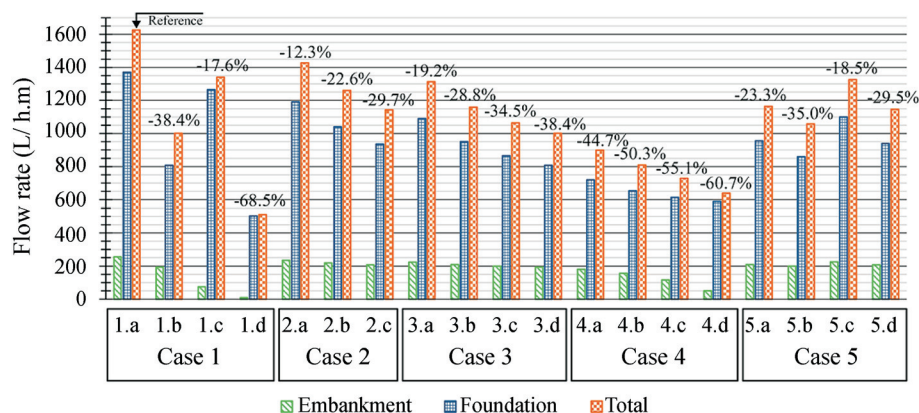


Figure 13 - Flow rate reduction in relation to all the studies.

Flow reduction in the embankment was detected even when geomembrane was applied over the upstream slope of the dam with just the necessary length for anchoring it, making them work together. Since the permeability of the foundation is 50 times higher than the permeability of the embankment, most of the percolation occurred through the soil foundation, justifying the use of geomembrane only on permeable foundation soil (Case 1) for the studied case.

Predicted values considering only the use of compacted soil as a barrier (Case 2) showed that the flow rates were greater than the ones with the use of geomembrane. For 0.8 m thick soil layer, the total flow rate has increased 43%, whereas for 3 and 6 m thick layers, the increase was equal to 26% and 14%, respectively, when compared to Case 1b. Therefore, even considering that the compacted soil layer has no cracks, its efficiency is lower when compared to the use of geomembrane without defects for the studied case. For this reason, the construction of thick layers of compacted soil might not be economically feasible when compared to solutions with geomembranes and each case must be evaluated by the engineers.

Based on the simulations that considered the variation of the geomembrane length (Case 3), it was found that the seepage flow through the foundation depends on the length of the water percolation path. Although there is a reduction in flow through the embankment, its magnitude is small when compared to the flow through the foundation.

According to the obtained results from numerical analyses that considered the length of geomembrane over the upstream slope of the dam (Case 4), when the length increases the flow rate through the embankment decreases. However, the decrease in total flow is small, because most of the flow occurred through the foundation and the geomembrane is covering most of it. For this reason, it is sufficient to adopt just the necessary length for anchoring the geomembrane on the slope.

The obtained seepage flow rates considering the existence of one longitudinal tear showed that if there is not a compacted soil layer over the geomembrane (Case 5a), the total flow increases approximately 25% when compared

with the geomembrane without defect (Case 1b). However, if an 80 cm thick protective soil layer is placed over the geomembrane (Case 5b), the flow rate increases only 6% in comparison with the case of geomembrane without defect (Case 1b). Predicted values of total flow, when three defects were considered in the geomembrane, indicated that the flow rate increase was approximately 32% (Case 5c) higher than that obtained for the geomembrane without defect (Case 1b), however this value was only 14% considering the presence of a protection layer (Case 5d). Thus, the presence of a layer of lower permeability than the foundation above the geomembrane is of great relevance for the proper performance of the system.

4.2.3. Hydraulic gradient

According to the results presented for Case 1, the hydraulic gradients in most of the embankment were between 0.8 and 1 for the analyses without the presence of geomembrane. Considering the use of geomembrane on foundation soil, the hydraulic gradient in the embankment, specifically near the anchor trench area, reached values above 1.5, as shown in Fig. 14 (A). For this reason, the anchorage area must be carefully constructed to avoid unexpected percolation between the geomembrane and the compacted soil.

In Case 2, the hydraulic gradients were found between 0.5 and 1 for most of the embankment for the case when an 80 cm thick compacted soil liner was employed. In the simulations considering soil liner 3 and 6 m thick, gradients in the embankment were between 0.8 and 1.2. High hydraulic gradients were observed near the connection with the embankment dam, with values ranging between 1.4 and 1.8, as shown in Fig. 14 (B), which suggests that the anchorage region between the embankment dam and the compacted soil liner must have high execution process control.

The hydraulic gradients observed in Case 3 ranged between 0.8 and 1.0 in most of the embankment, when a geomembrane with length $L = H = 24$ m was used. For higher lengths, the hydraulic gradients were greater, with values between 1 and 1.5 in the embankment, with greater values near the anchor trench area. In all the studied cases,

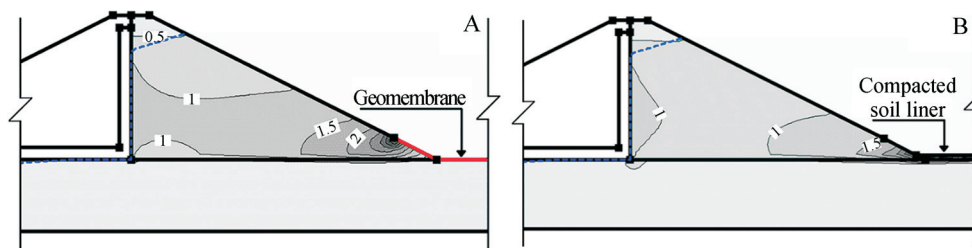


Figure 14 - Hydraulic gradients in the embankment dam: (A) Case 1b, and (B) Case 2a.

hydraulic gradients lower than 0.5 were observed in the foundation.

Regarding Case 4, it was observed that the installation of the geomembrane over the upstream slope of the dam reduced the hydraulic gradient in the embankment. However, the flow through the embankment corresponds to a small portion of the total flow collected by the drainage system. High hydraulic gradients in anchor trench areas, with values greater than 1.5, were observed in all analyses, with small differences due to different lengths.

The presence of defects in the geomembrane (evaluated in Case 5) led to the increase of hydraulic gradient in the soil foundation when compared to the case of the geomembrane with no defects. However, the values were below 0.5. Particularly in the damaged areas, high hydraulic gradients were found, which can contribute to the formation of percolation paths below the geomembrane. This is confirmed by the high values of pressure head of some piezometers below the defects, shown in the last section (Fig. 6).

5. Conclusions

This paper presented an experimental and numerical study of the performance of HDPE geomembrane as an impermeable blanket installed upstream of embankment dams. Data from the Brazilian Salto Hydroelectric Power Plant contributed to the development of a small-scale seepage model and the numerical modelling. After the laboratory tests, some parameters were calibrated and some numerical analyses of those tests have been performed. Additionally, some hypothetical conditions varying the presence of defects in the geomembrane, the impermeable blanket thickness and the length of the geomembrane were carried out.

For the small scale model, the obtained results indicated that the geomembrane impermeable blanket increased the percolation path through the dam soil foundation, reducing the pressure head in both embankment and foundation, as well as the flow collected by the drainage system. The higher reduction in pressure head occurred in the dam foundation, below the geomembrane and in the dam embankment upstream of the vertical filter. At the downstream side of the dam, on the other hand, a small variation of pressure head was observed. It indicates that the flow in the downstream side is controlled by the chim-

ney drain. The tests also have shown that if the applied geomembrane has damage, the total flow collected by the drainage system and the pressure heads are similar to those observed in the test with no geomembrane.

Based on the results of the scaled and the numerical model, it can be inferred that the anisotropy coefficient from the embankment influences the percolation flow rates for the case studied. The anisotropy coefficient that leads to results closest to the values obtained in small-scale modelling is equal to 1. However, it must be considered that compacted soils in actual dams present anisotropy relative to permeability. For this reason and in accordance with Salto Dam results, the anisotropy coefficient adopted for the embankment in the numerical model was $k_h/k_v = 5$.

Regarding the use of impermeable blanket of compacted soil as a single barrier with a horizontal permeability of 1×10^{-3} cm/s and vertical permeability of 2×10^{-4} cm/s (same material of dam), even considering it without cracks, the seepage reduction was not as significant as that found when geomembranes were used. Even for a 6 m thick layer, the performance of compacted soil was worse than that obtained by using geomembrane. The flow rates were greater than those calculated by software simulation with the use of geomembrane. Thus, even considering that the compacted soil layer has no cracks, its efficiency in some cases is lower when compared to the use of geomembrane without damage for the case studied.

For the analyses that considered the length of the geomembrane, pressure head reduction was detected in the foundation soil treated, upstream of the dam. Thus, the magnitude of the reduction is dependent on the treated foundation extension. It was also found that the seepage flow through the foundation depends on the length of the water percolation path.

The analyses considering the length of the geomembrane over the upstream slope of the dam have shown that the pressure head in the foundation soil had small variation in relation to the geomembrane length installed over the upstream slope of the dam, once most of the flow occurred through the foundation. However, the pressure head within the embankment have reduced when the geomembrane length along the upstream slope increased. Considering that most of the total flow occurred through the foundation, increasing the length of the geomembrane over the upstream slope of the dam is not effective for reducing the magnitude

of this parameter. For this reason, it was sufficient to adopt just the necessary length for anchoring the geomembrane on the slope.

For the analyses with the occurrence of defects in the geomembrane, a compacted soil layer over the geomembrane resulted in good performance for the foundation treatment. In the simulation that considered longitudinal tears in the geomembrane without the compacted soil layer, the flow increased approximately 25%, when compared to the simulation with undamaged geomembrane. However, considering a soil with lower permeability than the foundation protection layer in addition to the geomembrane liner, the flow reduction was only 6%.

Relating to the hydraulic gradients, the use of the geomembrane on foundation soil resulted in gradient values higher than 1.5. For this reason, it is recommended to carefully construct the anchor trench to avoid unexpected percolation between the geomembrane and the compacted soil. Major care must also be taken in case of defects in the geomembrane.

Based on all the results of this analysis, the use of geomembrane for treating permeable foundations can provide a good solution to reduce flow and pressure loads on dams.

Acknowledgments

The authors thank Rio Verde Energia S.A., Triunfo Participações e Investimentos S.A. and Intertechne Consultores S.A. for providing design and instrumentation data of the Salto Hydroelectric Dam. Authors would like to thank the Ministry of Education (CAPES) and the National Council for Scientific and Technological Development (CNPq).

References

- ASTM (2015). Standard Terminology for Geosynthetics - D 4439-15. ASTM International, West Conshohocken, Pennsylvania, USA, 6 p.
- Brandon, T.L.; Clough, G.W. & Rahardjo, P.P. (1991). Fabrication of silty sand specimens for large- and small-scale tests. *Geotechnical Testing Journal*, 14(1):46-55.
- Bhowmik, R.; Shahu, J.T. & Datta, M. (2018). Failure analysis of a geomembrane lined reservoir embankment. *Geotextiles and Geomembranes*, 46(1):52-65.
- Cardoso, R.M.; Calcina, A.M.; Oliveira, C.A.; Carvalho, A.H.E. & Sarlo, R.J.F. (2010). Use of HDPE geomembrane in foundation soil treatment on São Salvador Hydroelectric Power Plant. (In Portuguese). Proc. Brazilian Conference of Soil Mechanics and Geotechnical Engineering, Gramado, Brazil.
- Cruz, P.T. (2004). 100 Brazilian Dams: historical cases, construction materials, project. (In Portuguese). *Oficina de Textos, Brazil*, 2nd ed., 648 p.
- Dong, H.; Chen, J. & Li, X. (2016). Delineation of leakage pathways in an earth and rockfill dam using multi-tracer tests. *Engineering Geology*, 212(1):136-145.
- FHWA (1998). *Geosynthetic Design and Construction Guidelines, Participant Notebook*. Federal Highway Administration, U.S. Department of Transportation, National Highway Institute, Washington, DC, 460 p.
- GEO-SLOPE International Ltd. (2012). *Seepage Modeling with SEEP/W - An Engineering Methodology*. Calgary, Alberta, 199 p.
- Giroud, J.P. & Bonaparte, R. (1989). Leakage through liners constructed with geomembranes - Part I. *Geomembrane liners. Geotextiles and Geomembranes*, 8(1):27-67.
- Giroud, J.P. & Touze-Foltz, N. (2003). Empirical equations for calculating the rate of liquid flow through composite liners due to geomembrane defects. *Geosynthetics International*, 10(6):215-233.
- Koerner, R.M. (2012). *Designing with geosynthetics*. Xlibris Corporation, USA, 6th ed., v. 1, 914 p.
- Lo Presti, D.C.F.; Pedroni, S. & Crippa, V. (1992). Maximum dry density of cohesionless soils by pluviation and by ASTM D 4253-83: A comparative study. *Geotechnical Testing Journal*, 15(2):180-189.
- Mahinroosta, R.; Alizadeh, A. & Gatzmiri, B. (2015). Simulation of collapse settlement of first filling in a high rockfill dam. *Engineering Geology*, 187(1):32-44.
- Messerklinger, S. (2014). Failure of a geomembrane lined embankment dam - Case study. *Geotextiles and Geomembranes*, 42(3):256-266.
- Needham, A.D.; Smith, J.W.N. & Gallagher, E.M.G. (2006). The service life of polyethylene geomembrane barriers. *Engineering Geology*, 85(1-2):82-90.
- Nicholson, P.G. (2015). *Soil Improvement and Ground Modification Methods*. Butterworth Heinemann, Oxford, 455 p.
- Nosko, V.; Andreazal, T.; Gregor, T. & Ganier, P.G. (1996). SENSOR Damage Detection System (DDS) – The unique geomembrane testing method. *Geosynthetics: applications, design and construction*. Proc. First European Geosynthetics Conference Eurogeo 1, Maastricht, pp. 743-748.
- Petaccia, G.; Lai, C.G.; Milazzo, C. & Natale, L. (2016). The collapse of the Sella Zerbino gravity dam. *Engineering Geology*, 211(1):39-49.
- Pierozan, R.C. (2014). The use of geomembrane as impermeable blankets upstream embankment dams. (In Portuguese). Master's thesis, Department of Civil Construction, Federal University of Paraná, Curitiba, 182 p.
- Poulain, D.; Peyras, L. & Meriaux, P. (2011). Feedback and guidelines for geomembrane lining systems of mountain reservoirs in France. *Geotextiles and Geomembranes*, 29(4):415-424.
- Rad, N.S. & Tumay, M.T. (1987). Factor affecting sand specimen preparation by raining. *Geotechnical Testing Journal*, 10(1):31-37.

- Rollin, A.L.; Marcotte, M.; Jacquelin, T. & Chaput, L. (1999). Leak location in exposed geomembrane liners using an electrical leak detection technique. Proc. Geosynthetics'99, Boston, United States of America, pp. 615-626.
- Rollin, A.L.; Marcotte, M.; Chaput, L. & Caquel, F. (2002). Lessons learned from geo-electrical leaks surveys. Proc. Geosynthetics 2002, Nice, France, pp. 527-530.
- Rollin, A.L.; Jacquelin, T.; Forget, B. & Saunier, P. (2004). A guide to detect leaks on installed geomembranes. Proc. EuroGEO, Munich, Germany, pp. 235-240.
- Scuero, A.M. & Vaschetti, G.L. (2004). Watertightness and Safety of Dams Using Geomembranes. Long-Term Benefits and Performance of Dams. Thomas Telford, London, 15 p.
- Shukla, S.K. (2002). Geosynthetic Applications – General Aspects and Selected Case Studies. Handbook of Geosynthetic Engineering. Department of Civil Engineering, Harcourt Butler Technological Institute, Kanpur, 422 p.
- Tao, T.; Yan, J.; Tao, X.; Fu, F.F. & Zhou, H. (1996). Application of geotextile/geomembrane composite liner for infiltration prevention in Xiaolingtuo rock-fill dam. Geosynthetics International, 3(1):125-136.
- Touze-Foltz, N. (2009). Evaluation of flow in lining systems of Brazilian landfills. Version 4. Unité HBAN, Cedex, France, 18 p.
- Whitfield, B.L. (1996). Geomembrane application for an RCC dam. Geotextiles and Geomembranes, 14(5-6):253-264.
- Wu, W.; Wang, X.T. & Aschauer, F.F. (2008). Investigation on failure of a geosynthetic lined reservoir. Geotextiles and Geomembranes, 26(4):363-370.

Predicting the Shear Strength of Unfilled Rock Joints with the First-Order Takagi-Sugeno Fuzzy Approach

Y.M.P. Matos, S.A. Dantas Neto, G.A. Barreto

Abstract. As a result of a number of studies, some analytical models have been developed to predict the shear behavior of unfilled rock joints, but they all present a purely deterministic nature because their input variables are defined without considering the uncertainties inherent in the formation processes of the rock masses and related discontinuities. This work aims to present a model for predict the shear strength of unfilled rock joints by incorporating uncertainties in the variables that govern its shear behavior with a First-Order Takagi-Sugeno fuzzy controller. The model is developed based on the results of 44 direct shear tests carried out on different types of joints. The model input variables are the normal boundary stiffness and initial normal stress acting on the joint, its roughness (expressed by the JRC value), the uniaxial compressive strength, the basic friction angle of the intact rock and the shear displacement imposed to the joint. The results show that the predicted shear strength of unfilled rock joints obtained by the fuzzy model fits satisfactorily the experimental data and allows the shear behavior of the discontinuities to be defined. A practical application of the model in a stability analysis of a rock mass is also presented.

Keywords: Fuzzy, shear strength, Takagi-Sugeno, unfilled rock joints.

1. Introduction

One of the main difficulties with analyzing and designing geotechnical structures in rock is predicting the behavior of the rock masses correctly because it depends on the shear strength of the existing discontinuities. The shear behavior of unfilled discontinuities depends on their boundary conditions, *i.e.*, constant normal loading (CNL) or constant normal stiffness (CNS) conditions, their roughness, and on the properties of the intact rock (Patton, 1966; Barton, 1973; Benmokrane & Ballivy, 1989; Skinas *et al.*, 1990; Papaliangas *et al.*, 1993; Indraratna *et al.*, 1998, 1999, 2005, 2008, 2010a, 2010b, 2015; Indraratna & Haque, 2000, among others).

Several analytical models have been used to predict the shear strength of unfilled discontinuities (Patton, 1966; Barton, 1973; Barton & Choubey, 1977; among others). However, these models can only predict the peak shear strength of discontinuities that has been developed from shear tests conducted under CNL conditions, which many times do not represent the behavior of the discontinuity due the confinement imposed by the surrounding rock mass leading it to a CNS condition. Barton & Bandis (1990) presented the JRC-JCS method which allows the definition of the complete shear stress-displacement behavior of unfilled rock joints by considering the concept of the mobilized JRC (roughness), providing a more realistic prediction for the

nonlinear shear behavior of rock joints. Barton (2013, 2016) and Prassetyo *et al.* (2017) warn for the need to consider the nonlinearity for the shear behavior of rock joints. According to these authors, the dilation which occurs during the shearing process leads to a degradation of the joint asperities represented by the variation of JRC mobilized resulting in a nonlinearity in the shear behavior of the unfilled rock discontinuities.

Results of a number of direct shear strength tests indicate that normal boundary stiffness affects the shear behavior of unfilled rock joints as it increases their shear strength and reduces dilation in the shearing process (Skinas *et al.*, 1990; Papaliangas *et al.*, 1993; Indraratna *et al.*, 1998, 1999, 2005, 2008, 2010a, 2010b, 2015). Indraratna & Haque (2000) presented an analytical model where the shear strength of unfilled rock joints is estimated as a function of the boundary conditions (CNL or CNS) of the discontinuity; it is expressed by the initial normal stress and normal boundary stiffness of the joint such as its roughness which is expressed by the asperity inclination angle and the basic friction angle. The model of Indraratna & Haque (2000) is one of the most advanced models used to predict the shear strength of unfilled rock joints because unlike some traditional models, the shear stress and shear displacement in CNL and CNS conditions can be predicted. However, this model is somewhat laborious to use because the variation of rock joint dilation with shear displacement must be

Yago Machado Pereira de Matos, M.Sc., Departamento de Engenharia Hidráulica e Ambiental, Universidade Federal do Ceará, Fortaleza, CE, Brazil, e-mail: yago_mpm@hotmail.com.

Silvrano Adonias Dantas Neto, Ph.D., Assistant Professor, Departamento de Engenharia Hidráulica e Ambiental, Universidade Federal do Ceará, Fortaleza, CE, Brazil, e-mail: silvrano@ufc.br.

Guilherme de Alencar Barreto, Ph.D., Assistant Professor, Departamento de Engenharia de Teleinformática, Universidade Federal do Ceará, Fortaleza, CE, Brazil, e-mail: guialenbar@gmail.com.

Submitted on February 22, 2018; Final Acceptance on February 21, 2019; Discussion open until August 30, 2019.

DOI: 10.28927/SR.421021

known, and since they are obtained through large-scale direct shear, they are not always available under the same boundary conditions acting on the discontinuity.

Dantas Neto *et al.* (2017) proposed a model to predict the shear behavior of unfilled rock joints developed using artificial neural networks. Since the model proposed by Indraratna & Haque (2000), this neural model enables the shear behavior of discontinuities to be completely defined without the need for any special laboratory test. The results obtained using this model fit the experimental data of a wide variety of rock types better than the model by Indraratna & Haque (2000).

Despite these mentioned models being able to predict the shear behavior of unfilled rock joints quite well, they still do not consider any existing uncertainties in the input parameters along a certain discontinuity because there is no consideration on how the rock mass and discontinuities were formed. In this scenario of uncertainties, the Fuzzy Sets Theory (Zadeh, 1965) is a useful tool to model complex real systems with input parameters involving uncertainty, such as those observed in geotechnical works designed and built in rock masses.

The use of Fuzzy Sets Theory in a logical context to solve practical problems is known as Fuzzy Logic; Fuzzy Logic enables phenomena to be modelled by mathematical equations and also allows heuristics to be adopted to explain real problems. The heuristic method determines the solution of a given problem according to previous specialist experience or frequently used inference rules. These rules can be applied by expert systems that according to Grima (2000), aim to provide solutions for complex engineering problems without resorting to mathematical models. These expert systems are known as fuzzy controllers that use past experiences, and theoretical knowledge of the investigated phenomenon to determine the fuzzy inference rules which will provide solutions to the problem.

Several studies related to the application of fuzzy controllers in Rock Mechanics have been developed, such as Grima & Babuska (1999), Gokceoglu (2002), Kayabasi *et al.* (2003), Nefeslioglu *et al.* (2003), Sonmez *et al.* (2003), Gokceoglu & Zorlu (2004), Sonmez *et al.* (2004), Daftariresheli *et al.* (2011), Monjezi & Rezaei (2011), Akgun *et al.* (2012), Asadi (2016), and Sari (2016). However, since none of them can study the behavior of unfilled rock discontinuities during shearing, they provided the motivation for developing this present work.

This paper will therefore present the results of predicting the shear strength in unfilled rock joints as a function of the main variables that influence this phenomenon such as normal boundary stiffness, the initial normal stress acting on the discontinuity, joint roughness represented by the joint roughness coefficient (JRC), the intact rock properties such as the compressive strength and basic friction angle, as well as the shear displacement imposed onto the discontinuity. Thus, the results of 44 direct shear tests from

different joints and boundary conditions were used. This model was developed using a First-Order Takagi-Sugeno fuzzy controller. The results from predicting the shear strength of unfilled rock joints by the actual fuzzy model fit the experimental results used in the model development quite well, while also considering how the model responded to variability or uncertainty of the input variable of the studied phenomenon. A practical application of the model in a slope stability analysis of a rock mass is also presented.

2. Literature Review

2.1 Fuzzy logic

The Fuzzy Sets Theory conceived by Zadeh (1965) is a more general case of the classical Theory of Sets since it allows to consider the vague aspect of information, while admitting that a certain variable can assume a set of possible values rather than a single and unique one. Fuzzy Logic therefore uses Fuzzy Sets Theory in a logical context to solve practical problems.

Unlike classical (bivalent) logic, with Fuzzy Logic the existing sets do not have precise boundaries so the degree of membership (μ) of an element measures the possibility that that element belongs to a given set (see Fig. 1), *i.e.*, this degree of membership of a variable can vary between zero and one, depending on how much that one belongs to the analyzed set data. That is a fundamental difference between fuzzy and crisp sets, once in crisp sets the values of some element are unique and they do not consider the uncertainties possibly involved on that variable definition.

Fuzzy Logic is very useful when the number of data available is not enough to characterize the uncertainty involved in the studied phenomenon using the Theory of Probability. By making an analogy of it, Ganoulis (1994) states that fuzzy numbers are equivalent to random variables and that membership functions correspond to proba-

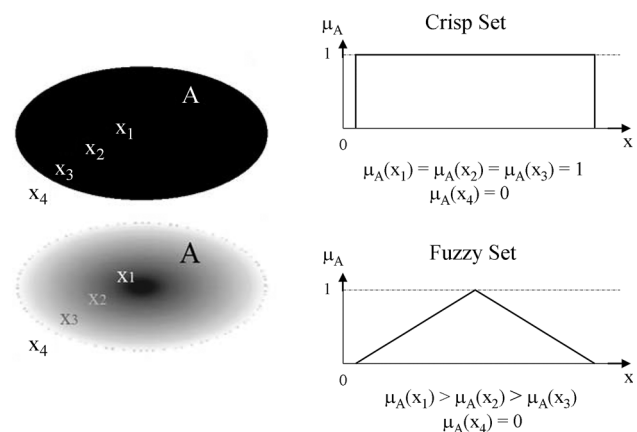


Figure 1 - Difference between classic and fuzzy logic (Jalalifar *et al.*, 2011).

bility density functions. However, the basic arithmetical rules of fuzzy sets are quite different from the Theory of Probability.

The membership function establishes the relationship between the values of a variable and their respective degrees of membership with regard to a given set, and since there are several types of membership functions, the most common are triangular, trapezoidal, Gaussian, and sigmoidal. The definition of membership functions of any variable is based on the knowledge of a specialist or on the analysis of a known series of observed values of the regarded variable. The delimitation of these functions is fundamental to the use of fuzzy controllers.

2.2 Fuzzy controller

A fuzzy controller is a system that contains a set of “IF ... THEN” inference rules that define the controlling actions based on different ranges of values that the governing variables of the problem can assume. Systems constructed in this way are even more interesting when the response of the existing mathematical model is subject to their input variables uncertainties.

Unlike conventional controllers where control is described analytically through a deterministic mathematical model, fuzzy controllers use logical rules to control a process where the modelled phenomenon can involve the human experience and intuition. These systems use fuzzy sets to describe the input and output variables, so instead of an exact value for the variables, possible sets of values could be adopted. It is important to mention that the fuzzy controllers allow to express the human experience and intuition, and therefore the uncertainty of a certain value, by considering the fuzzy set as a linguistic variable to which values as “low”, “high”, “very high” can be assigned.

Figure 2 presents a fuzzy controller which relates the uniaxial compressive strength of intact rock (σ_c) and the JRC with the shear strength (τ_h) of an unfilled rock joint. This example illustrates that the shear strength is not defined by unique values for the uniaxial compressive strength and JRC values but considering the uncertainties expressed by the range of values of each fuzzy linguistic membership function. The Boolean operator is called the antecedent part of the inference rule and its function is to combine the influence of the input variables on the fuzzy output, which is the consequent one.

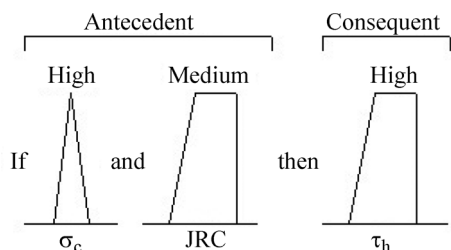


Figure 2 - Example of an inference rule using fuzzy numbers.

Simões & Shaw (2007) state that the basic structure of a fuzzy controller represents the transformation that occurs from the real domain to the fuzzy domain, known as the fuzzification step, where a set of fuzzy inference rules is used for decision-making that will provide the fuzzy outputs. At the end of the process, these outputs, which are currently fuzzy numbers, must be transformed into real numbers by a defuzzification process.

2.3 Takagi-Sugeno fuzzy model

Different fuzzy controllers may differ with regard to how the operators use them in their implementation and how they represent the fuzzy outputs of each specific rule. One of the most common types of fuzzy controllers is the interpolation model presented by Takagi & Sugeno (1983); it is known as the Takagi-Sugeno controller. The Takagi-Sugeno controller establishes that only the antecedent of the rules (premise part) is formed by fuzzy variables, and the output of each rule (consequent part) is defined as a function of these input variables. The operation of this controller is illustrated in Fig. 3.

The first step taken by a Takagi-Sugeno controller is the fuzzification process in which the membership functions for each input variable (x and y) are established, and the i rules of inference are defined based on the judgment of specialists. In the activation of each R_i rule of inference, a Boolean operator AND or OR is defined to establish how the input variables x and y are combined to define the response z of the model. When a connector AND is used, at each R_i rule the multiplication of degrees of membership of the input variables (μ_{xi} and μ_{yi}) is performed and a weight W_i is then obtained. Otherwise, when a connector “OR” is used, the highest value of the degree of membership of the input variables is adopted. Analyzing the rule R_1 presented in Fig. 3 and adopting real values for the two inputs x and y , it was observed that x belongs to the fuzzy set A_1 with degree of membership μ_{x1} , and y belongs to the fuzzy set B_1 with degrees of membership μ_{y1} . Therefore, using the connector AND to combine the variables x and y , the weight W_1 can be determined by multiplying μ_{x1} and μ_{y1} .

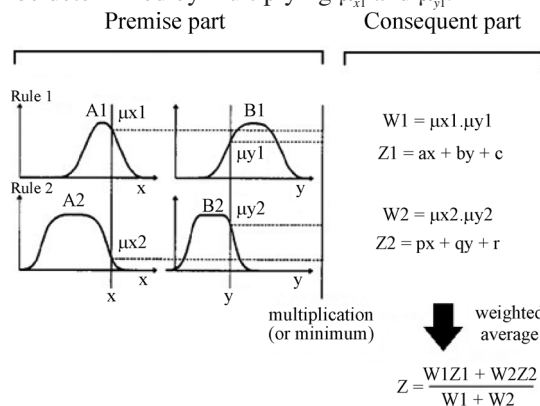


Figure 3 - Functioning of a Takagi-Sugeno fuzzy controller (Jang, 1993).

The implication step consists of defining a linear function that relates the consequents of rules z_i to the input variables x and y . This definition does not force the use of a specific implication function and may even be a constant value, but linear equations are normally adopted, as shown in Fig. 3, to present the functions for z_1 e z_2 . These linear equations are obtained by interpolating inside the dataset representing the experience on the modelled phenomenon the output variable as a function of the input variables in order to obtain the parameters a, b, c, p, q and r presented in Fig. 3.

Finally, the output z is the weighted average of the consequent of each rule, evaluated by the respective membership values that result from processing the antecedent of the rule (W_1 and W_2).

According to MathWorks (2006), Takagi-Sugeno controllers are computationally efficient and better suited for mathematically analyzing phenomena because adjustments to customize the membership functions and implication functions can be used to improve the fuzzy system.

Regarding the use of Takagi-Sugeno fuzzy controllers in Rock Mechanics, Grima & Babuska (1999) developed a fuzzy system to predict the uniaxial compressive strength of rock samples. The authors found that the Takagi-Sugeno fuzzy model could potentially model complex, non-linear and multivariable geological engineering systems. Grima & Babuska (1999) highlight the importance of intelligent computational systems that can be applied to Rock Mechanics because vague and imprecise information can be used about the materials and data whose physical meaning is not obvious.

3. Fuzzy Model Development

The proposed fuzzy model uses logical implications to describe the relationships between control variables and the physical phenomenon analyzed, *i.e.*, the shear strength in discontinuities of rock masses. This model was built based on a dataset of 44 direct shear tests presented by Benmokrane & Ballivy (1989), Skinas *et al.* (1990), Pappaliangas *et al.* (1993), Indraratna & Haque (2000), and Indraratna *et al.* (2010a), performed in different types of discontinuities (saw-tooth, tension-model, field-model and field-natural) and distinct boundary conditions.

The model was developed using 673 examples as the dataset, while considering as input variables the main factors governing the shear behavior of unfilled rock joints: the normal boundary stiffness (k_n), the initial normal stress (σ_{n0}) acting on the discontinuity, the JRC, the uniaxial compressive strength of the intact rock (σ_c), the basic friction angle (ϕ_b), and the shear displacement (δ_h) having as its response the shear strength of the discontinuity (τ_h).

The model was implemented using MATLAB and consists of a Takagi-Sugeno fuzzy controller (Takagi & Sugeno, 1983), where the linear (first-order) equations of the input variables are implied, and the shear strength is the

weighted average of the consequent of each rule that varies according to a combination of values assumed by the inputs as previously explained.

To develop this model, the membership function of each input variable had to be defined, *i.e.*, the type of function and its parameters. From the types of functions available, the authors used trapezoidal functions at the edges of the intervals of each variable and triangular functions to fill in the remaining values not comprised by the trapezoidal functions.

The parameters of the membership functions were defined by considering some values provided in the literature (when available), the results of direct shear tests, and the judgment of specialists. The membership functions of JRC, σ_c and ϕ_b were defined by considering the suggestions made by Barton & Choubey (1977), Bieniawski (1984) and Barton (1973), respectively. Due to the lack of data in literature regarding other variables, the parameters of the membership functions of k_n , σ_{n0} and δ_h are based on the results of direct shear tests only, and on the previous experience of specialists. The membership functions for each input variable presented in Figs. 4 to 9 cover the entire range of variables in the available dataset.

After defining all the membership functions for each variable, were also defined 57 fuzzy inference rules by analyzing how the input variables affected the shear strength values available in the experimental dataset used to develop the fuzzy model presented in this paper. An example of one of these rules is: if k_n is VERY HIGH and σ_{n0} is MEDIUM

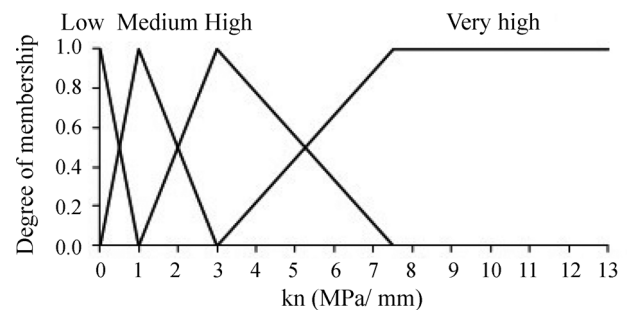


Figure 4 - Membership functions for the normal boundary stiffness (k_n) variable.

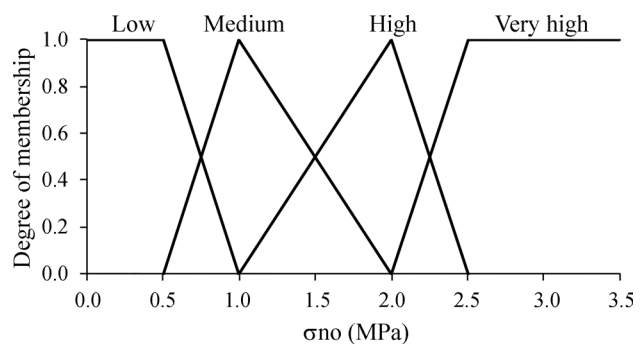


Figure 5 - Membership functions for the initial normal stress (σ_{n0}) variable.

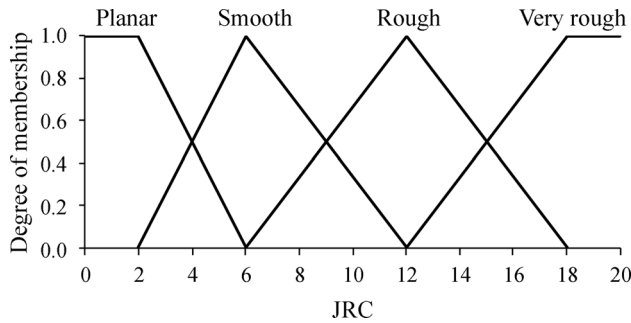


Figure 6 - Membership functions for the JRC variable.

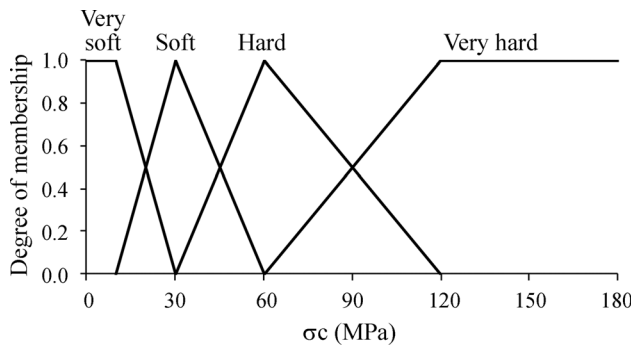


Figure 7 - Membership functions for the uniaxial compressive strength (σ_c) variable.

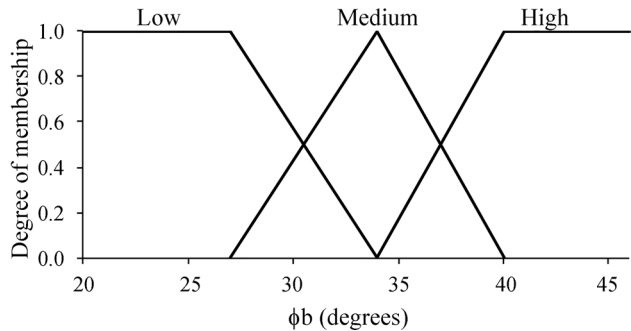


Figure 8 - Membership functions for the basic friction angle (ϕ_b) variable.

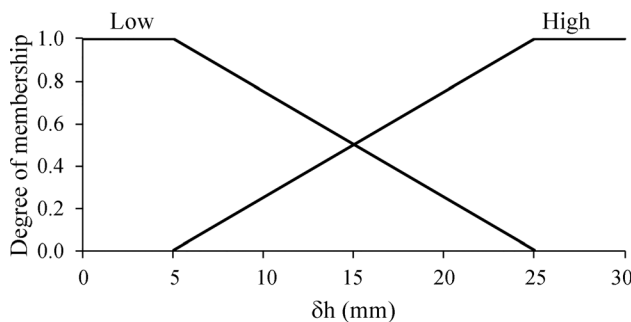


Figure 9 - Membership functions for the horizontal displacement (δ_h) variable.

and JRC is VERY ROUGH and σ_c is HARD and ϕ_b is MEDIUM and δ_h is LOW then τ_n is HIGH.

The coefficients of the implication functions were obtained by multiple linear regressions of the results of direct shear tests. The prediction of the shear strength of an unfilled rock joint by using the Takagi-Sugeno controller is a result of the defuzzification procedure of a membership function obtained by combining all the established inference rules.

4. Results and Discussion

Figures 10 to 12 present comparisons between the experimental data and values predicted by the Takagi-Sugeno model to evaluate whether the model can represent the influence of the governing parameters on the shear behavior of an unfilled rock joint with values for the uniaxial compressive strength and basic friction angle of 12 MPa and 37.5°, respectively.

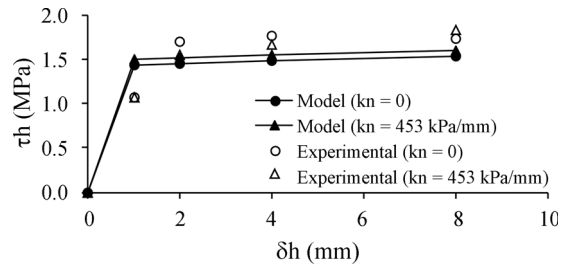


Figure 10 - Influence of normal boundary stiffness on the shear strength of unfilled rock joints.

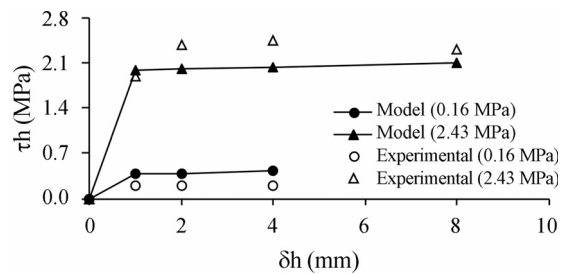


Figure 11 - Influence of the initial normal stress on the shear strength of unfilled rock joints.

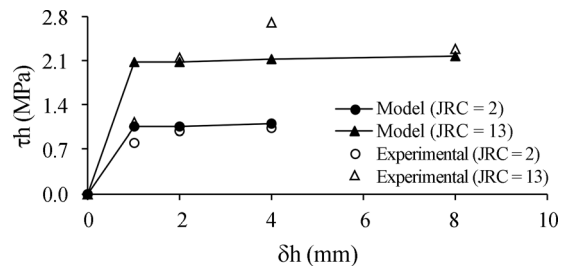


Figure 12 - Influence of the JRC values on the shear strength of unfilled rock joints.

The results in Figs. 10 to 12 show that the First-Order Takagi-Sugeno fuzzy controller fits the experimental data very well. Moreover, the model also represents the influence of the input variable on the shear behavior of the unfilled rock joints considered, as shown by an increase in the shear strength as the normal boundary stiffness, the roughness of the joint, and the initial normal stress also increased.

Figure 13 shows the correlation between experimental and predicted values of τ_h obtained for the fuzzy model. The fuzzy model has a high value of 0.85 for the coefficient of determination, which means it is a useful tool for predicting the shear behavior of unfilled rock joints and present as an advantage in relation to the existing models the fact of considering the uncertainties of their input variables.

5. Practical Application of the Fuzzy Model in a Rock Slope Stability Analysis

The initial application of the fuzzy model was made by assuming the general configuration of a rock slope subjected to a surcharge F , with height H , inclination α_s and whose potential slip surface is defined by an unfilled discontinuity with angle α_j , as shown in Fig. 14. The presence of the force T applied by the bolts defines the constant normal stiffness condition for the discontinuity.

The weight of the rock wedge (W) delimited by the rock discontinuity considering its unit weight (γ) can be determined according to Eq. 1.

$$W = 0.5\gamma H^2 (\cot \alpha_j - \cot \alpha_s) \quad (1)$$

The normal stress (σ_n) acting on the discontinuity can be determined as a function of the increase in the normal force (N) which acts on the discontinuity, due to the CNS

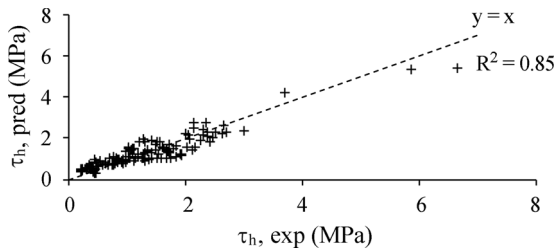


Figure 13 - Comparison between the experimental data with the shear strength predicted by the First-Order Takagi-Sugeno fuzzy model.

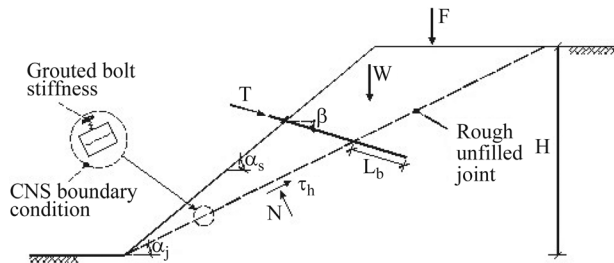


Figure 14 - Stability analysis of rock slope (Indraratna *et al.*, 2010a).

boundary condition imposed by the bolts. This increase in the normal force depends on the number of bolts inserted in the slope (n), and their horizontal spacing (s_h) and inclination (β), as well as the initial normal force (N_0) acting on the discontinuity.

$$\sigma_n = \frac{N \sin \alpha_j}{H} \quad (2)$$

$$N = N_0 + \frac{n}{s_h} T \sin(\alpha_j + \beta) \quad (3)$$

If there are no bolts, the normal force is constant and calculated according to Eq. 4.

$$N_0 = (W + F) \cos \alpha_j \quad (4)$$

The value of T can be calculated by using Eq. 5, which considers the characteristics of the bolts and the discontinuity dilation (δ_v), and whose measurement is obtained by laboratory tests or by using the Dantas Neto *et al.* (2017) neural model.

$$T = \frac{E_b A_b}{L_b} \frac{\delta_v}{\sin(\alpha_j + \beta)} \quad (5)$$

where E_b is the modulus of elasticity of the bolts; A_b is the cross-sectional area of the bolts; and L_b is the length of the ground anchored section of the bolts.

The normal boundary stiffness acting on the discontinuity can be defined by the elastic properties of the bolts and the geometry of the discontinuity (Eq. 6).

$$k_n = \frac{n E_b A_b \sin \alpha_j}{H L_b s_h \sin(\alpha_j + \beta)} \quad (6)$$

Finally, the factor of safety (FS) is obtained by the relation between the resisting forces acting on the wedge and the forces that cause its failure.

$$FS = \frac{\tau_h \left(\frac{H}{\sin \alpha_j} \right) + \left(\frac{n}{s_h} \right) T \cos(\alpha_j + \beta)}{(W + F) \sin \alpha_j} \quad (7)$$

The shear strength (τ_h) can be determined by laboratory tests or estimated by any available calculation methodology. In this paper, the analytical model of Indraratna & Haque (2000) and the neural model proposed by Dantas Neto *et al.* (2017) are used to predict the shear behavior of the unfilled rock joint in the rock slope stability analysis presented. A comparison of the results obtained by applying the First-Order Takagi-Sugeno fuzzy model is also presented.

Based on results of CNL and CNS direct shear tests, Indraratna & Haque (2000) proposed that the shear strength of an unfilled rock joint, presented in Eq. 8, can be defined as a function of the characteristics of the discontinuity, the

normal boundary stiffness, the initial normal stress acting on the joint, and the shear displacement.

$$\tau_h = \left(\sigma_{n0} + \frac{k_n \delta_v(\delta_h)}{A_j} \right) \left(\frac{\tan(\phi_b) + \tan(i_0)}{1 - \tan(\phi_b) \tan(i_h)} \right) \quad (8)$$

where A_j is the surface area of the discontinuity; $\delta_v(\delta_h)$ is the dilation during shearing; ϕ_b is the basic friction angle; i_0 is the initial asperity angle of the discontinuity; and i_h is the dilation angle at the horizontal displacement δ_h .

To use the analytical model proposed by Indraratna & Haque (2000), the dilation during shearing must be measured in large-scale direct shear tests. Once their values are known, the variation of dilation with the shear displacement to be inserted in Eq. 8 can be represented using a Fourier series, as presented in Eq. 9.

$$\delta_v(\delta_h) = \frac{a_0}{2} + \sum_{n=1}^{\infty} \left[a_n \cos\left(\frac{2\pi n \delta_h}{T_F}\right) + b_n \sin\left(\frac{2\pi n \delta_h}{T_F}\right) \right] \quad (9)$$

where a_0 , a_n e b_n are the coefficients of the Fourier series; n is the number of harmonics; and T_F is the period of the Fourier series.

The terms a_0 , a_n , b_n e T_F are determined by interpolating the dilation vs. shear displacement curve, as obtained by direct shear tests.

Indraratna *et al.* (2005, 2010a, 2010b) and Oliveira & Indraratna (2010) have shown that the model proposed by Indraratna & Haque (2000) can predict the shear behavior of unfilled rock discontinuities, but they also highlight the difficulties involved in obtaining its parameters because the results of laboratory tests are required and may not be easily available. Note also that the experimental data can only represent the field behavior if the boundary conditions imposed in laboratory tests are the same as those observed in the field, a fact that is not always possible, due to the limitations of the test equipment and the sampling process (Dantas Neto *et al.*, 2017).

In this practical application, the parameters representing the rock mass are: $H = 30.5$ m, $\alpha_s = 80^\circ$, and $\alpha_r = 50^\circ$, $\gamma = 27.5$ kN/m³ and $F = 25,000$ kN. The bolts are 63.5 mm in diameter by $L_b = 1.0$ m long, are inclined at $\beta = 15^\circ$ to the horizontal. The horizontal spacing of $s_h = 1.4$ m is assumed. Assuming $E_b = 200$ GPa and $n = 30$ bolts leads the discontinuity to an initial normal stress and boundary normal stiffness of 540 kPa and 380 kPa/mm, respectively.

The Indraratna & Haque (2000) model is used by applying the results of a direct shear test in a saw-tooth unfilled rock joint with $\sigma_c = 12$ MPa, $\phi_b = 37.5^\circ$ and JRC = 12 conducted under $k_n = 453$ kPa/mm and $\sigma_{n0} = 0.56$ MPa to obtain the coefficients of the Fourier series presented in Table 1. A saw-tooth unfilled rock joint was adopted to facilitate the calculations for applying the analytical model of Indraratna & Haque (2000). Note that the results of the direct shear test were obtained under boundary conditions

Table 1 - Fourier coefficients used in the stability analysis.

σ_{n0} (MPa)	Fourier coefficients							
	T_F	a_0	a_1	a_2	a_3	b_1	b_2	b_3
0.56	35.67	2.16	-1.14	0.04	0.00	-0.08	0.15	0.00

that differed from those imposed on the unfilled rock joint considered in the rock slope stability analysis. However, the fuzzy model proposed in this paper allows the shear strength of rock joints for the actual conditions of the rock slope to be evaluated, *i.e.*, normal boundary stiffness of 380 kPa/mm, and initial normal stress of 540 kPa.

This is one of the main advantages of this fuzzy model because it can predict the shear strength of unfilled discontinuities when carrying out laboratory tests to reproduce field boundary conditions that become difficult or unfeasible. Likewise, the neuronal model of Dantas Neto *et al.* (2017) also allows for a direct application, and it does not require laboratory tests.

Figure 15 shows the variation of the factor of safety with the shear displacement of the unfilled rock joint obtained by applying the First-Order Takagi-Sugeno fuzzy model and the results of shear strength obtained with models by Indraratna & Haque (2000) and Dantas Neto *et al.* (2017). The use of shear stresses provided by laboratory tests under boundary conditions, other than those imposed onto the analyzed rock slope, may have overestimated the factor of safety in most of the tangential displacements considered.

Other than what has been portrayed in the models proposed by Indraratna & Haque (2000) and Dantas Neto *et al.* (2017), the displacements could not initiate the degradation of the joint asperities, a phenomenon that leads to a loss of shear strength during shearing. This is possibly due to the previously established fact that the model provides predictions close to the residual strength of the joints.

Furthermore, to apply the fuzzy model to practical problems of rock slopes under CNS conditions, the dilation of the discontinuity must be determined in order to estimate the force applied by the bolts T , which defines the normal boundary stiffness of the discontinuity. In their analysis the authors used the dilations obtained by the model of Indraratna & Haque (2000).

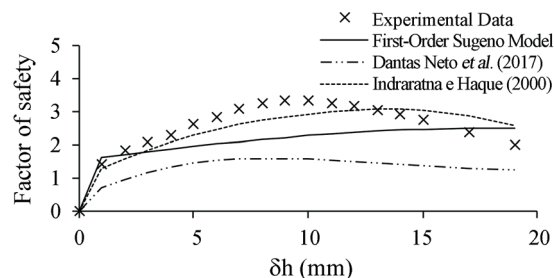


Figure 15 - Factors of safety vs. shear displacement for the analyzed rock slope.

6. Conclusions

The proposed fuzzy model is a Takagi-Sugeno controller with linear (first-order) implication functions used in the prediction of the shear strength of unfilled discontinuities; it was developed using a robust data set with 673 examples and was defined based on previous studies that identified the main factors that govern the shear behavior of unfilled joints. The proposed fuzzy model fits the experimental data very well, presenting a coefficient of correlation of 0.85. It presents as advantage in relation to the existing models the fact of considering the uncertainties of their input variables in its response, *i.e.*, in the shear strength of unfilled rock discontinuities, leading to more rational and safer analyses and design of structures in rock masses.

By analyzing the errors, the proposed Takagi-Sugeno model can explain the shear behavior of unfilled rock joints because it only needs some information about the characteristics of the discontinuities, the intact rock, and the boundary conditions imposed onto them.

In the rock slope stability problem presented, this limitation was confirmed, and the fuzzy model did not portray the degradation of joint asperities that can occur during the wedge movement which reduces the factor of safety. However, the model was very useful for analyzing the rock slope stability and for predicting the residual strength of unfilled discontinuities, especially where laboratory tests would be difficult or unfeasible, and the joint is subject to Constant Normal Loading (CNL) conditions.

Finally, it is important to mention that the main limitations of this fuzzy model are the domains of its input variables, which are defined during its construction, *i.e.*, they do not allow the insertion of values that are outside their pre-defined range of occurrence as input data. In the present work, the Takagi-Sugeno controller was conditioned to the domain of the measurements of direct shear tests for most of its parameters, but they can be adjusted as new data sets become available.

A suggestion for future studies would be to develop a Takagi-Sugeno fuzzy controller to predict the dilation of unfilled discontinuities of rock masses in order to apply the proposed model to practical problems of rock slopes under CNS conditions. Another interesting alternative would be to use neuro-fuzzy techniques to fully predict the shear behavior of unfilled rock joints.

Acknowledgments

The authors are thankful to FUNCAP (Fundação Cearense de Apoio ao Desenvolvimento Científico e Tecnológico) and CAPES/Proex for their financial support to the Post-Graduate Program in Civil Engineering of the Federal University of Ceará and to the Federal University of Ceará for the license of software MATLAB.

References

- Akgun, A.; Sezer, E.A.; Nefeslioglu, H.A.; Gokceoglu, C. & Pradhan, B. (2012). An easy-to-use MATLAB program (MamLand) for the assessment of landslide susceptibility using a Mamdani fuzzy algorithm. *Computers & Geosciences*, 38(1):23-34.
- Asadi, M. (2016). Optimized Mamdani fuzzy models for predicting the strength of intact rocks and anisotropic rock masses. *Journal of Rock Mechanics and Geotechnical Engineering*, 8(2):218-224.
- Barton, N.R. (1973). Review of a new shear strength criterion for rock joints. *Engineering Geology*, 7(4):287-332.
- Barton, N.R. (2013). Shear strength criteria for rock, rock joints, rockfill and rock masses: Problems and some solutions. *Journal of Rock Mechanics and Geotechnical Engineering*, 5(4):249-261.
- Barton, N.R. (2016). Non-linear shear strength for rock, rock joints, rockfill and interfaces. *Innovative Infrastructure Solutions*, 1(1):1-19.
- Barton, N.R. & Bandis, S.C. (1990). Review of predictive capabilities of JRC-JCS model in engineering practice. In: Barton N. & Stephansson O. (eds) *Proc. International Symposium on Rock Joints*, Loen, Norway. Balkema, Rotterdam, p. 603-610.
- Barton, N.R. & Choubey, V. (1977). The shear strength of rock joints in theory and practice. *Rock Mechanics*, 10(1-2):1-54.
- Benmokrane, B. & Ballivy, G. (1989). Laboratory study of shear behaviour of rock joints under constant normal stiffness conditions. In: Khair (ed) *Rock Mechanics as a Guide of Efficient Utilization of Natural Resources*. Balkema Publishers, Rotterdam, p. 899-906.
- Bieniawski, Z.T. (1984). *Rock mechanics design in mining and tunneling*. A.A. Balkema, Rotterdam, 272 p.
- Daftaribesheli, A.; Ataei, M. & Sereshki, F. (2011). Assessment of rock slope stability using the Fuzzy Slope Mass Rating (FSMR) system. *Applied Soft Computing*, 11(8):4465-4473.
- Dantas Neto, S.A.; Indraratna, B.; Oliveira, D.A.F. & Assis, A.P. (2017). Modelling the shear behaviour of clean rock discontinuities using artificial neural networks. *Rock Mechanics and Rock Engineering*, 50(7):1817-1831.
- Ganoulis, J.G. (1994). *Engineering Risk Analysis of Water Pollution. Probabilities and Fuzzy Sets*. VCH Publishers, New York, 327 p.
- Gokceoglu, C. (2002). A fuzzy triangular chart to predict the uniaxial compressive strength of the Ankara agglomerates from their petrographic composition. *Engineering Geology*, 66(1-2):39-51.
- Gokceoglu, C. & Zorlu, K. (2004). A fuzzy model to predict the uniaxial compressive strength and the modulus

- of elasticity of a problematic rock. *Engineering Applications of Artificial Intelligence*, 17(1):61-72.
- Grima, M.A. (2000). *Neuro-Fuzzy Modelling in Engineering Geology: Applications to Mechanical Rock Excavation, Rock Strength Estimation and Geological Mapping*. A.A. Balkema, Rotterdam, 244 p.
- Grima, M.A. & Babuska, R. (1999). Fuzzy model for the prediction of unconfined compressive strength of rock samples. *International Journal of Rock Mechanics and Mining Sciences*, 36(3):339-349.
- Indraratna, B.; Haque, A. & Aziz, A. (1998). Laboratory modelling of shear behaviour of soft joints under constant normal stiffness condition. *J. Geotech. Geol. Eng.*, 16(1):17-44.
- Indraratna, B.; Haque, A. & Aziz, A. (1999). Shear behaviour of idealized infilled joints under constant normal stiffness. *Géotechnique*, 49(3):331-355.
- Indraratna, B. & Haque, A. (2000). *Shear Behaviour of Rock Joint*. A.A. Balkema, Rotterdam, 164 p.
- Indraratna, B.; Welideniya, S. & Brown, E.T. (2005). A shear strength model for idealised infilled joints under constant normal stiffness. *Géotechnique*, 55(3):215-226.
- Indraratna, B.; Jayanathan, M. & Brown, E.T. (2008). Shear strength model for overconsolidated clay-infilled idealised rock joints. *Géotechnique*, 58(1):55-65.
- Indraratna, B.; Oliveira, D.A.F. & Brown, E.T. (2010a). A shear-displacement criterion for soil-infilled rock discontinuities. *Géotechnique*, 60(8):623-633.
- Indraratna, B.; Oliveira, D.A.F.; Brown, E.T. & Assis, A.P. (2010b). Effect of soil-infilled joints on the stability of rock wedges formed in a tunnel roof. *Int. J. Rock Mech. Min. Sci.*, 47(5):739-751.
- Indraratna, B.; Thirukumaran, S.; Brown, E.T. & Zhu, S. (2015). Modelling the shear behaviour of rock joints with asperity damage under constant normal stiffness. *Rock Mech. Rock Eng.*, 48(1):179-195.
- Jalalifar, H.; Mojedifar, S.; Sahebi, A.A. & Nezamabadi-Pour, H. (2011). Application of the adaptive neuro-fuzzy inference system for prediction of a rock engineering classification system. *Computers and Geotechnics*, 38(6):783-790.
- Jang, J.-S.R. (1993). ANFIS: Adaptive-network-based fuzzy inference systems. *IEEE Transactions on Systems, Man, and Cybernetics*, 23(3):665-685.
- Kayabasi, A.; Gokceoglu, C. & Ercanoglu, M. (2003). Estimating the deformation modulus of rock masses: a comparative study. *International Journal of Rock Mechanics & Mining Sciences*, 40(1):55-63.
- MathWorks, (2006). *Fuzzy Logic Toolbox for Use with MATLAB. User's Guide*. MathWorks, Natick, 227 p.
- Monjezi, M. & Rezaei, M. (2011). Developing a new fuzzy model to predict burden from rock geomechanical properties. *Expert Systems with Applications*, 38(8):9266-9273.
- Nefeslioglu, H.A.; Gokceoglu, C. & Sonmez, H. (2003). A Mamdani model to predict the weighted joint density. *Proc. 7th International Conference, KES 2003, Oxford, Part I*, pp. 1052-1057.
- Oliveira, D.A.F. & Indraratna, B. (2010). Comparison between models of rock discontinuity strength and deformation. *Journal of Geotechnical and Geoenvironmental Engineering*, 136(6):864-874.
- Papaliangas, T.; Hencher, S. R.; Manolopoulos, S. (1993). The effect of frictional fill thickness on the shear strength of rock discontinuities. *Int. J. Rock Mech. Min. Sci. Geomech.*, 30(2):81-91.
- Patton, F.D. (1966). Multiple modes of shear failure in rocks. *Proc. 1st Cong, Int. Soc. Rock Mech.*, Lisbon, v. 1, pp. 509-513.
- Prasetyo, S.H.; Gutierrez, M. & Barton, N.R. (2017). Non-linear shear behavior of rock joints using a linearized implementation of the Barton-Bandis model. *Journal of Rock Mechanics and Geotechnical Engineering*, 9(4):671-682.
- Sari, M. (2016). Estimating strength of rock masses using fuzzy inference system. *Proc. Eurock 2016, ISRM, Cappadocia*, v. 1, pp. 129-134.
- Simões, M.G. & Shaw, I.S. (2007). *Controle e Modelagem Fuzzy*. Blucher/FAPESP, São Paulo, 186 p.
- Skinas, C.A.; Bandis, S.C. & Demiris, C.A. (1990). Experimental investigations and modelling of rock joint behaviour under constant stiffness. In: Barton, Stephanson (eds) *Rock Joints*. Balkema Publisher, Rotterdam, p. 301-307.
- Sonmez, H.; Gokceoglu, C. & Ulusay, R. (2003). An application of fuzzy sets to the Geological Strength Index (GSI) system used in rock engineering. *Engineering Applications of Artificial Intelligence*, 16(3):251-269.
- Sonmez, H.; Gokceoglu, C. & Ulusay, R. (2004). A Mamdani fuzzy inference system for the Geological Strength Index (GSI) and its use in slope stability assessments. *Int. J. Rock Mech. Min. Sci.*, 41(3):1-6.
- Takagi, T. & Sugeno, M. (1983). Derivation of fuzzy control rules from human operator's control action. *IFAC Symposium on Fuzzy Information, Knowledge Representation and Decision Analysis*, Marseille, pp. 55-60.
- Zadeh, L.A. (1965). Fuzzy sets. *Information and Control*, 8(3):338-353.

Analysis of the Physical-Mechanical Behavior of Clayey Sand Soil Improved with Coir Fiber

L.C.P. Menezes, D.B. Sousa, S. Fucale, S.R.M. Ferreira

Abstract. The objective of this paper is to analyze the mechanical behavior of a clayey sand soil with added green coir fiber at 0.25%, 0.5%, 0.75%, and 1% by dry weight, through a series of laboratory tests that physically and mechanically characterize the samples in order to evaluate possible changes in the soil properties. Unconfined compression and indirect tensile tests were carried out. The addition of fibers to the soil resulted in a considerable increase in the strength of the composites. Unconfined compression strength for the soil and fiber mixtures was highest with 0.5% fiber content (50.8% higher than the soil without fibers), and the tensile strength was highest for 0.75% fiber content (85.4% increase). These results will hopefully encourage the use of vegetable fibers, specifically coir fiber, as an alternative material for use in civil engineering projects.

Keywords: alternative materials, coir fiber, indirect tensile test, reinforced soil, unconfined compression test.

1. Introduction

The usage of soil as a building material is common in civil engineering. However, some soils in their natural state have low strength. This characteristic intensifies when anthropogenic factors arise, such as the removal of vegetation cover, erosion, changes in drainage conditions, and disorganized human occupation, which occurs frequently in peripheral regions of large cities. This can exacerbate various socio-environmental problems, such as neighborhoods with poor infrastructure, residences located in high-risk areas, and degradation of natural systems (Souza, 2014), a common situation on the periphery of many Brazilian metropolises.

Awareness of the problem, and knowledge of the lack of strength capacity of some soils, makes it necessary to strengthen the soil by altering its properties to create a material capable of responding to the needs of the task (Cristelo, 2001).

Hejazi *et al.* (2011) cite soil improvement as “a procedure in which natural or synthetic additives are used to improve soil properties”, and typify this process in three different ways, as shown in Fig. 1. This paper deals with improvement through the addition of fibrous material.

The incorporation of fiber into fragile materials can provide various benefits, such as increased capacity to absorb energy before rupture, increased load capacity and unconfined compressive strength, and improved mechanical characteristics (Cabala, 2007).

The use of vegetable fibers in geotechnics has been studied with more emphasis in recent years, due to the demand for alternative materials and the need to dispose of

agricultural production waste. In order to substitute the use of synthetic materials with organic materials, however, studies are necessary to obtain conclusions and parameters on the viability of the use of these materials. The main objective of this paper is therefore to analyze the physical-mechanical behavior of composites of soil and coir fiber that can be used for soil stabilization projects.

1.1 Coir fiber

For Civil Engineering, vegetable fibers can have a number of applications, such as paving layers, retaining walls, temporary works, slope protection, foundations, and earthquake structures, among others (Kalita *et al.*, 2016). They have advantages over more conventional soil reinforcement materials, such as glass or carbon, but they also have certain disadvantages, as shown in Table 1.

Ali (2011) studied coir fiber and concluded that it is one of the most ductile vegetable fibers and capable of withstanding stress 4 to 6 times greater than other vegetable fibers. Table 2 shows the chemical composition of coir fiber according to various researchers. Coir fiber has a lower percentage of cellulose than other vegetable fibers, such as sisal and jute, between 33% and 43%, reaching 68.9% in some cases, according to Agopyan *et al.* (2005) and Asatutjarit *et al.* (2007). The hemicellulose content (0.15-31.1%) has the advantage of being low, since this material is attacked by microorganisms (Noguera *et al.*, 2000, apud Bolanões, 2013).

On the other hand, the amount of lignin is high, 20% to 40% (Passos, 2005), about two to four times more than jute and sisal fibers, providing compressive strength to cel-

Lucas Chagas Paes de Menezes, M.Sc., Universidade de Pernambuco, Recife, PE, Brazil, e-mail: lucas_cpm89@hotmail.com.

Danielle Barbosa de Sousa, B.Sc., Universidade de Pernambuco, Recife, PE, Brazil, e-mail: danielle.barbosa4@hotmail.com.

Stela Fucale Sukar, Dr., Full Professor, Universidade de Pernambuco, Recife, PE, Brazil, e-mail: sfucale@poli.br.

Sílvia Romero de Melo Ferreira, Dr., Full Professor, Universidade Federal de Pernambuco, Recife, PE, Brazil, e-mail: sr.mf@hotmail.com.

Submitted on March 03, 2018; Final Acceptance on December 13, 2018; Discussion open until August 30, 2019.

DOI: 10.28927/SR.421031

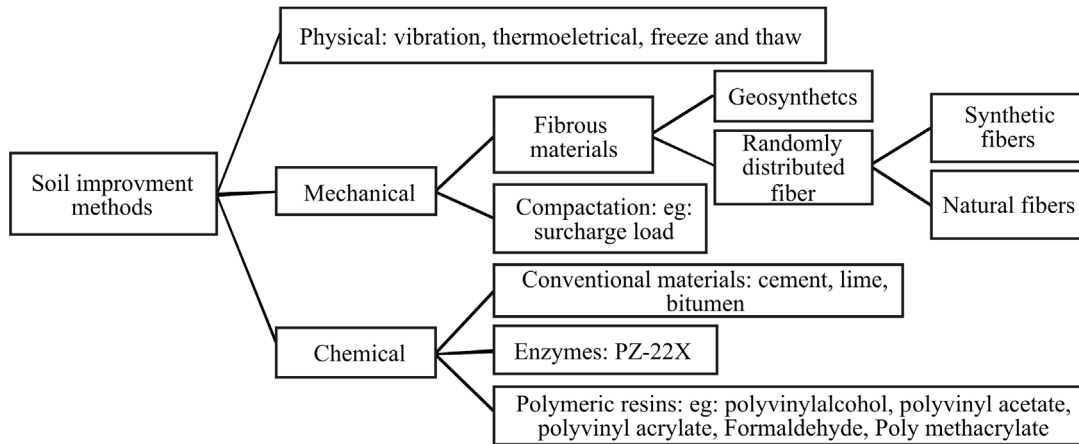


Figure 1 - Soil improvement methods. Source: Hejazi *et al.* (2011).

Table 1 - Advantages and disadvantages of the use of plant fiber for geotechnics.

Advantages	Disadvantages
Ecological and renewable;	Fibers degrade after being stored for a long time;
Low cost (or low cost by volume);	High moisture absorption (hygroscopicity);
Fully biodegradable;	Low strength to moisture;
Non-toxic;	Low thermal stability;
Easy to handle, low density, and light weight;	Weak adhesion in its natural state to numerous matrices;
Non-abrasive during processing and use;	Need for chemical, mechanical or thermal treatments to be used as reinforcement for cementitious composites.
Good insulation against heat and noise;	
Acceptable specific strength properties;	

Source: Bolaños (2013).

ular tissue and fibers. According to Babu & Vasudevan (2007), coir fiber is much more advantageous in certain applications, such as erosion control, or improvement of slope performance, due to the high lignin content.

It is also important to know the physical and mechanical properties of coir fiber, in order to better understand how it will behave in composites (Bledzeki & Gassan, 1999). Table 3 shows the physical and mechanical properties of coir fiber, as determined by several authors (Ali,

2011). The properties shown may differ among the studies cited, as the fibers may come from different origins, and may be tested using different methods and under different humidity conditions (Faruk *et al.*, 2012).

2. Materials and Methods

The soil was collected from the Alto do Reservatório hillside, located in Recife, Pernambuco. It is an area considered to have a high risk of slope instability (Meira *et al.*,

Table 2 - Coir fiber chemical composition.

Hemi-cellulose (%)	Cellulose (%)	Lignin (%)	Reference
-	43	45	Satyanarayana <i>et al.</i> (1990)
31.1	33.2	20.5	Ramakrishna <i>et al.</i> (2005)
15-28	35-60	20 - 48	Agopyan <i>et al.</i> (2005)
16.8	68.9	32.1	Asasutjarit <i>et al.</i> (2007)
0.15-0.25	36-43	41 - 45	Corradini <i>et al.</i> (2006)
0.25	43.4	45.8	Shankar <i>et al.</i> (2012)
0.15-0.25	32-35	40-45	Faruk <i>et al.</i> (2012)

Table 3 - Physical and mechanical properties of coir fiber.

Diameter (mm)	Length (mm)	Tensile strength (MPa)	Elongation (%)	Young's modulus (GPa)	Density (kN/m ³)	Reference
0.10-0.40	50-252	100 - 130	10-26	19-26	14.5-28	Aggarwal (1992)
0.11-0.53	-	108-252	13.3	2.5-4.5	10.0	Toledo <i>et al.</i> (2005)
0.1-0.4	-	174	10-25	16-26	-	Reis (2006)
-	-	500	-	-	11.5	Rao & Rao (2007)
0.27	50	142±36	24±10	2.0	-	Li <i>et al.</i> (2007)
0.13-0.23	-	100 - 250	-	3.0	-	Tomczak (2010)
-	-	175	30	4-6	12	Faruk <i>et al.</i> (2012)
-	-	220	15-25	6	12.5	Mohammed <i>et al.</i> (2015)

2006) and is susceptible to erosion. Coir fibers were supplied by an agricultural machinery company. They were cut to a length of 20 mm, a value based on previous studies (Babu *et al.*, 2008; Bolaños, 2013; Chaple & Dhattrak, 2013; Maliakal & Thiyyakkandi, 2013; Kar *et al.*, 2014; Aguilar, 2015). Following this, mixtures were prepared with proportions of 0.25%, 0.5%, 0.75%, and 1% with respect to the dry soil weight. These amounts were chosen based on previous studies (Bolaños, 2013; Chaple & Dhattrak, 2013; Maliakal & Thiyyakkandi, 2013; Singh & Mittal, 2014; Tiwari & Mahiyar, 2014; Aguilar, 2015; Anggraini *et al.*, 2015; Ayninola & Oladotun, 2016; Kalita *et al.*, 2016; Subramani & Udayakumar, 2016).

The following tests were carried out: Particle-size distribution (ABNT NBR 7181, 2016a), Consistency limits (ABNT NBR 7180, 2016b; ABNT NBR 6459, 2016c), Specific gravity (ABNT NBR 6508, 1984), and Proctor compaction (ABNT NBR 7182, 2016d). Four samples were produced (Fig. 2a) using static compaction method in a cylindrical mold (50 mm diameter x 100 mm height) for carrying out the mechanical tests: unconfined compressive strength (UCS) (ABNT NBR 12770, 1992) at a fixed strain rate of 0.5 mm/min (Fig. 2b) and tensile strength by diametral compression, or indirect tensile strength (ITS) (ABNT NBR 7222/2011) only, done at a strain rate of 0.25 mm/min (Fig. 2c).

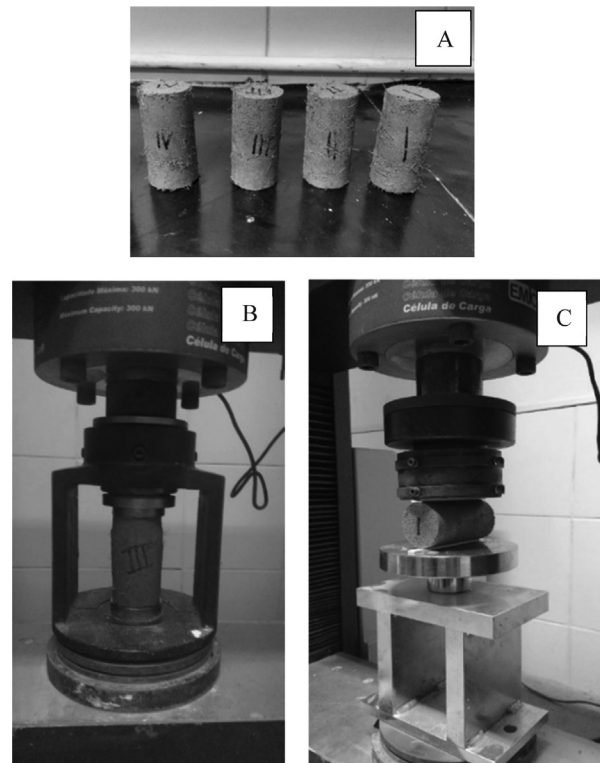

Figure 2 - (a) Samples; (b) Unconfined compression test; (c) Indirect tensile test.

Table 4 - Results of physical soil characterization and mixture tests.

Sample	Specific gravity	Liquid limit (%)	Plastic limit (%)	Plasticity index (%)	Optimum moisture content (%)	Maximum dry density (kN/m ³)	USCS	TRB
Soil	2.63	44	23	21	15.3	17.55	SC	A-7-6
S+0.25%	2.63	43	30	13	16.5	17.50	SM	A-7-5
S+0.5%	2.63	44	30	14	16.5	17.42	SM	A-7-5
S+0.75%	2.62	41	27	14	16.3	17.29	SM	A-7-6
S+1%	2.63	43	31	12	16.8	17.35	SM	A-7-6

An important feature to be analyzed when including fibers in soil mixtures is the form in which rupture occurs when the test is performed. Visual analysis of the increase

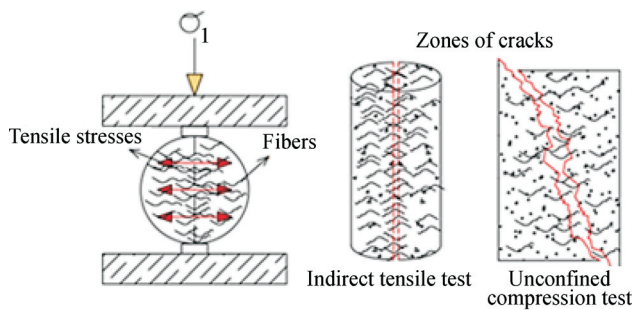


Figure 3 - Arrangement of the fibers in the rupture zones of the unconfined compression and indirect tensile tests. Source: Guedes *et al.*, 2016.

in fibrous ductility is interesting, and was used by other authors like Feuerharmel (2000) and Festugato (2008), considering that this characteristic tends to increase with the addition of fibers. The rupture patterns were analyzed in order to understand how the fibers acted as an improvement material. Figure 3 shows the probable ruptures that may occur (Guedes *et al.*, 2016).

3. Results and Discussion

Physical and mechanical characterization of soil and mixtures are presented and discussed.

3.1. Physical characterization

Figure 4 shows the particle size distribution curves for the soil and mixtures, and Table 4 presents the results of the specific gravity, consistency limit, and compaction test,

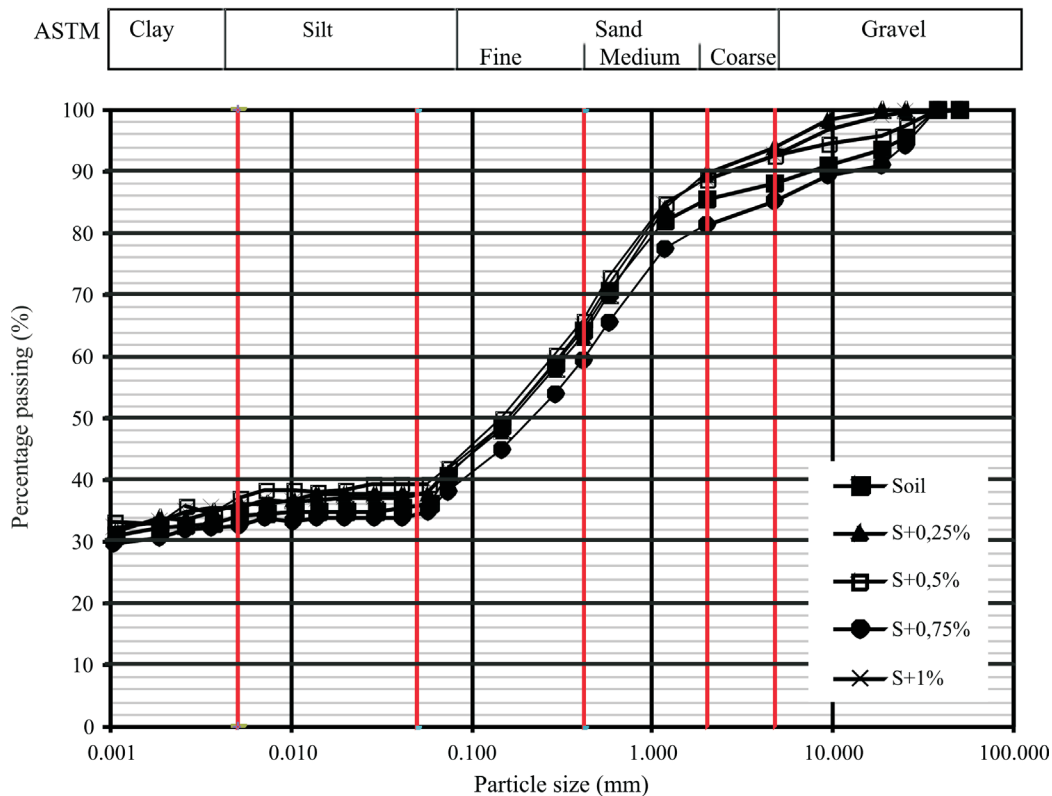


Figure 4 - Grain size distribution curves.

including Unified Soil Classification System (USCS) and Transportation Research Board (TRB) classifications.

The soil is a clayey sand, and the mixtures are silty sand. The insertion of the fibers decreased the plasticity index. The introduction of the fibers contributed to a slight decrease in the maximum dry density of the mixtures, because the fibers are lighter than the soil, while the increase of the optimum moisture values can be explained by the moisture absorption capacity of the fibers.

The same trend was observed by other authors, such as Chaple & Dhattrak (2013), who saw the maximum dry density decrease from 17.30 kN/m³ for the soil to 16.60 kN/m³ for the 1% coir fiber mixture. For all mixtures, the optimum moisture increased from 18.10% for the soil to 20.76% for the 1% coir fiber mixture. Soundara & Kumar (2015) obtained maximum dry densities of 19.80 kN/m³ for soil and 17.20 kN/m³ for 1.5% coir fiber, and optimum moisture of 6.50% for soil and 19% for 1.5% coir fiber.

3.2. Mechanical characterization

The results of the unconfined compressive strength and indirect tensile strength tests are presented and discussed.

3.2.1. Unconfined compression strength tests

Table 5 presents the unconfined compression strength results obtained from the samples, along with other important parameters. The values of simple compressive strength, for both the soil and the mixtures, had low dispersion (coefficient of variation less than 15%) and low modulus of elasticity, except for S+1%, which had medium dispersion of 22.9% (value between 15% and 30%) (Ferreira, 2018). The unconfined compressive strength increased with the insertion of coir fiber, reaching the highest value for the 0.5% fiber mixture. This effect may be caused by an interaction between the soil and fiber, indicating a possible optimum fiber content with the best soil-particle entanglement. For the higher fiber values of 0.75% and 1%, there was a small decrease in strength.

Similar behavior was obtained by Kar & Pradhan (2011) in soils of similar granulometry with 15-mm length fibers, where soil strength increased with 0.6% coir content. Chegenizadeh & Nikraz (2012 used 20-mm length fi-

bers, and found soil strength increased with 1.0% coir. Kar *et al.* (2014) performed this investigation in a clay-sand soil with 20 mm fibers and found that the best content was 0.8%, providing a 57% increase in UCS.

Stress-strain curves are shown in Fig. 5. The curves for the soil show a peak in strength, typical of friable material, reaching its maximum between 3 and 3.5% strain, following which, a decrease occurs for all applied stresses (Fig. 5a). For the mixtures, no strength peak was observed, but instead a hardening plastic behavior, characterizing a material more ductile than soil. There is a continuous increase in strength with higher deformations (Figs. 5b to 5d). Kar *et al.* (2014), and Subramani & Udayakumar (2016) obtained similar observations.

The increasing fiber addition was observed to turn the composite into a less rigid material, due to the fact that fiber is a more flexible material than soil (Fig. 5). The values for the rupture strain at this percentages increase with increasing fiber content; showing a tendency for the mixtures to be more ductile than soil. Therefore, the soil curve showed a behavior characteristic of a more rigid material, with a deformation peak and fragile rupture. With the inclusion of the fiber, this characteristic changes, indicating a less rigid and more ductile material.

Figure 6 shows 95% confidence intervals for the unconfined compressive strength test results. The S+ 0.5% and S+ 0.75% mixtures obtained the best results, considering that the S+ 0.25% and S+ 1% samples did not present statistically significant differences from the soil.

The results presented in this paper also point to a tendency of increase and decrease of strengths related to the elasticity modulus, reaffirming that it decreases with the insertion of fiber (Fig. 7), except for the 0.25% mixture, which showed a slight increase.

When the improved soil is subjected to an external load, the fibers become active, increasing the interconnection between the soil particles. This increases the strength of the composite. However, studies indicate that the addition of fibers beyond the ideal amount could actually reduce the effectiveness of this strength improvement, as the fibers would interact with each other, rather than with the soil (Sivakumar & Vassudevan, 2008; Anggraini, 2016).

Table 5 - Unconfined compression strength values.

	Average UCS (kPa)	Strength increase (%)	Variation coefficient (%)	Average elasticity modulus (MPa)	Variation coefficient (%)	Average rupture strain (%)
Soil	421.4± 22.4	-	5.3	17.2± 2.1	11.9	3.3
S+0.25%	513.3± 37.7	21,8	7,3	20.3± 1.9	9.3	4.5
S+0.5%	635.4± 84.6	50,8	13.3	16.6± 0.6	3.5	6
S+0.75%	553.9± 26.6	31.5	4.8	11.9± 0.6	5.1	6
S+1%	546.1± 40.9	29.6	7.5	6.3± 1.4	22.9	6.4

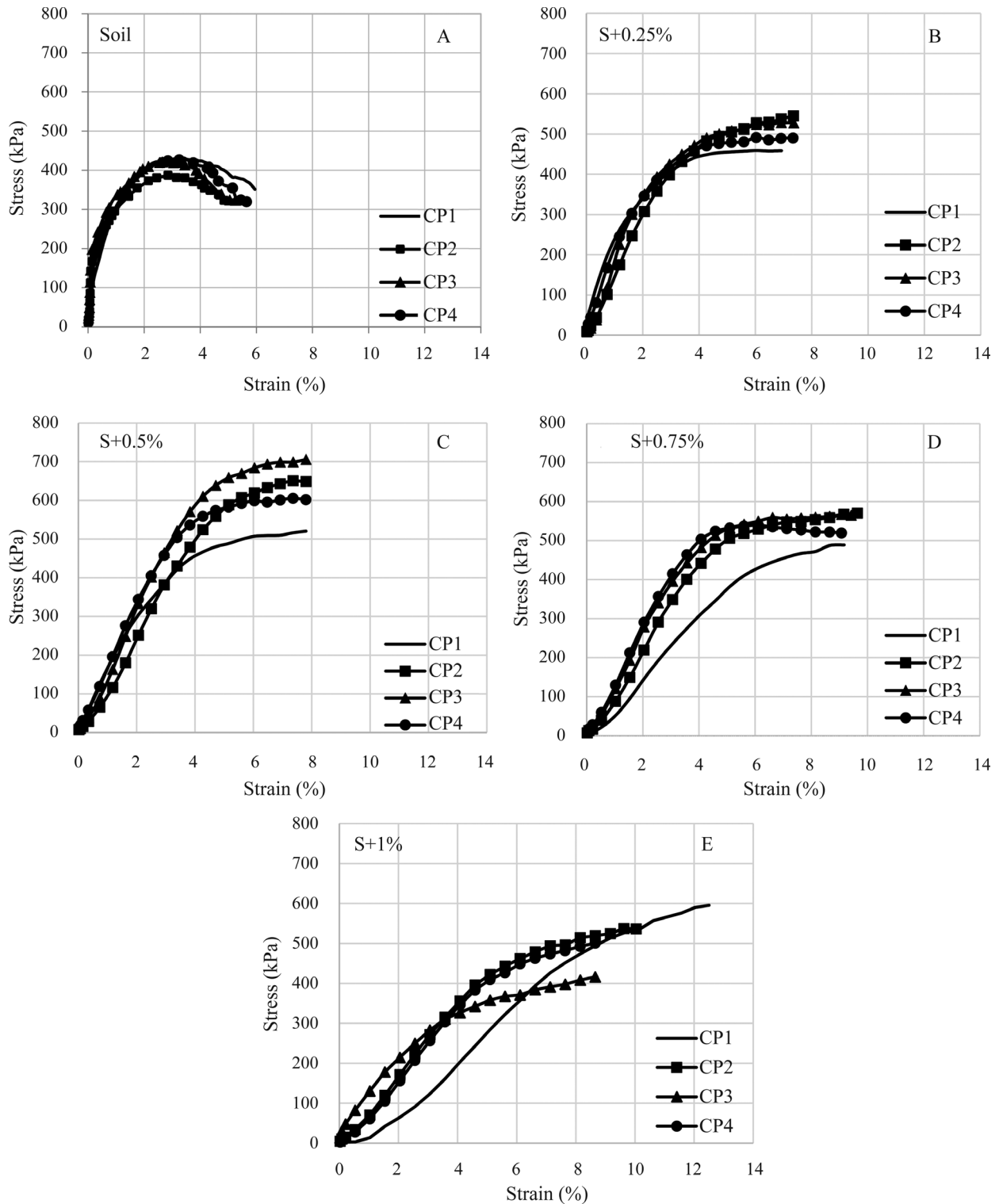


Figure 5 - Unconfined stress-strain curves for soil and mixtures.

Regarding the rupture pattern, as the fiber content increases, visible external ruptures occurred less frequently. Figure 8 shows the specimens following the test for the soil, S+0.5%, and S+1% mixtures. The S+0.5% mixture had the highest strength, but the S+1% sample was more ductile,

with fewer apparent ruptures distributed throughout the test body.

Bolaños (2013) and Maliakal & Thiyyakkandi (2013) verified similar behavior for fiber contents of 0.75%, 1%, and 1.5%. Kar & Pradhan (2011) also found a similar result

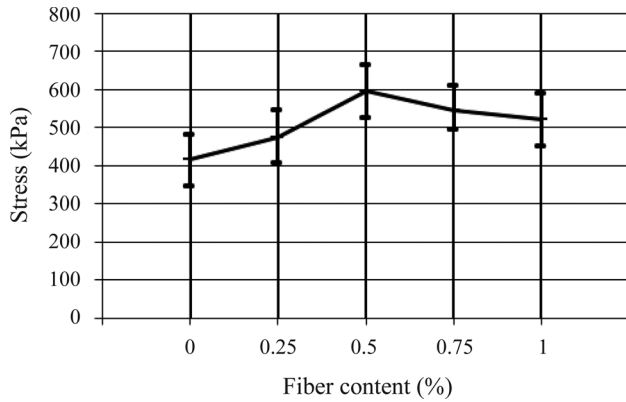


Figure 6 - Variation of unconfined compressive strength and 95% confidence intervals for the unconfined compressive strength test.

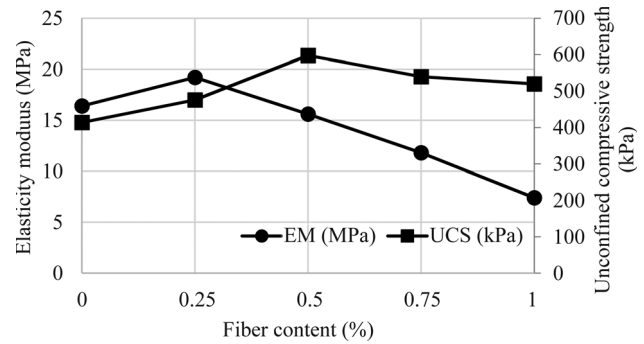


Figure 7 - Unconfined compressive strength and its relation to elasticity modulus.

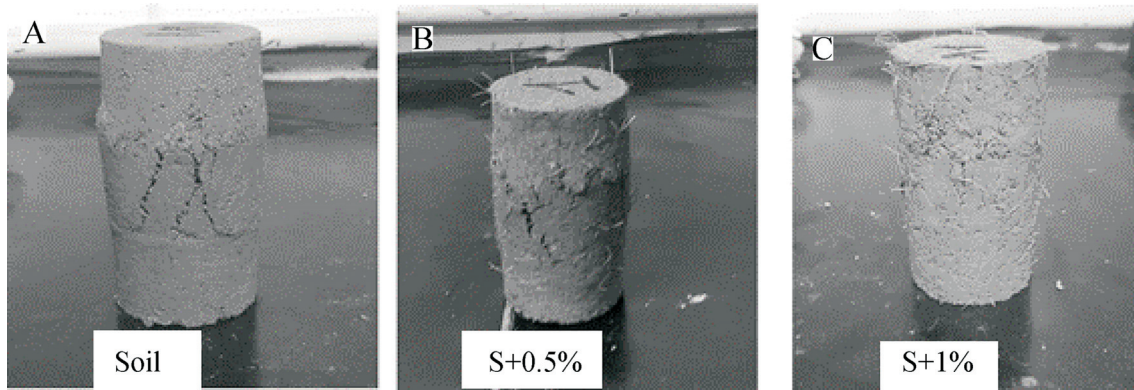


Figure 8 - Rupture patterns found in soil, S+0.5%, and S+1%.

for 0.4% fiber content, but with 15 mm fibers in clayey soil. Sebastian *et al.* (2011) found the best results with 0.8% of 20 mm fibers in a clay soil.

3.2.2. Indirect tensile strength test

Table 6 shows ITS test results, along with other parameters for the analyses. The values of tensile strength under diametral compression for both the soil and the mixtures, had low dispersion (coefficient of variation lower than 15%), except for the S+0.5% mixture, which had medium dispersion of 18.95% (value between 15% and 30%) (Ferreira, 2018).

The indirect tensile strength increased with the insertion of coir fibers, reaching the highest value for 0.75% fiber content. This effect may be due to interaction between soil and fiber, indicating that there is an optimum fiber content for the best soil-particle entanglement. Above the optimum fiber content value, the excess fibers in the mixture reduce the interaction between the materials. For 1% content, there was a small decrease in strength.

With the decrease in modulus of elasticity values and increase in rupture strain values, the tendency of the mixtures to become more ductile than the soil was identified. The stress-strain curves are shown in Fig. 9. The soil was found to

Table 6 - Indirect tensile strength values.

	Average ITS (kPa)	Strength increase (%)	Variation coefficient (%)	Average stiffness modulus (MPa)	Variation coefficient (%)	Average rupture strain (%)
Soil	20.5± 1.9	-	9.3	1.2± 0.1	9.9	1.4
S+0.25%	19.2± 1.9	-6.4	9.9	2.6± 0.2	7.9	3.5
S+0.5%	31.5± 5.9	53.7	18.9	2.3± 0.05	2.1	5
S+0.75%	38± 5.7	85.4	15.0	2.9± 0.7	24.9	8
S+1%	26.3± 3.5	28	13.3	1± 0.1	8.2	9.8

have low indirect tensile strength, where there is a peak, generally between 1 and 1.5% deformation, at which the soil completely ruptured across its longitudinal section. (Fig. 9a).

No strength peak was observed for the mixture samples S+0.25% and some of sample S+0.5% (Figs. 9b and

9c). Samples S+0.75% and S+1% showed no strength peak, however strength increased along the specific deformation, demonstrating the plastic behavior of the composite.

The soil indirect tensile strength is very low, and the insertion of fiber generated an improvement, especially for

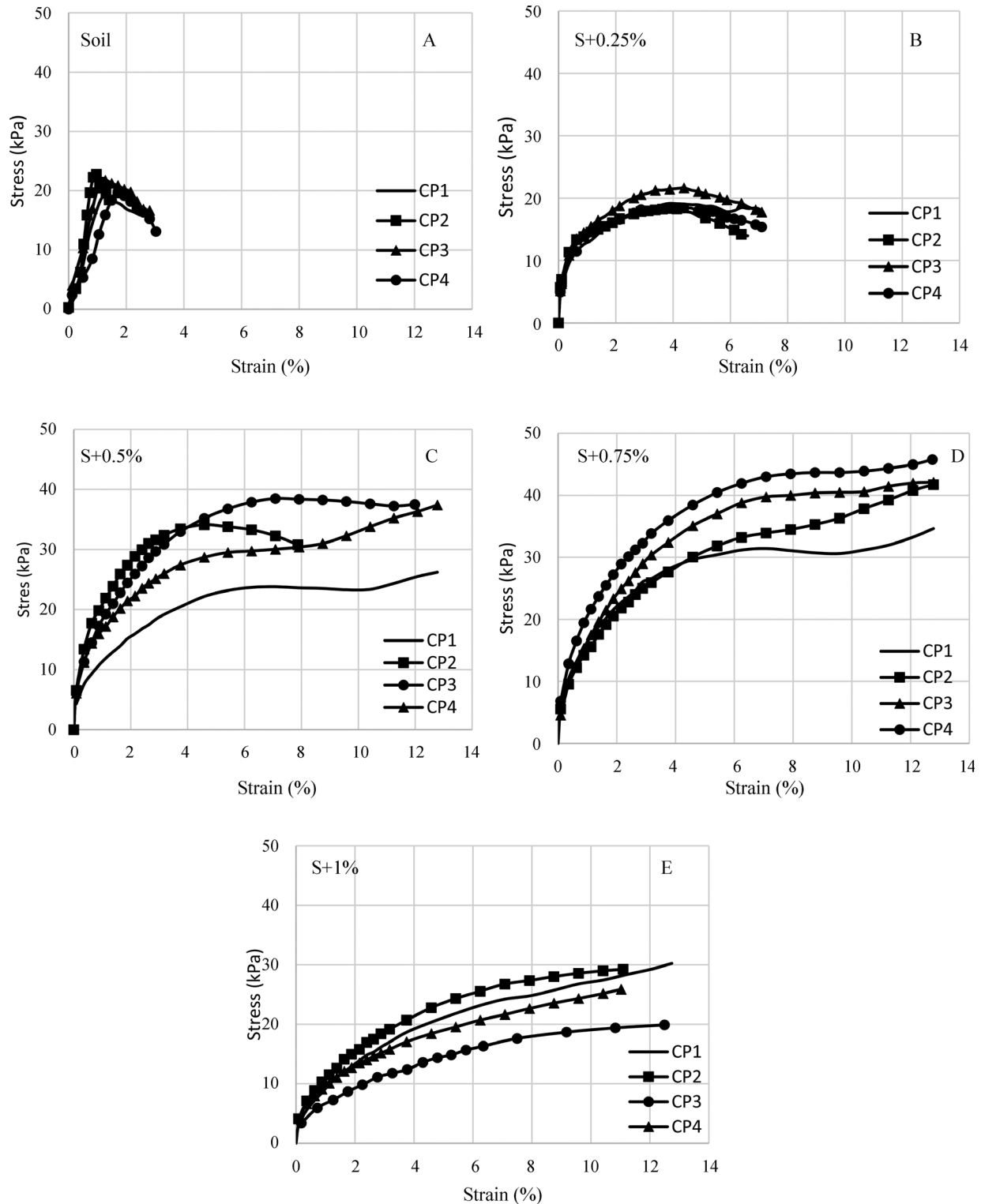


Figure 9 - Indirect tensile stress-strain curves.

the 0.75% content mixture, which provided the best inter-connection between the soil particles. For the 1% content mixture, there was a slight decrease in strength compared to the 0.75% content mixture. Figure 10 shows the 95% confidence intervals for the indirect tensile strength values. The S+0.75% mixture obtained the best results, considering that the S+0.25%, S+0.5%, and S+1% samples did not have a statistically significant difference in relation to the soil.

Similar results were obtained by Anggraini *et al.* (2014), for a clayey soil stabilized with lime, in which the addition of 1% fiber content showed strength gains, while a higher fiber content (1.5% and 2%) had reduced gain; and by Anggraini *et al.* (2015), for a clayey soil with 0.5% coir

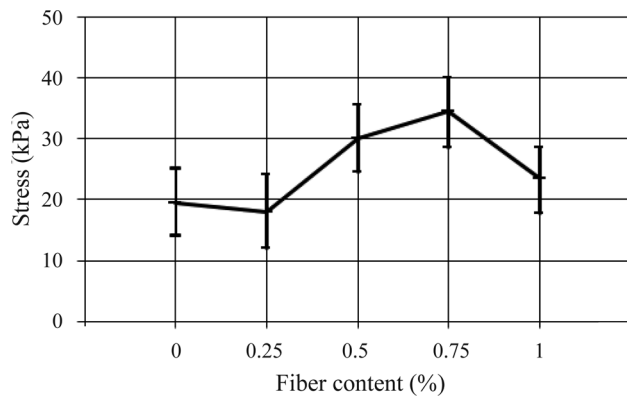


Figure 10 - Variation of indirect tensile strengths and 95% confidence intervals of indirect tensile strength.

fiber content, which decreased at higher content levels (1%, 1.5%, and 2%).

The ITS values were compared to the modulus of elasticity, reaffirming that it decreases as fiber content increases (Fig. 11). The stiffness modulus increases for the mixtures, making them more resistant materials than the soil, reaching the lowest value for 1% fiber content.

A definite vertical rupture plane, characteristic of a rigid material, is observed in the region where stress is applied (Fig. 12a). The specimens of sample S+0.75% (Fig. 12b) did not present a defined rupture plane, as the stress tended to dissipate to other regions of the specimen. Due to the presence of fibers, radial cracks also formed, but the soil remained cohesive.

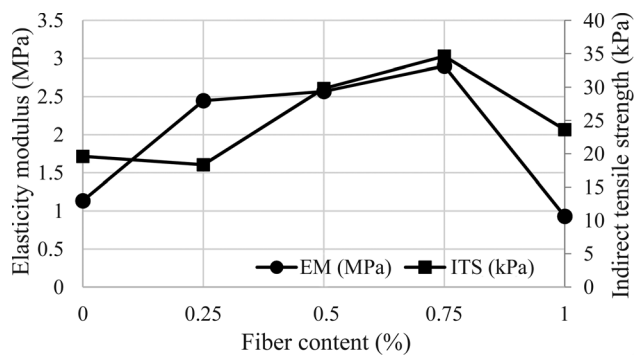


Figure 11 - Indirect tensile strength and its relationship with the elasticity modulus.

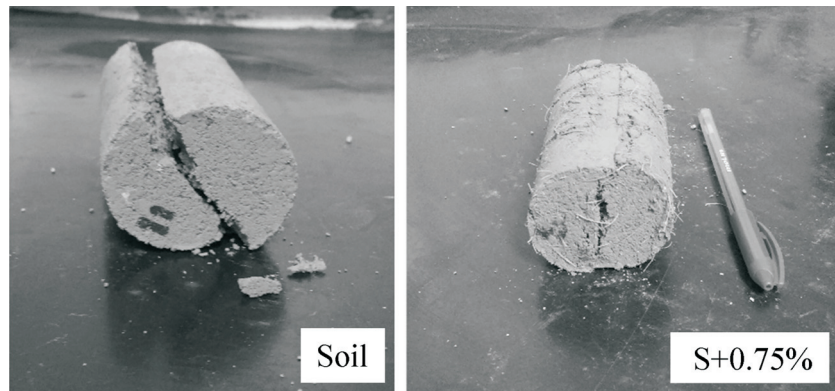


Figure 12 - Rupture pattern of the a) Soil and b) S+0.75% mixture after indirect tensile strength test.

Table 7 - Comparison between UCS and ITS values.

Mixture	Average strength (kPa)		Strength increase (%)		ITS/UCS (%)
	UCS	ITS	UCS	ITS	
Soil	421.4	20.5	-	-	4.8
S+0.25%	513.3	19.2	21.8	-6.4	3.7
S+0.5%	635.4	31.5	50.8	53.7	4.9
S+0.75%	553.9	38	31.5	85.4	6.8
S+1%	546.1	26.3	29.6	28	4.8

3.2.3. Unconfined compressive strength vs. indirect tensile strength

There is a general increase in strength when comparing the behavior of the average UCS and ITS values (Table 7). The UCS was highest at 0.5% fiber content, slightly decreasing for higher fiber contents, whereas the ITS showed little difference between the soil and S+0.25% mixture in numerical terms, although the test piece did not rupture or in half. There is a tendency for strength to increase up to 0.75% fiber, decreasing slightly at 1% content. ITS values were around 5% of the UCS values. Regardless of the content, the fibers contributed more to the ITS, providing an increase of around 40%, than to the UCS, whose average gain was 33%.

4. Conclusions

A comprehensive program of laboratory tests was performed to analyze the physical and mechanical properties of soil reinforced with coir fiber.

- The physical characteristics of the soil, such as specific gravity, optimum moisture content, and maximum dry density do not change significantly with the inclusion of coir fiber. The plasticity index decreased with the addition of fibers.
- Fibers in the soil matrix were verified to provided an increase in the unconfined compressive strength. The highest increases were reached at 0.5% coir fiber content, 50% greater than that of soil without fiber.
- The incorporation of fibers increased the indirect tensile strength. Higher increases were found with 0.75% coir fiber content, which was 85% higher than that untreated soil.
- The insertion of fibers made the soil a more ductile material, prone to reach higher strength with deformation.

Acknowledgments

The authors would like to thank all those who contributed to the research, especially Polytechnic School of Pernambuco (University of Pernambuco), as well as Fortalmag company, for supplying the fibers used in this study.

References

- ABNT (1992). Solo – Resistência à Compressão Simples. NBR 12770. Rio de Janeiro. Brasil (in Portuguese).
- ABNT (1984). Grãos de Solos que Passam na Peneira de 4.8 mm - Determinação da Massa Específica. NBR 6508. Rio de Janeiro. Brasil (in Portuguese).
- ABNT (2011). Argamassa e Concreto – Determinação da Resistência à Tração por Compressão Diametral de Corpos-de-Prova Cilíndricos. NBR 7222. Rio de Janeiro. Brasil (in Portuguese).
- ABNT (2016a). Solo – Análise Granulométrica. NBR 7181. Rio de Janeiro, Brasil (in Portuguese).
- ABNT (2016c). Solo – Determinação do Limite de Liquidez. NBR 6459. Rio de Janeiro. Brasil (in Portuguese).
- ABNT (2016b). Solo – Determinação do Limite de Plasticidade. NBR 7180. Rio de Janeiro. Brasil (in Portuguese).
- ABNT (2016d). Solo – Ensaio de Compactação. NBR 7182. Rio de Janeiro. Brasil (in Portuguese).
- Aggarwal, L. (1992). Studies on cement bonded coir fiber boards. *Cement Conc. Comp.*, 14(1):63-69.
- Agopyan, V.; Savastano JR., H.; John, V.M. & Cincotto, M.A. (2005). Developments on vegetable fibre-cement based materials in São Paulo, Brazil: An overview. *Cement and Concrete Composites*, 27(5):527-536.
- Aguilar, J.R.T. (2015). Analysis of Mechanical Behavior of a Sandy Soil Reinforced with Coir Fibers. MSc Dissertation, Pontifical Catholic University of Rio de Janeiro, 114 p. (in Portuguese).
- Ali, M. (2011). Coconut Fibre – A Versatile Material and its Applications in Engineering. 2nd International Conference on Sustainable Construction Materials and Technologies, Ancona, Italy. 2(9):189-197.
- Anggraini, V. (2016). Potential of coir fibres as soil reinforcement. *Pertanika Journal of Scholarly Research Reviews*, 2(1):95-106.
- Anggraini, V.; Asadi, A.; Huat, B.B.K. & Nahazanan, H. (2014). Effects of coir fibers on tensile and compressive strength of lime treated soft soil. *Measurement*, 59:372-381.
- Anggraini, V.; Huat, B.B.K.; Asadi, A. & Nahazanan, H. (2015). Effect of coir fibers on the tensile and flexural strength of soft marine clay. *Journal of Natural Fibers*, 12(2):185-200.
- Asasutjarit, C.; Hirunlabh, J.; Khedari, J.; Charoenvai, S.; Zeghmami, B. & Shin, U.C. (2007). Development of coconut coir-based lightweight cement board. *Construction and Building Materials*, 21(2):277-288.
- Ayininuola, G.M. & Oladotun, P.O. (2016). Geotechnical Properties of Coconut Coir Fiber Soil Mixture. *Journal of Civil Engineering Research*, 6(4):79-85.
- Babu, G.L.S. & Vasudevan, A.K. (2007). Evaluation of strength and stiffness response of coir-fibre-reinforced soil. *Ground Improvement*, 11(3):111-116.
- Babu, G.L.S.; Vasudevan, A.K. & Sayida, M.K. (2008). Use of coir fibers for improving the engineering properties of expansive soils. *Journal of Natural Fibers*, 5(1):61-75.
- Bledzeki, A.K. & Gassan, J. (1999). Composites reinforced with cellulose based fibres. *Progress in Polymer Science*, 24(2): 221-274.
- Bolaños, R.E.Z. (2013). Mechanical Behavior of Clayey Soil Reinforced with coconut fiber. MSc Dissertation, Pontifical Catholic University of Rio de Janeiro, Rio de Janeiro, 143 p. (in Portuguese).
- Cabala, G.V.E. (2007). Estudo do comportamento mecânico de estruturas de solo-cimento reforçado com fibras de coco e hastes de bambu. 113 p. MSc Dissertation,

- Federal University of Rio Grande do Norte. (in Portuguese).
- Chaple, P.M. & Dhattrak, A.I. (2013). Performance of Coir Fiber Reinforced Clayey Soil. *The International Journal of Engineering and Science*, 2(4):54-64.
- Chegenizadeh, A. & Nikraz, H. (2012). Effective parameters on strength of reinforced clayey sand. *International Journal of Material Science*, 2(1):1-5.
- Corradini, E.; Morais, L.C.; Rosa, M.F.; Mazzetto, S.E.; Mattoso, L.H.C. & Agnelli, J.A.M. (2006). A preliminary study for the use of natural fibers as reinforcement in starch-gluten-glycerol matrix. *Macromolecular Symposia*, 245-246(1):558-564.
- Cristelo, N.M.C. (2001). Stabilization of Residual Granitic Soils by the Addition of Lime. Master Dissertation, Minho University, Portugal. (in Portuguese).
- Faruk, O.; Bledzki, A.K.; Fink, H. & Sain, M. (2012). Biocomposites reinforced with natural fibers: 2000-2010. *Progress in Polymer Science*, 37(11):1552-1596.
- Ferreira, P.V. (2018). Estatística Experimental Aplicada às Ciências Agrárias. Editora UFV, Viçosa, 588 p. (in Portuguese).
- Festugato, L. (2008). Analysis of the Mechanical Behavior of a Micro-Reinforced Soil with Fibers of Different Aspect Ratio. Master Dissertation, Federal University of Rio Grande do Sul, Porto Alegre, 145 p. (in Portuguese).
- Feuerharmel, M. R. (2000). Behaviour of Soils Reinforced with Polypropylene Fibres. MSc Dissertation, Federal University of Rio Grande do Sul, Porto Alegre, 152 p. (in Portuguese).
- Guedes, S.B.; Coutinho, R.Q. & Fonseca, A.J.P.V. (2016). Influência do teor e do comprimento de fibras de polipropileno na resistência à tração por compressão diametral de um solo cimento. 18 Congresso Brasileiro de Mecânica dos Solos e Engenharia Geotécnica, Belo Horizonte. 8 p. (in Portuguese).
- Hezaji, S.M.; Sheikhzadeh, M.; Abtahi, S.M. & Zadhoush, A. (2011). A simple review of soil reinforcement by using natural and synthetic fibers. *Construction and Building Materials*, 30:100-116.
- Kalita, D.M.; Mili, I.; Baruah, H. & Islam, I. (2016). Comparative Study of Soil Reinforced with Natural Fiber, Synthetic Fiber and Waste Material. *International Journal of Latest Trends in Engineering and Technology*, 6(4):284-290.
- Kar, R.K. & Pradhan, P.K. (2011). Strength and compressibility characteristics of randomly distributed fiber-reinforced soil. *International Journal of Geotechnical Engineering*, 5(2):235-243.
- Kar, R.K.; Pradhan, P.K. & Naik, A. (2014). Effect of randomly distributed coir fibers on strength characteristics of cohesive soil. *Electronic Journal of Geotechnical Engineering*, 19:1567-1583.
- Li, Z.; Wang, L. & Wang, X. (2007). Cement composites reinforced with surface modified coir fibers. *J. Comp. Mat.*, 41(12):1445-1457.
- Maliakal, T. & Thiyyakkandi, S. (2013). Influence of randomly distributed coir fibers on shear strength of clay. *Geotechnical and Geological Engineering*, 31(2):425-433.
- Meira, F.F.D.A.; Coutinho, R.Q.; Cantalice, J.R.B. & Alheiros, M.M. (2006). Erosão do solo em encostas ocupadas. Proc. 2nd Simpósio Brasileiro de Jovens Geotécnicos, Nova Friburgo. 6 p. (in Portuguese).
- Mohammed, L.; Ansari, N.M.N.; Pua, G.; Jawaid, M. & Islam, M.S. (2015). A review on natural fiber reinforced polymer composite and its applications. *International Journal of Polymer Science*, 15 p.
- Motta, L.A.C.; Agopyan, V. & John, V.M. (2007). Caracterização de Fibras Curtas Empregadas na Construção Civil. *Boletim Técnico da Escola Politécnica da USP, São Paulo*. (in Portuguese).
- Passos, P.R.A. (2005). Sustainable disposal of green coconut (*cocos nucifera*) husks: producing roof tiles and fiberboards. DSc Dissertation, Federal University of Rio de Janeiro. 166 p. (in Portuguese).
- Ramakrishna, G. & Sundararajan, T. (2005). Studies on the durability of natural fibres and the effect of corroded fibres on the strength of mortar. *Cement and Concrete Composites*, 27(5):575-582.
- Rao, K.M.M. & Rao, K.M. (2007). Extraction and tensile properties of natural fibers: Vakka, date and bamboo. *Composite Struct.*, 77(3):288-295.
- Reis, J.M.L. (2006). Fracture and flexural characterization of natural fiber reinforced polymer concrete. *Constr. Build Mater.*, 20(9):673-678.
- Satyanarayana, K.G.; Sukumaran, K.; Mukherjee, P.S.; Pavithran, C. & Pillai, S.G.K. (1990). Natural fibre-polymer composites. *Cement and Concrete Composites*, 12(2):117-136.
- Sebastian, B.; Cyrus, S. & Jose, B.T. (2011). Effect of inclusion of coir fiber on the shear strength of marine clay. Proc. of Indian Geotechnical Conference, Kochi, pp. 379-382.
- Shankar, A.U.R.; Chandrasekhar, A. & Bhat Prakash, H. (2012). Experimental investigation on lithomargic clay stabilized with sand and coir. Indian highways: A review of road and road transport development. *Indian Highways*. 40(2):21-31.
- Singh R.R. & Mittal, S. (2014). Improvement of local subgrade soil for road construction by the use of coconut coir fiber. *IJRET: International Journal of Research in Engineering and Technology*, 3(5):707-711.
- Sivakumar, B.G.L. & Vasudevan, A.K. (2008). Strength and stiffness response of coir fiber-reinforced tropical soil. *Journal of Materials in Civil Engineering*, 20(9):571-577.

- Soundara, B. & Kumar, S. (2015). Effect of fibers on properties of clay. *International Journal of Engineering and Applied Sciences*, 2(5):123-128.
- Souza, A.P.L. de (2014). Estudos Geotécnicos e de Estabilidade de Taludes da Encosta do Alto do Padre Cícero no Município de Camaragibe-PE. Master Dissertation, Federal University of Pernambuco, 177 p. (in Portuguese).
- Subramani, T. & Udayakamur, D. (2016). Experimental study on stabilization of clay soil using coir fibre. *International Journal of Application or Innovation in Engineering & Management*, 5(5):192-204.
- Tiwari, A. & Mahiyar, H.K. (2014). Experiential study on stabilization of black cotton soil by fly ash, coconut coir fiber & crushed glass. *International Journal of Emerging Technology and Advanced Engineering*, 4(11):330-333.
- Toledo, F.R.D.; Ghavami, K. & England, G.L. (2005). Free, restrained and drying shrinkage of cement mortar composites reinforced with vegetable fibres. *Cement Conc. Comp.*, 27(5):537-546.
- Tomczak, F. (2010). Studies on the Structure and Properties of Coconut Fibers and Curauá of Brazil. DSc Dissertation, Federal University of Paraná, 150 p.

Numerical Simulation of Vertical Pullout of Plate Anchors Embedded in Reinforced Sand

A.T. Siacara, L. Festugato

Abstract. This paper presents a model to predict the ultimate pullout load (P_u) for a shallow single vertical plate anchor embedded in sand and fiber reinforced sand for depth (H)/diameter (D) ratios of 1.0, 1.5 and 2.0. The model was developed based on literature field test results and wide laboratory investigation. The numerical analysis was performed using the software ABAQUS considering elastoplasticity (Mohr Coulomb - Abaqus CAE) for modelling fiber reinforced sand. The results indicate that this type of fiber reinforced sand significantly increases the P_u of shallow anchor plates. Based on test results, critical values were discussed and recommended in order to estimate the P_u for shallow single vertical plate anchor embedded in sand and fiber reinforced sand. The proposed theory was compared against available bibliography of homogeneous material (sand) in field tests or analytical methods. The variability of the results shows that the proposed method is in the range of expected results. For fiber reinforced sand, no method for comparison has been found literature.

Keywords: elastoplasticity, fiber reinforced sand, numerical simulation, plate anchors, pullout load.

1. Introduction

A series of investigations and researches have been carried out to determine the pullout resistance of circular plate anchors placed horizontally in a homogeneous soil medium. Foundations subjected to pullout loadings rely heavily on the passive resistance developed on such elements. Anchors are known to be the best foundation elements to provide such resistance. The development of analytical models for these types of foundations depends on identifying a representative failure mechanism of the surrounding soil. This constitutes one of the major difficulties.

In the literature, the different studies were based on small-scale trials (Das & Seeley, 1975; Murray & Geddes, 1987), the limit equilibrium method (Meyerhof, 1973; Murray & Geddes, 1987; Jesmani *et al.*, 2013), the elastoplastic finite element method (Rowe & Davis, 1982a, 1982b; Andresen *et al.*, 2011; Jesmani *et al.*, 2013), models of centrifugal test (Dickin, 1988; Ovesen, 1981), the stress characteristics method (Subba Rao & Kumar, 1994), the upper limit-boundary analysis (Murray & Geddes, 1989; Kumar, 2001; Merifield & Sloan, 2006; Kumar & Kouzer, 2008; Kouzer & Kumar, 2009) and the lower limit-boundary analysis (Merifield & Sloan, 2006; Merifield *et al.*, 2006; Khatri & Kumar, 2011). Most of these studies were focused mainly on plates embedded in a homogeneous medium of a single layer of soil.

The lack of agreement between the various theories of tensile load capacity is due to the difficulty of predicting the geometry of the rupture zone. In the case of compressive load capacity tensions occur below the foundations in a continuous medium, which is assumed to be homogeneous

and isotropic; thus, the zones of rupture are predicted and coherent with the Classical Soil Mechanics (Bhattacharya & Kumar, 2016).

In the majority of earlier studies, a failure mechanism was assumed and the uplift capacity was then determined by considering the equilibrium of the soil mass above the anchor and contained by the assumed failure surface. Based on the underlying assumptions, these methods of analysis are commonly referred to as the “Soil cone” method (Mors, 1959) and the “Friction cylinder” method (Downs & Chieruzzi, 1966). A similar study to that of Pearce (2000) was performed by Ilamparuthi *et al.* (2002) who conducted a series of laboratory pullout tests on horizontal circular plate anchors pulled vertically in loose to dense sand. A discussion of the observed failure mechanisms, load displacement response and critical embedment depth was also provided. A set of empirical equations were presented for estimating the break-out factors for circular anchors with any friction angle.

At the ultimate pullout load (P_u) the tensile load tensions are distributed above the base and their distribution seems to be unique and influenced by the surface of the terrain: the behavior of deep foundations has been generally distinguished from shallow foundations in studies (CIGRÉ, 2008). Various prediction formulas based on an assumed failure mechanism have also been proposed (Vermeer & Sutjiadi, 1985; Trautmann *et al.*, 1985; Murray and Geddes, 1987). More rigorous solutions based on plasticity theory have been presented by Merifield *et al.* (2001) and Merifield & Sloan (2006). These various prediction methods, based on different assumed failure mechanisms, stress

Adrian T. Siacara, Ph.D. Student, Departamento de Engenharia de Estruturas e Geotécnica, Universidade de São Paulo, São Paulo, SP, Brazil, e-mail: adriantorricosiacara@gmail.com.

Lucas Festugato, D. Eng., Associate Professor, Departamento de Engenharia Civil, Universidade Federal do Rio Grande do Sul, Porto Alegre, RS, Brazil, e-mail: lucas@ufrgs.br. Submitted on April 21, 2018; Final Acceptance on February 14, 2019; Discussion open until August 30, 2019.

DOI: 10.28927/SR.421043

distributions and material behaviour, can lead to very different results. The solutions have a wide variation and these kinds of methods do not give a prediction for fiber reinforced sand.

The use of fiber reinforced sand has also attracted considerable interest in recent years in the research area (Silva dos Santos *et al.*, 2010; Consoli *et al.*, 2007a, b; Consoli *et al.*, 2009a, b). Despite that, no work has focused on determining the ultimate pullout load for a plate anchor embedded in fiber reinforced sand.

The studies available in the literature are mainly focused on the capacity of vertical anchors as well as the deformation mechanisms at the soil-plate interface. However, the effect of soil improvement with the use of fiber reinforced sand on the behaviour of a plate anchor has not yet been investigated. Therefore, the aim of this study is to develop more understanding about the behavior of loaded vertical anchor plates embedded in sand and fiber reinforced sand. This is achieved by studying the influence of the reinforcing element parameters, such as its length and diameter on the pullout resistance of the anchor plate. Also, the effect of these parameters is investigated on anchor plates with different geometry, embedment depth and the kind of soil (sand or fiber reinforced sand).

2. Objectives

The purpose of this research is to present the validation of a simple limit equilibrium solution for the vertical pullout resistance of plate anchors embedded in sand and fiber reinforced sand. The limit equilibrium solution is inspired by the formulation of Rowe & Davis (1982b) and Merifield *et al.*, 2003. The use of elastoplasticity (Mohr Coulomb - Abaqus CAE) in the analysis by the Finite Ele-

ment Method (FEM) for fiber reinforced sand was adopted, following Hibbit *et al.*, 2006, in order to establish the geometry of the mechanism, and the resistance mobilised on the failure planes. The solution is shown to provide agreement with a large database of model test results that have been assembled from the published literature (the solution shows the variation of the results that exist in the literature). Simple design charts are presented. It is shown that plasticity solutions for an ideal frictional material can be unconservative. Finite element solutions with a non-associated flow rule can give closer predictions. However, finite element analysis is not routinely used in practice, and simple analytical idealisations of the kind described in this paper remain the principal tool used by designers.

3. Problem Definition

The experimental program was carried out in two parts. First, all the description of the pull out of circular anchor plates embedded in sand and fiber reinforced sand test was developed in the experimental program by Consoli *et al.* (2012, 2013) such as the characterization of the backfill material (the configuration made for the test follows the instructions of ASTM D 1194, 1994). The foundation consists of a steel cable and a rigid circular steel plate 300.0 mm in diameter and 25.4 mm thick. Then a numerical 2D study was conducted using the source code of the commercial finite-element package ABAQUS, with further development to simulate the deformation analysis.

A basic explanation of the problem is now provided. The anchor plate is placed at a distance H measured from the top of the backfill and the diameter of the anchor plate is B as shown in Fig. 1. The thickness of the anchor is assumed to be negligible compared to its width. The soil mass

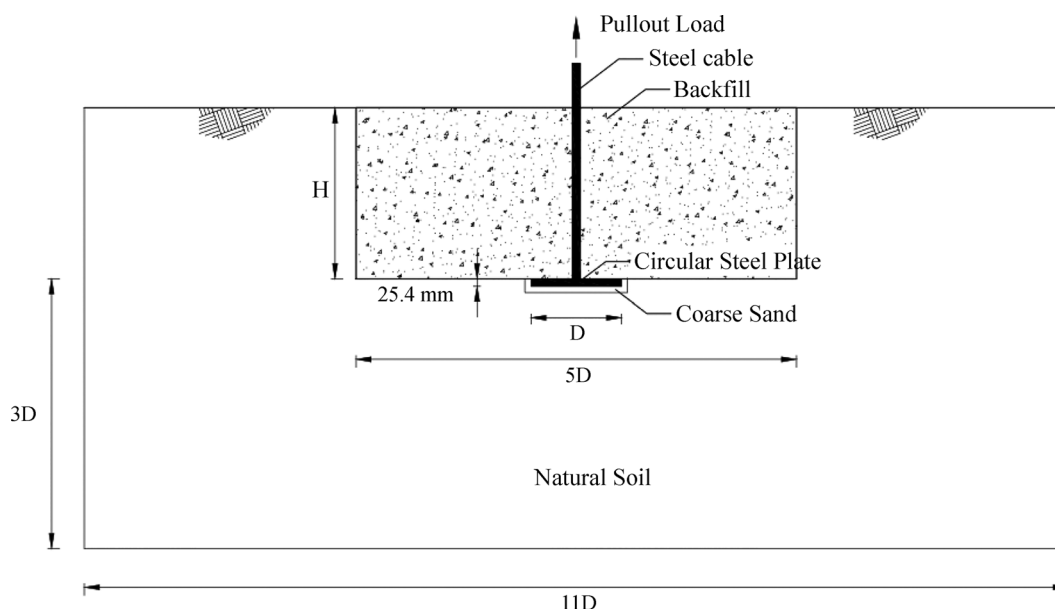


Figure 1 - Schematic diagram of the problem definition.

is perfectly plastic and is assumed to obey an associated flow rule. The Mohr-Coulomb failure criterion is applicable for the analysis. The objective of this work is to find the ultimate pullout load (P_u) per unit of length of the plate anchor for different values of H/D (1.0, 1.5 and 2.0) where the direction of the pullout is perpendicular to the anchor plate. The ultimate pullout capacity of the plate anchor is determined for the sand and fiber reinforced sand.

4. Elastoplasticity (Mohr Coulomb - Abaqus Cae)

The non-associative Drucker-Prager model (Drucker & Prager, 1952) was implemented in this work. Since ABAQUS (Hibbit *et al.*, 1998) requires parameters in the p - t coordinate system, calculations need to be performed to transfer soil parameters from the t - s to the p - t coordinate system. The following explanations will summarize references (Drucker & Prager, 1952 and Chen, 1982) which provide detailed explanation for obtaining parameters for the Drucker-Prager soil model.

The Mohr-Coulomb failure criterion is an elastoplastic constitutive model that is controlled by the laws of yield, flow, and expansion (hardening). The Mohr-Coulomb constitutive model, which can be provided by the Abaqus program, has some requirements that are important when studying or using the model in geotechnical problems (Hibbit *et al.*, 2006). The requirements are as follows:

- Stresses and deformations do not depend on time.
- The material studied should be isotropic.
- The material is expanding (hardening) or softening isotropically. The model does not use an equation that controls the expansion of the material, but this is controlled by the user through the control of the cohesion with the plastic deformation.
- Cohesion has two functions, i) first, the yield function where the resistance parameter of the material is known by the traditional Mohr-Coulomb constitutive model; ii) second, the function of the plastic potential where the stress is controlled when plastic deformations called Cohesion yield stress are generated.

The formulation of the Mohr-Coulomb failure criterion that is implemented in Abaqus is a function of three stress invariants and state parameters presented in the following equations. The Mohr-Coulomb yield criterion is associated with the flow function by forming a yield surface in Haigh-Westergaard co-ordinates, expressed in terms of principal stresses (Hibbit *et al.*, 1998) by.

$$F = Rmc \times q - p \tan(\varphi) - c \quad (1)$$

where F is the yield surface; Rmc is the Mohr-Coulomb deviatoric stress measure that is a function of the angle of Lode (θ) and the internal friction angle of the material (φ) according to Eq. 2; q is the second stress invariant that Abaqus calls equivalent Von Mises stress presented in

Eq. 6; p is the hydrostatic stress being the first stress invariant that is in Eq. 4; c is the cohesion of the material; and φ is the internal friction angle of the material.

$$Rmc(\theta, \varphi) = \frac{1}{\sqrt{3} \cos \varphi} \sin\left(\theta + \frac{\pi}{3}\right) + \frac{1}{3} \cos\left(\theta + \frac{\pi}{3}\right) \tan \varphi \quad (2)$$

where θ is the angle between the stress path of the material and the main stress present in Eq. 3 and r is the third stress invariant presented in Eq. 7.

$$\cos(3\theta) = \frac{r^3}{q^3} \quad (3)$$

$$p = \frac{-(\sigma_{11} + \sigma_{22} + \sigma_{33})}{3} \quad (4)$$

The Von Mises equivalent stress (q) and the third invariant (r) are in function of the deviatoric stress (S_y). In Eq. 5 the variables in terms of stress tensors are expressed

$$\sigma = S - pI \quad (5)$$

$$q = \sqrt{\frac{3}{2}(S:S)} \quad (6)$$

$$r = \left[\frac{9}{2}(S:S:S)\right]^{\frac{1}{3}} \quad (7)$$

The constitutive model is characterized by a non-associated plasticity where there is no equality between the yield function (F) and that of the plastic potential (G). The plastic potential function of Eq. 8 defines the direction of the plastic deformations that are perpendicular to the surface of the plastic potential.

$$G_1 = \sqrt{(E_1 c_2 \tan \psi)^2 + (Rmw \times q)^2} - p \tan \psi \quad (8)$$

where, E_1 is the eccentricity that controls the deformability of the function (G) in the meridional plane (Rmw - q) and approaches the asymptotic line. The Abaqus software defines the default ($E = 0.1$). The meridional plane represents a cut of the surface of the plastic potential in which the directions of the plastic deformations are perpendicular to the surface.

The c_2 is the initial cohesion yield stress, ψ is the angle of dilatancy that relates the volumetric and shear deformation in the plastic range, different to the angle of friction due to the selection of the non-associated flow (Houlsby, 1991). Rmw is the elliptic function presented by Menétrey & Willam (1995) that generates the concave shape to the function of the plastic potential by means of the Lode angle (θ) and the variable (e) called the out-of-roundedness parameter. The variable (e) allows smoothing the function that governs the surface of the plastic potential.

$$e = \frac{(3 - \sin \varphi)}{(3 + \sin \varphi)} \quad (9)$$

$$Rmc\left(\frac{\pi}{3}, \varphi\right) = \frac{(3 - \sin \varphi)}{(6 \cos \varphi)} \tag{10}$$

$$Rmw(\theta, e) = \frac{\left(4(1 - e^2)(\cos \theta)^2 + (2e - 1)^2\right)}{\left(2(1 - e^2)(\cos \theta) + (2e - 1)\sqrt{\left(4(1 - e^2)(\cos \theta)^2\right)(5e^2 - 4e)}\right)} Rmc\left(\frac{\pi}{3}, \varphi\right) \tag{11}$$

The model hardening law is controlled by the cohesion parameter under confinement pressure and the load level of the test.

5. Finite Element Simulation

Numerical simulations have been often used to analysed various types of geotechnical models in pullout testing using the finite element approach (Susila *et al.*, 2003; Song *et al.*, 2008; Bhattacharya & Kumar, 2014 and Bhattacharya & Kumar, 2016). However, there are not models that have been used to investigate the pull out of circular anchor plates embedded in fiber reinforced sand.

Steel plates with tensile stresses can be solved in axissimetry, planar or three-dimensional, but in this research they will be solved in axissimetry (Fig. 2a) due to the ease provided and the type of model. Loading by prescribed displacement was chosen (due to being a facilitator while

the model converged), with subsequent response to the re-action force.

It is assumed that the steel plate is in perfect contact with the ground at the beginning. The interaction between the plate and the soil is simulated using interface elements, with coefficient of friction of 0.30 for the interaction between the materials. This type of interface is able to reproduce the Coulomb-type frictional interaction between the surface of the plate and the ground in contact (Hellwany, 2007).

The extent of the mesh must be large enough to prevent discrepancies due to the boundary conditions. Thus, a minimum spacing of 11 times the diameter of the plate was adopted, and 3 times the length at depth (Fig. 2b). Bhattacharya *et al.* (2008) adopted a lateral distance and depth of 5D, relative to the center of the foundation, for their sand simulations. Consoli *et al.* (2007c) and Ratley *et al.* (2008),

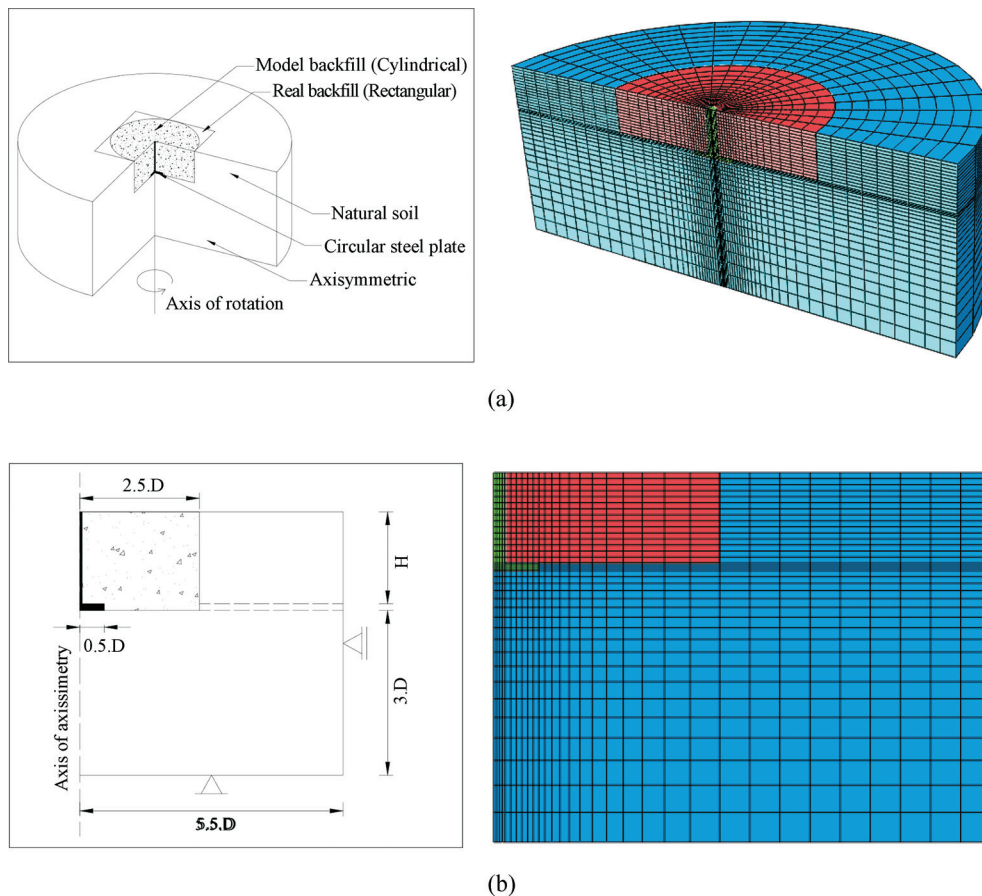


Figure 2 - Axisymmetric analysis a) Parts of the model b) Dimensions of the model.

in their numerical simulations, adopted a radius and depth of 3D for sand-fiber backfills. The extent of the mesh is sufficiently large to avoid discrepancies with the boundary conditions according to the Fig. 2b.

After the step of applying the initial stress state, one must check the value of vertical displacements, which should tend to zero. It is suggested a tolerance around 1×10^{-5} m.

The Fig. 2a and 2b show the finite element model for the analysis. Both the soil and the plate anchors are modelled using four node axisymmetric elements (CAX4 ABAQUS element) and axisymmetric pore pressure elements (CAX4P ABAQUS element) are also used but only in the soil, but the pore pressure will be not considered. The structured mesh is of square type elements in the entire model. In order to optimize the processing time and reduce the possibility of errors, the finite element mesh is more concentrated in the landfill area. This same procedure was also adopted by Mántaras (1995), Thomé (1999), Consoli *et al.* (2007c) and Ratley *et al.* (2008).

The base of the model is restricted in the X and Y directions, while the sides are constrained only in the X direction. The boundary conditions for the displacement constraints are shown in Fig. 2b.

The elasto-perfectly plastic Mohr-Coulomb constitutive model was adopted for the natural soil and sand, in which the input parameters are relatively easy to obtain, and the results would show good agreement with the field results.

In the fiber reinforced sand numerical model the Mohr-Coulomb hardening option was used; this option is used to define the linear behavior of the material in hardening/softening (Abaqus, 2010).

All analyses were performed in the isotropic condition ($K = 1.0$). According to Burd & Frydman (1997) and Thomé (1999), the consideration of different anisotropic conditions ($K \neq 1.0$) for surface foundations submitted to compression did not show differences from the results obtained with the elasto-perfectly plastic model.

Three steps were determined for the algorithm sequence: a) Initial, the numerical insertion of the initial stress state, its boundary conditions, and contact properties between the different parts is done; b) Geostatic, the geostatic control is activated, which verifies if the geostatic stresses applied in the previous step caused significant deformations; c) Loading, in this step the displacement is gradually applied in the steel tube, and the reading of reaction forces and displacements are checked.

5.1. Material properties of the Analysis

5.1.1. Sand

The sand used in this study comes from a deposit located in the municipality of Osório-Rio Grande do Sul. This material is characterized as a fine sand (NBR 6502-ABNT,

1995 and ASTM-D 2487, 1993), being uniform, fine, non-plastic, with grain specific gravity 26.5 kN/m^3 and average particle size 0.16 mm (Cruz, 2008 and Dalla Rosa, 2009).

The geotechnical parameters of cohesion (c) and the angle of friction (ϕ) were obtained directly from the triaxial test of Festugato (2008) and Santos (2008). In terms of modulus of elasticity, Thomé (1999) defined as the secant value for a 0.1% deformation. This same criterion was adopted in this work. Alternatively, the modulus of elasticity (E) can be obtained by correlation with the shear modulus (G) by the elasticity theory relations as shown in Eq. 12, where a shear modulus of 20.0 MPa is obtained according to Consoli *et al.*, 2013.

$$E = 2(1 + \nu)G \quad (12)$$

In the preliminary analyses, the value of Poisson ratio (ν), between 0.2 and 0.4, was varied for both the natural soil and the material of the landfill, and no influence was verified on the stress vs. relative displacement curves for the adopted range. Thus, an average value of 0.3 was considered for all materials involved. These considerations are consistent with the results of Rowe & Booker (1981) who verified that, for a homogeneous soil, there is no variation in the displacement for a variation of ν between the values 0.0 and 0.5. Cudmani (1994) verified the same result for his analyses of foundations subject to compression.

The dilatation curves (stress ratio - q vs. dilatation - $\delta\varepsilon_v / \delta\varepsilon_s$) for the triaxial sand tests are presented by Festugato (2008) and Santos (2008). The dilatancy angle Ψ can be obtained directly through these curves and through Eq. 13.

$$\tan(\Psi) = \frac{\delta\varepsilon_v}{\delta\varepsilon_s} \quad (13)$$

where $\delta\varepsilon_v$ is the volumetric deformation and $\delta\varepsilon_s$ is the shear deformation.

As $\phi \neq \psi$ (non-associated flow) the stiffness matrix is non-symmetric. It is necessary to use the “Unsymmetric Matrix Storage” option in ABAQUS (Abaqus, 2010).

5.1.2. Sand with fiber

The fibers used consist of polypropylene monofilaments of 50.0 mm in length and 0.01 mm in diameter, relative density of 0.91, tensile strength of 120.0 MPa , modulus of elasticity of 3.0 GPa and deformation at rupture of 80.0%. The fiber content used was 0.50% of the weight of the dry sand.

From the results of the triaxial tests, performed under different effective confinement stresses for a sand with fiber with 50.0% of relative density, the resistance parameters of the analyzed mixtures, angle (ϕ'), and cohesive intercept (c'), are defined through their rupture envelope (Festugato, 2008) and the value adopted in the initial numerical model is presented in Table 1.

Table 1 - Calibrated properties of the studied soils

Description	Properties	Sand	Sand - fiber	Natural soil	Steel plate	Steel tube
Density	ρ (kg/m ³)	1770.0	1770.0	1650.0	7850.0	1600.0
Elasticity	E (kPa)	60000.0	80000.0	15000.0	210000000.0	210000000.0
ν	0.3	0.3	0.3	0.3	0.3	
Plasticity	c' (kPa)	3.0	0.3-2.0	-	-	-
φ' (°)	39.2	43.0	-	-	-	-
ψ (°)	7.0	8.0	-	-	-	-

In terms of modulus of elasticity, the same criterion of the sand was adopted in this work.

The internal friction angle values of the blends are not influenced by the fiber aspect ratio. The rupture envelopes are parallel. In contrast, the values of cohesive intercept of the composites are strongly influenced by the aspect ratio of reinforcements. The higher the aspect ratio, the greater the cohesive intercept (Festugato, 2008).

The same criterion of the sand was used for obtaining the value of ν (Cudmani, 1994) and the dilation angle (Festugato, 2008).

5.1.3. Natural soil

The excavated soil that served as the base for the execution of the load tests is of the homogeneous residual type, originating from the decomposition of basaltic rocks (igneous) and sandstones (sedimentary). Standard penetration test (SPT) was performed in the experimental field by Lopes Jr. and Thomé, 2005.

Dalla Rosa *et al.* (2004a, b) conducted a geotechnical investigation along the profile to a depth of 5.0 m to determine the physical properties and indices along the depth (moisture, specific gravity, particle size distribution and limits of liquidity and plasticity).

Considering the geotechnical parameters presented above (granulometry and Atterberg limits), the soil of the experimental field can be classified as an A-5-7 soil (silt-clay soil) by the American Association of State Highway and Transportation Officials (AASHTO) and CL (low to high liquidity clay) by the unified soil classification system (USCS).

Dalla Rosa *et al.* (2004a, b) performed oedometric tests in the natural and flooded conditions, simple compression tests and Thomé *et al.* (2005) carried out consolidated drained (CD) triaxial tests.

In addition to the geotechnical characterization of the experimental field, Dalla Rosa *et al.* (2004a) performed compressive load tests on steel plates with diameters of 30, 60 and 90 cm and set at a depth of 80.0 cm. Lopes Jr. & Thomé (2005) performed six static load tests on excavated cuttings (three of which were isolated with styrofoam),

with a diameter of 25.0 cm and drilled between the depths of 3.86 and 4.70 m.

5.1.4. Steel

For the steel plate, the technical characteristics of the type of steel used in its manufacture were used (Souza, 1974).

Table 1 provides a summary of the calibrated material properties that were used in the present study.

6. Results and Comparison

6.1. Results of the model

Figure 3 shows the comparison of the results of the experimental tests with the numerical simulation of vertical pullout of plate anchors embedded in sand and fiber reinforced sand.

The ultimate pullout load (P_u) of plate anchors embedded in sand was 5.0 kN and in fiber reinforced sand was 4.1 kN, from the numerical modeling was 5.1 kN and 5.1 kN respectively for a displacement of 1.5 mm and 6.0 mm in the cases of a H/D ratio of 1.5 and 1.0 respectively with a steel plate of 30.0 cm. There is a difference in P_u of 0.1 kN that is approximately 2.0% higher in the numerical model than in the field test, which is considered a satisfactory result.

Figure 4a presents the initial stress state for an embedded sand of H/D ratio of 1.5. The S, S22 (stress components at integrations points) view helps to show that points A, B and C meet the state of initial stress. Hence, it can be inferred that all the points in the model meet the state of initial stress. Figure 4b, for an embedded fiber reinforced sand with H/D ratio of 1.0, shows the U, U2 (spatial displacement at nodes) view that helps check the initial displacements. In the same figure, it is shown that points A, B and C meet the state of initial displacements with displacements close to zero. Therefore, all the model satisfactorily meets the initial displacement expected conditions.

The displacement occurring during the initial step is not due to the external load, but it is due to the difference between initial stresses predicted in the computational program by the user and the converged stresses calculated by ABAQUS which are in equilibrium with the external load.

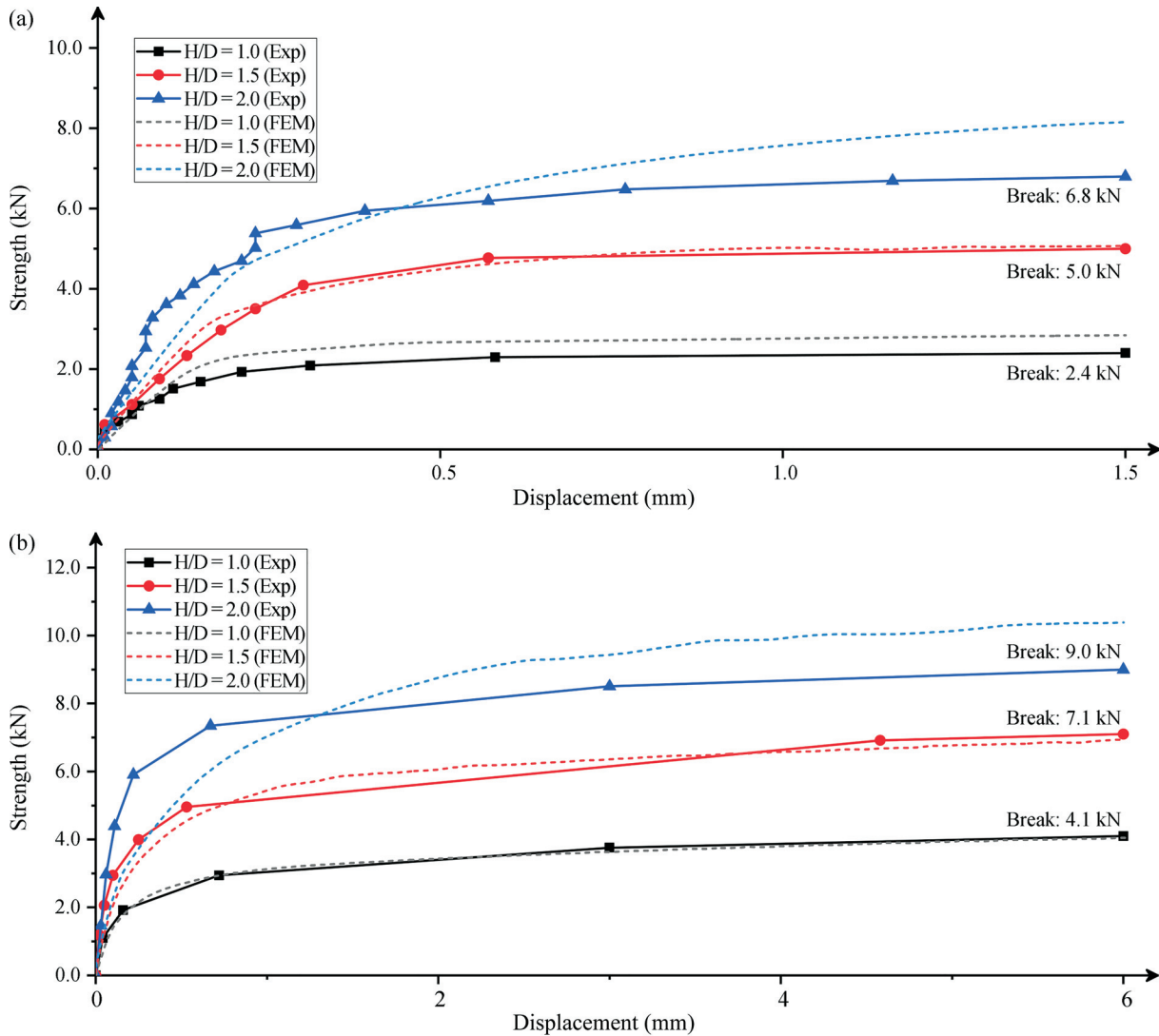


Figure 3 - Results of the vertical pullout test and the numerical model in an embedded a) sand b) fiber reinforced sand for $H/D = 1.0, 1.5$ and 2.0 .

The verification of the state of initial stresses and the initial displacements helps check that the numerical model behaves close to reality.

In Figure 5 the largest displacements (U) are observed in the soil that is on top of the upper face of the steel plate. In this case the simulation was done with continuous elements and that is why the solid does not present cracks. However, the displacement gradient indicates the probable location of the rupture surface, which can be observed with a frustoconical shape. The generatrix of the failure surfaces in the case of fiber reinforced sand forms a larger angle with the vertical compared to the sand case. From the same figure we can see that a displacement of 2.0 mm was used for the sand model and for the fiber reinforced sand model a displacement of 6.0 mm.

The stresses and deformations are developed in several directions and one way of presenting these stresses is to

combine them in the so called equivalent von Mises (S). In three-dimensional models the combination of the six stress components in a single equivalent stress is related to the real stress system (Abaqus, 2010). Von Mises stresses or equivalent stresses are concentrated in the landfill zone as shown in Fig. 6 and they increase as the H/D ratio increases. It can be seen that in the case of sandy soil the stresses are distributed more randomly than in the case of fiber reinforced sand in which they concentrate in the direction of failure. In general, reinforced soils (sand-fiber) reach higher values of stress than in sandy soil.

The plastic deformation at the integration points (E_2) is a scalar variable used to present the non-elastic deformation of the material. When the variable is greater than zero, it means that the material has yielded and when the variable is less than zero it means that the material is still in elasticity (Abaqus, 2010). The blue color zone in Fig. 7 indicates that

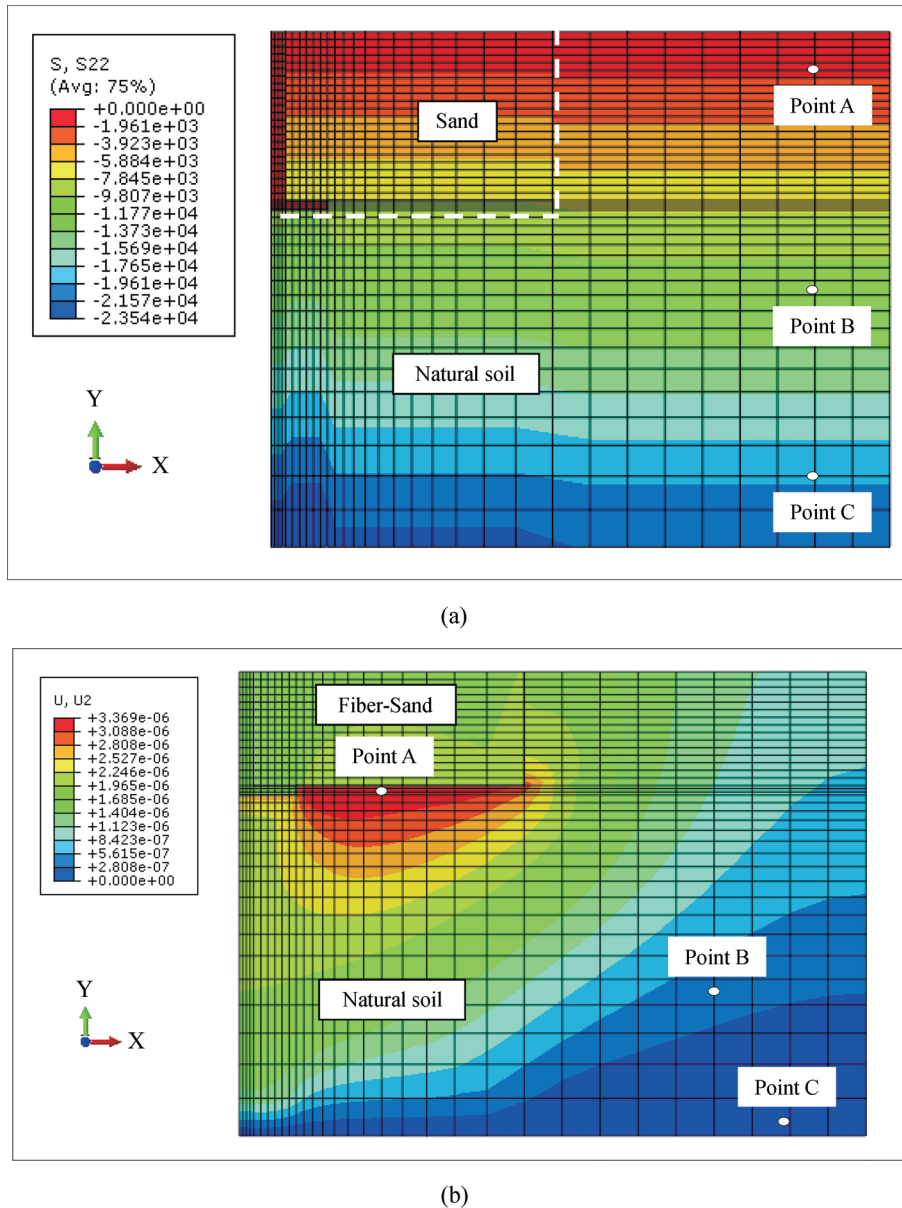


Figure 4 - Initial conditions of the numerical model a) Initial stress state in an embedded sand for $H/D = 1.5$ b) Initial displacements in an embedded fiber reinforced sand for $H/D = 1.0$.

the material has elastic behaviour; it can be observed that the plastification in all cases is concentrated in the elements that are near the upper corner of the plate and follow the trajectory of the rupture surface obtained experimentally.

6.2. Comparison

Figure 8a shows the ultimate pullout load (P_u) for each H/D ratio of the numerical models and the field tests. It can be seen that in the comparisons of the P_u for the fiber reinforced sand, the H/D ratio of 1.0 and 1.5 presents very similar strength gains with a difference of 0.1 kN and 0.2 kN respectively. Additionally, the difference of P_u for the sand was 0.4 kN and for the fiber reinforced sand was

0.1 kN for H/D ratio of 1.0. For the H/D ratio of 1.5 the difference of P_u for the sand was 0.1 kN and for the fiber reinforced sand was 0.2 kN; nevertheless, for the H/D ratio of 2.0 there is a considerable difference since for both sand and fiber reinforced sand we have a difference of 1.4 kN. In other words, there are variations between the numerical model and the field test from 0.1 to 0.4 kN for a H/D ratio of 1.0 and 1.5 in sand and fiber reinforced sand, but in the H/D ratio of 2.0 we have a variation of 1.4 kN.

In Fig. 8a the comparison of the strength gains between the sand and the fiber reinforced sand in field tests for a H/D ratio of 1.0 show 2.4 kN and 4.1 kN respectively, which is an approximate gain of 40.0%. The numerical

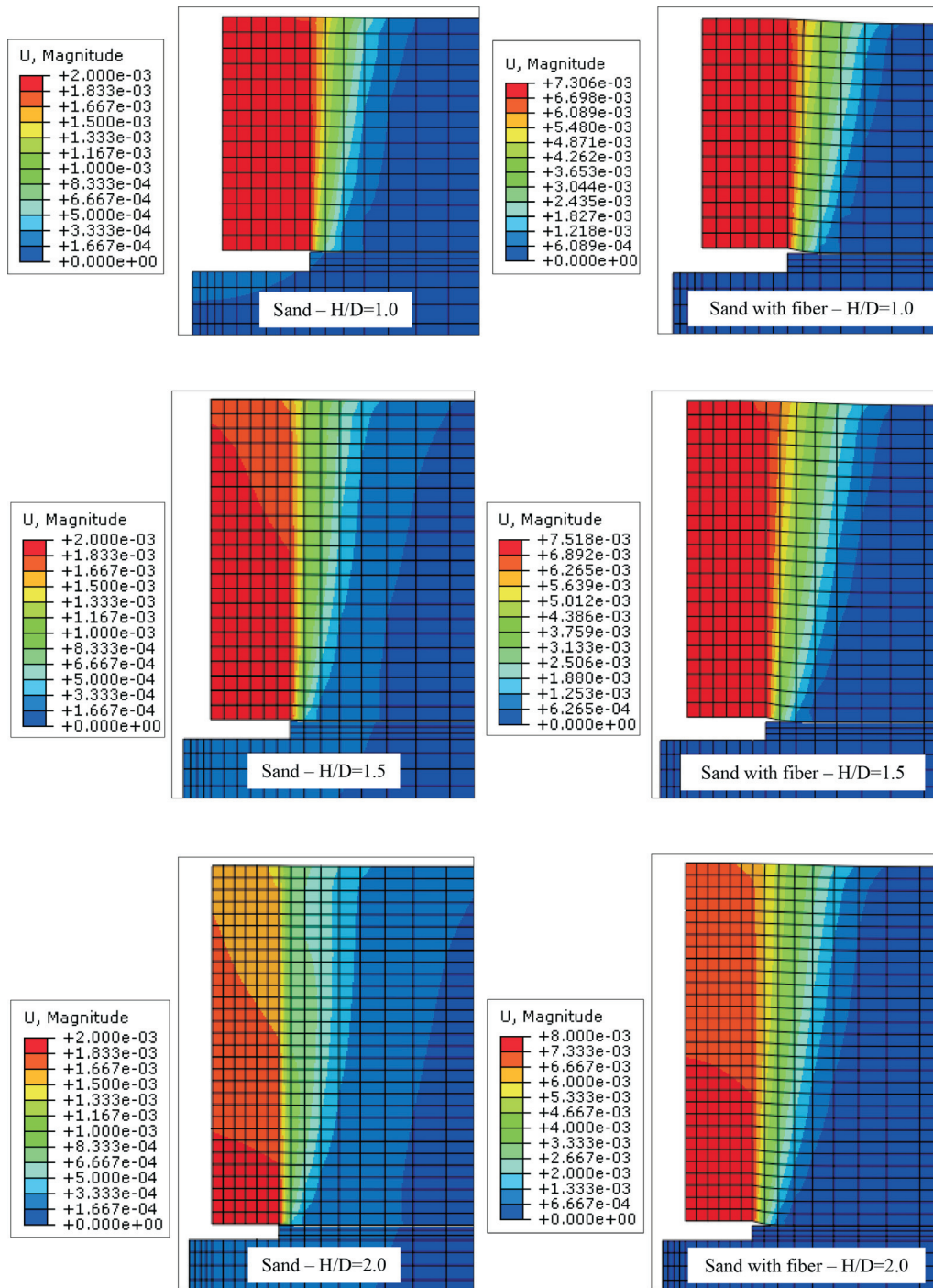


Figure 5 - Displacements (U , mm) for an embedded sand and fiber reinforced sand.

model, with the resistance parameters adjusted for the same relation, has 2.8 kN in a sand backfill and 4.0 kN in a fiber reinforced sand backfill which is a gain of approximately 30.0%. In the same figure, the H/D ratios of 1.5 and 2.0 for a field test and numerical model show a gain resistance of approximately 30.0%. In other words, in an arithmetic mean there are resistance gains from 35.0 to 40.0% for fiber

reinforced sand backfill in the field tests and in the numerical model.

Although Fig. 8a showed 35.0 to 40.0% strength gain, when the analysis considers the ratio of the P_u reinforced against P_u , a tendency of strength gain decrease is observed (Fig. 8b). Figure 8a showed the gain of P_u with the use fiber reinforced, and the Fig. 8b showed that the gain rate decreased with the increase of the H/D ratio.

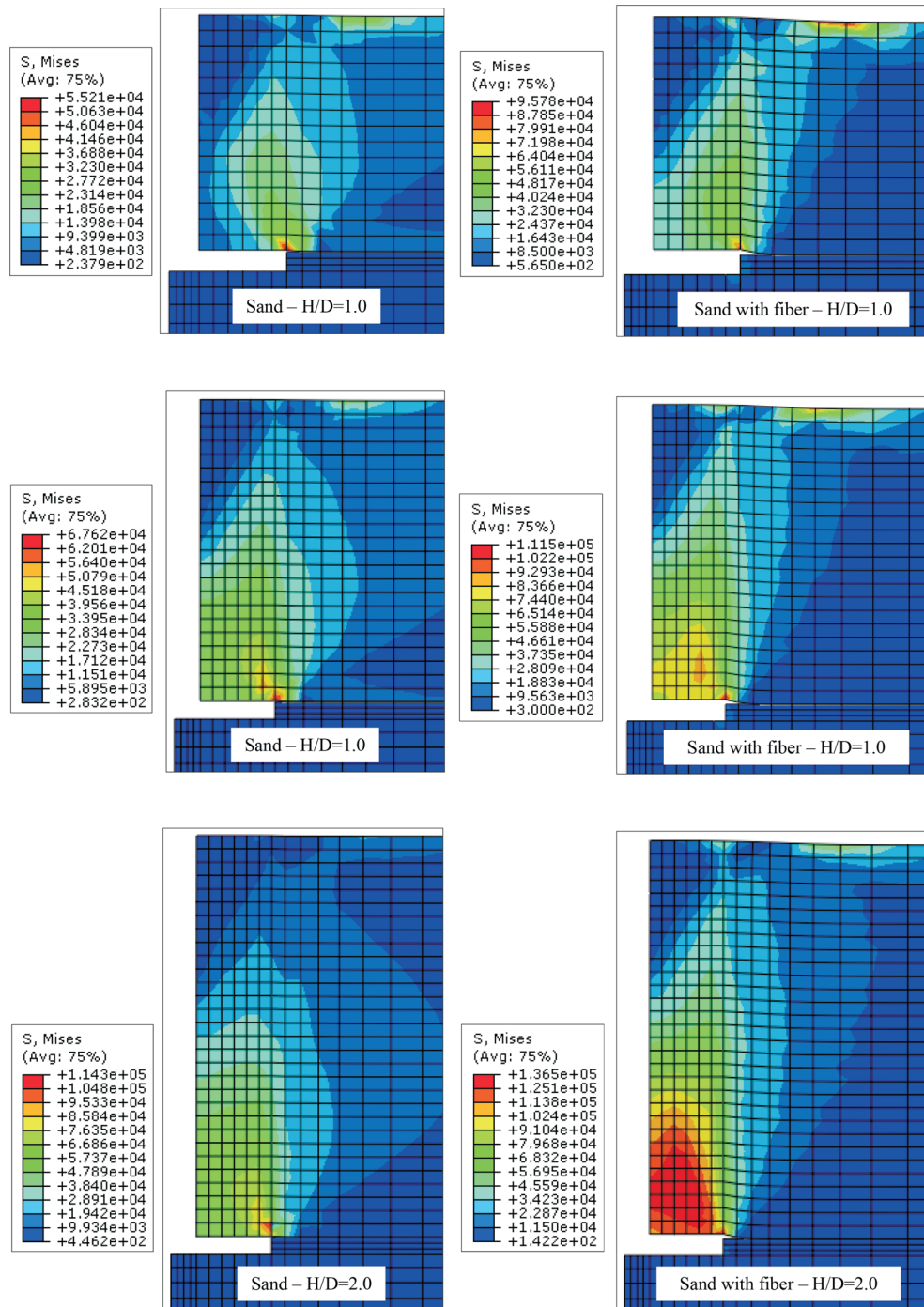


Figure 6 - Stress at the integration points - Mises (S , Pa) for an embedded sand and fiber reinforced sand.

7. Estimation of the Ultimate Pullout Capacity of Plate Anchors

The ultimate pullout load (P_u) of a steel plate in sand is generally expressed as a function of the landfill weight (γ) and the depth of the plate anchor (H) as shown in Eq. 14 (Rowe & Davis, 1982b; Merifield *et al.*, 2003). There are not other equations in the literature that refer to a fiber reinforced sand backfill.

$$q_u = \gamma \times H \times N_\gamma \tag{14}$$

The pullout factor N_γ was obtained from numerical modeling with Abaqus for H/D ratios of 1.0, 1.5 and 2.0 and for different friction angles (ϕ) and for a sand and sand-fiber backfill as shown in Figs. 9a and 9b. The presented figures can be used for steel plates of different dimensions, but between the H/D ratios of 1.0, 1.5 and 2.0 in order to de-

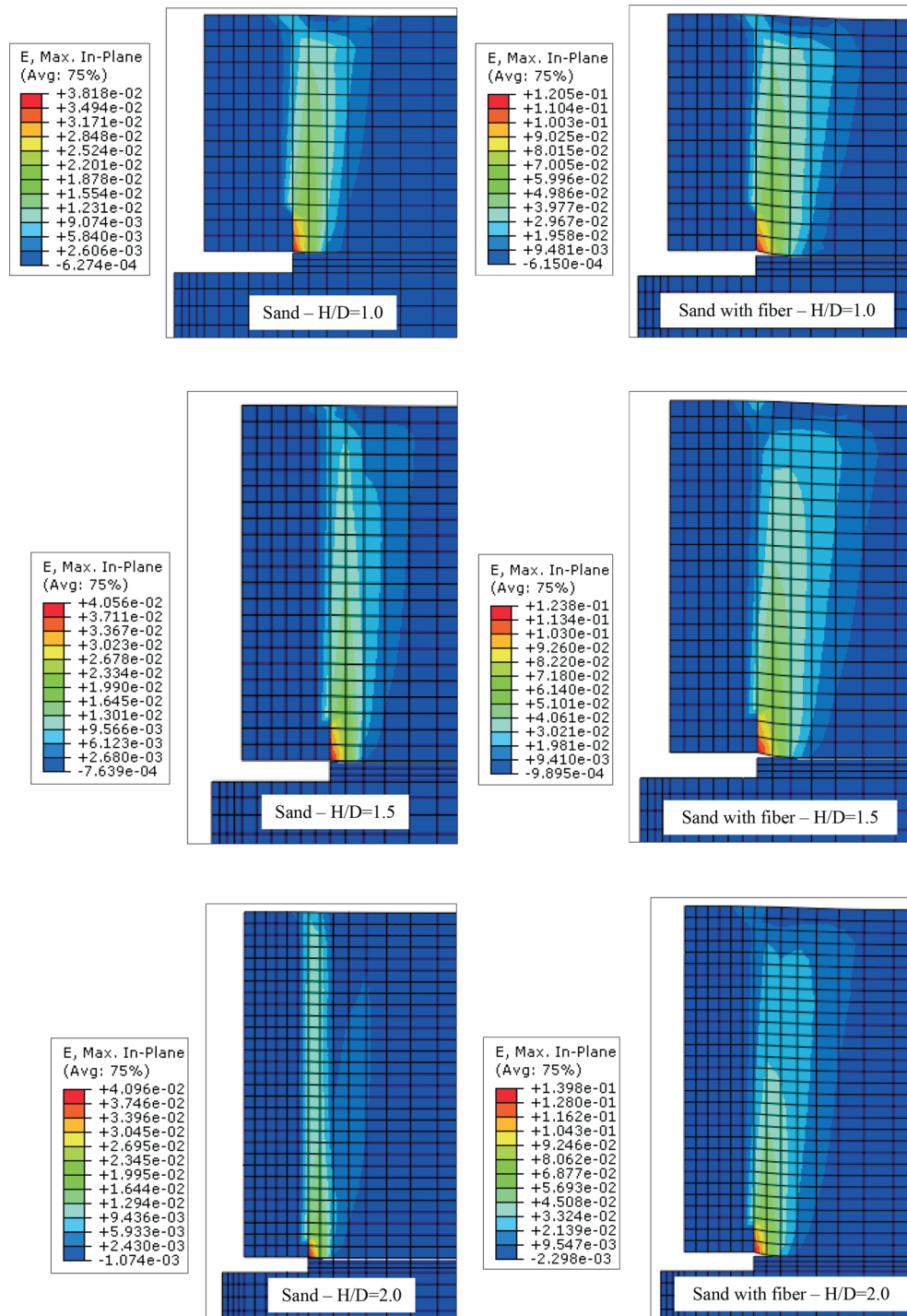


Figure 7 - Deformation at the integration points - Maximum in the main plane (E_2) for an embedded sand and fiber reinforced sand.

termine the P_u value in sand and fiber reinforced sand embankments from the friction angle of the material.

7.1. Comparison

Figure 10a shows the Pullout factor values obtained by FEM and some methods presented in the literature for H/D ratios of 1.0, 1.5 and 2.0 at a friction angle (ϕ) of 30.0°

in sand backfill. The use of this friction angle was only for comparing the present numerical model with other methods in the literature; in addition, the methods used for estimating the pullout factor were not used for fiber reinforced sand backfill. The different factors N_γ were obtained from the literature and this factor depend of the H/D ratio, γ and ϕ of the material backfill.

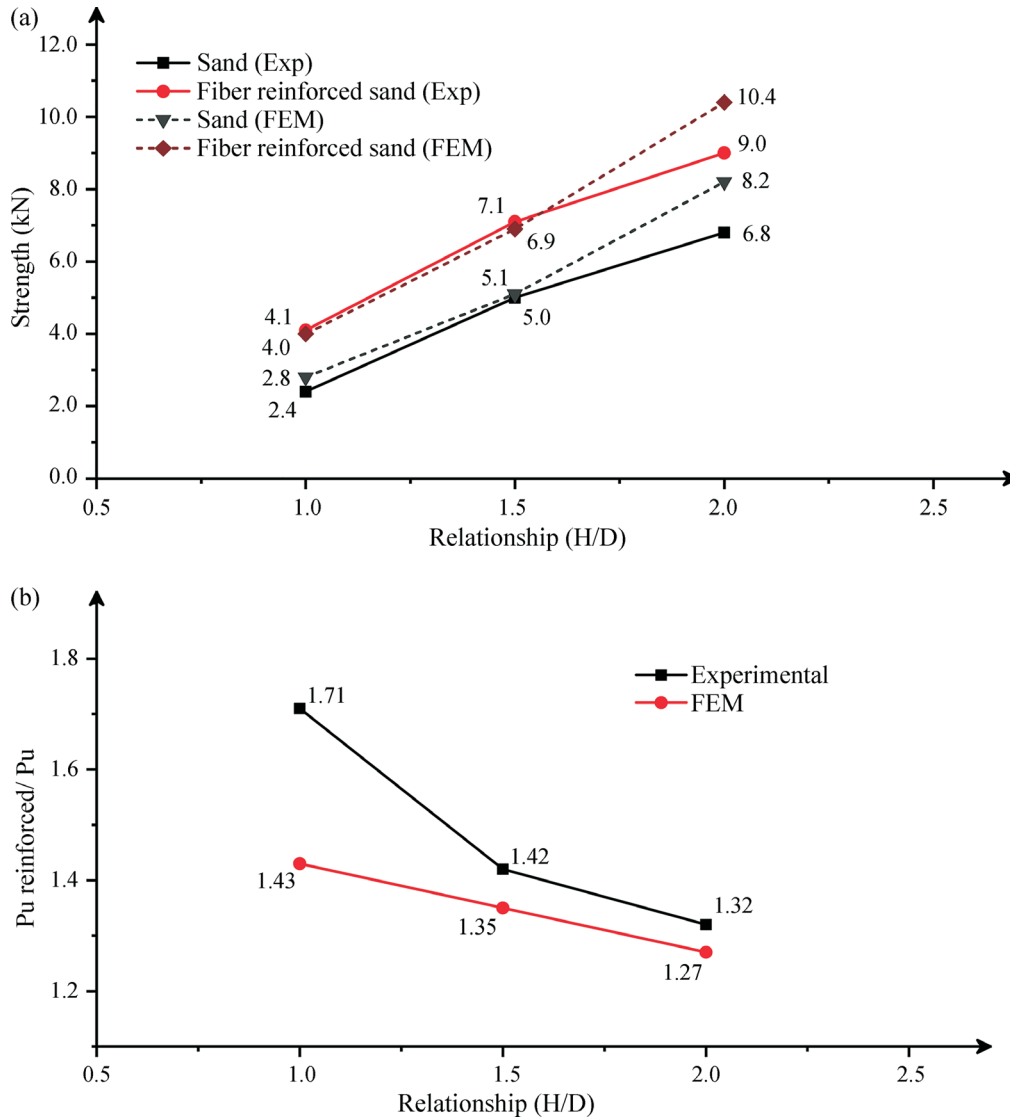


Figure 8 - Comparison in different H/D ratios of (a) the ultimate pullout load (P_u) (b) the relationship P_u reinforced and P_u .

Of the nine remaining methodologies employed in the Fig. 10a, five methods (Balla, 1961; Meyerhof & Adams, 1968; Murray & Geddes, 1987; Saedy, 1987; Merifield *et al.*, 2003) were extremely conservative in comparison with the proposed method. Three methods (Sarac, 1989; Ghaly & Hanna, 1994; Grenoble method in Biarez & Baraud, 1968; Martin, 1963 & 1966) presented overestimates for all load tests. The Hanna model (Hanna *et al.*, 2007) presented the best estimates, with differences between 18.0% for a H/D ratio of 1.0, 7.0% for a H/D ratio of 1.5 and 10.0% for a H/D ratio of 2.0 compared to the proposed model.

Also for sand backfill, Fig. 10b presents a comparison between the values of the load tests done in the laboratory or field by different authors where five authors (Murray & Geddes, 1987 for a friction angle (ϕ) of 44.0°; Ilamparuthi

et al., 2002 for a ϕ of 43.0°; Balla, 1961 for a ϕ of 38.0°; Ghaly *et al.*, 1991 for a ϕ of 30.0°; Baker & Kondner, 1966 for a ϕ of 42.0°) were extremely conservative when compared with the proposed method. Two papers (Ghaly *et al.*, 1991 for friction angles (ϕ) of 35.0° and 40°; Kwasniewski *et al.*, 1975 for a ϕ of 28.0°) presented overestimates for all load tests. The field tests of Bembem & Kupferman (1975) for a ϕ of 46.0° and Ruver (2011) for a ϕ of 39.2° presented the best estimates, with differences of 0.40% for a H/D ratio of 2.0 in Bembem & Kupferman (1975) and the proposed method. For the Ruver (2011) tests, there is a difference of 16.9% for a H/D ratio of 1.0, 3.0% for a H/D ratio of 1.5 and 16.6% for a H/D ratio of 2.0 compared to the proposed model.

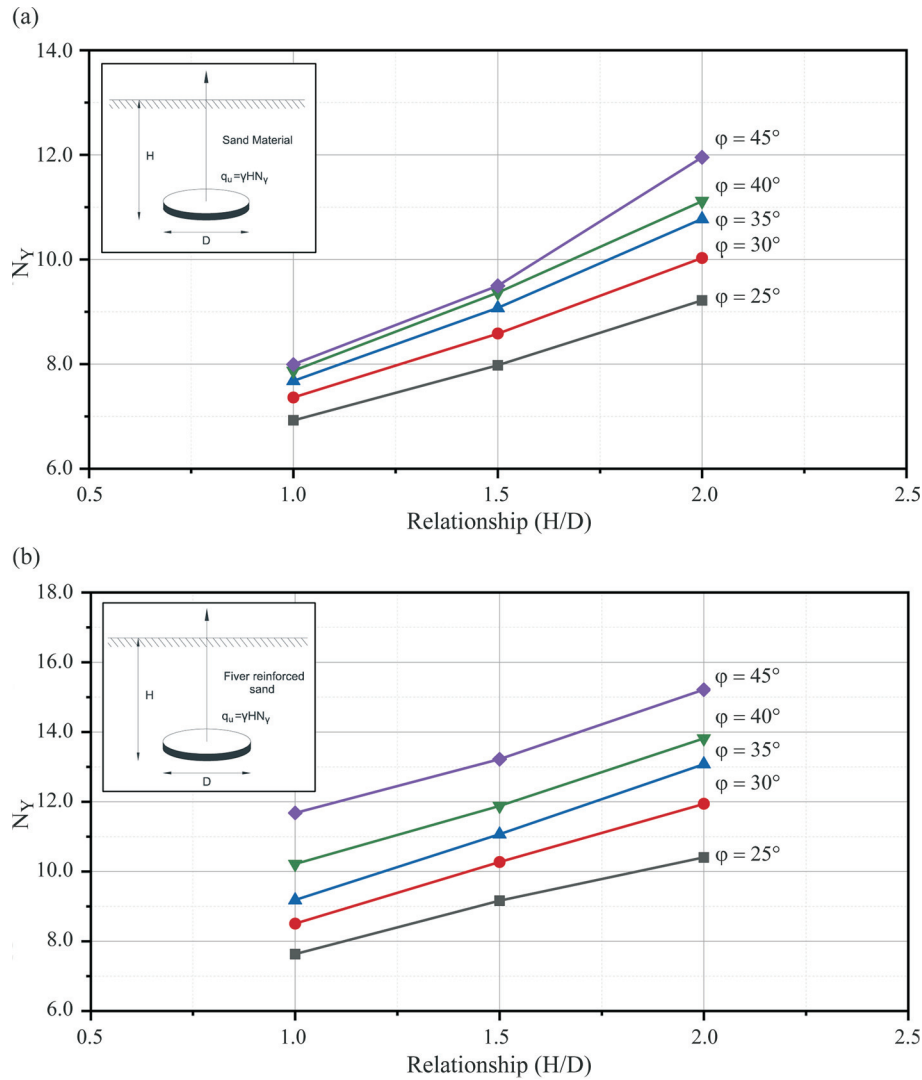


Figure 9 - Pullout factor for embedded a) sand and b) fiber reinforced sand.

8. Conclusions

The outcomes from this work can be summarized as follows:

- The present work introduces a method for designing and analyzing vertical pullout of plate anchors embedded in sand and fiber reinforced sand. There are still divergences in determining the pullout factor ($N\gamma$). Hence, further investigations are needed to clarify this basic but important topic. The present work emphasizes the criterion for determining the $N\gamma$ of plate anchors in sand and fiber reinforced sand. After a review of current studies on this topic, the criterion for determining γ based on finite element analysis is recommended. This criterion is validated firstly by model tests and then applied to circular plate anchors with different embedment ratios in both

sand and fiber reinforced sand to calculate bearing capacity factors.

- The proposed methodology conforms to two capacity factors. The first, the value of $N\gamma$ can be obtained by using a sand backfill. The second, to be obtained by using a fiber reinforced sand backfill can be generally applied for different H/D ratios. The ultimate pullout load (P_u) in the present analysis is definitely recommended, in which a non-associated flow ($\phi \neq \psi$) was used.
- The numerical model for a sand backfill had an approximate difference of $\pm 2.0\%$ from the ultimate pullout load (P_u) in the field test for a H/D ratio of 1.5 which shows that the model reproduced with satisfactory accuracy the result obtained in real scale. In the same way, the numerical model calibrated for a fiber reinforced sand backfill had an approximate difference of $\pm 3.0\%$ from the P_u in the field test for a H/D ratio of 1.0.

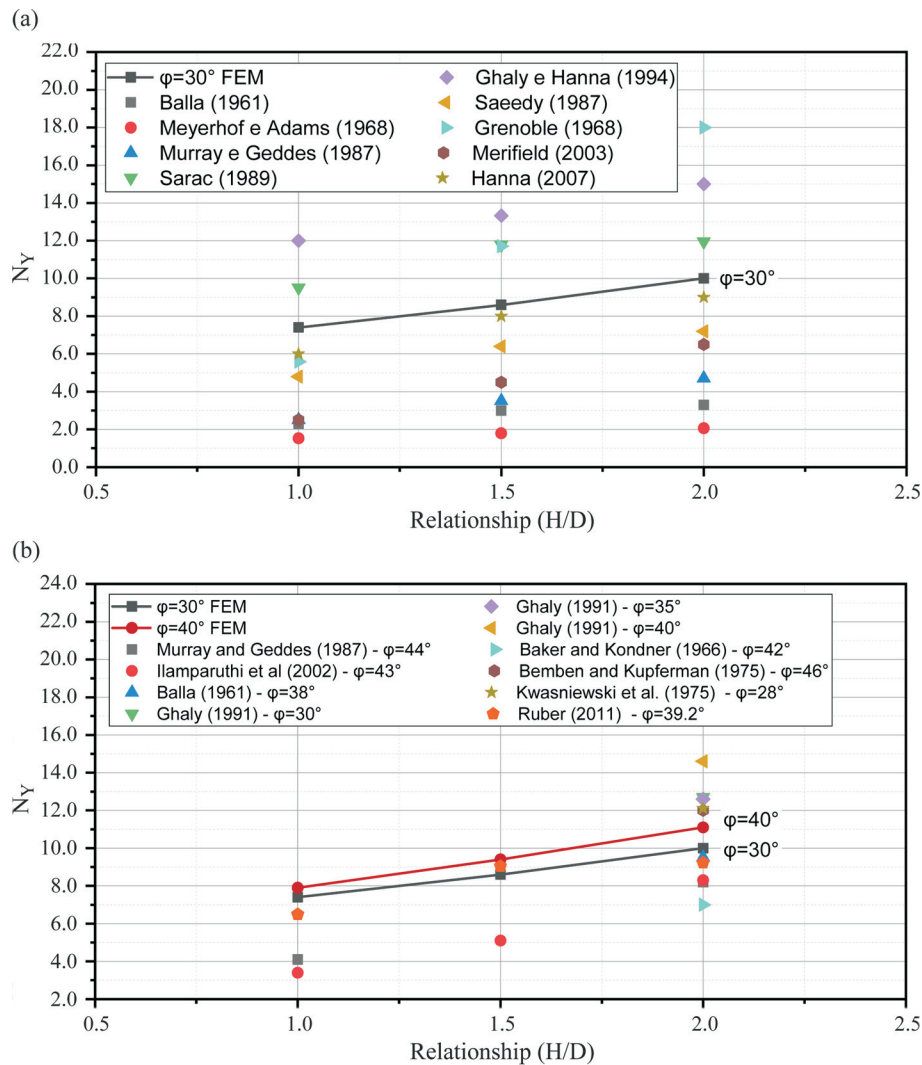


Figure 10 - Comparison of pullout factor for embedded sand in a) methods of the literature and b) field tests.

- By comparing the resistance gains in the numerical models of sand and fiber reinforced sand backfill with those from the field tests for a H/D ratio of 1.0, 1.5 or 2.0, the average resistance gain is about 40.0% to 35.0%. The gain rate decreases with the increase of the H/D ratio.
- Although the H/D ratio varied within a limited range of 1.0, 1.5 and 2.0, the simulations and their respective results for the ultimate pullout load (P_u) represent an important step towards understanding the application of this approach in sand and fiber reinforced sand backfills.

Acknowledgments

The authors wish to thank the Brazilian Research Council (CNPq), the Federal University of Rio Grande do Sul (UFRGS) and the São Paulo University (USP) for funding the research group.

References

Abaqus (2010). Analysis User's Manual. Version 6.10. Dassault Systemes Simulia Corp.

Andresen, L.; Petter Jostad, H. & Andersen, K. (2011). Finite element analysis applied in design of foundations and anchors for offshore structures. *Int. J. Geomech.*, 11(6): 417-430.

ASTM (1993). Standard Practice for Classification of Soils for Engineering Purposes (Unified Soil Classification System). ASTM D 2487, West Conshohocken, Philadelphia.

ASTM (1994). Standard Test Method for Bearing Capacity of Soil for Static Load and Spread Footings. ASTM D 1194, West Conshohocken, Philadelphia.

ABNT (1995). Rochas e Solos, NBR 6502. Rio de Janeiro, Brasil.

- Balla, A. (1961). The resistance to breaking-out of mushroom foundations for pylons. Proc. 5th International Conference on Soil Mechanics and Foundations Engineering, Paris, France, vol. 1, pp. 569-576.
- Baker, W.H. & Kondner, R.L. (1966). Pullout load capacity of a circular earth anchor buried in sand. Highway Research Record, No. 108, pp 1-10.
- Bemben, S.M. & Kupferman, M. (1975). The vertical holding capacity of marine anchor flukes subjected to static and cyclic loading. In: Proceedings of the 7th Offshore Technology Conference, Houston, Texas, OTC2185, pp. 363-374.
- Bhattacharya, P.; Bhowmik, D.; Mukerjee, S.P. & Chattopadhyay, B.C. (2008). Pullout behavior of square anchors in reinforced clay. Proc. 12th Conference of International Association for Computer Methods and Advances in Geomechanics (IACMAG); proceedings of the Goa/India.
- Bhattacharya, P. & Kumar, J. (2014). Pullout capacity of inclined plate anchors embedded in sand. Can. Geotech. J., 51:1365-1370.
- Bhattacharya, P. & Kumar, J. (2016). Uplift capacity of anchors in layered sand using finite-element limit analysis: formulation and results. Journal of Geotechnical and Geoenvironmental Engineering, 16(3): 04015078.
- Biarez, J. & Barraud, Y. (1968). Adaptation des fondations de pylônes au terrain par les méthodes de la mécanique des sols. Rapport 22-06 de la CIGRÉ, Paris.
- Burd, H.J. & Frydman, S. (1997). Bearing capacity of plane-strain footings on layered soils. Canadian Geotechnical Journal, 34: 241-253.
- Chen, W.F. (1982). Constitutive Equations for Engineering Materials. Wiley-Interscience Publication, John Wiley & Sons, New York, 580 p.
- CIGRÉ (2008). Reliability Based Calibration of Foundation Strength Factor Using Full-Scale Test Data. A Guide for Design Engineers, Technical brochures WG B2.07, March 2008, 116 p.
- Consoli, N.C.; Heineck, K.S.; Casagrande, M.D.T. & Coop, M.R. (2007a). Shear strength behavior of fiber-reinforced sand considering triaxial tests under distinct stress paths. Journal of Geotechnical and Geoenvironmental Engineering, 133(11):1466-1469.
- Consoli, N.C.; Casagrande, M.D.T. & Coop, M.R. (2007b). Performance of fibre-reinforced sand at large shear strains. Géotechnique, 57(9):751-756.
- Consoli, N.C.; Lehane, B.M.; Helinski, M.; Richards, D.J. & Rattley, M.J. (2007c). On the pullout of footing backfill with cemented sand. Proc. International Workshop on Applications of Computational Mechanics in Geotechnics Engineering, Portugal, 2007. Taylor and Francis Group, London, pp. 331-339.
- Consoli, N.C.; Festugato, L. & Heineck, K.S. (2009a). Strain hardening behaviour of fibre-reinforced sand in view of filament geometry. Geosynthetics International, 16(2):109-115.
- Consoli, N.C.; Casagrande, M.D.T.; Thomé, A.; Dalla Rosa, F. & Fahey, M. (2009b). Effect of relative density on plate tests on fiber reinforced sand. Géotechnique, 59(5):471-476.
- Consoli, N.C.; Ruver, C.A.; Girardello, V.; Festugato, L. & Thomé, A. (2012). Effect of polypropylene fibers on the uplift behavior of model footings embedded in sand. Technical Note. Geotextiles and Geomembranes, 19(1): 79-84.
- Consoli, N.C.; Ruver, C.A. & Schnaid, F. (2013). Uplift Performance of anchor plates embedded in cement-stabilized backfill. Journal of Geotechnical and Geoenvironmental Engineering, 139(3): 511-517.
- Cruz, R.C. (2008). Influência de Parâmetros Fundamentais na Rigidez, Resistência e Dilatância de uma Areia Artificialmente Cimentada. Tese de Doutorado em Engenharia Civil, Universidade Federal do Rio Grande do Sul, 216 p.
- Cudmani, R.O. (1994). Estudo do Comportamento de Sapatas Assentes em Solos Residuais Parcialmente Saturados através de Ensaios de Placa. Dissertação de Mestrado em Engenharia Civil, Universidade Federal do Rio Grande do Sul, 150 p.
- Dalla Rosa, F. & Thomé, A. (2004a). Obtenção das Características de Resistência e Deformabilidade de um Solo Residual de Basalto Através de Ensaios de Placa. Proc. XXXI Jornadas Sud-Americanas Engenharia Estrutural, CD-Rom, p. 112.
- Dalla Rosa, F.; Thomé, A. & Ruver, C.A. (2004b). Determinação de alguns parâmetros geotécnicos do campo experimental de geotecnia da Universidade de Passo Fundo - RS. Proc. 1^o Simpósio Brasileiro de Jovens Geotécnicos (Geo Jovem 2004), CD-Rom, pp. 1-6.
- Dalla Rosa, F. (2009). Efeito do Estado de Tensões de Cura no Comportamento de Uma Areia Artificialmente Cimentada. Tese de Doutorado em Engenharia Civil, Universidade Federal do Rio Grande do Sul, 191 p.
- Das, B.M. & Seeley, G.R. (1975). Breakout resistance of shallow horizontal anchors. J. Geotech. Engrg. Div., 101(9):999-1003.
- Dickin, E.A. (1988). Uplift behavior of horizontal anchor plates in sand. J. Geotech. Engrg., 10.1061/(ASCE)0733-9410(1988)114:11(1300), 1300-1317.
- Thomé, A., Donato, M., Consoli, N.C. & Graham, J. (2005). Circular footings on a cemented layer above weak foundation soil. Canadian Geotechnical Journal, v. 42, 1569-1584.
- Downs, D.I. & Chieruzzi, R. (1966). Transmission tower foundations. Journal of the Power Division, ASCE, 92(2):91-114.

- Drucker, D.C. & Prager W. (1952). Soil mechanics and plastic analysis or limit design. *Quarterly of Applied Mathematics*, 10(2):157-165.
- Festugato, L. (2008). Análise do Comportamento mecânico de um solo micro-reforçado com fibras de distintos Índices Aspecto. Dissertação de Mestrado, Universidade Federal do Rio Grande do Sul, Porto Alegre, Brasil.
- Ghaly, A.M.; Hanna, A.M. & Hanna, M. (1991). Uplift behavior of screw anchors in sand. I: Dry sand. *J Geotech Eng ASCE* 117(5):773-793.
- Ghaly, A.M. & Hanna, A.M. (1994). Ultimate Pullout resistance of single vertical anchors. *Can Geotech Journal*, 31(5):661-672.
- Hanna, A.; Ayadat, T. & Sabry, M. (2007). Pullout resistance of single vertical shallow helical and plate anchors in sand. *Geotech Geol Eng.*, 25:559-573.
- Hellwany, S. (2007). *Applied Soil Mechanics with ABAQUS Applications*. John Wiley & Sons, New Jersey, 400p.
- Hibbit, D.; Karlsson, B. & Sorensen, P. (1998). Inc. ABAQUS/Explicit User's Manual. Version. 5.8. Ed. Hibbitt, Karlsson & Sorensen, Dallas, USA, 1306 p.
- Hibbit, D.; Karlsson, B. & Sorensen, P. (2006). ABAQUS/Standard User's Manual. Ed. Hibbitt, Karlsson & Sorensen, Dallas, USA, 1505 p.
- Houlsby, G. (1991). How the Dilatancy of Soils Effects Their Behaviour. University of Oxford, Department of Engineering Science, 1-30p.
- Ilamparuthi, K.; Dickin, E.A. & Muthukrisnaiah, K. (2002). Experimental investigation of the uplift behaviour of circular plate anchors embedded in Sand. *Can Geotech J.*, 39(3): 648-664.
- Jesmani, M.; Kamalzare, M. & Nazari, M. (2013). Numerical study of behavior of anchor plates in clayey soils. *Int. J. Geomech.*, 10.1061/(ASCE)GM.1943-5622.0000236:502-513.
- Khatri, V.N. & Kumar, J. (2011). Effect of anchor width on pullout capacity of strip anchors in sand. *Can. Geotech. J.*, 48(3):511-517.
- Kouzer, K.M. & Kumar, J. (2009). Vertical uplift capacity of equally spaced horizontal anchors in sand. *Int. J. Geomech.*, 10.1061/(ASCE)1532-3641(2009)9:5(230):230-236.
- Kumar, J. (2001). Seismic vertical uplift capacity of strip anchors. *Géotechnique*, 51(3):275-279.
- Kumar, J. & Kouzer, K.M. (2008). Vertical uplift capacity of horizontal anchors using upper bound limit analysis and finite elements. *Can. Geotech. J.*, 45(5):698-704.
- Kwasniewski, J.; Sulikowska, I. & Walker, A. (1975). Anchors with vertical tie rods. In: *Proc. 1st Baltic Conference, Soil Mechanics and Foundation Engineering*, Gdansk, Poland, pp 122-133.
- Lopes Junior, L.S. & Thomé, A. (2005). Provas de Carga Estática em Estacas Escavadas de Pequeno Diâmetro, Executadas na Região de Passo Fundo, Rio Grande do Sul. *Seminário de Engenharia Geotécnica do Rio Grande do Sul (GEORS2005)*, Passo Fundo/RS, 2005.
- Mántaras, F.M. (1995). Análise Numérica do Ensaio Presiométrico Aplicada à Previsão do Comportamento de Fundações Superficiais em Solos Não Saturados. Dissertação de Mestrado em Engenharia Civil, Universidade Federal do Rio Grande do Sul, PPGEC, p150 p.
- Martin, D. (1963). *Fondations Profondes Soliciitées à L'Arrachement en Milieu Cohérent Tridimensionnel*. Thèse de Doctorat de Spécialité, Université de Grenoble.
- Martin, D. (1966). *Étude a la Rupture de Different Ancrages Soliciitées Verticalement*. Thèse Docteur-Ingénieur, Faculté des Sciences de Grenoble, Grenoble.
- Menétrey, P. & Willam, K. (1995). Triaxial failure criterion for concrete and its generalization. *ACI Structural Journal*, 92(3): 311-318.
- Merifield, R.S.; Sloan, S.W.; Abbo, A.J. & Yu, H.S. (2001). The ultimate pullout capacity of anchors in frictional soils. *Proc. 10th Int. Conf. on Computer Methods and Advances in Geomechanics*, Tucson, pp. 1187-1192.
- Merifield, R.S.; Sloan, S.W. & Lyamin, A.V. (2003). Three Dimensional Lower Bound Solutions for the Stability of Plate Anchors in Sand. *Faculty of Engineering and Surveying Technical Reports*, University of Southern Queensland, 40 p.
- Merifield, R.S. & Sloan, S.W. (2006). The ultimate pullout capacity of anchors in frictional soil. *Can. Geotech. J.*, 43(8):852-868.
- Merifield, R.S.; Lyamin, A.V. & Sloan, S.W. (2006). Three-dimensional lower-bound solutions for the stability of plate anchors in sand. *Géotechnique*, 56(2):123-132.
- Meyerhof, G.G. & Adams, J.I. (1968). The ultimate uplift capacity of foundations. *Canadian Geotechnical Journal*, 5(4): 225-244.
- Meyerhof, G.G. (1973). Uplift resistance of inclined anchors and piles. *Proc. 8th Int. Conf. on Soil Mech.*, A.A. Balkema, Rotterdam, v. 2, pp. 167-172.
- Mors, H. (1959). The behaviour of mast foundations subject to tensile forces. *Bautechnik*, 36(10):367-378.
- Murray, E.J. & Geddes, J.D. (1987). Uplift of anchor plates in sand. *J. Geotech. Eng.*, 10.1061/(ASCE)0733-9410(1987)113:3(202):202-215.
- Murray, E.J. & Geddes, J.D. (1989). Resistance of passive inclined anchors in cohesionless medium. *Géotechnique*, 39(3):417-431.
- Ovesen, N.K. (1981). Centrifuge tests on the uplift capacity of anchors. *Proc. 10th Int. Conf. on Soil Mechanics and Foundation Eng.*, A.A. Balkema, Rotterdam, v. 1, pp. 717-722.

- Pearce, A. (2000). Experimental Investigation Into the Pullout Capacity of Plate Anchors in Sand. M.Sc. Thesis, University of Newcastle, Australia.
- Ratley, M.J.; Lehane, B.M.; Consoli, N.C. & Richards, D.J. (2008). Uplift of shallow foundations with cement-stabilised backfill. Proc. Institution of Civil Engineers, Ground Improvement, ICE, 161(2):103-110.
- Rowe, R.K. & Booker, J.R. (1981). The elastic displacement of single and multiple underream anchors in a Gibson soil. Géotechnique, 31(1):125-141.
- Rowe, R.K. & Davis, E.H. (1982a). The behaviour of anchor plates in clay. Géotechnique, 32(1):9-23.
- Rowe, R.K. & Davis, E.H. (1982b). The behaviour of anchor plates in sand. Géotechnique, 32(1):25-41.
- Ruver, C.A. (2011). Estudo do Arrancamento de Fundações em Solos Tratados com Cimento. Tese de Doutorado, Escola de Engenharia, Universidade Federal do Rio Grande do Sul, 220 p.
- Saedy, H.S. (1987). Stability of circular vertical anchors. Can. Geotech. J., 24(3):452-456.
- Santos, A.P.S. (2008). Estudo do Comportamento de Misturas Solo-Cimento-Fibra sob Altas Tensões. Tese de Doutorado em Engenharia Civil, Universidade Federal do Rio Grande do Sul, 171 p.
- Sarac, D.Z. (1989). The uplift capacity of shallow buried anchor slabs. Proc. International Conference on Soil Mechanics and Foundation Engineering. Montreal, Canada, pp. 1213-1216.
- Silva dos Santos, A.P.; Consoli, N.C. & Baudet, B.A. (2010). The mechanics of fibre-reinforced sand. Géotechnique, 60(10):791-799.
- Souza, S. (1974). Ensaios Mecânicos de Materiais Metálicos. Edgard Blucher, São Paulo, 304 p.
- Song, Z.; Hu, Y. & Randolph, M.F. (2008). Numerical simulation of vertical pullout of plate anchors in clay. Journal of Geotechnical and Geoenvironmental Engineering ASCE, 134(6): 866-875.
- Subba Rao, K.S. & Kumar, J. (1994). Vertical uplift capacity of horizontal anchors. J. Geotech. Engrg., 10.1061/(ASCE)0733-9410(1994)120:7(1134):1134-1147.
- Susila, E. & Hryciw, R.D. (2003). Large displacement FEM modelling of the cone penetration test (CPT) in normally consolidated sand. International Journal for Numerical and Analytical Methods in Geomechanics, 27(7): 585-602.
- Thomé, A. (1999). Comportamento de fundações superficiais apoiadas em aterros estabilizados com resíduos industriais. Tese de Doutorado em Engenharia, CPGEC/UFRGS, Porto Alegre, 245 p.
- Trautmann, C.H.; O'Rourke, T.D. & Kulhawy, F.H. (1985). Uplift force-displacement response of buried pipe. J. Geotech. Engng ASCE 111(9):1061-1076.
- Vermeer, P.A. & Sutjiadi, W. (1985). The uplift resistance of shallow embedded anchors. Proc. 11th International Conference on Soil Mechanics and Foundation Engineering, San Francisco, A.A. Balkema, Rotterdam, v. 4, pp. 1635-1638.

List of Symbols

- c : Cohesion of the material
 c_2 : Cohesion that controls the cohesion Yield Stress
 CAX4: Four node axisymmetric elements
 CAX4P: Four node axisymmetric pore pressure elements
 CD: Consolidated drained
 D: Diameter of the plate anchor (m)
 e: Diverting eccentricity
 E: Modulus of elasticity
 E_1 : Meridian eccentricity
 E_2 : Plastic deformation at the integration points
 FEM: Finite Element Method
 F: Flow function
 G: Shear modulus
 G_1 : Plastic potential
 K: Isotropic condition
 H: Depth of the plate anchor (m)
 I: Stress invariant
 $N\gamma$: Pullout factor
 P_u : Ultimate pullout load (kN)
 p : Hydrostatic stress
 q : Equivalent Von Mises Stress
 p - t : Coordinate system
 r: Third invariant
 Rmc: Measure of the surface formation
 Rmw: Elliptic function
 S: Von Mises
 S_y : Deflection effort
 SPT: Standard penetration test
 t - s : Coordinate system
 U: Displacements
 X: Horizontal axis
 Y: Vertical axis
 $\delta\epsilon$: Small change of deformation
 ϵ_s : Shear deformation
 ϵ_v : Volumetric deformation
 θ : Lode angle
 ν : Poisson Ratio
 σ_u : Axial stress
 ϕ : Internal friction angle of the material
 ψ : Angle of dilatancy
 γ : Unit weight

Obtaining the Mechanical Parameters for the Hardening Soil Model of Tropical Soils in the City of Brasília

J.F.R. Rebolledo, R.F.P. León, J. Camapum de Carvalho

Abstract. In this article, the mechanical parameters of characteristic soils of the city of Brasília are obtained, calibrated and validated for the Hardening Soil (HS) model, based on laboratory and field test results obtained in previous research studies conducted in the Experimental Field of the University of Brasília (CEGUnB). The strength and compressibility parameters are obtained from triaxial CU tests (with isotropic and anisotropic consolidation) and one-dimensional consolidation tests, respectively. The obtained parameters are calibrated *via* explicit numerical modeling using the finite element method and the *SoilTest* module of Plaxis software. After the parameters are evaluated and calibrated, a geotechnical model characterizing the city of Brasília for HS is proposed. Finally, this geotechnical model is validated through the numerical modeling of load testing on footings and piles conducted at the CEGUnB. It is concluded that the mechanical behavior of the Brasília soils under natural moisture conditions can be modeled using the HS model.

Keywords: finite element method, Hardening Soil model, tropical soils, model validation and calibration, load testing.

1. Introduction

The tropical soils of the city of Brasília have been extensively studied in the Postgraduate Program in Geotechnics of the University of Brasília. A significant number of theses and dissertations have been developed on these soils, focusing on the investigation of their physical-chemical, mineralogical, structural, mechanical and hydraulic properties as well as the behavior of shallow and deep foundations. The use of numerical tools for research related to these soils is becoming increasingly common, including Plaxis software, among others. Plaxis is a more versatile analysis tool than other commercial programs for the analysis of practical problems and is increasingly employed by geotechnical companies all over the world. One of the most complete constitutive models of Plaxis is the Hardening Soil (HS) model (Schanz *et al.*, 1999; Brinkgreve *et al.*, 2014, 2015), which is capable of:

- 1) calculating the total strains using a stress-dependent stiffness that is different for loading and unloading/re-loading conditions;
- 2) modeling irreversible strains due to primary deviatoric loading (shear hardening); and modeling irreversible plastic strains due to primary compression under oedometric and isotropic loading (compression hardening).

Given this context, the objective of this study is to obtain, adjust and validate the mechanical parameters of characteristic soils of the city of Brasília for the HS model, making use of laboratory and field test results obtained in previous research studies conducted in the Experimental

Field of the Graduate Program in Geotechnics of the University of Brasília, and additionally to present a validation methodology that can be applied to any other soil type.

The methodology proposed herein begins with the evaluation of the strength and compressibility parameters of triaxial CU tests (with isotropic and anisotropic consolidation) and one-dimensional consolidation tests, respectively (Guimarães, 2002). Then, the parameters obtained for the HS model are calibrated through the explicit numerical modeling of the tests using the finite element method (FEM) and the *SoilTest* module of Plaxis software. Based on the evaluation and calibration of these parameters, a geotechnical model profile of the Experimental Field of the University of Brasília (CEGUnB) is proposed for the HS model. The profile is composed of characteristic soils of the city of Brasília: a deeply weathered soil mantle composed of lateritic soil, followed by a thin layer of transitional soil that overlaps the poorly weathered residual saprolite soil.

Finally, this geotechnical model is validated through the numerical modeling of the load testing of footings and piles conducted in the CEGUnB (Sales, 2000; Guimarães, 2002).

2. General Description of the Problem

2.1. General characteristics of the Federal District subsoil

The Federal District (DF) is located in the Central Plateau in the Center-West region of Brazil and is home to the city of Brasília, which is the federal capital of the country. The DF region is covered by a mantle of Tertiary-Quaternary detritus-lateritic soil composed mainly of red-yellow latosols, according to the Brazilian soil classifica-

Juan Félix Rodríguez Rebolledo, Dr., Associate Professor, Programa de Pós-Graduação em Geotecnia, Universidade de Brasília, Brasília, DF, Brazil, e-mail: jrodriguezr72@hotmail.com.

Raimundo Francisco Pérez León, Ph.D. Student, Programa de Pós-Graduação em Geotecnia, Universidade de Brasília, Brasília, DF, Brazil, e-mail: rai88mundo@gmail.com.

José Camapum de Carvalho, Ph.D., Professor, Programa de Pós-Graduação em Geotecnia, Universidade de Brasília, Brasília, DF, Brazil, e-mail: camapumdecarvalho@gmail.com.

Submitted on July 17, 2018; Final Acceptance on April 04, 2019; Discussion open until August 30, 2019.

DOI: 10.28927/SR.421061

tion system (Fig. 1). The thickness of this cover is quite diverse depending on the topography, vegetation and original rock and can range from centimeters to tens of meters. High degrees of weathering and leaching were responsible for the formation of this soil, which led to the development of a very porous, metastable aggregate structure with a large proportion of voids and, consequently, low density, called “porous clay” by local geotechnicians. Due to its aggregate state and metastable structure, this clay has a low penetration resistance standard (N_{SPT} from 1 to 6 strokes; stable meta structure) and high permeability (from 10^{-3} to 10^{-4} m/s; particles in an aggregate state), similar to that of fine granular soils, which, incidentally, is how its texture is presented in its natural state. Due to its high porosity and cementitious bond type, it has a highly unstable structure when subjected to increased moisture and/or changes in the stress state, almost always presenting a volume variation as high as the variation of these factors (referred to as a collapsible structure).

According to Ortigão & Macedo (1993), in the city of Brasília, along the pathway designed for the subway (*Asa Sul* neighborhood), it was found that the porous clay has a variable thickness ranging from 20 to 30 m, generally with a deep groundwater level, in some cases at 5.0 m depth, as occurs at the end of *Asa Sul*. The end of the porous clay layer is clearly identified in percussion drillings by the significant increase of N_{SPT} at the transition, followed by contact with the underlying saprolite soil.

For this study, the stratigraphy of the Experimental Field of the Postgraduate Program in Geotechnics of the University of Brasília (CEGUnB, Fig. 2) was considered representative of the city of Brasília. This Program has valuable geotechnical information obtained from surveys, field trials, laboratory tests and loading tests on superficial and deep foundations (Perez, 1997; Jardim, 1998; Sales, 2000; Guimarães, 2002; Mota, 2003; Coelho, 2013; Sales *et al.*, 2015). According to this information and the tropical

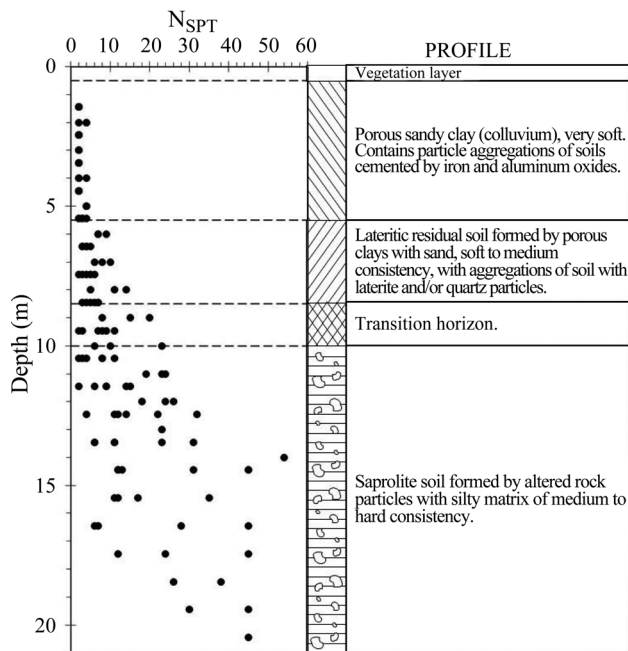


Figure 2 - Stratigraphic profile of the Experimental Field of the Postgraduate Program in Geotechnics of the University of Brasília (CEGUnB).

soil profiles proposed by Cruz (1987) and Cardoso (2002), it was possible to define the typical stratigraphic profile of the CEGUnB, as shown in Fig. 2.

2.2. Soil properties characteristic of the CEGUnB

The mechanical parameters for the HS model of the tropical soils of the CEGUnB were obtained through laboratory tests conducted by Guimarães (2002). Characterization, shear strength and compressibility tests were performed on undisturbed samples obtained at each meter depth in two open pit wells excavated up to eight and ten meters deep. Table 1 presents a summary with some of the

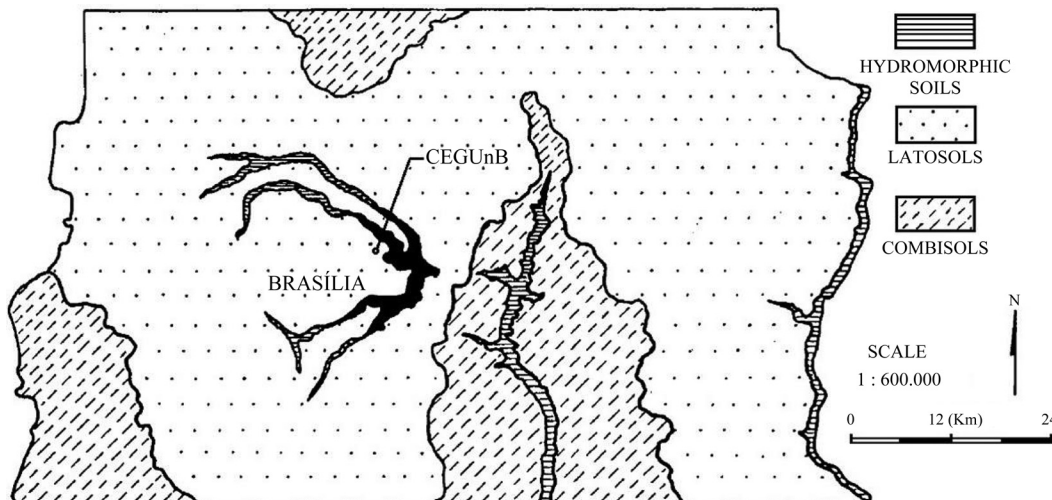


Figure 1 - Soils of the Federal District (modified from Mortari, 1994).

index properties of the most representative layers of the CEGUnB, and it should be noted that the particle size percentages were obtained by using the sodium hexameta-phosphate deflocculant for the fraction passing through a no. 10 sieve.

One-dimensional consolidation tests were conducted to obtain the compressibility and soil collapse parameters of the CEGUnB. For each collected sample, the following were performed: a “conventional” consolidation test, according to the Brazilian standard, and a “simple” consolidation test, according to the procedure recommended by Jennings and Knight (1975). In the “conventional” test, the samples were saturated after the first loading (5 kPa) and loaded until reaching a stress of 800 kPa. In the “simple” test, the sample was loaded with a natural moisture content until it reached a stress of 200 kPa; the specimen was then saturated and loaded until reaching a stress of 800 kPa. Fig. 3 shows the compressibility curves for the undisturbed sample obtained at 2 m depth.

In addition to the compressibility tests, consolidated undrained (CU) triaxial tests were performed. The test specimens were consolidated both isotropically and anisotropically following the K_0 (lateral earth pressure at rest) path. Both tests were performed with natural moisture (unsaturated) and saturated samples. The results of these tests

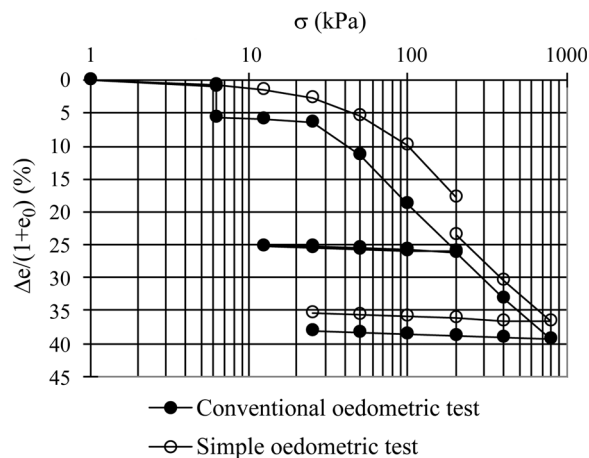


Figure 3 - Compressibility curves obtained from conventional and simple consolidation tests at a depth of 2 m (Guimarães, 2002).

Table 1 - Index properties of the characteristic layers of the CEGUnB.

Layer	G_s	γ (kN/m ³)	γ_{sat} (kN/m ³)	e	n (%)	G (%)	S (%)	M (%)	C (%)	S_{mat} (%)
A	2.65	14.2	16.9	1.4	58	0.7	38.0	26.5	34.8	44
B	2.63	15.9	18.0	1.0	51	3.3	27.4	25.0	44.3	51
C	2.74	17.7	18.6	1.0	50	0.3	6.8	86.8	6.1	82

A: porous sandy clay, B: residual lateritic soil, C: saprolitic soil, G_s : density of solids, γ : apparent specific weight of moist soil, γ_{sat} : saturated specific gravity, e : void ratio, n : porosity, G : percentage of gravel, S : percentage of sand M : percentage of silt, C : percentage of clay S_{mat} : degree of saturation under natural conditions.

are presented in section 5.2, with the validation of the constitutive model.

In the case of this study, the soil properties were analyzed exclusively in natural moisture conditions; therefore, only “simple” consolidation tests and triaxial tests with unsaturated test specimens were used.

2.3. Load tests conducted at the CEGUnB

The stratigraphic model and the mechanical parameters obtained for the HS model were validated through the simulation of load tests on piles and footings performed at the CEGUnB by Guimarães (2002) and Sales (2000), respectively.

Guimarães (2002) conducted five load tests on piles mechanically excavated at the site (0.3 m in diameter and 7.25 to 7.85 m in length). Table 2 presents the characteristics of the piles and the results obtained for each test, and Fig. 4 presents the load vs. displacement curves.

Sales (2000) performed a load test on a single concrete footing at the CEGUnB for natural moisture and saturated conditions. The footing (1 × 1 m² concrete plate, 15 cm thick) was built at the bottom of a square pit 80 cm deep. Figure 5 shows the results of the load tests under natural moisture and porosity conditions.

3. Hardening Soil Model

Soil constitutive models have advanced significantly from basic models that idealize the soil as a linear elastic medium or a perfectly plastic linear elastic medium. The Hardening Soil (HS) model is implemented in Plaxis soft-

Table 2 - Pile characteristics and load test results (Guimarães, 2002).

Pile #	Date	Length (m)	Maximum applied load (kN)	Maximum displacement (mm)
1	02/2000	7.65	270	16.10
2	08/2000	7.25	300	3.82
3	10/2000	7.80	240	8.71
4	03/2001	7.30	210	6.82
5	06/2000	7.85	270	9.42

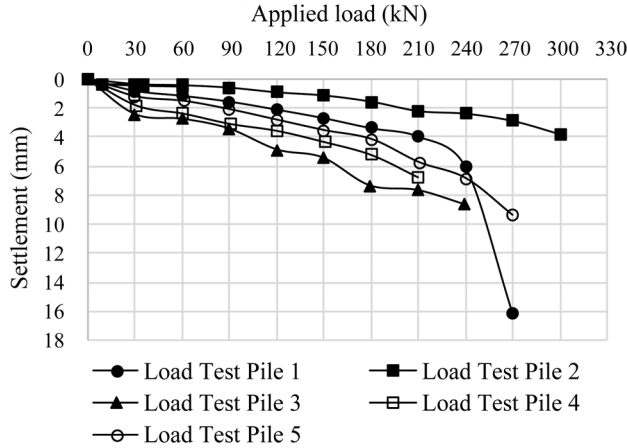


Figure 4 - Load vs. displacement curves (Guimarães, 2002).

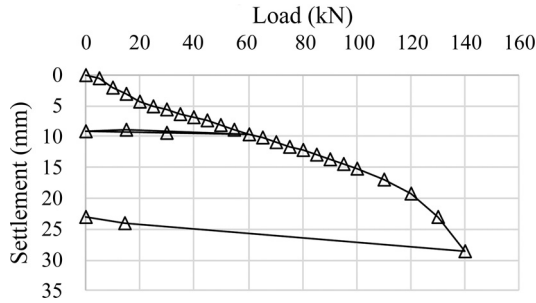


Figure 5 - Load tests of a single footing (Sales, 2000).

ware and is based on the theory of plasticity. Its main characteristics are described as follows:

- 1) The total strains are calculated using a stress-dependent stiffness.
- 2) The stiffness is defined for both loading and unloading/reloading conditions.
- 3) Modeling of irreversible strains due to primary deviatoric loading (shear hardening).
- 4) Modeling of irreversible plastic strains due to primary compression under oedometric and isotropic loading (compression hardening).
- 5) A non-associated flow rule is assumed for shear hardening, and an associated flow rule is assumed for compression hardening.
- 6) The Mohr-Coulomb failure criterion is applied.

In the HS model, the stress-strain relationship ($q - \varepsilon_1$) due to the primary load is hyperbolic (Kondner, 1963; Duncan & Chang, 1970) for a drained triaxial test (Fig. 6).

We then have:

$$\varepsilon_1 = \frac{1}{E_i} \frac{q}{1 - \frac{q}{q_a}}, \text{ for } q < q_f \quad (1)$$

where the initial stiffness E_i is related to E_{50} by:

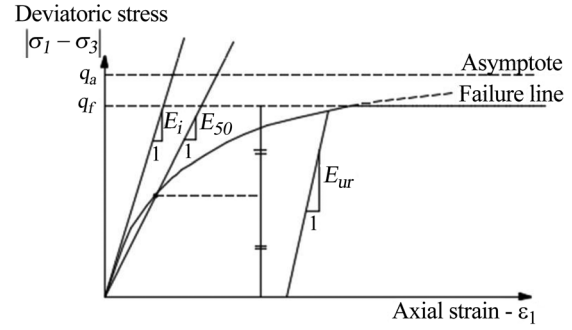


Figure 6 - Hyperbolic strain-strain relationship for an isotropic load in a drained triaxial test (modified from Schanz *et al.*, 1999).

$$E_i = \frac{2E_{50}}{2 - R_f} \quad (2)$$

where ε_1 is the axial strain, q is the deviatoric stress, and q_a is the asymptote of the shear strength:

$$q_a = \frac{q_f}{R_f} \quad (3)$$

where R_f is the failure ratio (0.9 by default in the software) and q_f is the ultimate deviatoric stress, defined by the Mohr-Coulomb criterion:

$$q_f = \frac{2 \sin \phi'}{1 - \sin \phi'} (\sigma'_3 + c' \cot \phi') \quad (4)$$

where c' and ϕ' are the effective shear strength parameters, σ'_3 is the confining stress in the triaxial test (in the software, σ'_3 is negative in compression), and E_{50} is the confining stress-dependent stiffness modulus for the primary load, defined as follows:

$$E_{50} = E_{50}^{ref} \left(\frac{c' \cos \phi' + \sigma'_3 \sin \phi'}{c' \cos \phi' + p^{ref} \sin \phi'} \right)^m \quad (5)$$

where E_{50}^{ref} is the reference secant stiffness modulus for the drained triaxial test, p^{ref} is the reference isotropic stress (100 kPa by default in the software), and m is the exponent that defines the strain dependence value of the stress state. In natural soil, the exponent m varies between 0.3 and 1.0. As suggested by Brinkgreve *et al.* (2014), to simulate a logarithmic compression behavior, as observed in soft clays, m should be taken equal to 1.0. As noted by Obrzud & Truty (2018) and by Brinkgreve *et al.* (2014), Janbu (1963) reported values of $m = 0.5$ for Norwegian sands and silts, Kempfert (2006) provided values between 0.38 and 0.84 for soft lacustrine clays and von Soos (1990) reported various different values in the range $0.5 < m < 1.0$.

The confining stress-dependent stiffness modulus for unloading and reloading conditions is defined as:

$$E_{ur} = E_{ur}^{ref} \left(\frac{c' \cos \phi' + \sigma'_3 \sin \phi'}{c' \cos \phi' + p^{ref} \sin \phi'} \right)^m \quad (6)$$

Table 3 - Compressibility parameters calculated from one-dimensional consolidation tests.

Depth (m)	E_{oed}^{ref} (MPa)	m	$E_{ur,oed}^{ref}$ (MPa)	m	$E_{ur,oed}^{ref} / E_{oed}^{ref}$
1	5.0	0.19	-	-	-
2	1.25	0.21	14.05	1.67	11.25
4	2.33	0.20	36.86	1.02	15.82
6	10.0	0.15	37.52	0.96	3.75
8	6.67	0.45	9.63	1.70	1.44
10	6.51	0.57	7.71	1.22	1.18

kok soils, the parameter m and moduli E_{oed}^{ref} and $E_{ur,oed}^{ref}$ were obtained as follows:

- 1) The tangent stiffness moduli E_{oed} and $E_{ur,oed}$ for several vertical stress values σ'_1 were determined as indicated in Fig. 9;
- 2) As shown in Fig. 10, the E_{oed}/p^{ref} and $E_{ur,oed}/p^{ref}$ normalized moduli were plotted vs. the σ'_1/p^{ref} normalized stress on a double logarithmic graph considering a p^{ref} value of 100 kPa (any value can be used as a reference, but the authors decided to use the value proposed by the software manual);
- 3) Finally, the values of the E_{oed}^{ref} and $E_{ur,oed}^{ref}$ moduli were

found for σ'_1/p^{ref} (stiffness moduli for the reference isotropic stress value). Because the exponent m (Eq. 14) represents the amount of stress dependency, to simulate the logarithmic compression behavior of the soil, the m values were obtained from the slopes of the double logarithmic trend lines of the graphs of Fig. 10.

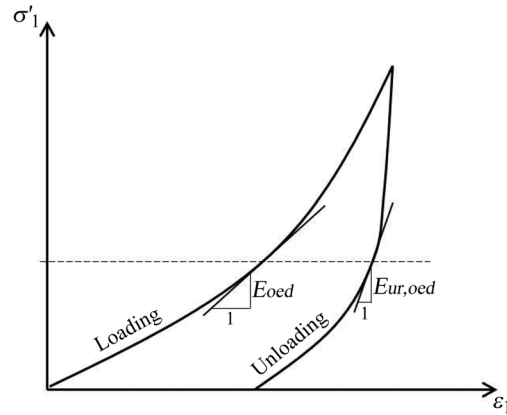


Figure 9 - Determination of moduli E_{oed} and $E_{ur,oed}$ from oedometer test result.

As shown in Table 3, the E_{oed}^{ref} modulus values for depths of 1 to 6 m vary from 1.25 to 10 MPa, with a mean value of 4.7 MPa, while from depths of 8 to 10 m, the mean value is approximately 6.6 MPa, almost 1.4 times greater than the mean superficial value. In contrast, for the $E_{ur,oed}^{ref}$ modulus, the mean value from depths of 8 to 10 m is just 8.7 MPa, while the superficial obtained mean value is approximately 29.5 MPa, 3.4 times greater than the mean deep value. For the $E_{ur,oed}^{ref} / E_{oed}^{ref}$ ratio, it can be seen that the superficial soils (porous sandy clay) show considerably higher values (up to 15.82) than the deepest ones (up to 1.18). This may be because superficial soils may collapse during primary loading, inducing major changes in the soil response for unloading conditions. On the other hand, the average obtained value of the exponent m for primary loading is approximately 0.3, near the values obtained by Jambu

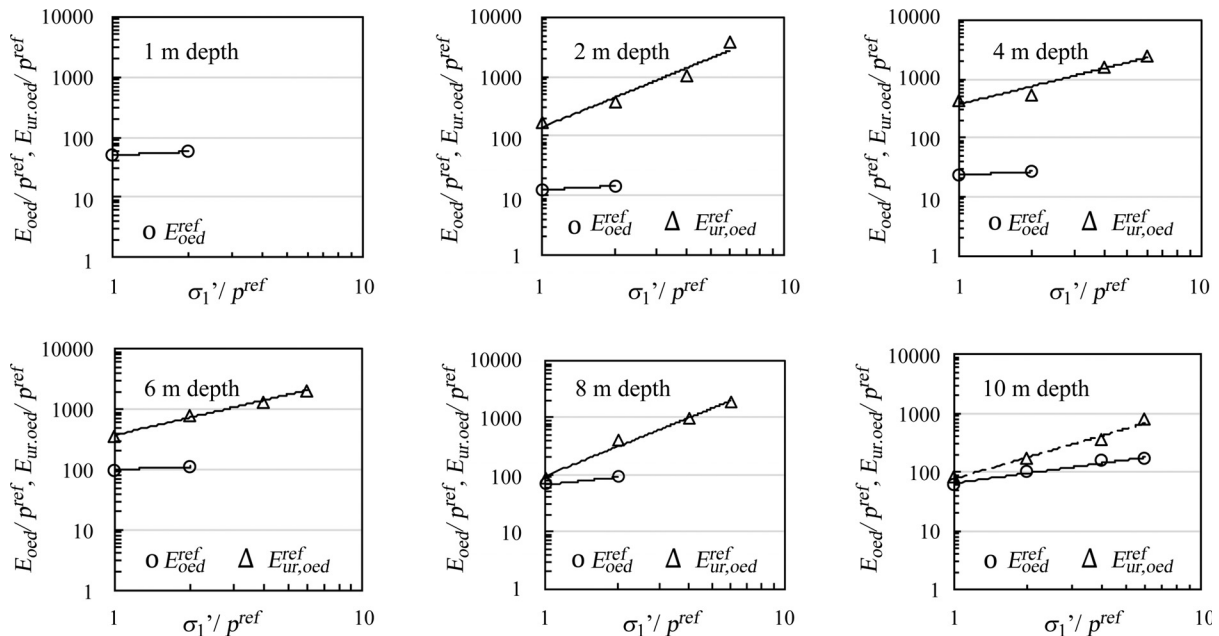


Figure 10 - Oedometric modulus vs. consolidation pressure calculated from one-dimensional consolidation tests.

(1963) for Norwegian sands and silts ($m = 0.5$). This is not the case for the average value of the exponent m for unloading conditions, where the obtained mean value is approximately 1.3, closer to the behavior of a normally consolidated clay ($m = 1$). The results reported by Surarak *et al.* (2012), for Bangkok stiff clays, show values of the exponent m for primary loading from 0.5 to 0.7 and from 1.0 to 1.2 for unloading conditions. Additionally, studies developed by Kempfert (2006) in three lacustrine soft soils demonstrated that the exponent m can be greater for unloading conditions than for primary loading.

4.2. Information obtained from triaxial tests

The CIU triaxial tests (consolidated under isotropic conditions and failure under undrained conditions) were conducted at depths of 2, 4 and 6 m, and the CKOU triaxial tests (consolidated under K_0 anisotropic conditions and failure under undrained conditions) were conducted at depths of 8 and 10 m in undisturbed samples under natural moisture conditions. The shear strength parameters (c' and ϕ'), the reference modulus at 50% strength (E_{50}^{ref}), and the modulus m were calculated; Table 4 summarizes the obtained values. The parameter m and modulus E_{50}^{ref} were obtained as follows:

- 1) The secant stiffness modulus E_{50} for each triaxial deviatoric stress ($\sigma'_1 - \sigma'_3$) vs. axial strain (ε_1) curve of each confining stress pressure (σ'_3) was determined;
- 2) As shown in Fig. 11, the E_{50}/p^{ref} normalized modulus was plotted vs. the σ'_3/p^{ref} normalized confining stress on a double logarithmic graph considering a p^{ref} value of 100 kPa;

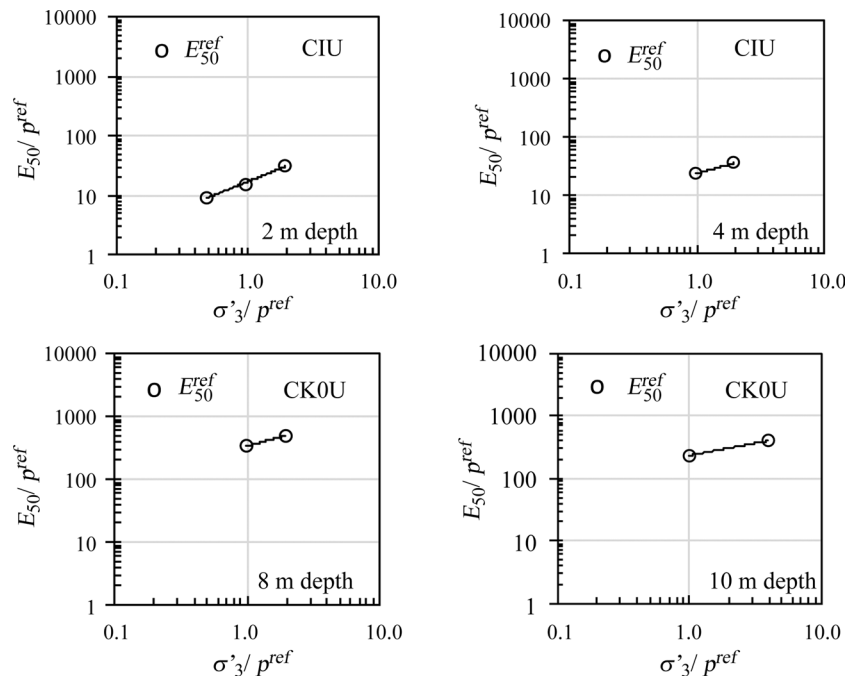


Figure 11 - Variation in E_{50} with confining pressure.

Table 4 - Stiffness and strength parameters obtained from triaxial tests.

Depth (m)	CIU				
	c' (kPa)	ϕ' ($^\circ$)	E_{50}^{ref} (MPa)	m	$E_{50}^{ref} / E_{oed}^{ref}$
2	0	25	1.65	0.88	1.32
4	5	26	2.36	0.52	1.01
6	20	35	-	-	-
Depth (m)	CKOU				
	c' (kPa)	ϕ' ($^\circ$)	E_{50}^{ref} (MPa)	m	$E_{50}^{ref} / E_{oed}^{ref}$
8	76	19	33.78	0.49	5.06
10	20	21	23.48	0.31	3.61

- 3) Finally, the values of the E_{50}^{ref} modulus were found for σ'_3/p^{ref} (stiffness modulus for the reference isotropic stress value). Because the exponent m (Eq. 5) represents the amount of stress dependency, to simulate the logarithmic behavior of the soil, the m values were obtained from the slopes of the double logarithmic trend lines of the graphs of Fig. 11.

Unfortunately, some $\sigma'_1 - \sigma'_3$ vs. ε_1 curves had to be discarded because they were inconsistent with the other results, so for the depths of 4, 8 and 10 m, only two points were plotted, and for 6 m, all points were discarded.

Table 4 shows that for superficial soils (2 and 4 m depths), the mean E_{50}^{ref} modulus is approximately 2 MPa, while for the deeper soils (8 and 10 m depths) the mean value is 28.3 MPa, 14.3 times greater. Additionally, for superficial soils, the obtained mean $E_{50}^{ref} / E_{oed}^{ref}$ ratio is ap-

proximately 1.17, close to the default value of 1.25 proposed by the software; this is not the case for the deeper soils, where the mean $E_{50}^{ref} / E_{oed}^{ref}$ value is approximately 4.3, very far from the proposed value. The high E_{50}^{ref} moduli for the 8 and 10 m depths are because, despite the undrained condition of the tests, the large air volume present in the macropores of the superficial soils ($S_r < 50\%$) prevents the generation of a significant pore pressure, thus generating a behavior closer to the drained condition. However, at greater depths, the porosity decreases, and the degree of saturation considerably increases ($S_r > 80\%$); therefore, the porosity values generated are more relevant, and the stiffness of the material is closer to that of the undrained condition.

5. Calibration of the Parameters Obtained for the HS Model

5.1. Numerical modeling through FEM

To obtain the best representation of the stress-strain curves and the stress paths, once the compressibility and strength parameters were evaluated from the laboratory tests, it was considered important to simulate those tests using the HS constitutive model to see if it was necessary to make adjustments to those parameters. Mainly, two techniques can be used for this simulation to calibrate the initially obtained parameters: one is the explicit simulation of the test by finite element software, and the other is the *SoilTest* module of Plaxis software (Brinkgreve *et al.*, 2014). To show the use of both techniques, in this work, the modeling of the triaxial test was carried out considering the explicit numerical modeling and the one-dimensional consolidation tests using the *SoilTest* module.

The numerical modeling of the triaxial tests was performed considering the axisymmetric geometry of the problem. Figure 12 shows the developed finite element mesh and the boundary conditions considered. Because the tests were performed for soils under natural moisture conditions ($S_{mat} = 34$ to 84%), in the model, the test type was considered as drained (CD), and therefore the development of a positive pore pressure was not allowed.

For the tests corresponding to depths of 2, 4 and 6 m, the initial stage was simulated considering isotropic loading conditions (distributed load system A = B = σ'_3 , Fig. 12), whereas for the depths of 8 and 10 m, the loading was anisotropic (B equal to K_0A , Fig. 12); the considered stress values are shown in Table 5. The failure was generated under drained conditions by increasing the value of the distributed load A that, in this step of the test, represents the deviatoric stress ($A = \sigma'_1 - \sigma'_3$, Fig. 12).

5.2. Calibration of the obtained parameters

The compressibility parameters obtained from the consolidation tests (Table 3) and the stiffness and strength

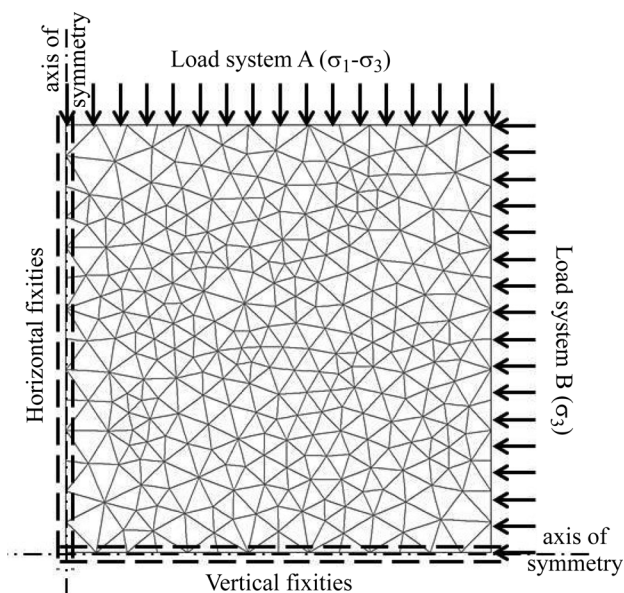


Figure 12 - Finite element mesh used for the simulation of the triaxial test.

Table 5 - Loading conditions considered for the simulation of the initial stage of the triaxial tests.

Depth (m)	Type	Load A (kPa)	K_0	Load B (kPa)
2	CIU	49, 98, 196	1	49, 98, 196
4	CIU	49, 98, 196	1	49, 98, 196
6	CIU	49, 98, 196	1	49, 98, 196
8	CK0U	140, 280, 566	0.7	98, 196, 396
10	CK0U	140, 280, 566	0.7	98, 196, 396

parameters obtained from the triaxial tests (Table 4) were used for the calibration of the HS model for the soils of the CEGUnB.

To obtain the best representation of the stress-strain curves and the stress paths of the laboratory tests, the following parameter-adjusting criteria were adopted:

- The c' , ϕ' and E_{oed}^{ref} parameters obtained from laboratory tests (Tables 3 and 4) were used as initial values and were kept (as much as possible) without major changes during the calibration process;
- The modulus E_{ur}^{ref} was defined equal to $E_{ur,oed}^{ref}$ (Table 3) as the initial value and was considered one of the main parameters of adjustment during the calibration process;
- The modulus E_{50}^{ref} obtained from laboratory tests (Table 4) was defined as the initial value and was considered one of the main parameters of adjustment during the calibration process;
- An initial value of $m = 0.5$ was considered (sand behavior) and was kept (as much as possible) without major changes during the calibration process;

- e) An initial value of $R_f = 0.9$ was considered (default setting) and was kept (as much as possible) without major changes during the calibration process;
- f) The default settings for the parameters ψ , v_{ur} and K_0^{nc} were considered without changes during the calibration process.

Table 6 shows the parameters that best fit the deviatoric stress vs. axial strain, stress path (p vs. q) and one-dimensional compressibility (axial strain vs. vertical stress). As part of the obtained results, Figs. 13 and 14 shows the adjustment curves of the CIU and consolidation tests for a depth of 2 m and for the CKOU and consolidation tests for the depth of 10 m, respectively.

In general, good agreement is observed between the laboratory results and the HS model, but it is important to

identify and analyze the major differences observed. However, for illustration purposes, only the CIU test for the 2 m depth and the CKOU test at a 10 m depth are presented and discussed:

- a) In the ε_1 vs. q curves (Figs. 13a and 14a), the material develops softening during failure, especially for the CKOU tests at 8 and 10 m in depth, and this behavior cannot be simulated with the HS model.
- b) The strain by material collapse during saturation under a stress of 200 kPa (Fig. 13b) was not simulated; however, the predictions of the model before saturation and during unloading show strong correlations.
- c) There is a strong correlation between the strains obtained in the ε_1 vs. q diagrams for the 2, 4 and 6 m depth tests (Fig. 13a), however, for the CKOU tests at 8 and 10 m

Table 6 - Parameters obtained for the HS model that best fit the laboratory tests.

Depth (m)	Type	c' (kPa)	ϕ' (°)	ψ (°)	E_{50}^{ref} (MPa)	E_{oed}^{ref} (MPa)	E_{ur}^{ref} (MPa)	m	v_{ur}	K_0^{nc}	R_f
1*	CIU	0	25	0	3.2	4.9	14.0	0.5	0.2	0.58	0.8
2	CIU	0	25	0	2.5	1.45	14.0	0.5	0.2	0.58	0.8
4	CIU	5	26	0	4.0	2.20	36.9	0.5	0.2	0.56	0.9
6	CIU	20	32	0	12.0	6.90	37.5	0.5	0.2	0.47	0.9
8	CKOU	75	20	0	13.2	7.00	54.0	0.5	0.2	0.66	0.9
10	CKOU	20	22	0	12.2	5.69	54.0	0.7	0.2	0.63	0.8

* parameters adjusted from the results of the 2 m triaxial test and the 1 m consolidation test.,

ψ = dilatancy angle, considered = 0 (default setting).

v_{ur} = unloading/reloading Poisson's ratio = 0.2 (default setting).

K_0^{nc} = coefficient of earth pressure at rest for normal consolidation = $1 - \sin\phi'$ (default setting).

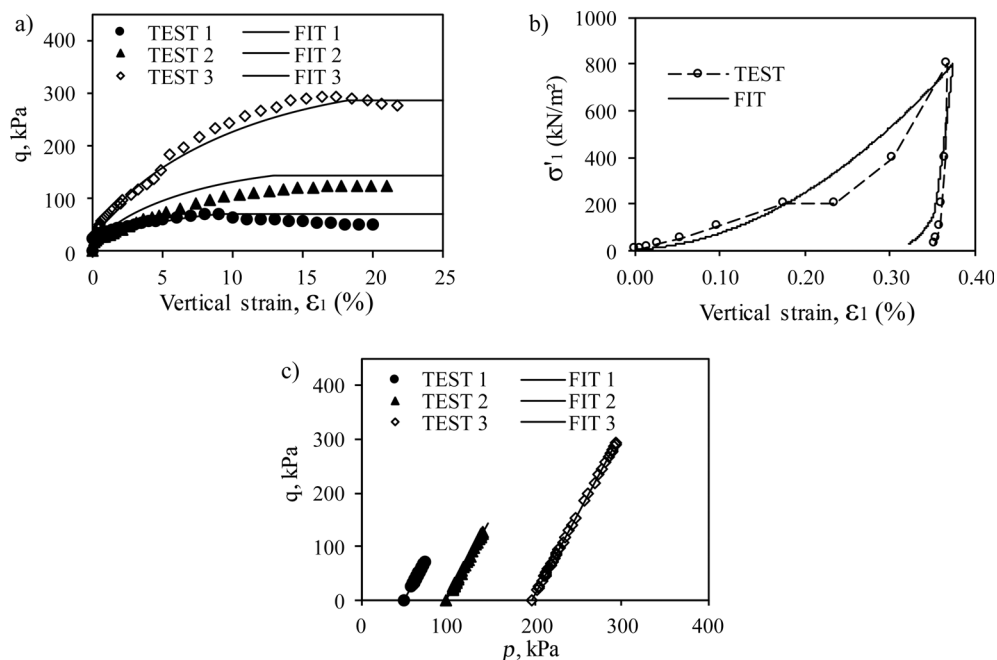


Figure 13 - Laboratory results and adjustment curves obtained with the HS model for the CIU test and for the 2 m depth consolidation. (a) Axial strain vs. deviatoric stress (ε_1 vs. q); (b) Compressibility curve (ε_1 vs. σ'_1); (c) Stress path (p vs. q).

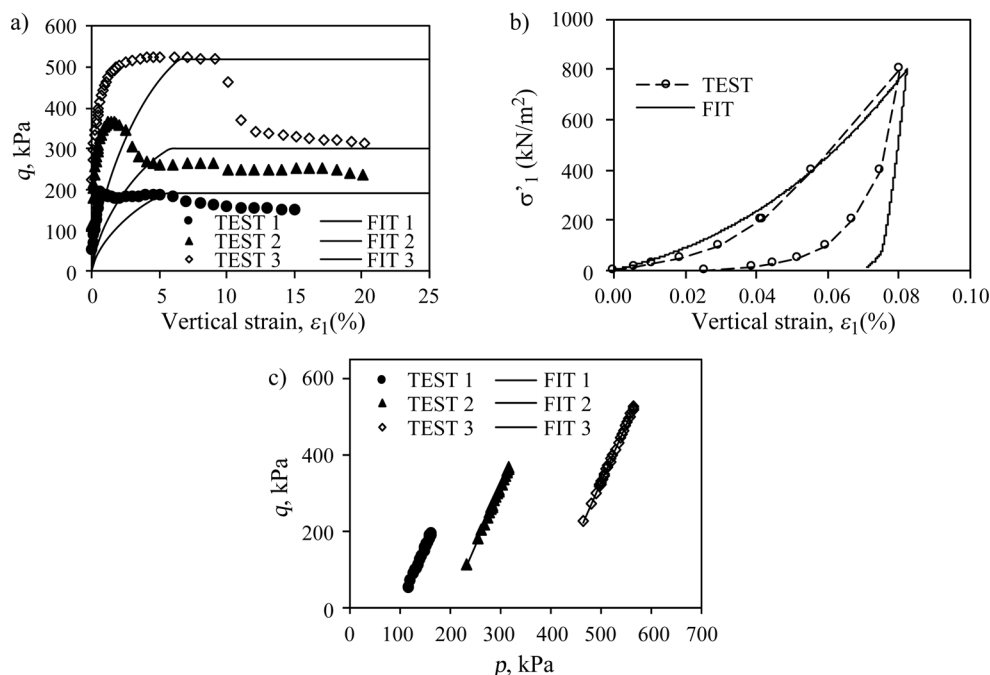


Figure 14 - Laboratory results and adjustment curves obtained with the HS model for the CK0U test and consolidation test at a 10 m depth. (a) Axial strain vs. deviatoric stress (ϵ_1 vs. q); (b) Compressibility curve (ϵ_1 vs. σ'_1); (c) Stress path (p vs. q).

depths (Fig. 14a), the displacement obtained by the HS model is considerably greater than that of the triaxial tests. As mentioned before, this is because, despite the undrained condition of the test, the large air volume present in the macropores of the surface soils ($S_r < 50\%$) prevents the generation of a significant pore pressure, thus generating a behavior closer to that of the drained condition, obtaining a better prediction of the initial stiffness of the material (E_{50}). However, at greater depths, the porosity decreases, and the degree of saturation considerably increases ($S_r > 80\%$); therefore, the porosity values generated are more relevant, and the stiffness of the material is closer to the undrained condition, obtaining high initial stiffness values far away from the drained adopted condition.

For future studies, it will be advisable to carry out a calibration process by triaxial CD tests to avoid the influence of excess water pore pressure generation during the failure step and to obtain a more realistic stiffness modulus.

6. Proposed Geotechnical Model

According to the stratigraphic profile of the CEGUnB (Fig. 2) and the parameters obtained for the HS model (Table 6), the proposed geotechnical model is presented in Table 7. The cohesion values for the soils of layers 1 and 2 were modified, which is explained in greater detail in the following section. The POP (pre-overburden pressure = effective preconsolidation stress - initial effective stress = $\sigma'_p - \sigma'_0$) values were obtained from the compressibility curves (σ'_p) of the consolidation tests and initial stress profile (σ'_0); the K_0^{nc} values (lateral earth pressure at rest for non-

mal consolidation) were based on Jaky's criterion (1944); and the K_0 values (lateral earth pressure at rest) were based on the equation proposed by Mayne and Kulhawy (1982).

7. Validation of the Proposed Geotechnical Model

7.1. Validation through load testing of a single footing

The first part of the validation of the proposed geotechnical model and the mechanical parameters obtained for the HS model was performed for the porous clay surface layer through the numerical simulation of a single-footing load test conducted by Sales (2000) at CEGUnB. The general characteristics of the test are described in section 2.3.

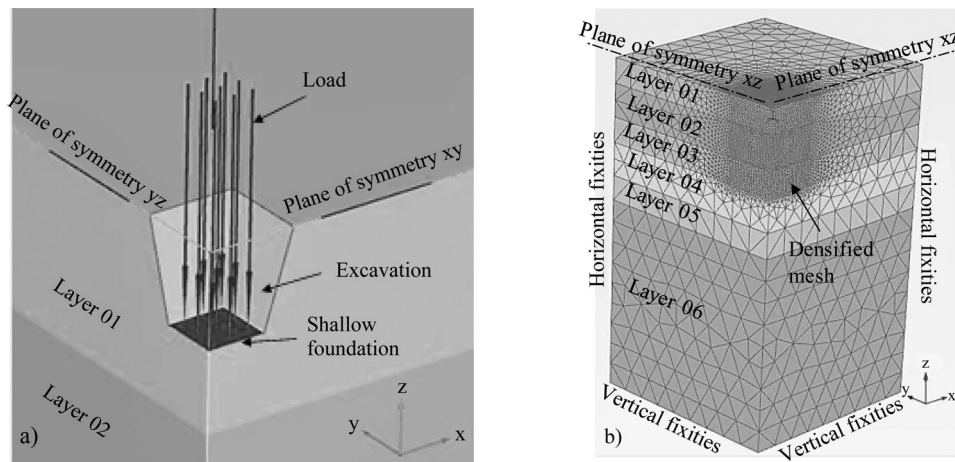
The numerical simulation was performed using the 3D finite element method (Plaxis 3D, Brinkgreve *et al.*, 2015). As shown in Fig. 15a, the symmetry conditions of the problem were considered. Fig. 15b shows the finite element mesh developed and the boundary conditions considered. The medium was discretized by a finite element mesh with more than 161,907 10-node tetrahedral elements, and the footing was discretized by six-node triangular elements. The densification of the mesh around and under the footing was considered. The lateral boundary conditions were fixed in the horizontal direction, and the bottom boundary conditions in both directions. Sensitivity analyses showed that the mesh density was sufficient to obtain accurate results.

The test was simulated considering the following steps:

- 1) Excavation to 0.8 m depth.

Table 7 - Proposed geotechnical model of the CEGUnB for the HS model.

Parameters	Layer number					
	1	2	3	4	5	6
	Porous sandy clay			Lateritic residual soil		Saprolitic soil
Depth (m)	0 - 1.5	1.5 - 3.5	3.5 - 5.0	5.0 - 7.0	7.0 - 8.5	8.5 - 20.0
γ (kN/m ³)	13.1	12.8	13.9	14.3	16.0	18.2
c' (kPa)	5	5	5	20	75	20
ϕ' (°)	25	25	26	32	20	22
ψ (°)	0	0	0	0	0	0
E_{50}^{ref} (MPa)	3.2	2.5	4.0	12.0	13.2	12.2
E_{oed}^{ref} (MPa)	4.9	1.45	2.2	6.9	7.0	5.7
E_{ur}^{ref} (MPa)	14.0	14.0	36.9	37.5	54.0	54.0
m	0.5	0.5	0.5	0.5	0.5	0.7
ν_{ur}	0.2	0.2	0.2	0.2	0.2	0.2
p^{ref} (kPa)	100	100	100	100	100	100
R_f	0.8	0.8	0.9	0.9	0.9	0.8
POP (kPa)	65.7	31.8	0	31.4	0	0
K_0^{nc}	0.58	0.58	0.56	0.47	0.66	0.63
K_0	1.37	0.77	0.56	0.56	0.66	0.63


Figure 15 - Square footing model developed in 3D Plaxis: a) Symmetry and boundary conditions. Geometry of the model: b) finite element mesh.

- 2) The displacement values were reset, and an incremental vertical load was placed above the footing until the maximum site value was reached (140 kN, Fig. 5);
- 3) Total removal of the load.

To simulate the excavation and get the best fit of the simulation with the loading *vs.* settlement graph obtained on-site, it was necessary to increase the cohesion value of the porous clay determined in the triaxial tests, *i.e.*, $c' = 0$ kPa (Table 6, 1 and 2 m depth samples) to $c' = 5$ kPa (Table 7, layers 1 and 2). Figure 16 shows the comparison of the simulated and on-site load *vs.* settlement curves, and good agreement is observed between them. The increase

considered in the cohesion value seems reasonable since it is possible to observe that this superficial soil in the city of Brasília generally maintains verticality in cuts without any type of support up to 2 m height. Likewise, due to the complex structure of this type of porous and collapsible soil, a loss of cohesion may occur during the collection, transport, and assembly of the undisturbed sample.

7.2. Validation by load testing on piles

The complete stratigraphic model and the mechanical parameters obtained for the HS model were validated through the numerical simulation of load tests on rein-

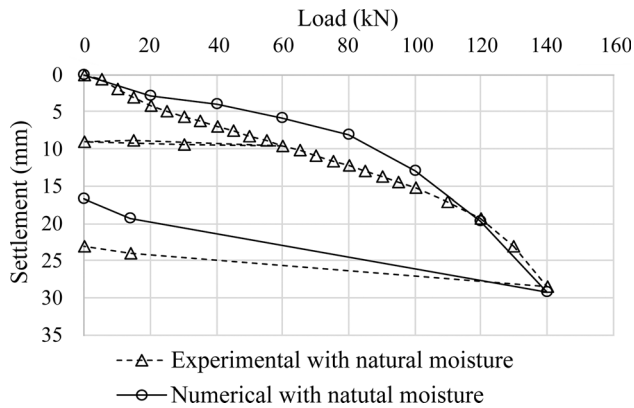


Figure 16 - Comparison of the load vs. settlement curves obtained from the experimental test and the explicit numerical modeling of the problem.

forced concrete piles conducted at the CEGUnB by Guimarães (2002; Table 2 and Fig. 4). The piles were built by the excavation method, with lengths of 7.25 to 7.8 m and diameter of 0.3 m.

Due to the cylindrical geometry of the problem, the model was considered axisymmetric (Fig. 17). The me-

dium was discretized by a finite element mesh with 4,298 15-node triangular elements. Densification of the mesh around the pile was considered. The lateral boundary conditions were fixed in the horizontal direction, and the bottom boundary conditions in both directions. Sensitivity analyses demonstrated that the mesh density was sufficient to obtain accurate results. The pile concrete was assumed to be linearly elastic, with a stiffness modulus of 25 GPa and a Poisson ratio of 0.20. To adequately consider the interactions between the pile surface and the soil, five pairs of node interface elements were added.

The simulation was performed considering the following analysis steps:

- 1) Pile construction *via* direct replacement of the soil by the pile material (reinforced concrete).
- 2) Incrementation of the external loads in the same sequence as applied in the load tests (30, 60, 90, 120, 150, 180, 210, 240 and 270 kN).
- 3) Total unloading of the pile.

Piles 1 and 5 were simulated (Table 2). Figure 18 shows the comparison between the simulated and on-site

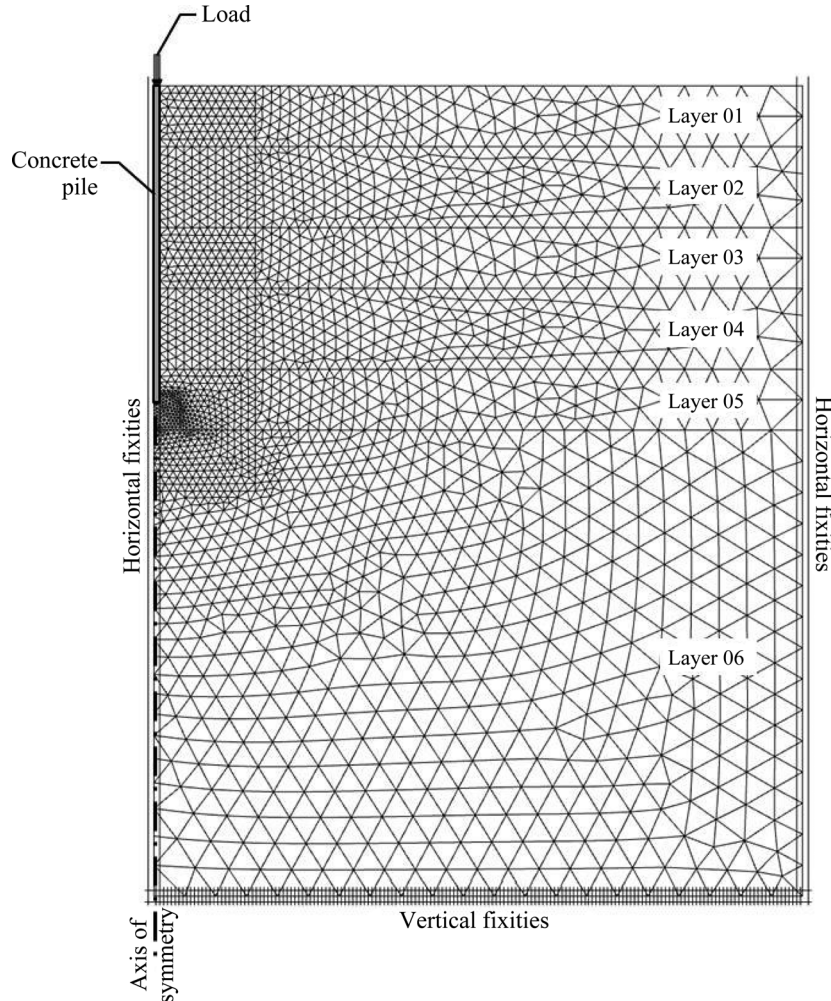


Figure 17 - Finite element mesh and boundary conditions considered for the pile load test.

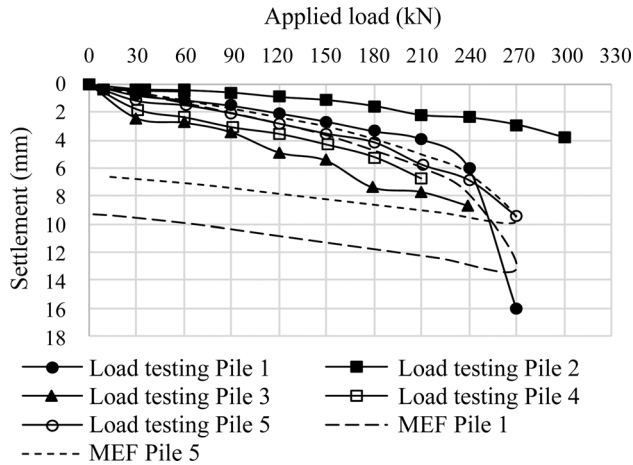


Figure 18 - Load vs. settlement curves obtained from on-site load testing and numerical modeling.

load testing results, and good agreement is observed between the two load capacity assessments.

8. Conclusions

In this study, based on laboratory and field tests conducted as part of previous experimental field studies at the University of Brasília (CEGUnB), the mechanical parameters of characteristic soils of the city of Brasília were obtained, adjusted and validated for the Hardening Soil (HS) model of Plaxis software.

The methodology and main conclusions are summarized below:

- With the information available from the different research studies, it was possible to define a stratigraphic profile typical of the CEGUnB, which is considered to be characteristic of the city of Brasília.
- The compressibility parameters (E_{oed}^{ref} , $E_{ur,oed}^{ref}$ and m) were obtained from six “simple” one-dimensional consolidation tests (under natural moisture and saturated conditions until reaching a stress of 200 kPa). The parameter m and moduli E_{oed}^{ref} and $E_{ur,oed}^{ref}$ were obtained by plotting the moduli E_{oed} and $E_{ur,oed}$ vs. σ'_1 on a double logarithmic graph.
- The shear strength (c' , ϕ') and stiffness (E_{50}^{ref} , m) parameters were obtained from CIU (consolidation under isotropic conditions and failure under undrained conditions) and CK0U (consolidation under anisotropic conditions and failure under undrained conditions) triaxial tests. The parameter m and modulus E_{50}^{ref} were obtained by plotting E_{50} vs. σ'_3 on a double logarithmic graph.
- Through the explicit numerical modeling of triaxial tests and the use of the *SoilTest* module of Plaxis software for one-dimensional consolidation tests, the parameters obtained for the HS model were adjusted to obtain the best representation of the curves of deviatoric

stress vs. axial strain, isotropic stress vs. deviatoric stress (stress path) and axial strain vs. vertical stress (compressibility curve). In general, good agreement was observed between the laboratory results and the HS model. The main differences are because the HS model cannot simulate softening during failure or material collapse during saturation.

- Based on the stratigraphic profile and on the parameters obtained for the HS model, a geotechnical model of the CEGUnB was defined.
- The first part of the validation of the proposed geotechnical model and the mechanical parameters obtained for the HS model was performed for a porous clay surface layer through the numerical simulation of an isolated footing load test by Sales (2000) at the CEGUnB. The numerical simulation was performed using the 3D finite element method (Plaxis 3D). To simulate the excavation and obtain the best fit with the on-site loading vs. settlement curve, it was necessary to increase the cohesion value of the porous clay obtained in the triaxial tests to $c' = 5$ kPa. This cohesion value seems reasonable, since it is possible to observe that this superficial soil in the city of Brasília generally maintains verticality in cuts without any type of support up to 2 m heights. Likewise, due to the complex structure of this type of porous and collapsible soil, a loss of cohesion may occur during the collection, transport, and assembly of the undisturbed sample.
- The complete stratigraphic model and the mechanical parameters obtained for the HS model were validated through the numerical simulation of the load testing on reinforced concrete piles conducted at the CEGUnB. Due to the cylindrical geometry of the problem, the model was considered axisymmetric. The loading vs. settlement graphs obtained for the on-site load testing and for the numerical simulation show good agreement between the two cases.

Finally, it can be concluded that the mechanical behavior of the soils of Brasília under natural moisture conditions can be modeled using the HS model. The parameter values obtained herein can be considered as representative of soils of the city of Brasília, but they must be determined for each particular site and project, and the methodology presented in this study may help in their determination and validation.

Acknowledgments

The authors acknowledge the Coordination for the Improvement of Higher Education (CAPES), the National Council for Scientific and Technological Development (CNPq) and the Federal District Development Support Fund (FAPDF) for their support and partnership and Dr. Renato Cabral Guimarães for sharing laboratory test results performed at the UnB Experimental Field site as part of his Master's thesis.

References

- Brinkgreve, R.B.J.; Engin E. & Swolfs W.M. (2014). Plaxis 2D Anniversary Edition, Plaxis bv.
- Brinkgreve, R.B.J.; Kamarswamy S. & Swolfs W.M. (2015). Plaxis 3D Anniversary Edition, Plaxis bv.
- Cardoso, F.B.F. (2002). Propriedades e Comportamento Mecânico de Solos do Planalto Central Brasileiro. Tese de Doutorado, Departamento de Engenharia Civil e Ambiental, Universidade de Brasília, Brasília, DF, 357 p.
- Coelho, R.S. (2013). Relatório das sondagens executadas na área destinada à construção da obra Casa do Professor. FUNDEX, Infrasolo, Brasília, DF, 11 p.
- Cruz, P.T. (1987). Solos residuais: algumas hipóteses de formulações teóricas de comportamento. Seminário em Geotecnia de Solos Tropicais, ABMS-UNB, Brasília, DF, pp. 79-111.
- Duncan, J.M. & Chang, C.M. (1970). Nonlinear analysis of stress and strain in soils. *Journal of Soil Mechanics and Foundations Division, ASCE*, 96(SM5):1629-1653.
- Guimarães, R.C. (2002). Análise das Propriedades e Comportamento de um Perfil de Solo Laterítico Aplicada ao Estudo do Desempenho de Estacas Escavadas. Dissertação de Mestrado em Geotecnia, Departamento de Engenharia Civil e Ambiental, Universidade de Brasília, Brasília, DF, 183 p.
- Jaky, J. (1944). The coefficient of earth pressure at rest. *J. Society Hungarian Arch. and Eng.*, v. 1, pp. 355-358.
- Janbu, N. (1963). Soil compressibility as determined by oedometer and triaxial tests. *Proc. ECSMFE, Wiesbaden*, v. 1, pp. 19-25.
- Jardim, N.A. (1998). Metodologia de Previsão de Capacidade de Carga Vertical e Horizontal com o Dilatômetro de Marchetti. Dissertação de Mestrado em Geotecnia, Departamento de Engenharia Civil e Ambiental, Universidade de Brasília, Brasília, DF, 141 p.
- Jennings, J.E. & Knight, K. (1975). A guide to construction on or with materials exhibiting additional settlement due to collapse of grain structure. *Regional Conference for Africa on Soil Mechanics & Foundation Engineering, Durban*, v. 1, pp. 99-105.
- Kempfert, H. (2006). *Excavations and foundations in soft soils*. Springer, Heidelberg, 523 p.
- Kondner R.L. (1963). Hyperbolic stress-strain response: cohesive soils. *Journal of the Soil Mechanics and Foundations Division, ASCE*, 89(SM1):115-143.
- Mayne, P.W. & Kulhawy, F.H. (1982). K₀-OCR relationships in soil. *J. Geotech. Engng. ASCE*, 108(GT6):851-872.
- Mortari, D. (1994). Caracterização Geotécnica e Análise do Processo Evolutivo das Erosões no Distrito Federal. Dissertação de Mestrado, Universidade de Brasília, 200 p.
- Mota, N.M.B. (2003). Ensaio Avançados de Campo na Argila Porosa Não Saturada de Brasília: Interpretação e Aplicação em Projetos de Fundação. Tese de Doutorado, Departamento de Engenharia Civil e Ambiental, Universidade de Brasília, Brasília, DF, 335 p.
- Obrzud, R. & Truty, A. (2018). *The hardening soil model - a practical guidebook*. Zace Services Ltd, Software Engineering, Switzerland, 205 p.
- Ortigão, J.A.R. & Macedo, P. (1993). Large settlements due to tunnelling in porous clay. *AFTES Association Française des Tunnels et Ouvrages Souterrains, Paris*, v. 119, pp. 245-250.
- Perez, E.N.P. (1997). O Uso da Teoria da Elasticidade na Determinação do Módulo de Young de Solo Adjacente a Estacas Carregadas Verticalmente na Argila Porosa de Brasília. Dissertação de Mestrado em Geotecnia, Departamento de Engenharia Civil e Ambiental, Universidade de Brasília, Brasília, DF, 146 p.
- Sales, M.M. (2000). Análise do Comportamento de Sapatas Estaqueadas. Tese de Doutorado em Geotecnia, Departamento de Engenharia Civil e Ambiental, Universidade de Brasília, Brasília, DF, 229 p.
- Sales, M.M.; Vilar O.M.; Mascarenha, M.M.A.; Silva, C.M.; Pereira, J.H.F & Camapum de Carvalho, J. (2015). Fundações em solos não saturados. Solos não saturados no contexto geotécnico. Camapum de Carvalho, J.; Gitirana Jr, G.; Machado, S.; Mascarenha, M.M. & Filho, F. (eds.), ABMS, São Paulo, pp. 651-685.
- Schanz, T.; Vermeer, A. & Bonnier, P. (1999). The hardening soil model: formulation and verification. *Proc. Int. Symp. beyond 2000 Comput. Geotech. 10 years Plaxis, Amsterdam, Netherlands*, 281 p.
- Surarak, Ch.; Likitlersuang, S.; Wanatowski, D.; Balasubramaniam, A.; Oh, E. & Guan, H. (2012). Stiffness and strength parameters for hardening soil model of soft and stiff Bangkok clays. *Soils and Foundations*, 52(4):682-697.
- von Soos, P. (1990). Properties of soil and rock (in German). In: *Grundbautaschenbuch Part 4*. Ernst & Sohn, Berlin.

Technical Notes

Soils and Rocks
v. 42, n. 1

Rockburst From Floors

S.S. Andreyko, T.A. Lyalina

Abstract. The purpose of this work is the calculation of the optimal parameters involved with advanced drilling of gas-draining holes. These holes are made to floor entryways and provide an efficiency test for floor degas extractions, like the AB bed at the Uralkali's Berizniki Ore Development Unit No 2 and Unit No 4 (Mine 2 and Mine 4). Current conditions and entry floor mechanisms affect the gassy outburst analysis of the potash mines. The optimal parameters of gas-draining holes at the Mine 2 and Mine 4 are calculated. The effectiveness test of advance drilling in a potash mine is made. Promising technologies for preparation and extraction, that help reduce the dangers associated with rockbursts from entry floors, have been proposed. Implementation of advance drilling in potash mines have significantly improved the safety of Mine 2's and Mine 4's AB bed preparation and extraction. A conclusion was made, based on the results of gassy outburst calculations of entry floors, that mitigation of hazards can be achieved by both degassing, and through the use of mining equipment that minimizes the size of floor cutting layers. The remaining ore, in the floor, helps eliminate the adverse effects of rockbursts.

Keywords: floor, gas-draining hole, gassy outburst, potash mines, rockburst, sylvinite bed, trapped gas pressure.

1. Introduction

It is understood that factors such as the pressure of trapped gas, gas found in the contact zone of lithological rock varieties (known as contact gas), the stress-strain placed upon rock salt mass, variations in physical and mechanical properties found in the rock, and the ore zone structure, will affect gas generation and subsequent gassy outbursts from the entry floor of potash mines (Proskuriakov *et al.*, 1974, 1988; Proskuriakov, 1980, 1991; Kovalev *et al.*, 1982; Duchrow, 1961; Ekkart, 1965).

A rockburst from the floor first occurred in France in 1959, during the development of the Alsatian potash deposit (Permyakov and Proskuryakov, 1972).

Since that time, effective techniques for anticipating gassy outburst hazards and mine control procedures for entry have been developed. Sudden roof breaks, often accompanied by gassing, can be avoided. These techniques have been implemented for Upper Kama mining districts (JSC «Uralkaliy», 2005; JSC «Sil'vinit», 2009).

The All-Russian Vedenev Hydraulic Engineering Research Institute (VNIIG), the Saint-Petersburg Mining University, the Perm National Research Polytechnic University, the Ural Branch of VNIIG and other organizations have contributed significant investigations on the mechanisms associated with rockburst generation and how to handle it.

Implementation of this research has resulted in the mining operations ability to significantly minimize gassy outburst related problems experienced during the extrac-

tions conducted at the sylvinite bed at the Upper Kama mining districts.

However, mining operations in the Uralkali's potash mines showed that the rockburst problem still is a topical problem.

Over the last few years, gassy outburst from entry floors has again become a relevant problem, during Mine 2's and Mine 4's AB bed extractions (Fig. 1).

Rockburst may lead to the sudden destruction of the rock floor, accompanied by gassing, which poses a threat to the life and well-being of miners, and may result in the need to shut down a mine for several months.

In this context, there was an urgent need to assess the effectiveness of advanced drilling techniques for gas-draining holes, which mitigate gassy outburst events, and the proper calculation of the optimal parameters related to degas drilling at Uralkali's Mine 2 and Mine 4.

2. Material and Methods

It is understood that the gassy outburst occurrence, as seen by sudden floor breakage, accompanied by gassing, is possible if the active force (pressure of the contact gas) exceeds the force supporting the floor.

Analysis of the conditions associated with rockburst occurrence has shown that the bottom base of the cavity is where contact gas is confined (contact zone of lithological rock varieties, clay seams, high-shale ore).

For the safety of miners during entries, the floor which contains contact gas needs to have an assessment of floor stability, with calculation of the minimal forces that

Sergey Semenovich Andreyko, D.Eng. Science, Mining Institute of the Ural Branch, Russian Academy of Sciences, 614007 78-A, Sibirskaya, St. Perm, Russia, e-mail: ssa@mi-perm.ru.

Tamara Alexandrovna Lyalina, M.Sc., Mining Institute of the Ural Branch, Russian Academy of Sciences, 614007 78-A, Sibirskaya, St. Perm, Russia, e-mail: lyalina@mi-perm.ru.

Submitted on March 10, 2016; Final Acceptance on December 13, 2018; Discussion open until August 30, 2019.

DOI: 10.28927/SR.421077



Figure 1 - Rockburst in the sudden destruction of the rock floor, accompanied by gassing at Mine 4 AB bed.

could affect its balance (Kovalev *et al.*, 1982; Proskuriakov *et al.*, 1988; Proskuriakov, 1991; Obert, 1964; Obert & Duvall, 1967; Gasausbruch-richtlinien, 1981).

As already indicated, floor stability will vary, depending on the effects of the contact gas on or near the face zone position (face zone or a distance from face of 20 m (off-face zone)) (Fig. 2).

Thereby, the conditions of gassy outburst occurrence from entry floors at the face zone or the off-face zone can be calculated using the following formula (Kovalev *et al.*, 1982; Proskuryakov *et al.*, 1988):

$$P_{critical} \geq (0.7925 \times \sigma_t \times h_c^2 \times a^{-2} + \gamma h_c) + \Delta_{c.s.} \quad (1)$$

$$P_{critical} \geq (0.5 \times \sigma_t \times h_c^2 \times a^{-2} + \gamma h_c) + \Delta_{c.s.} \quad (2)$$

When potential rockburst from entry floors at the face zone is assessed using Eq. 1 and consideration is given to the weight of mining machines, a reduction in the occurrence of gassy outbursts results.

At the face zone, two sub zones were located.

The first sub zone is characterized by the pressure caused by the weight of mining machines.

Mining machine weight distribution is made on the area, which is determined by the entry width and length, the undercarriage dimensions of the mining machine, and the stiffness of Krasnyy I-A rock-salt bed.

Thus, weight application area is 19.2 m² for ore excavating machines PC-8 or Ural-61; weight application area for Ural-10KSA is 32 m²; weight application areas are 44 m², 46.4 m² and 48.8 m² and depend on entry width for Ural-20, making Eq. 1 for the first sub zone:

$$P_{critical} \geq (0.7925 \times \sigma_t \times h_c^2 \times a^{-2} + \gamma h_c) + \Delta_{c.s.} + \Delta_{m.m.} \quad (3)$$

Equation 1 will be correct for the second face sub zone.

Gas is associated with the contact and clay seams, which results in a force to stability mass structure (apart from geological faults zone).

The condition of rockburst occurrence at the off-face zone is also overworking of a gas pocket of the contact zone. It is possible, when the gas has larger pressure or migrates to this area through the change of the stress environment.

When the face zone is distant from a gas-containing region, the change of floor stability near the contact gas may result in gassy outburst occurrence of this type even with constant physical and mechanical characteristics of the rocks and the mass (with the same tensile strength, at the same gas content, gas pressure, etc.).

Thus, rockburst from the floor at the off-face zone may occur at a contact gas pressure not enough for the occurrence near the face. Gassy outburst at the off-face zone is therefore particularly dangerous, since it occurs suddenly. This fact must be considered when developing measures for the elimination of rockburst of this type. The criteria of a loss in floor stability were assessed for operating panels and unmined areas at Uralkali's Mine 2 and Mine 4.

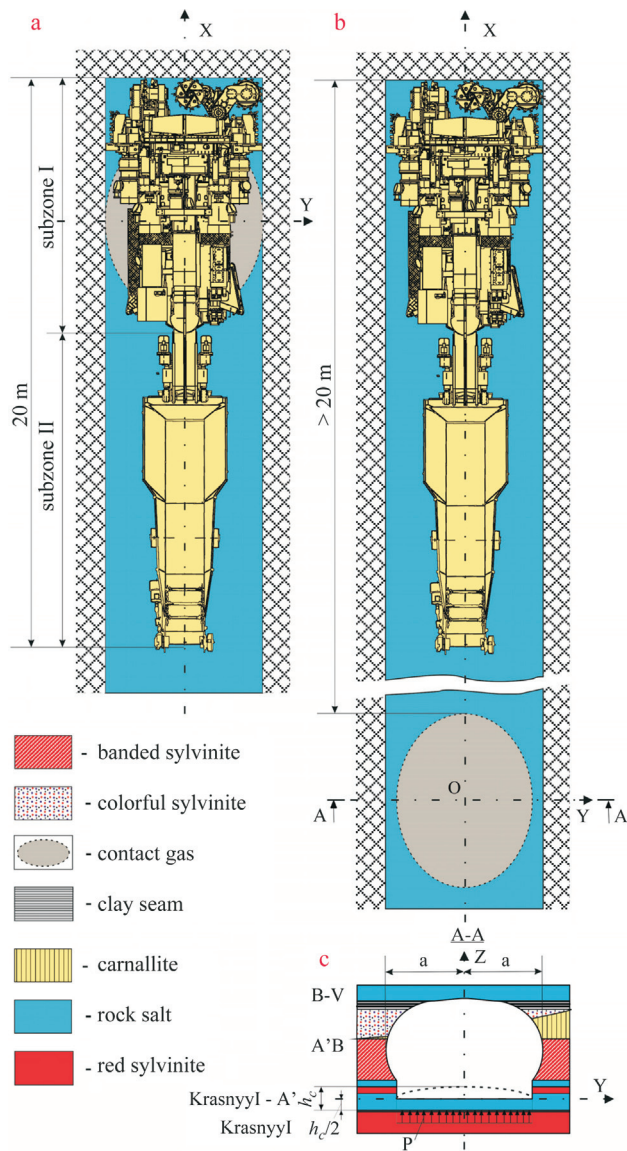


Figure 2 - Definition scheme of the contact gas critical pressure: a - at the face zone; b - at the off-face zone; c - for the rock floor.

3. Results

3.1. Assessment of a potential gassy rockburst

Assessment is made of a potential rockburst from the entry floor, where contact gas is located in clay seam of 3-5 cm thickness, between the Krasnyy I and KrasnyyI-A' rock salt beds, at the Berizniki Ore Development Unit No. 2. Assessment of a potential breakage of the entry floor is made for north-western and south-eastern areas of Mine 2: 8, 10, 12, 14, 16, 18 and 20 western panels (W. P.); 11, 13, 15 and 17 eastern panels (E. P.). It was calculated using Eqs 1, 2 and 3. Calculations were made for the types of ore excavating machines being used at the mined panels. Results of the calculations are shown in Table 1 (h_c , floor distance from the contact gas).

At the 8 W.P., the floor distance from the contact gas for “Ural-61” varies two fold, between 1.5-2.9 m as shown in Table. The distance of the floor from the contact gas is between 1.0-2.4 m, when using “Ural-20R”, which is also a very important factor. At 16 W. P., h_c was predicted to be at 2.0 m, due to insufficient data on the AB bed structure and the surrounding rock, when using “Ural-61”.

Table 2 shows the results of the calculation of the safe gas pressure at the floor entries, driven by Mine 2’s AB bed.

At the 14 W.P. the minimum gas safety pressure P_s on the floor, is 0.47 MPa (subzone II) and 0.49 MPa (subzone I) in extraction AB bed in Mine 2 north-western area when using “Ural-10A” as shown in Table 2. At the 14 W.P. P_s is 0.26 MPa (sub-zone II) and 0.28 MPa (subzone I) when using “Ural-61”. At 14 W.P. P_s is 0.02 MPa (subzone II) and 0.04 MPa (subzone I) when using “Ural-20R”. At the other panels in the north-western area, pressure is also minimum when using “Ural-20R” compared to the other types of mining machines.

Table 3 shows the results of an assessment of a potential gassy outburst from the entry floor at the off-face zone at Mine 2, as seen by sudden breakage of the entry floor.

In a similar manner, the criterium for loss in floor stability was assessed for Mine 4.

3.2. Justification for drilling optimal gas-draining holes in the entry floor at Mine-2, using advanced drilling techniques

There was a total of eighteen gassy outbursts with sudden breakage of the entry floor, that were accompanied by gassing at Mine 2. The histogram of distribution of the value h_c is shown in Fig. 3. On the horizontal axis, the floor distance h_c is set with a 0.3 m interval between values - with an interval of 0.3 m between them. The vertical axis displays the number of rockburst accidents having this distance.

The distribution is verified by checking the conformity with the normal probability law, and it was confirmed that it follows the rule (Ryzhov, 1973; Kalosha *et al.*, 1982). The next step was to determine the confidence interval for the value h_c .

The confidence interval for a normal distribution of value h_c at Mine-2 with a probability of 94% is:

$$3 \text{ m} < h_c < 1.7 \text{ m} \tag{4}$$

4. Discussion

The analysis of the extract from the Mine 2 north-western area subsequently showed that the distance of the floor from the contact gas is minimal at 10 and 14 W. P. when using “Ural-20R” and at 14 W.P. when using “Ural-61”, with h_c between 0.8-3.7 m.

As a result, the analysis of the extract from Mine 2 south-eastern area subsequently showed that 13, 15 and 17

Table 1 - Floor distances from the contact gas at Mine 2.

No.	Panel	Thickness of bed A'B, m		Thickness of bed Krasnyy I - A', m		h_c , floor distance from the contact gas, m					
						Ural 10A		Ural 61		Ural 20R	
		from	to	from	to	from	to	from	to	from	to
1.	8 western	2.65	3.41	1.8	2.44	-	-	1.5	2.9	1.0	2.4
2.	10 western	2.5	4.08	1.66	2.58	1.8	4.3	1.2	3.7	0.7	3.2
3.	12 western	2.50	3.18	1.84	2.21	2.0	3.0	1.4	2.4	-	-
4.	14 western	2.30	4.15	1.45	2.50	1.4	4.3	0.8	3.7	0.3	3.2
5.	16 western	2.78	2.78	2.15	2.15	-*	-	2.0	2.0	-	-
6.	18 western	2.70	4.37	2.00	3.30	-	-	1.8	4.7	1.3	4.2
7.	20 western	2.45	3.40	2.00	2.40	2.1	3.5	1.5	2.9	1.0	2.4
8.	11 eastern	2.30	2.60	1.62	2.18	-	-	1.0	1.8	-	-
9.	13 eastern	1.73	2.55	1.29	1.67	-	-	0.1	1.3	-	-
10.	15 eastern	1.98	2.54	1.30	1.82	-	-	0.3	1.4	-	-
11.	17 eastern	1.69	2.63	1.62	3.25	-	-	0.4	2.9	-	-

*- A line in the table means that the mining machine is not used at this panel.

Table 2 - Calculation results of gas safety pressure in Mine 2 entries floor (subzones I and II of the face).

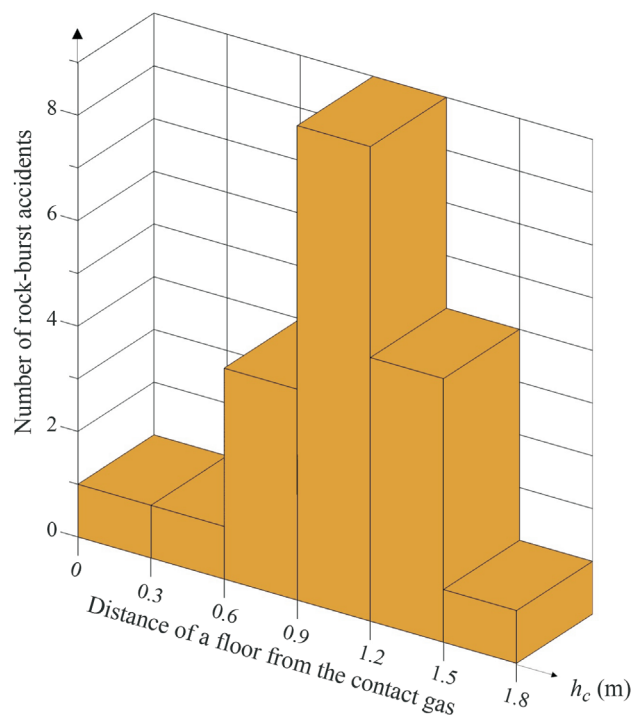
Panel	Ural 10A				Ural 61				Ural 20R			
	Gas safety pressure P_g , MPa				Gas safety pressure P_g , MPa				Gas safety pressure P_g , MPa			
	(subzone I)		(subzone II)		(subzone I)		(subzone II)		(subzone I)		(subzone II)	
	from	to	from	to	from	to	from	to	from	to	from	to
8 W.P.	-	-	-	-	0.90	3.22	0.87	3.19	0.19	0.92	0.17	0.89
10 W.P.	0.80	4.32	0.78	4.30	0.60	5.22	0.57	5.19	0.11	1.60	0.09	1.58
12 W.P.	0.96	2.18	0.94	2.16	0.78	2.29	0.75	2.26	-	-	-	-
14 W.P.	0.49	4.30	0.47	4.28	0.28	5.19	0.26	5.17	0.04	1.59	0.02	1.57
16 W.P.	-	-	-	-	1.53	1.53	1.50	1.50	-	-	-	-
18 W.P.	-	-	-	-	1.20	8.41	1.18	8.38	0.28	2.72	0.26	2.70
20 W.P.	1.06	2.79	1.04	2.77	0.90	3.11	0.87	3.08	0.19	0.88	0.17	0.86
11 E.P.	-	-	-	-	0.40	1.31	0.37	1.28	-	-	-	-
13 E.P.	-	-	-	-	0.03	0.66	0.00	0.63	-	-	-	-
15 E.P.	-	-	-	-	0.08	0.80	0.05	0.77	-	-	-	-
17 E.P.	-	-	-	-	0.09	3.28	0.06	3.25	-	-	-	-

Table 3 - Assessment results of a potential rockburst at Mine 2.

No.	Panel	Gas safety pressure P_g , MPa					
		Ural 10A		Ural-61		Ural 20R	
		from	to	from	to	from	to
1.	8 western	-	-	0.56	2.03	0.11	0.58
2.	10 western	0.51	2.75	0.37	3.31	0.06	1.02
3.	12 western	0.61	1.39	0.48	1.45	-	-
4.	14 western	0.31	2.73	0.17	3.29	0.01	1.01

Table 3 (cont.)

No.	Panel	Gas safety pressure P_s , MPa					
		Ural 10A		Ural-61		Ural 20R	
		from	to	from	to	from	to
5.	16 western	-	-	0.96	0.96	-	-
6.	18 western	-	-	0.76	5.32	0.17	1.73
7.	20 western	0.68	1.77	0.56	1.97	0.11	0.56
8.	11 eastern	-	-	0.24	0.82	-	-
9.	13 eastern	-	-	0	0.41	-	-
10.	15 eastern	-	-	0.03	0.5	-	-
11.	17 eastern	-	-	0.04	2.08	-	-

**Figure 3** - Histogram of floor distance from the contact gas at Mine 2.

E.P. are the areas with the greatest the possibility of a rockburst, as seen by an entry floor sudden breakage.

The possible occurrence of a potential gassy outburst is significant, as seen by an entry floor sudden breakage, during extraction of the AB bed in the north-western area using “Ural-20R”.

Based on the calculated pressures of the mining operations, there are dangers found at the East Panels when using “Ural-61”. It would appear to be useful to use a machine with a lower cutting height, or to use a drum miner, which would increase h_c and P_s .

Similar results for gas safety pressure calculations at the off-face zone were obtained, using face zone calculations. At the south-eastern area, rockburst, as seen by entry floor sudden breakage, at the off-face zone, is most proba-

ble at 14 W.P. when using “Ural-61” and at 8, 10, 14, 18, 20 W.P. when using “Ural-20R”.

For security reasons, the lower limit of 0.3 m for the confidence interval of the h_c value is not a preferred practice for mining operations at a bed with gassy outburst hazards.

Conclusions

The calculated results of contact gas safe pressure suggest that a technological solution is possible through the use of a mining machine that allows for minimized floor cutting (rock salt KrasnyyI-A’ bed). This approach, with rockburst problems from entries floor through advance drilling of gas-draining holes, differs from the traditional approach. Using a drum miner may be most appropriate in this mining engineering situation.

The upper limit of the confidence interval of value h_c reveals important practical findings:

- sudden breakage of the entry floor, accompanied by gassing, has a probability of 94% when cutting of 1.7 m thickness at Mine-2;
- it can be argued, that by drilling gas-draining holes in entries floor at AB bed of 1.7 m in depth, contact gas with a probability of 94%, will be degassed and the sudden breakage of the entry floor will be eliminated at Mine-2;
- it can be argued, that in the floor layers (ore leaved on the floor, in order to eliminate gassy outburst - value h_c) of more than 1.7 m thickness, rockburst of the entry floor, accompanied by gassing, will not occur when gas-draining holes are drilled.

References

- Duchrow G. (1961). Methoden zur Bekämpfung mechanischer Zerstörungen bei schweren Gasausbrüchen im Kalibergbau. Freiburg. Forsh, A 183:64-81.
- Ekkart D. (1965). Beitrag zur Bekämpfung plotzlicher Ausbrüche von Salz und Gas. Freiburger Forschungshefte. Bergakademie, 17(8):759-760.
- Gasausbruch-richtlinien (1981). Richtlinien des landes oberbergamtes nordrhein-westfalen über die abwehr von gefahren des plötzlichen freiwerdens grosser gru-

- bengasmengen mit oder ohne auswurf von kohle oder gestein. August, v. 13.
- JSC «Sil'vinit» (2009). Spetsial'nyye Meropriyatiya Po Bezopasnomu Vedeniyu Gornyykh Rabot Na Verkhnekamskom Mestorozhdenii Kaliynykh Soley V Usloviyakh Gazovogo Rezhima V OAO «Sil'vinit», Perm'-Solikamsk, 75 p.
- JSC «Uralkaliy» (2005). Spetsial'nyye Meropriyatiya Po Bezopasnomu Vedeniyu Gornyykh Rabot Na Verkhnekamskom Mestorozhdenii Kaliynykh Soley V Usloviyakh Gazovogo Rezhima V OAO «Uralkaliy», Perm'-Berezniki, 67 p.
- Kaloshka V.K., Lobko S.I., Chikova T.S. (1982). Matematicheskaya obrabotka rezul'tatov eksperimenta, Vysshaya shkola, Minsk, 103 p.
- Kovalev O.V., Livenskij V.S., Bylino L.V. (1982). Osobennosti Bezopasnoy Otrabotki Kaliynykh Mestorozhdeniy, Polymya, Minsk, 96 p.
- Obert, L. (1964). In situ determination of stress in rock. Mining Engineer, No 8 (august): 51-58.
- Obert, L. & Duvall W. (1967). Rock mechanics and the design of structures in rock, John Wiley & Sons Inc, pp.582-610.
- Permyakov, R.S. & Proskuryakov, N.M. (1972). Vnezapnyye Vybrosoy Soli I Gaza, Nedra, Leningrad, 180 p.
- Proskuryakov N.M., Fomina V.D., Rozhkov V.K. (1974). Gazodinamicheskkiye Yavleniya Na Soligorskikh Rudnikakh, Polymya, Minsk, 211 p.
- Proskuryakov N.M. (1980). Vnezapnyye Vybrosoy Porody I Gaza V Kaliynykh Rudnikakh, Nedra, Moscow, 263 p.
- Proskuryakov N.M., Kovalev O.V., Meshcheryakov V.V. (1988). Upravleniye Gazodinamicheskimi Protssami V Plastakh Kaliynykh Rud, Nedra, Moscow, 239 p.
- Proskuryakov N.M. (1991). Upravleniye Sostoyaniyem Massiva Gornyykh Porod, Nedra, Moscow, 368 p.
- Ryzhov P.A. (1973). Matematicheskaya statistika v gornom dele, Vysshaya shkola, Moscow, 287 p.

List of Symbols

- X, Y, Z: coordinate axis
 Ural 10A, Ural 61, Ural 20R: mining machine name
 E. P.: eastern panel
 P_s : safe gas pressure, MPa
 A'B, Krasnyy I - A': bed name
 W. P.: western panel
 for Eq. 1:
 $P_{critical}$: gas critical pressure, MPa
 σ_f : tensile strength of rock floor, MPa
 h_c : distance of a floor from the contact gas, m
 a : half entry width, m
 γ : unit weight of rock floor, H/m³
 $\Delta_{c.s.}$: shear strength of clay seams in floor, MPa
 for Eq. 2:
 $P_{critical}$: gas critical pressure, MPa
 σ_f : tensile strength of rock floor, MPa
 h_c : distance of a floor from the contact gas, m
 a : half entry width, m
 γ : unit weight of rock floor, H/m³
 $\Delta_{c.s.}$: shear strength of clay seams in floor, MPa
 for Eq. 3:
 $P_{critical}$: gas critical pressure, MPa
 σ_f : tensile strength of rock floor, MPa
 h_c : distance of a floor from the contact gas, m
 a : half entry width, m
 γ : unit weight of rock floor, H/m³
 $\Delta_{c.s.}$: shear strength of clay seams in floor, MPa
 $\Delta_{m.m.}$: pressure of the mining machine weight, MPa
 for Eq. 4:
 h_c : distance of a floor from the contact gas, m

Maximum Tensile Strength of Sand - Coal Fly Ash - Lime Blends for Varying Curing Period and Temperature

C. Silvani, M. Benetti, N.C. Consoli

Abstract. The pozzolanic reactions, responsible for the resistance of soil-lime blends, are endothermic. As such, increasing the curing temperature in turn increases the strength of lime-stabilized soil. Recent research has shown that there is a maximum limit to the resistance of a specimen, based on its curing time. This study aims to predict the maximum tensile strength of sand-coal fly ash-lime blends for several curing times. To achieve that, a series of splitting tensile tests were carried out using cylindrical specimens with diameter and length equal to 50 mm and 100 mm, respectively. Lime content varied from 3% to 7%, dry unit weight ranged from 14 kN/m³ to 16 kN/m³, curing temperatures were 20, 35, 50, 65, 80 and 90 °C, curing periods were 1, 3 and 7 days and fly ash content was established as 25%. Results show that the increase in curing temperature boosts the tensile strength of sand-coal fly ash-lime blends up to a limit that varies with curing time. The porosity/lime index, defined as the ratio of the compacted mixture's porosity and volumetric lime content adjusted by an exponent, proves to be an appropriate parameter to estimate the splitting tensile strength of the soil-coal fly ash-lime studied for all curing times and temperatures studied. Using this index, curves were obtained for the calculation of the maximum temperature that influences the resistance of the studied mixture for each curing time. An equation capable of determining the maximum resistance that can be reached in each curing time, independent of curing temperature, was also obtained through the index.

Keywords: coal fly ash, curing temperature, curing time, lime, maximum splitting tensile strength, sand, soil stabilization.

1. Introduction

Lime stabilization in quartzitic soil, like Osório sand, is not possible since lime needs to react with amorphous silica or alumina to become a water-resistant cementitious material. Quartz is a crystalline material, so it does not react with lime. To be able to stabilize Osório sand with lime, adding a source of amorphous material, such as the coal fly ash used in this research, is necessary.

The development of alternatives for Portland cement, such as reusing industrial by-products (*e.g.* coal fly ash, carbide lime) as a cementitious material, brings environmental and economical benefits. In southern Brazil, materials such as coal fly ash (by-product of coal combustion in thermal power plants) and carbide lime (by-product of acetylene gas manufacture) are profusely produced. From an environmental perspective the use of by-products and wastes instead of Portland cement is a more sustainable solution, since it reduces the use of Portland cement, whose manufacture is the origin of about 8% of the world's CO₂ pollutant emissions (Zhang *et al.*, 2014). From an economical viewpoint, the use of coal fly ash plus carbide lime, in-

stead of Portland cement, comes from the fact that such industrial by-products have a very reduced cost at their place of production. The commercial feasibility of using such by-products is related to the distance from the production sites to the place where they are going to be used (the main cost is linked to transportation), the shorter the distance, the lower the cost and the higher the economic feasibility of using them. Soil-coal fly ash-carbide lime blends have been successfully used to enhance the bearing capacity of footings leaning on improved layers above weak foundation soil (*e.g.*, Pedreira, 2000; Pedreira *et al.*, 2002; Consoli *et al.*, 2009a), as well as the base/sub-base of pavements (*e.g.*, Kampala *et al.*, 2014). Other procedures have focused on assessing the use of wastes to produce building materials such as bricks (*e.g.* Consoli *et al.*, 2014a) and new products from reclaimed asphalt pavement, coal fly ash and carbide lime blends (Consoli *et al.*, 2018).

The porosity/lime index (η/L_{iv}) has been shown to be useful to design lime-stabilized soil (Consoli *et al.*, 2009b, 2011, 2015). One problem in lime stabilization is that the reaction between lime and the amorphous materials is slow. That can be accelerated with the increase of curing temper-

Carina Silvani, Lecturer, D. Eng., Programa de Pós-graduação em Engenharia Civil e Ambiental, Universidade Federal de Campina Grande, Campina Grande, PB, Brazil. E-mail: carinasilvani@hotmail.com.

Mozara Benetti, Ph. D. Student, Programa de Pós-Graduação em Engenharia Civil, Universidade Federal do Rio Grande do Sul, Porto Alegre, RS, Brazil. E-mail: mozara.benetti@hotmail.com.

Nilo Cesar Consoli, Full Professor, Ph. D., Programa de Pós-Graduação em Engenharia Civil, Universidade Federal do Rio Grande do Sul, Porto Alegre, RS, Brazil. E-mail: consoli@ufrgs.br.

Submitted on November 30, 2017; Final Acceptance on December 1, 2018; Discussion open until August 30, 2019.

DOI: 10.28927/SR.421083

ature (Thompson, 1966, Toohey *et al.*, 2013, Saldanha & Consoli, 2016). However, according to Consoli *et al.* (2014a, 2014b, 2014c), the maximum strength of coal fly ash-lime and soil-coal fly ash-lime blends is limited by curing time.

Thomé *et al.* (2005) and Consoli *et al.* (2008, 2009a) have shown that the failure in stabilized layers usually starts with fissures at the bottom of the layer once tensile strength (q_t) is reached. For this reason, tensile strength is a good parameter to evaluate failure of lime-stabilized soils. This research looks for a way to predict the maximum tensile strength for each curing time. The temperature at which that maximum tensile strength can be reached for sand-coal fly ash-lime blends is also investigated.

2. Experimental Program

The experimental program was carried out in two parts. First, soil and fly ash had their geotechnical properties established. The second part was a series of splitting tensile tests for sand-coal fly ash-lime specimens cured for 1, 3 and 7 days at temperatures of 20, 35, 50, 65, 80 and 90 °C. Temperature variation was chosen in a way that the maximum strength for each curing time could be reached. Since temperature works as a catalyzer, it is expected that there will be no need of a curing period longer than a few days to develop the full cementation for higher curing temperatures.

2.1. Materials

Quartzitic rounded wind sand (Osório Sand) was used in this study. The samples were collected in a disturbed state, through manual excavation, in the region of Osório, southern Brazil. According to the Unified Soil Classification System (ASTM D2487, 2006), Osório sand is classified as poorly graded sand (SP).

The coal fly ash (FA) used was obtained from a coal-fired power plant and such residue is composed predominantly by amorphous minerals (SiO_2 and Al_2O_3) according to X-ray diffraction tests. The FA used has only 0.8% of lime, so it is classified as Class F fly ash, according to ASTM C618 (ASTM 1998) and it has the granulometry

of a sandy silt. The results of the characterization tests of Osório sand and the FA are shown in Table 1.

Carbide lime was used throughout this investigation; such lime is a by-product of the manufacture of acetylene gas. In ambient temperature (about 20 °C) the gain of strength due to chemical reactions between Ca^{++} [from $\text{Ca}(\text{OH})_2$], SiO_2 and Al_2O_3 (from coal fly ash) is relatively slow, when compared to other binders (such as Portland cement) at equal curing temperatures. The specific gravity of the lime grains is 2.49.

Distilled water was used for both the characterization tests and molding of the specimens for the splitting tensile tests. The use of distilled water in all testing is due to the necessity of guaranteeing that no impurities (*e.g.*, minerals) that might exist in the tap water will affect the results.

2.2. Initial consumption of lime

The minimum amount of lime required for full stabilization, based on the initial consumption of lime (ICL) (Rogers *et al.*, 1997), was established on the basis of the interpretation of pH tests carried out on soil-coal fly ash with lime added - water (proportions of 1:3) mixtures. Tests carried out in the present study have shown that the variation of pH due to lime addition presented an asymptotic pH result with varying lime amount starting at 3% lime content. So, according to such methodology, 3% lime content is the minimum amount that will guarantee full stabilization of the studied blends.

2.3. Methods

2.3.1. Molding and curing of specimens

All the tests in this study used cylindrical specimens, 50 mm in diameter and 100 mm in length. The first step in the preparation of the specimens was the weighing of dry Osório sand, coal fly ash and lime. The second step was the hand mixing of the dry materials until they reached a uniform consistency. The third step was the addition of water and subsequently hand-mixing the blend for 5 min. It is important to say that the amount of FA (25%) was calculated based on the mass of the dry sand, while the amount of lime (3% to 7%) was calculated based on the mass of the dry sand plus the mass of the fly ash. Eq. 1 was used in the cal-

Table 1 - Physical properties of Osório sand and coal fly ash samples.

Properties	Osório sand	Coal fly ash
Specific gravity	2.63	2.28
Medium sand size particles (0.2 mm < diameter < 0.6 mm)	-	1.0%
Fine sand size particles (0.06 mm < diameter < 0.2 mm)	100.0%	13.6%
Silt size particles (0.002 mm < diameter < 0.06 mm)	-	84.9%
Clay size particles (diameter < 0.002 mm)	-	0.5%
Mean particle diameter (D_{50})	0.16 mm	0.018 mm

calculation of the porosity of a sand-fly ash-lime specimen (Consoli *et al.*, 2011).

$$\eta = 100 - \frac{100 \left[\frac{\left(\frac{\gamma_d V_s}{1 + \frac{L}{100}} \right) \left(\frac{s}{100} \right)}{G_{s_s}} + \frac{\left(\frac{\gamma_d V_s}{1 + \frac{L}{100}} \right) \left(\frac{FA}{100} \right)}{G_{s_{FA}}} + \frac{\left(\frac{\gamma_d V_s}{1 + \frac{L}{100}} \right) \left(\frac{L}{100} \right)}{G_{s_L}} \right]}{V_s} \quad (1)$$

where: η = porosity of the sand-coal fly ash-lime specimen, FA = coal fly ash content (percentage of dry weight of sand), L = lime content (percentage of dry weight of soil plus fly ash), γ_d = dry unit weight of the specimen and V_s = volume of specimen, G_{s_s} = specific gravity of the sand grains, $G_{s_{FA}}$ = specific gravity of the fly ash grains and G_{s_L} = specific gravity of the lime grains.

During the confection of the specimens, the sand-coal fly ash-lime mixture was kept in a covered container to avoid moisture loss. The water content was obtained through two small portions retrieved from the mixture.

The static compaction of the specimens was carried out in three layers inside a lubricated cylindrical split mold. To ensure sample integrity the top of the first and the second layers were scarified. When the three layers were done the specimen was removed from the mold. The specimen was then measured and weighed with accuracies of about 0.01 g and 0.1 mm. The specimens were cured inside plastic bags in a humid room at distinct temperatures and relative humidity above 95% for 1, 3 or 7 days.

The samples were accepted for testing if they met the following tolerances: *Dry Unit Weight* (γ_d): degree of compaction between 99% and 101% (the degree of compaction being defined as the value obtained in the molding process divided by the target value of γ_d); *Moisture Content* (ω): within $\pm 0.5\%$ of the target value and *Dimensions*: diameter to within ± 0.5 mm and height ± 1 mm.

2.3.2. Splitting tensile tests

Carneiro & Barcellos (1953) developed a simple test able to measure the tensile strength of brittle materials: the splitting tensile test. ASTM C496 (ASTM 2011) follows the concepts established by Carneiro & Barcellos (1953). After curing, the specimens were soaked in water at 20 °C for 24 h to minimize suction (Consoli *et al.*, 2011). After these 24 h period immersed in water, all specimens had a degree of saturation above 85%, irrespective of the initial porosity or cementitious material content. All specimens have had their matric suction measured using the filter paper technique (Marinho, 1995). Such tests were carried out with pieces of artificially cemented material collected from the center of the specimens just after they have been taken to failure. The values of suction measured were low, ranging from about zero up to 10 kPa, allowing suction to be eliminated as a variable in the analysis. For the test, the

samples were removed from water and placed horizontally between two stainless steel plates in an automatic loading machine with a maximum capacity of 50 kN and a proving ring with a capacity of 10 kN and a resolution of 0.005 kN. The tests were carried out by compressing the samples along two opposite generatrices leading to failure in tension along the diameter contained in the plane formed by these two generatrices. Tests in which the average strength deviated by more than 10% were disregarded.

2.3.3. Program of splitting tensile tests

In the program of splitting tensile tests, the molding points were positioned in a vertical line (Points A1, A2, and A3), with the same moisture content and three different dry unit weights (16 kN/m³, 15 kN/m³ and 14 kN/m³). Such values were chosen after standard Proctor compaction test results carried out by Silvani (2013) on a sand-coal fly ash-lime blend (containing 25% of coal fly ash and 7% lime) presented maximum dry unit weight (γ_{dmax}) of about 16.0 kN/m³ at optimum moisture content (ω_{opt}) of 14% (Fig. 1). It is important to state that standard Proctor compaction tests were also carried out on sand-coal fly ash-lime blends containing 3% and 5% lime, which resulted in about the same $\gamma_{dmax} = 16.0$ kN/m³ and $\omega_{opt} = 14\%$ as the mixture containing 7% lime. Three different lime percentages (calculated based on the mass of dry soil plus coal fly ash) were

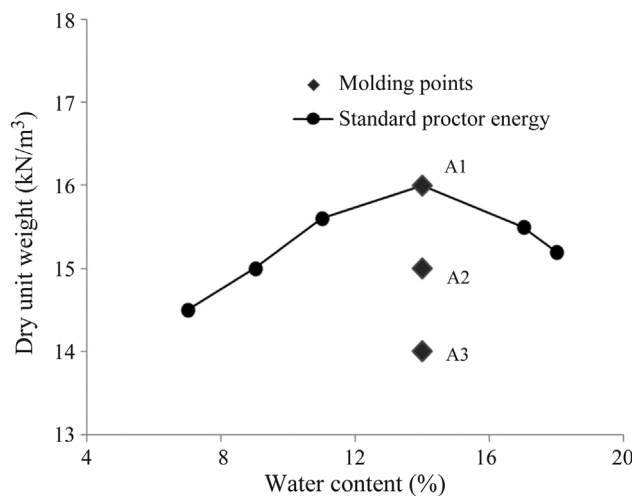


Figure 1 - Compaction curve of sand-coal fly ash (25%) -lime (7%) blend under standard Proctor energy.

chosen starting with 3% [minimum amount to guarantee full stabilization of the studied blends according to Initial Consumption of Lime (ICL) proposed by Rogers *et al.* (1997)], plus two other values above it, 5% and 7% (Mitchell, 1981). Consoli *et al.* (2014b) studied the same sand-coal fly ash-lime blends studied here in (considering the same compaction conditions - same molding points, curing method, and curing temperatures of 20, 35 and 50 °C), but only contemplating 28 days of curing time. Since temperature can be a catalyzer in lime-fly ash reactions, this research focused on shorter curing times (1, 3 and 7 days) and considered the following range of curing temperatures: 20, 35, 50, 65, 80 and 90 °C. All specimens had 25% FA content. This agrees with Brazilian practice (Consoli *et al.*, 2001). Three specimens were tested for each molding point so as to account for the typical scatter of data from the strength tests.

3. Results and Analysis

3.1. Effect of porosity/lime index

Consoli *et al.* (2014b) showed that the tensile strength of sand-fly ash-lime blends, cured for 28 days, can be evaluated by the porosity/lime index (η/L_v), defined by the porosity (η) of the compacted blend divided by the volumetric lime content (L_v) (defined as the volume of lime in relation to the total specimen volume) adjusted by an exponent (0.30). Figures 2, 3 and 4 show that the $[\eta/(L_v)]^{0.30}$ can also be used to evaluate the tensile strength of the studied mixture when the curing time is 1, 3 and 7 days. All fits were based in the whole raw experimental data.

It can be observed in Figs. 2, 3 and 4 that for the lower curing temperatures, q_t does not change much with increas-

ing values of $[\eta/(L_v)]^{0.30}$, and consequently the coefficient of determination (R^2) is low. In the extreme, if q_t was constant with increasing values of $[\eta/(L_v)]^{0.30}$ the coefficient of determination would be close to zero.

Consoli *et al.* (2014b) found that for 28 days of curing the q_t increased with temperature up to 35 °C, after which it stabilized. Figure 2 presents that for 7 days of curing, q_t increases with the temperature up to 50 °C. According to Figs. 3 and 4, the temperature of 80 °C seems to be the limit temperature for 1 and 3 days of curing time. For any tem-

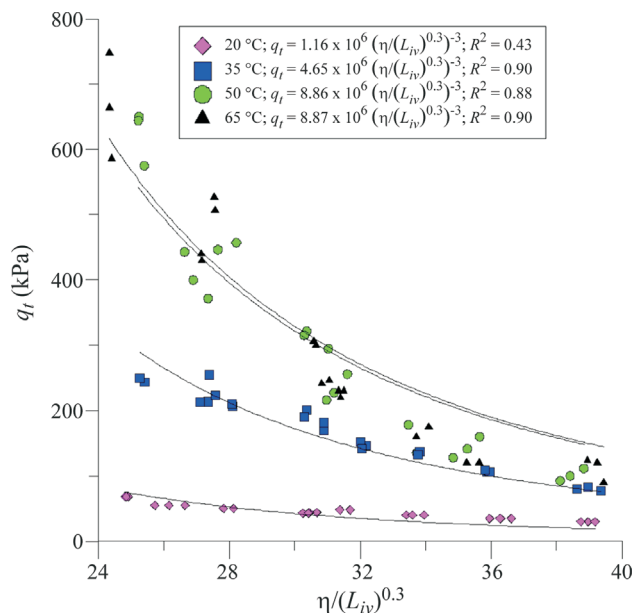


Figure 2 - Variation of splitting tensile strength with adjusted porosity/lime index considering 7 days of curing time.

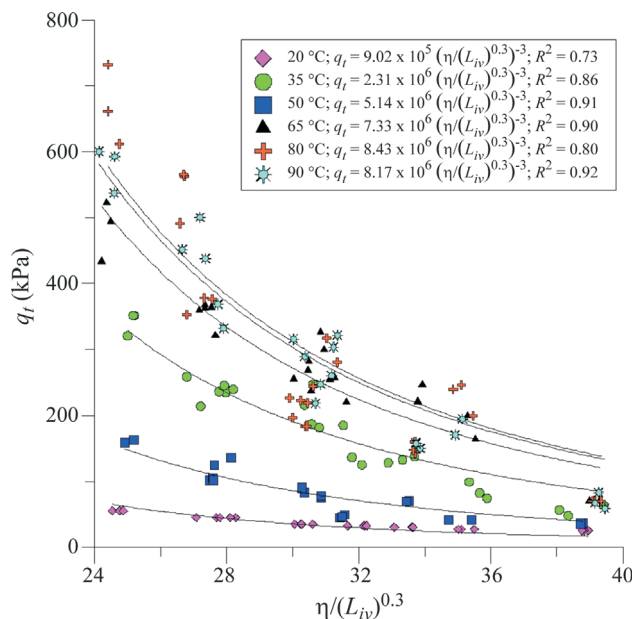


Figure 3 - Variation of splitting tensile strength with adjusted porosity/lime index considering 3 days of curing time.

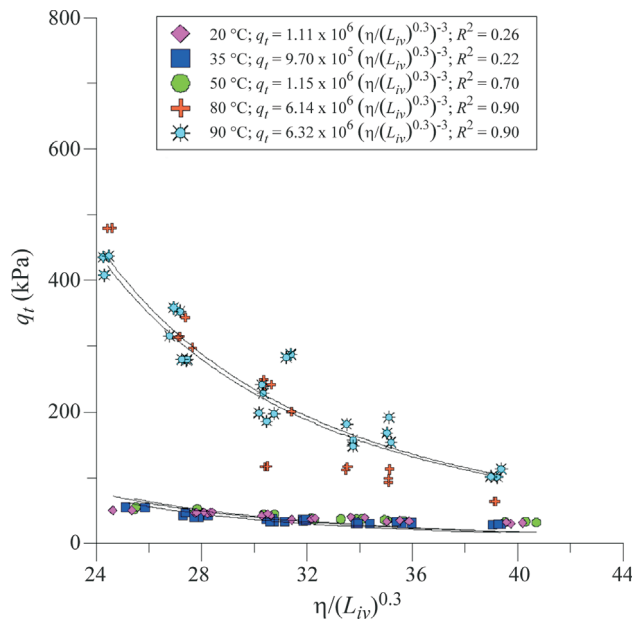


Figure 4 - Variation of splitting tensile strength with adjusted porosity/lime index considering 1 day of curing time.

perature beyond 50 °C for 7 days of curing time and 80 °C for 1 and 3 days of curing time, the q_t remains constant. The data of Figs. 2 to 4 plus the result of Consoli *et al.* (2014b) can be summarized in Fig. 5. Figure 5 presents the variation of normalized splitting tensile strength $q_t / [\frac{\eta}{(L_{iv})^{0.30}}]^{-3}$ with curing temperatures (T). Figure 5 shows that for each curing time $q_t / [\frac{\eta}{(L_{iv})^{0.30}}]^{-3}$ increases linearly with rising temperatures up to a threshold and after that it becomes an

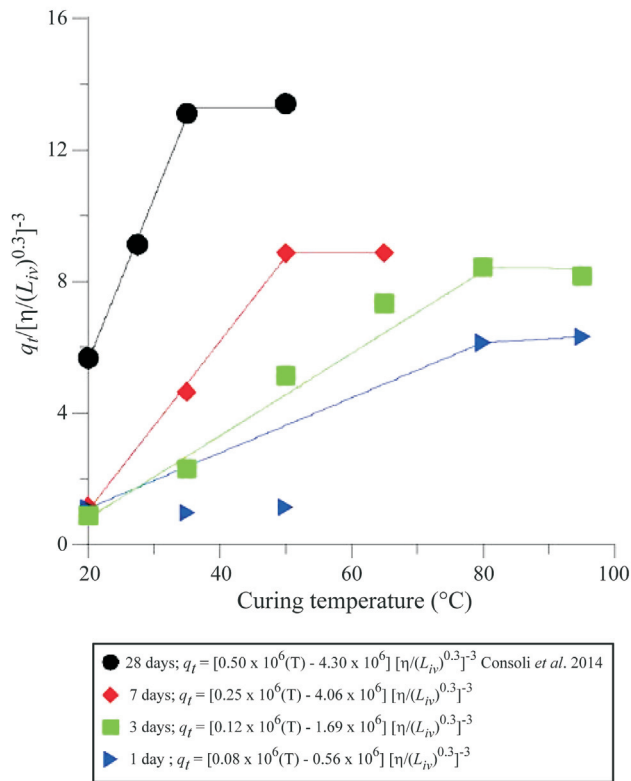


Figure 5 - Variation of normalized splitting tensile strength with curing temperatures (for 1, 3, 7 and 28 days curing).

asymptote. The strength gain leveled off for each specific curing time period because there is a maximum velocity for the chemical reactions between silica and alumina in amorphous phase (from the coal fly ash) and Ca^{++} from the $Ca(OH)_2$ that can occur. As such, increasing temperature expedites pozzolanic reactions up to a certain temperature (until the kinematic of the reactions reach a maximum) and increasing temperature beyond that will not cause any strength increase. Figure 5 also shows that $q_t / [\frac{\eta}{(L_{iv})^{0.30}}]^{-3}$ depends on the time and temperature of curing. Thus in order to optimize the tensile strength, it is necessary to know the maximum temperature capable of effectively increasing q_t for each curing time and the maximum tensile strength that can be reached in each curing time. Figure 6 presents the maximum temperature that is effective in growing q_t . That temperature decreases with the rise of curing time according with a power function [Eq. 2]. So, Eq. 2 is useful to optimize the expenditure of energy in the form of heat to increase q_t .

$$T_i = 88.89(t_{curing})^{-0.27} \tag{2}$$

The space $q_t / [\frac{\eta}{(L_{iv})^{0.30}}]^{-3}$ vs. curing time (t_{curing}) can be divided in two areas (see Fig. 7): one possible (below the curve represented in Fig. 7) and one impossible (above the curve represented in Fig. 7). These areas are divided by a power equation [Eq. 3]. Equation 3 enables the calculation of the maximum tensile strength that can be reached for each curing time.

$$q_t = [6.22(t_{curing})^{0.22}] \left[\frac{\eta}{(L_{iv})^{0.3}} \right]^{-3} \tag{3}$$

where T_i = temperature of stabilization (maximum) of the increase in tensile strength, and t_{curing} = curing time.

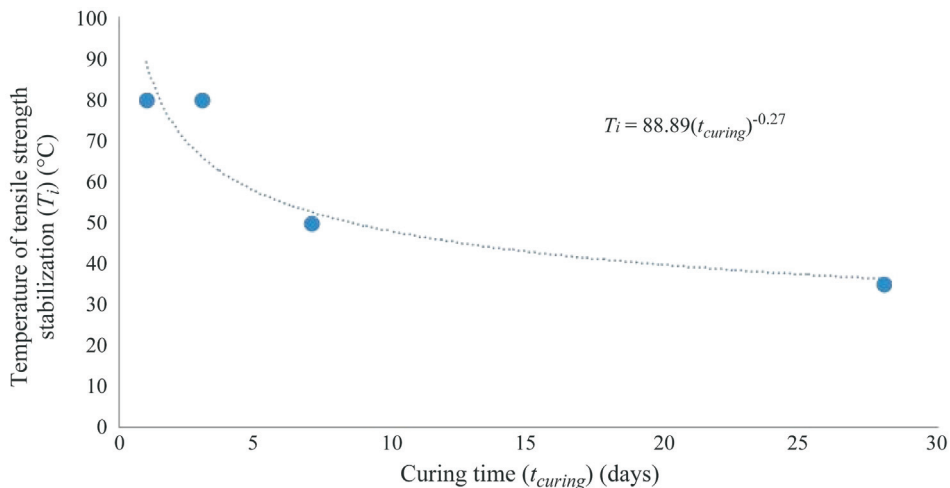


Figure 6 - Relationship between the temperature of tensile strength stabilization (T_i) and the curing time (t_{curing}).

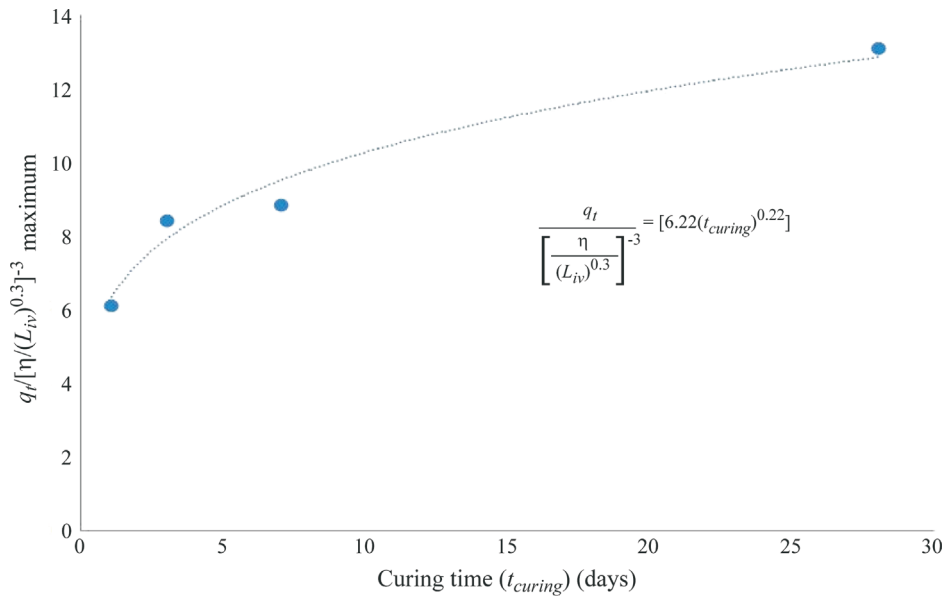


Figure 7 - Relationship between the normalized splitting tensile strength and the curing time (t_{curing}).

4. Concluding Remarks

From the data presented in this manuscript the following concluding remarks can be drawn:

- Increase in temperature boosts tensile strength of sand-coal fly ash-lime blends up to a limit. This limit varies with curing time. To optimize the dosage of sand-coal fly ash-lime mixtures, it is necessary to know the maximum temperature (T_i) capable of effectively increasing q_t [see Eq. 2]. The maximum tensile strength, for each curing time (t_{curing}), is also a restraining value. This information can be calculated from Eq. 3. Equations 2 and 3 are valid for the sand, coal fly ash and lime used in the present study and further studies are necessary to check if analogous equations are found for other soils, ashes and limes. Additionally, subsequent investigation shall be carried out to assess if similar trends are also observed regarding initial shear stiffness (G_0);
- The porosity/lime index, defined by the porosity of the compacted mixture divided by the volumetric lime content, adjusted by an exponent, $[\eta / (L_{iv})^{0.30}]$ has been shown to be an appropriate parameter for evaluating the splitting tensile strength of several combinations of curing temperatures and curing times for the sand-coal fly ash-lime blends studied. Further studies are being carried out by the authors considering the efficiency of the porosity/lime index to detect the impact of distinct curing temperatures and curing times on similar blends considering clayey soils;
- Curing temperature only works as a catalyzer, meaning that increasing temperature only expedites strength gain but does not increase it (final strength depends only on dosage and time to reach such strength is the only aspect affected by temperature). However, given the possibility of encountering temperatures above 40 °C in the field

during certain times of year (mainly in summer), it is important to know that in such situations shorter curing periods will be required in order to develop the full cementation using coal fly ash - lime blends. Finally, the development of strength of sand-coal fly ash-lime blends due to field temperatures above the ambient temperature commonly considered for design (about 20 °C) is key to soil stabilization and ground improvement, since the faster the final target strength is reached in the field, the sooner the earthwork can be used for the purpose for which it has been built.

Acknowledgments

The authors wish to express their appreciation to Edital 12/2014 FAPERGS/CNPq - PRONEX (project # 16/2551-0000469-2), CNPq (INCT-REAGEO and Produtividade em Pesquisa) and CAPES for funding the research group.

References

- ASTM (1998). Standard specification for coal fly ash and raw or calcined natural pozzolan for use as a mineral admixture in concrete. ASTM C618, West Conshohocken, PA.
- ASTM (2006). Standard classification of soils for engineering purposes. ASTM D2487, West Conshohocken, Philadelphia.
- ASTM (2011). Standard test method for splitting tensile strength of cylindrical concrete specimens. ASTM C496, West Conshohocken, PA.
- Carneiro, F.L.L.B. & Barcelos, A. (1953). Concrete tensile strength. R.I.L.E.M. Bulletin, 13:97-108.
- Consoli, N.C.; Prietto, P.D.M.; Carraro, J.A.H. & Heineck, K.S. (2001). Behavior of compacted soil-fly ash-car-

- bide lime-fly ash mixture. *Journal Geotechnical Geoenvironmental Engineering*, 127(9):774-782.
- Consoli, N.C.; Thomé, A.; Donato, M. & Graham, J. (2008). Loading tests on compacted soil, bottom ash and lime layers. *Proceedings of the ICE - Geotechnical Engineering*, 161(GE1):29-38.
- Consoli, N.C.; Dalla Rosa, F. & Fonini, A. (2009a). Plate load tests on cemented soil layers overlaying weaker soil. *Journal of Geotechnical and Geoenvironmental Engineering*, 135(12):1846-1856.
- Consoli, N.C.; Lopes Junior, L.S. & Heineck, K.S. (2009b). Key parameters for the strength control of lime stabilized soils. *Journal of Materials in Civil Engineering*, 21(5):210-216.
- Consoli, N.C.; Dalla Rosa, A. & Saldanha, R.B. (2011). Variables governing strength of compacted soil-fly ash-lime mixtures. *Journal of Materials in Civil Engineering*, 23(4):432-440.
- Consoli, N.C.; Da Rocha, C.G. & Saldanha, R.B. (2014a). Coal fly ash-carbide lime bricks: An environment friendly building product. *Construction and Building Materials*, 69:301-309.
- Consoli, N.C.; Da Rocha, C.G. & Silvani, C. (2014b). Devising dosages for soil-fly ash-lime blends based on tensile strength controlling equations. *Construction and Building Materials*, 55:238-245.
- Consoli, N.C.; Da Rocha, C.G. & Silvani, C. (2014c). Effect of curing temperature on strength of sand - coal fly ash - lime blends. *Journal of Materials in Civil Engineering*, 26(8):06014015.
- Consoli, N.C.; Festugato, L.; Consoli, B.S. & Lopes Junior, L.S. (2015). Assessing failure envelopes of soil-fly ash-lime blends. *Journal of Materials in Civil Engineering*, 27(5):04014174.
- Consoli, N.C.; Scheuermann Filho, H.C.; Godoy, V.B.; Rosenbach, C.M.D.C. & Carraro, J.A.H. (2018). Durability of RAP-industrial waste mixtures under severe climate conditions. *Soils and Rocks*, 41(2):149-156.
- Kampala, A.; Horphibulsuk, S.; Prongmanee, N. & Chinkul-kijniwat, A. (2014). Influence of wet-dry cycles on compressive strength of calcium carbide residue-fly ash stabilized clay. *Journal of Materials in Civil Engineering*, 26(4):633-643.
- Marinho, F.A.M. (1995). Suction measurement through filter paper technique. *Proc. Unsaturated Soils Seminar, UFRGS, Porto Alegre*, pp. 111-125 (in Portuguese).
- Mitchell, J.K. (1981). Soil improvement - State-of-the-art report. *Proc. 10th Int. Conf. on Soil Mechanics and Foundation Engineering. International Society of Soil Mechanics and Foundation Engineering, Stockholm*, pp. 509-565.
- Pedreira, C.L.S. (2000). The use of industrial by-products to build a cemented layer above compressible soil: Case study. M.Sc. Dissertation, Programa de Pós-Graduação em Engenharia Civil, Universidade Federal do Rio Grande do Sul, Porto Alegre, Brazil (in Portuguese).
- Pedreira, C.L.S.; Dias, C.R.R. & Schnaid, F. (2002). Settlement of a building constructed on the top of an artificially cemented layer bearing on a compressible soil. *Proc. XII Brazilian Congress of Soil Mechanics and Geotechnical Engineering (ABMS), São Paulo, Brazil* (in Portuguese).
- Rogers, C.D.F.; Glendinning S. & Roff, T.E.J. (1997). Lime modification of clay soils for construction expediency. *Proceedings of the Institute of Civil Engineers - Geotechnical Engineering*, 125(4):242-249.
- Saldanha, R.B. & Consoli, N.C. (2016). Accelerated mix design of lime stabilized materials". *Journal of Materials in Civil Engineering*, 28(3):06015012.
- Silvani, C. (2013). Influence of curing temperature in the mechanical behavior of sand-coal fly ash-lime blends. M.Sc. dissertation, Programa de Pós-Graduação em Engenharia Civil, Universidade Federal do Rio Grande do Sul, Porto Alegre, Brazil (in Portuguese).
- Thomé, A.; Donato, M.; Consoli, N.C. & Graham, J. (2005). Circular footings on a cement layer above weak foundation soil. *Canadian Geotechnical Journal*, 42(6):1569-1584.
- Thompson, M.R. (1966). Shear strength and elastic properties of lime soil mixtures. *Highway Research Record, Washington*, pp. 139, 1-14.
- Toohey, N.M.; Mooney, M.A. & Bearce, R.G. (2013). Stress-strain-strength behavior of lime-stabilized soils during accelerated curing. *Journal of Materials in Civil Engineering*, 25(12):1880-1886.
- Zhang, J.; Liu, G.; Chen, B.; Song, D.; Qi, J. & Liu, X. (2014). Analysis of CO₂ emission for the cement manufacturing with alternative raw materials: A LCA-based framework. *Energy Procedia*, 61:2541-2545.

List of Symbols

- L : lime content (expressed in relation to mass of dry soil)
- L_{iv} : volumetric lime content (expressed in relation to the total specimen volume)
- D_{50} : mean particle diameter
- q_t : splitting tensile strength
- T : curing temperature
- T_i : temperature of stabilization (maximum) of the increase in tensile strength
- t_{curing} : curing time
- V_L : volume of lime
- V_s : total volume of specimen
- V_v : volume of voids
- γ_d : dry unit weight
- γ_{dmax} : maximum dry unit weight
- η : porosity
- η/L_{iv} : porosity/lime index
- ω : moisture content
- ω_{opt} : optimum moisture content

Discussion

Soils and Rocks
v. 42, n. 1

Discussion

Behavior of Geosynthetic-Encased Stone Columns in Soft Clay: Numerical and Analytical Evaluations

Discussion by:

B. Pulko and J. Logar

Faculty of Civil and Geodetic Engineering, University of Ljubljana
Jamova 2, Ljubljana, Slovenia.

1. Introduction

The authors presented numerical analysis of an embankment underlain by soft clay improved with geosynthetic-encased stone columns and comparison of results with analytical methods developed by Raithel & Kempfert (2000), Pulko *et al.* (2011) and Zhang & Zhao (2014). The authors conclude that among the three methods, the results of R&K generally show better agreement with the results of FEM than the results of PEA and ZZ methods. The readers would like to address that statement and point to some shortcomings and inconsistencies regarding the use of analytical procedures according to R&K and PEA methods.

2. Discussion

When comparing R&K and PEA methods, it should be considered that both are based on the same fundamental assumptions. The methods differ only in treatment of the stone column (SC). In the R&K method, the SC is considered as a rigid plastic material with constant volume at yield. On the other side, the PEA method assumes elastoplastic behavior with the ability to take into account the SC dilation. Another difference with minor influence on calculation results is that the R&K method assumes finite strains, while the PEA method assumes small strain theory. Due to these differences, the calculated settlements according to the PEA method will always exceed the values of the R&K method, if the equivalent input data are used (Pulko *et al.*, 2011). Because in the paper the PEA method is shown to produce settlements lower than the R&K method, the readers believe that the soil stiffness used for both methods was not the same but is unfortunately not given in the paper.

From theoretical equations behind both methods, it is evident that under constant SC volume and considering small strain theory ($\varepsilon_v = \varepsilon_1 - 2\varepsilon_r = 0$), the total settlement s

can be obtained with the integration of axial strains ε_1 over depth, which can be related to the geosynthetic tensile force $\Delta F_g(z)$:

$$\begin{aligned} s &= \int_0^H \varepsilon_1 dz = \int_0^H 2\varepsilon_r dz = \int_0^H \frac{2\Delta F_g(z)}{J} dz = \\ &= \frac{2}{J} \int_0^H \Delta F_g(z) dz \end{aligned} \quad (1)$$

If the SC volume is constant, then the settlement is proportional to the area under the graph of geosynthetic tensile force $\Delta F_g(z)$. If the SC is compressible, then the settlement is even larger. In Fig. 5 of the paper (Fig. 1 below), the areas under the graphs of tensile force for the R&K method are significantly smaller than for the FEM and PEA methods. This does not support the authors' conclusion that the R&K method produces settlements in line with the FEM results, while the PEA method produces smaller settlements.

3. Conclusions

Under given assumptions both analytical methods (R&K and PEA) are able to provide comparable results in good agreement with FEM, as long as equivalent material data are taken into account. When using simplified elastic methods, the determination of equivalent stiffness is essential to provide comparability with the results of advanced nonlinear FEM. Any comparison of different analytical methods without proper representation of the equivalent input data (*i.e.* stiffness) is incomplete and can lead to misleading conclusions.

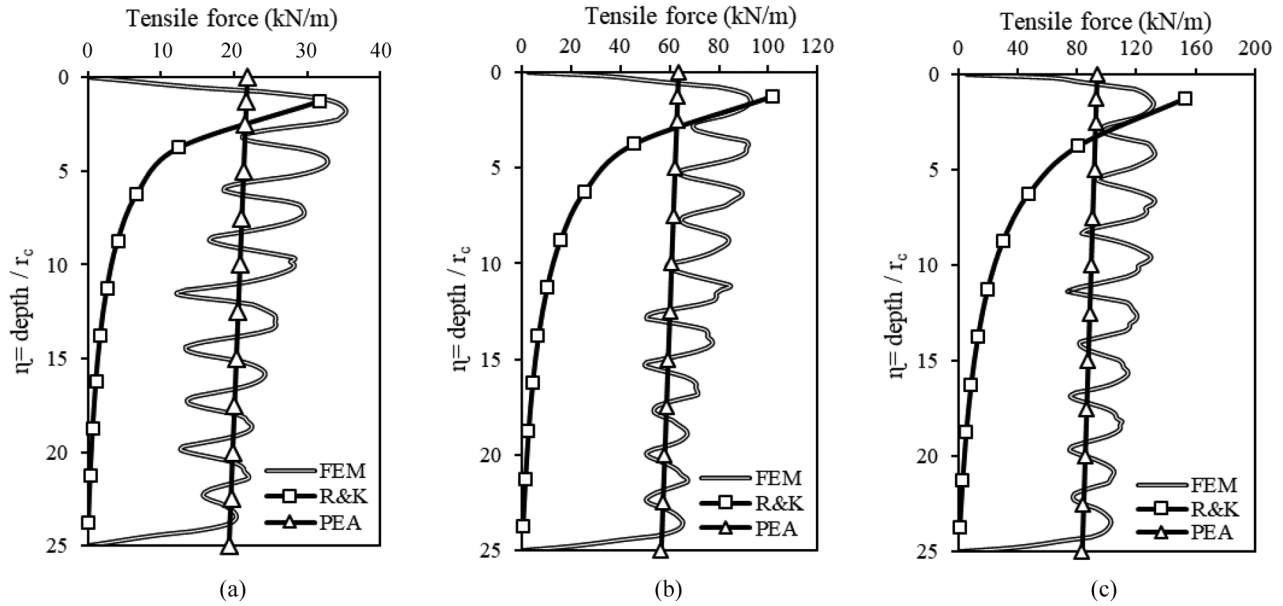


Figure 1 - Tensile force vs. depth ratio for different geosynthetic stiffnesses; (a) Tensile force for $J = 500$ kN/m, (b) Tensile force for $J = 2000$ kN/m, (c) Tensile force for $J = 4000$ kN/m (Fig. 5 after Alkhorshid *et al.*, 2018).

References

Alkhorshid, N.R.; Araújo, G.L.S. & Palmeira, E.M. (2018). Behavior of geosynthetic-encased stone columns in soft clay: Numerical and analytical evaluations. *Soils and Rocks*, 41(3):333-343.

Pulko, B.; Majes, B. & Logar, J. (2011). Geosynthetic-encased stone columns: Analytical calculation model. *Geotextiles and geomembranes*, 29(1):29-39.

Raithel, M. & Kempfert, H.G. (2000). Calculation models for dam foundation with geotextile coated sand columns. Proc. International Conference on Geotechnical & Geological Engineering, Geo-Eng -2000, Melbourne.

Zhang, L. & Zhao, M. (2014). Deformation analysis of geotextile-encased stone columns. *Int. J. Geomech.*, 15(3):1-10.

Closure by authors

1. Introduction

The authors would like to thank the writers' interest in the paper and constructive comments. The writers present some theoretical statements about PEA and R&K methods. It is stated that both methods come from same fundamental assumptions, except for the column behavior which is treated as a rigid plastic material in R&K and is expected to have an elastoplastic behavior in PEA. It is also commented that another difference is that PEA presumes small strain theory while R&K assumes finite strains. Then it concluded that these differences cause PEA values always to exceed R&K values if equivalent input data are employed.

2. Reply to the Discussion

Both methods, PEA and R&K, use the oedometric modulus of the soil, which can be obtained from $E_{oed,ref}$ presented in Table 1 of the paper ($E_{oed,ref} = 1850$ kPa). Thus, the R&K greater settlements than the PEA settlements can not be due to the different input data since in both methods the very same value of soil stiffness was used.

Considering the values of tensile forces, the result for R&K shown in Fig. 5 of the paper was produced using the values of radius variation for different depths obtained from the following equation (Raithel & Kempfert, 2000):

$$\Delta r_c = \frac{K_{a,c} \left(\frac{1}{a_E} \cdot \Delta \sigma_{v,s} + \sigma_{v,0,c} \right) - K_{0,s} \cdot \Delta \sigma_{v,s} - K_{0,s} \cdot \Delta \sigma_{v,0,s} + \frac{(r_{geo} - r_c) \cdot J}{r_{geo}^2}}{\frac{E^*}{\left(\frac{1}{a_E} - 1 \right) \cdot r_c} + \frac{J}{r_{geo}^2}} \quad (1)$$

where $k_{a,c}$, a_E , $\Delta \sigma$, $\Delta \sigma_{v,s}$, $\sigma_{v,0,c}$, $K_{0,s}$, $\sigma_{v,0,s}$, r_{geo} , r_c and J are coefficient of active earth pressure of column, area replacement ratio, applied stress at the top of unit cell, increase of vertical stress on soft ground, initial stress on the column before loading, coefficient of lateral earth pressure at rest for soft soil, initial stress on soft soil before loading, radius of the surrounding geotextile, column radius and geosynthetic tensile stiffness.

The discussion also addresses the constant stone column volume and the assumption of incompressible column material. Hence, the values of tensile forces calculated using R&K were double-checked considering the constant stone column volume and it was found that R&K predictions were wrongly plotted. Thus, the correct values are now presented as R&K2 in Fig. 2.

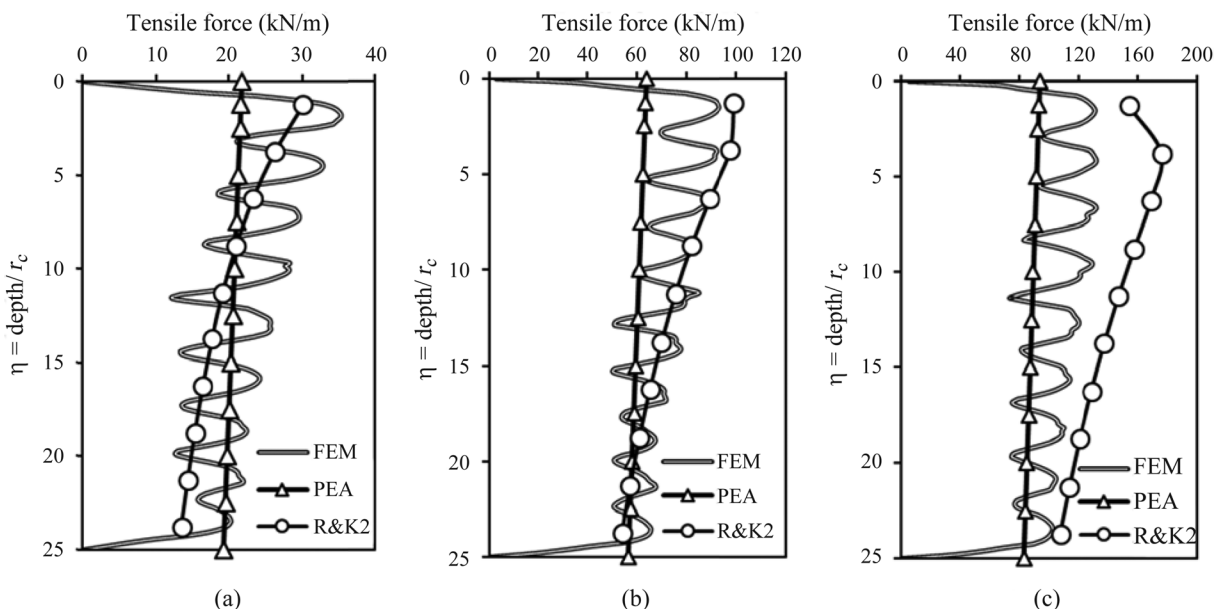


Figure 2 - Tensile force vs. depth ratio for different geosynthetic stiffness: (a) Tensile force for $J = 500$ kN/m, (b) Tensile force for $J = 2000$ kN/m, (c) Tensile force for $J = 4000$ kN/m.

3. Conclusion

The writers suggest that under equivalent material data both methods, PEA and R&K, can provide comparable results in good agreement with those of FEM. Since both methods take E_{oed} of soil into account, the calculations were made using the same value ($E_{oed,ref} = 1850$ kPa) for both methods. The authors do not believe that using different oedometric modulus for the soil would be fair for the comparisons between predictions from different methods. In addition, Khabbazian *et al.* (2011) presented a discussion on PEA method and in Fig. 1 of their paper, PEA settlements were compared with those from FEM for different diameter ratios ($N = r_e/r_c$). They also found that settlements predicted by PEA were smaller than those from FEM.

PEA is capable of producing results that are in good agreement with FEM. Yet, the settlement results shown in Fig. 3 of the paper suggest that under constant value of

geosynthetic tensile stiffness ($J = 2000$ kN/m) and different diameter ratios ($N = r_e/r_c$), R&K radius variations and settlements were in better agreement with those from FEM. On the other hand, under constant diameter ratio ($N = 3.5$) and different tensile stiffness values both methods can provide satisfactory results (Fig. 2).

References

Alkhorshid, N.R.; Araújo, G.L.S. & Palmeira, E.M. (2018). Behavior of geosynthetic-encased stone columns in soft clay: Numerical and analytical evaluations. *Soils and Rocks*, 41(3):333-343.

Khabbazian, M.; Meehan, C.L. & Kaliakin, V.N. (2011). Discussion of “Geosynthetic-encased stone columns: Analytical calculation model” by Bostjan Pulko, Bojan Majes & Janko Logar, [*Geotextiles and Geomembranes* 29:29-39 (2011)]. *Geotextiles and Geomembranes* 29:581-583 (2011).

SOILS and ROCKS

An International Journal of Geotechnical and Geoenvironmental Engineering

Publication of

ABMS - Brazilian Association for Soil Mechanics and Geotechnical Engineering

SPG - Portuguese Geotechnical Society

Volume 42, N. 1, January-April 2019

Author index

Andreyko, S.S.	77	Matos, Y.M.P.	21
Araújo, G.L.S.	3	Menezes, L.C.P.	31
Barreto, G.A.	21	Neto, S.A. Dantas	21
Benetti, M.	83	Pierozan, R.C.	3
Camapum de Carvalho, J.C.	61	Pulko, B.	93
Consoli, N.C.	83	Rebolledo, J.F.R.	61
Ferreira, S.R.M.	31	Siacara, A.T.	43
Festugato, L.	43	Silvani, C.	83
León, R.F.P.	61	Sousa, D.B.	31
Logar, J.	93	Sukar, S.F.	31
Lyalina, T.A.	77	Teixeira, C.A.	3
		Teixeira, S.H.C.	3

BUILDING A BETTER WORLD



TPF

PLANEGE CENOR



Engineering and Architectural Consultancy

Geology, Geotechnics, Supervision of Geotechnical Works
Embankment Dams, Underground Works, Retaining Structures
Special Foundations, Soil Improvement, Geomaterials



www.tpfplanegecenor.pt



- > **Prospecção Geotécnica**
Site Investigation
- > **Consultoria Geotécnica**
Geotechnical Consultancy
- > **Obras Geotécnicas**
Ground Treatment-Construction Services
- > **Controlo e Observação**
Field Instrumentation Services and Monitoring Services
- > **Laboratório de Mecânica de Solos**
Soil and Rock Mechanics Laboratory

Certificada ISO 9001 por



Geocontrole



Parque Oriente, Bloco 4, EN10
2699-501 Bobadela LRS
Tel. 21 995 80 00
Fax. 21 995 80 01
e.mail: mail@geocontrole.pt
www.geocontrole.pt


Geocontrole
Geotecnia e Estruturas de Fundação SA



COBA

GEOLOGY AND GEOTECHNICS

Hydrogeology • Engineering Geology • Rock Mechanics • Soil Mechanics • Foundations and Retaining Structures • Underground Works • Embankments and Slope Stability
Environmental Geotechnics • Geotechnical Mapping



- Water Resources Planning and Management
- Hydraulic Undertakings
- Electrical Power Generation and Transmission
- Water Supply Systems and Pluvial and Wastewater Systems
- Agriculture and Rural Development
- Road, Railway and Airway Infrastructures
- Environment
- Geotechnical Structures
- Cartography and Cadastre
- Safety Control and Work Rehabilitation
- Project Management and Construction Supervision



PORTUGAL

CENTER AND SOUTH REGION
Av. 5 de Outubro, 323
1649-011 LISBOA
Tel.: (351) 210125000, (351) 217925000
Fax: (351) 217970348
E-mail: coba@coba.pt
www.coba.pt

Av. Marquês de Tomar, 9, 6º.
1050-152 LISBOA
Tel.: (351) 217925000
Fax: (351) 213537492

NORTH REGION

Rua Mouzinho de Albuquerque, 744, 1º.
4450-203 MATOSINHOS
Tel.: (351) 229380421
Fax: (351) 229373648
E-mail: engico@engico.pt

ANGOLA

Praceta Farinha Leitão, edifício nº 27, 27-A - 2º Dto
Bairro do Maculusso, LUANDA
Tel./Fax: (244) 222338 513
Cell: (244) 923317541
E-mail: coba-angola@netcabo.co.ao

MOZAMBIQUE

Pestana Rovuma Hotel. Centro de Escritórios.
Rua da Sé nº114. Piso 3, MAPUTO
Tel./Fax: (258) 21 328 813
Cell: (258) 82 409 9605
E-mail: coba.mz@tdm.co.mz

ALGERIA

09, Rue des Frères Hocine
El Biar - 16606, ARGEL
Tel.: (213) 21 922802
Fax: (213) 21 922802
E-mail: coba.alger@gmail.com

BRAZIL

Rio de Janeiro
COBA Ltd. - Rua Bela 1128
São Cristóvão
20930-380 Rio de Janeiro RJ
Tel.: (55 21) 351 50 101
Fax: (55 21) 258 01 026

Fortaleza

Av. Senador Virgílio Távora 1701, Sala 403
Aldeota - Fortaleza CEP 60170 - 251
Tel.: (55 85) 3261 17 38
Fax: (55 85) 3261 50 83
E-mail: coba@esc-te.com.br

UNITED ARAB EMIRATES

Corniche Road - Corniche Tower - 5th Floor - 5B
P. O. Box 38360 ABU DHABI
Tel.: (971) 2 627 0088
Fax: (971) 2 627 0087

Reliable solutions with **technology, quality,** and **innovation** for Civil Engineering proposes



MACCAFERRI POLIMAC

New polymeric coating with high performance
PoliMac™



Long-life galvanising
GalMac® 4R

Intermetallic coating

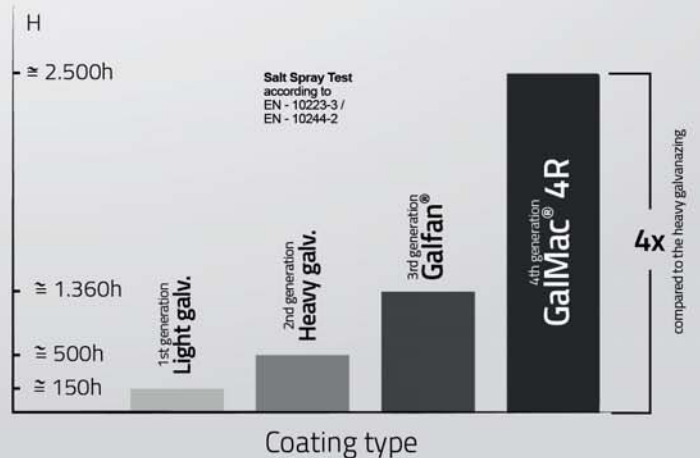
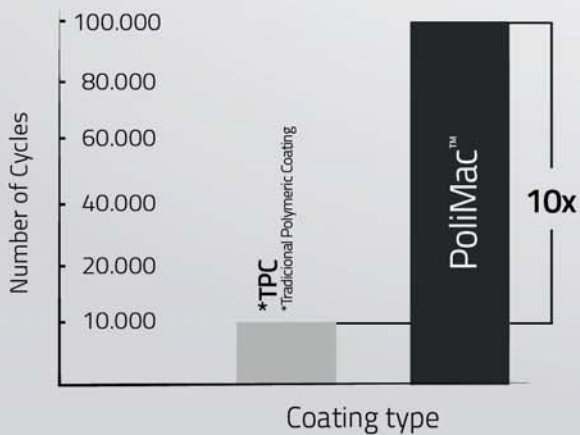
Steel wire LCC*
*Low Carbon Content



The **PoliMac™** in controlled abrasion resistance tests, it showed its excellent performance by resisting up to 100,000 cycles in the standard tests **ABNT NBR 7577** and **EN 10223-3**; about **10x more** than the traditional coating.



The **GalMac® 4R** coating complies with the main national and international standards such as: **EN 10223-3: 2013, ASTM B860** and **NBR 8964**.



Follow us on our **social media**



/maccaferri



/maccaferriatriz



@Maccaferri_BR



+MaccaferriWorld

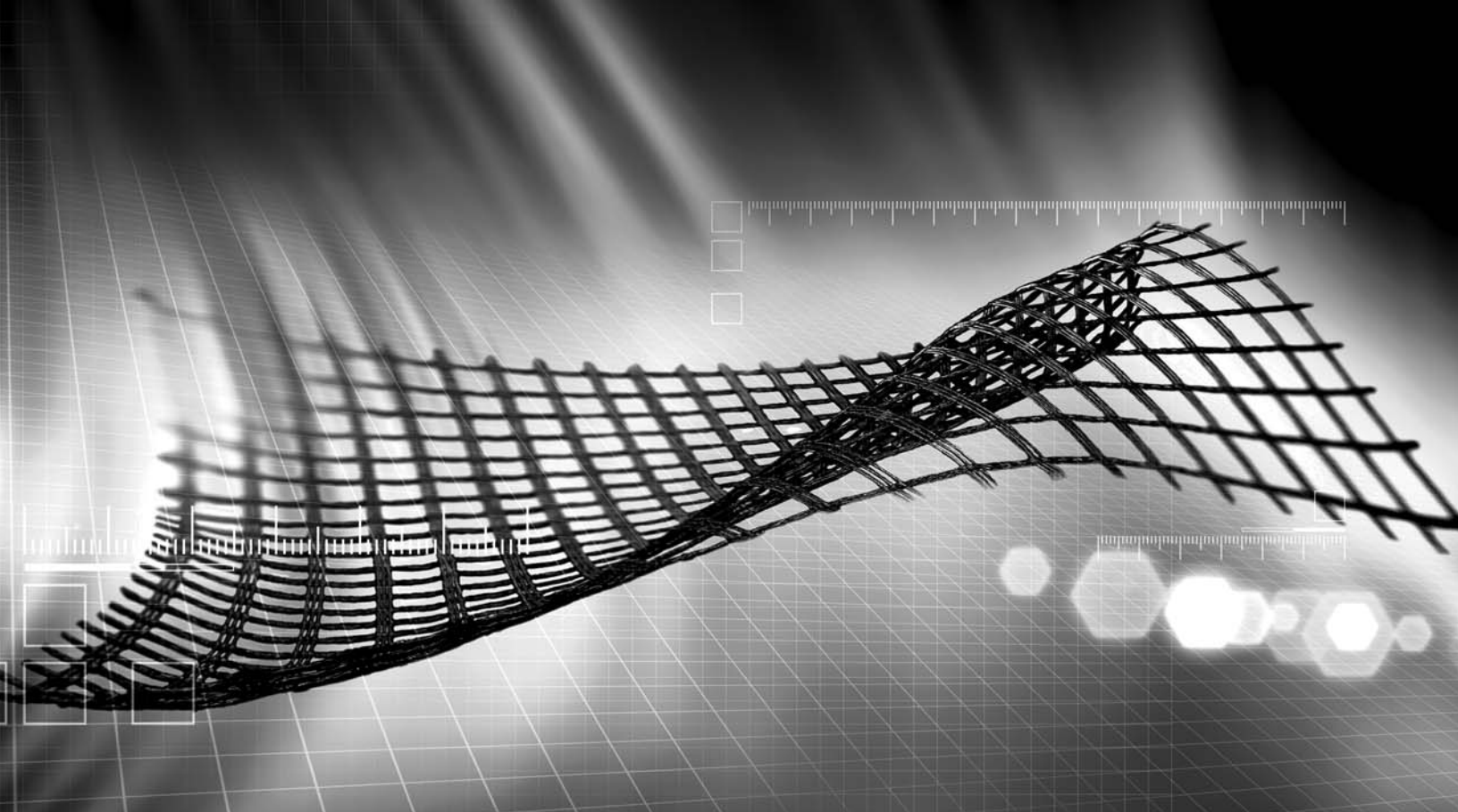


/maccaferriworld



MACCAFERRI

www.maccaferri.com/br



A strong, lasting connection.

With a history of over 150 years of pioneering in geosynthetics, we strive to create solutions for the most diverse engineering challenges.

Our business areas:



Earthworks and Foundations



Environmental Engineering



Roads and Pavements



Hydraulic Engineering

Talk to HUESKER Brasil:
www.HUESKER.com.br
HUESKER@HUESKER.com.br
+55 (12) 3903 9300

Follow HUESKER Brasil in social media:



HUESKER
Ideen. Ingenieure. Innovationen.



Geotechnic and Rehabilitation

TEIXEIRA DUARTE ENGENHARIA E CONSTRUÇÕES, S.A.

- **Head Office**
Lagoas Park - Edifício 2
2740-265 Porto Salvo - Portugal
Tel.: [+351] 217 912 300
Fax: [+351] 217 941 120/21/26
- **Algeria**
Parc Miremont - Rua A, Nº136 - Bouzareah
16000 Alger
Tel.: [+213] 219 362 83
Fax: [+213] 219 365 66
- **Spain**
Avenida Alberto Alcocer, nº24 - 7º C
28036 Madrid
Tel.: [+34] 915 550 903
Fax: [+34] 915 972 834
- **Angola**
Alameda Manuel Van Dunen 316/320 - A
Caixa Postal 2857 - Luanda
Tel.: [+34] 915 550 903
Fax: [+34] 915 972 834
- **Brazil**
Rua Iguatemi, nº488 - 14º - Conj. 1401
CEP 01451 - 010 - Itaim Bibi - São Paulo
Tel.: [+55] 112 144 5700
Fax: [+55] 112 144 5704
- **Mozambique**
Avenida Julyus Nyerere, 130 - R/C
Maputo
Tel.: [+258] 214 914 01
Fax: [+258] 214 914 00

Instructions for Submission of Manuscripts

Category of the Papers

Soils and Rocks is the international scientific journal edited by the Brazilian Association for Soil Mechanics and Geotechnical Engineering (ABMS) and the Portuguese Geotechnical Society (SPG). The aim of the journal is to publish (in English) original research and technical works on all geotechnical branches.

According to its content the accepted paper is classified in one of the following categories: Article paper, Technical Note, Case Study or Discussion. An article paper is an extensive and conclusive dissertation about a geotechnical topic. A paper is considered as a technical note if it gives a short description of ongoing studies, comprising partial results and/or particular aspects of the investigation. A case study is a report of unusual problems found during the design, construction or the performance of geotechnical projects. A case study is also considered as the report of an unusual solution given to an ordinary problem. The discussions about published papers, case studies and technical notes are made in the Discussions Section.

When submitting a manuscript for review, the authors should indicate the category of the manuscript, and is also understood that they:

- assume full responsibility for the contents and accuracy of the information in the paper;
- assure that the paper has not been previously published, and is not being submitted to any other periodical for publication.

Manuscript Instructions

Manuscripts must be written in English. The text is to be typed in a word processor (preferably MS Word), **single column**, using ISO A4 page size, left, right, top, and bottom margins of 25 mm, Times New Roman 12 font, and line spacing of 1.5. All lines and pages should be numbered. The text should be written in the third person.

The first page of the manuscript must include the title of the paper followed by the names of the authors with the abbreviation of the most relevant academic title. The affiliation, address and e-mail must appear below each author's name. An abstract of 200 words follows after the author's names. A list with up to six keywords at the end of the abstract is required.

Although variations on the sequence and title of each section are possible, it is suggested that the text contains the following sections: Introduction, Material and Methods, Results, Discussions, Conclusions, Acknowledgements, References and List of Symbols. A brief description of each section is given next.

Introduction: This section should indicate the state of the art of the problem under evaluation, a description of the problem and the methods undertaken. The objective of the work should be clearly presented at the end of the section.

Materials and Methods: This section should include all information needed to the reproduction of the presented work by other researchers.

Results: In this section the data of the investigation should be presented in a clear and concise way. Figures and tables should not repeat the same information.

Discussion: The analyses of the results should be described in this section.

Conclusions: The content of this section should be based on the data and on the discussions presented.

Acknowledgements: If necessary, concise acknowledgements should be presented in this section.

References: References to other published sources must be made in the text by the last name(s) of the author(s), followed by the year of publication, similarly to one of the two possibilities below:

...while Silva & Pereira (1987) observed that resistance depended on soil density... or It was observed that resistance depended on soil density (Silva & Pereira, 1987).

In the case of three or more authors, the reduced format must be used, e.g.: Silva *et al.* (1982) or (Silva *et al.*, 1982). Two or more citations belonging to the same author(s) and published in the same year are to be distinguished with small letters, e.g.: (Silva, 1975a, b, c.). Standards must be cited in the text by the initials of the entity and the year of publication, e.g.: ABNT (1996), ASTM (2003).

Full references shall be listed alphabetically at the end of the text by the first author's last name. Several references belonging to the same author shall be cited chronologically. Some examples are listed next:

Papers: Bishop, A.W. & Blight, G.E. (1963). Some aspects of effective stress in saturated and unsaturated soils. *Geotechnique*, 13(2):177-197.

Books: Lambe, T.W. & Whitman, R.V. (1979). *Soil Mechanics*, SI Version. John Wiley & Sons, New York, 553 p.

Book with editors: Sharma, H.D.; Dukes, M.T. & Olsen, D.M. (1990). Field measurements of dynamic moduli and Poisson's ratios of refuse and underlying soils at a landfill site. Landva, A. & Knowles, G.D. (eds), *Geotechnics of Waste Fills - Theory and Practice*, American Society for Testing and Materials - STP 1070, Philadelphia, pp. 57-70.

Proceedings (printed matter or CD-ROM): Jamiolkowski, M.; Ladd, C.C.; Germaine, J.T. & Lancellotta, R. (1985). New developments in field and laboratory testing of soils. Proc. 11th Int. Conf. on Soil Mech. and Found. Engn., ISSMFE, San Francisco, v. 1, pp. 57-153. (specify if CD ROM).

Thesis and dissertations: Lee, K.L. (1965). *Triaxial Compressive Strength of Saturated Sands Under Seismic Loading Conditions*. PhD Dissertation, Department of Civil Engineering, University of California, Berkeley, 521 p.

Standards: ASTM (2003). *Standard Test Method for Particle Size Analysis of Soils - D 422-63*. ASTM International, West Conshohocken, Pennsylvania, USA, 8 p.

Internet references: Soils and Rocks available at <http://www.abms.com.br> and downloaded on August 6th 2003.

On line first publications must also bring the digital object identifier (DOI) at the end.

Figures shall be either computer generated or drawn with India ink on tracing paper. Computer generated figures must be accompanied by the corresponding digital file (.tif, .jpg, .pcx, etc.). All figures (graphs, line drawings, photographs, etc.) shall be numbered consecutively and have a caption consisting of the figure number and a brief title or description of the figure. This number should be used when referring to the figure in text. Photographs should be black and white, sharp, high contrasted and printed on glossy paper.

Tables shall be numbered consecutively in Arabic and have a caption consisting of the table number and a brief title. This number should be used when referring to the table in the text. Units should be indicated in the first line of the table, below the title of each column. Acronyms should be avoided. When applicable, the units should come right below the corresponding column heading. Additional comments can be placed as footnotes.

Equations shall appear isolated in a single line of the text. Numbers identifying equations must be flushed with the right margin. International System (SI) units must be used. The definitions of the symbols used in the

equations must appear in the List of Symbols. It is recommended that the symbols used are in accordance with Lexicon in 8 Languages, ISSMFE (1981) and the ISRM List of Symbols.

The text of the submitted manuscript (including figures, tables and references) intended to be published as an article paper or a case history should not contain more than 30 pages, formatted according to the instructions mentioned above. Technical notes and discussions should have no more than 15 and 8 pages, respectively. Longer manuscripts may be exceptionally accepted if the authors provide proper explanation for the need of the required extra space in a cover letter.

Discussion

Discussions must be written in English. The first page of a discussion should contain:

The title of the paper under discussion;

Name of the author(s) of the discussion, followed by their position, affiliation, address and e-mail. The author(s) of the discussion should refer to himself (herself/themselves) as the reader(s) and to the author(s) of the paper as the author(s).

Figures, tables and equations should be numbered following the same sequence of the original paper. All instructions previously mentioned for the preparation of article papers, case studies and technical notes also apply to the preparation of discussions.

Editorial Review

Each paper will be evaluated by reviewers selected by the editors according to the subject of the paper. The authors will be informed about the results of the review process. If the paper is accepted, the authors will be required to submit a version of the revised manuscript with the suggested modifications. If the manuscript is rejected for publication, the authors will be informed about the reasons for rejection. In any situation comprising modification of the original text, classification of the manuscript in a category different from that proposed by the authors, or rejection, the authors can reply presenting their reasons for disagreeing with the reviewer comments.

Submission

The author(s) must upload a digital file of the manuscript to the Soils and Rocks website.

Follow Up

The online management system will provide a password to the corresponding author, which will enable him/her to follow the reviewing process of the submitted manuscript at the Soils and Rocks website.

Volume 42, N. 1, January-April 2019**Table of Contents***ARTICLES*

- Geomembrane as an Upstream Impermeable Blanket of Embankment Dams - Laboratory and Numerical Study*
R.C. Pierozan, S.H.C. Teixeira, G.L.S. Araújo, C.A. Teixeira 3
- Predicting the Shear Strength of Unfilled Rock Joints with the First-Order Takagi-Sugeno Fuzzy Approach*
Y.M.P. Matos, S.A. Dantas Neto, G.A. Barreto 21
- Analysis of the Physical-Mechanical Behavior of Clayey Sand Soil Improved with Coir Fiber*
L.C.P. Menezes, D.B. Sousa, S.F. Sukar, S.R.M. Ferreira 31
- Numerical Simulation of Vertical Pullout of Plate Anchors Embedded in Reinforced Sand*
A.T. Siacara, L. Festugato 43
- Obtaining the Mechanical Parameters for the Hardening Soil Model of Tropical Soils in the City of Brasilia*
J.F.R. Rebolledo, R.F.P. León, J. Camapum de Carvalho 61
- TECHNICAL NOTES*
- Rockburst From Floors*
S.S. Andreyko, T.A. Lyalina 77
- Maximum Tensile Strength of Sand - Coal Fly Ash - Lime Blends for Varying Curing Period and Temperature*
C. Silvani, M. Benetti, N.C. Consoli 83
- DISCUSSION*
- Behavior of Geosynthetic-Encased Stone Columns in Soft Clay: Numerical and Analytical Evaluations*
N.R. Alkhorshid, G.L.S. Araújo, E.M. Palmeira 93